MECHANISMS OF PULP LOSS IN FLOTATION DEINKING

By

MICHAEL AJERSCH, B.A.Sc., M. Eng.

A Thesis
Submitted to the School of Graduate Studies
in Partial Fulfillment of the Requirements
for the Degree
Doctor of Philosophy

McMaster University

This thesis is dedicated to my parents, to Duane (who may now call me "Doctor"), and to Basil Watson.

DOCTOR OF PHILOSOPHY (1997)

McMaster University
Hamilton, Ont.

TITLE: Mechanisms of Pulp Loss in Flotation Deinking

AUTHOR: Michael John Ajersch, B.A.Sc. (Waterloo University)
M. Eng. (McMaster University)

SUPERVISOR: Professor Robert Pelton

NUMBER OF PAGES: xviii, 283

ABSTRACT

A key unit operation in most recycled paper mills is the flotation deinking process. In an ideal flotation cell, the froth (rejects) should only contain ink and other hydrophobic contaminants. In actual flotation cells, however, the rejects also contain small amounts of useful cellulosic pulp material. These pulp losses are a waste of raw material.

The objectives of this thesis were to identify the dominant mechanism(s) responsible for pulp loss in flotation systems, and to attempt to quantify these mechanisms. Three potential causes of pulp loss were investigated: pulp flotation by bubble adhesion, pulp flotation by bubbles mechanically-trapped within fibre networks, and the transport of pulp fibres and pulp fines into the froth by hydraulic entrainment.

Direct observation of bubble-fibre interactions in both bubble generation tests and in flow visualization studies revealed that bubbles are unlikely to adhere to wetted pulp fibres. The flow visualization studies also demonstrated that while bubbles can become trapped in fibre networks, these bubbles are easily released under flowing conditions. Mechanical entrapment is considered to cause significant pulp flotation only under quiescent conditions where pulp flocs were present.

Based on results obtained from batch flotation experiments, it was determined that hydraulic entrainment is the dominant pulp loss mechanism. Entrainment was largely affected by flocculation, as rising bubbles tended to be channeled around the flocs. Two

regimes of entrainment were proposed, which depended on flocculation. When no flocs were present, the consistency of the foam and feed were similar. In flocculated pulp suspensions, the consistency of the foam represented that of the pulp existing in regions between the flocs.

A three-parameter model was derived which predicted the consistencies and the pulp fines fractions of the foams from the flotation experiments. By combining these experimental results with independently-measured pulp sedimentation curves, the model characterized the pulp suspensions' state of flocculation in terms of floc volume fraction, floc consistency and the distribution of pulp fines between the flocculated and non-flocculated regions. The model was more applicable when flow conditions were such that small bubbles were channeled around the flocs. The model also indicated that pulp fines tend to be excluded from flocs.

PREFACE

The majority of the work involved in completing this thesis is summarized in Chapters 2 to 6. The format of this thesis was chosen with the intention that each of these key chapters will be submitted, as is, for publication in the literature. To aid the reader in keeping a sense of continuity with this work, an introductory chapter and a generalized summary have also been added. Chapters 2 and 5 have already been published: the appropriate references to the journals are given at the beginning of each of these chapters. The content of these published chapters has been kept intact, but slight modifications in the text and figures have been made in order to be consistent with the rest of the text.

ACKNOWLEDGMENTS

While writing this thesis, I've come to realize that a Ph.D. is similar to other life experiences, such as having one's wisdom teeth removed or having knee ligament surgery. It's something that one cannot go through alone without having to depend others for help. There are many people who have been a great support to me over the past 4 years who deserve mentioning.

First, and foremost, I would like to thank my parents, John and Mary Ajersch, for making this thesis possible. Without their moral and financial support, I probably would have quit this degree long ago and become a gold miner in the Yukon, or a Level One ski instructor in Kamloops. I am extremely grateful for the money they lent me, which enabled me keep a semblance of my former (pre-student) life. Without their help, I wouldn't have been able to keep my prized vintage Honda Civic on the road for those important trips to Ottawa to get a dose of home cooking and my laundry done. Nor could I have afforded to go on my "male bonding" camping and fishing trips which helped keep my sanity. Those extra treats like ski tickets for Master's races, winter tires, and the odd bit of gas money were really appreciated. In addition to helping me financially, my parents have always been there for me when I needed them, especially during times when my luck ran out. (Like the time I almost totaled my car hitting a deer, or when I needed someone to "babysit" me while recovering from surgery). I must also mention my brother and sister, Peter and Jennifer. We've always kept in touch even though we have

been hundreds, or sometimes thousands of miles away. Now that I'm done, I hope we will spend more time together (Peter, Jennifer PLAY!).

Next, I would like to acknowledge all my friends who have a great help over the past four years. Someone I definitely have to mention is Duane Clifton, for two reasons. First, Duane has been my best friend for 17 years. Also, Duane "suggested" that it would be in my best interests to acknowledge him. (He's bigger than me so I better do what he says). Duane has always been a good listener and phoning him every month has probably saved me thousands of dollars in therapy bills. Part of my reason for those road-trips to Ottawa was to get a "dose of Duane", so we could do something stupid just to amuse ourselves. Like eating Jean-Burgers, doing downhill races down the Crescendo at Mte. Ste. Marie, or finding lost car keys in a school yard at 2 a.m. Our 9-day trip to Banff and back is something I'll never forget, which ended with me being kidnapped on my 30th birthday. Duane is also the best Honda mechanic there is, and he's saved thousands of dollars by doing my car repairs for free. Thanks, Duane. I hope someday I can use my own special skills to return the favor. Just call me if you ever need some estimates of surface tension or an enthalpy balance.

I have had three "homes away from home" while living in Hamilton. One of them has been the Lipper Ferrets' residence, which I visited at least 3-4 times a week. I was always welcome to come over and terrorize Lipper, Cara and Mark. The psycho mountain biking adventures, predator Scrabble, and watching the "Boy's" antics were always fun. I fondly remember the Temagami Canoe Incident, or being left stranded on

the ice in Cootes Paradise. (Thanks to Cara). Lipper's "McBain" knife-throwing exercise was just one example of the countless hours of entertainment I enjoyed while visiting.

The Larue Knobs (Lee, Karen, Kathleen, Stinkin' Lincoln Dog and Scotty, a recent addition) also welcomed me into their home. Especially Kathleen and Lincoln, who constantly shoved each other aside to get closer to "Uncle Mike". This was always good ego-booster: at least two critters in the world thought I was someone terrific. Karen has always on the same wave-length as me (even though I joke about her red hair) and understands where I come from. She has fed me countless home-cooked meals, and has been a great friend. Lee Larue, on the other hand, has "helped" me in other ways. He has always played the devil's advocate with me, ever since high school. Lee has sucessfully inveigled me to take time off and go on countless bush-whacking trips which I had no time to go on, and to buy camping and fishing toys which I could not afford. I hold Lee personally responsible for delaying my defence by at least 6 weeks. However, I'm glad I listened to Lee; those trips were worth it, and he always showed me how to keep things in perspective. If I were to get hit by a truck tomorrow, I would have regretted not taking the time off. There are often occasions when spending time with best friends is more important than studying.

My third "home" has been the residence of Sally and Basil Watson. Sally has taken me under her wing many times when I was having an off-day, and has played Florence Nightingale, bringing me nourishment and medicine whenever I've been too

sick to leave my apartment. She is also one of the most wonderful cooks I know, and I think I owe more than a few nice meals. (Notice that there's a pattern between people I like and people who feed me?). Basil, on the other hand, cannot cook, but he will try to pull a 2-inch log through a picket fence sideways. Basil is an energetically-challenged Labrador Retriever and the most "intelligent" dog I know. I don't know many people who will actually acknowledge dogs in their thesis, but I must honestly say that Basil has contributed significantly towards making my Ph.D. easier. He has been a great stress reliever and a lot of fun. He is a complete, lovable idiot who is one of my best doggie friends (even when eating my shoes or trying to drill his head into my chest, or trying to do "both").

Next, I would like to thank Nancy Price-Munn, another good friend and wonderful listener. Whenever I was in a slump, Nancy would tell me about her own Ph.D. that did not always go perfectly smoothly. At times, I felt she was one of the few people who could relate to me, and I truly respect her opinion. As a veteran of academia, Nancy has given me many suggestions and helpful hints which made this last year go more smoothly.

I would also like to acknowledge the technical staff in our Department. Paul Gatt has done outstanding machine-shop work on some pretty bizarre equipment I've asked him to make over the years. His "Flusha-Matic" attachment to my flotation apparatus changed my outlook on my thesis. Gord Slater did not have to build anything electronic for me this time, but he has saved my skin on several occasions by overhauling my

computer when I've had problems with viruses or (say it ain't so, Mr. Gates!) Windows. Justyna Derkach is the one person at McMaster who has had put up with me the longest (almost a decade). She has always been cheerful and helpful, and has always been willing to lend me equipment for my experiments (which is quite amazing, considering my reputation). I would also like to thank Doug Keller, whose rare skills in communicating with Gilmour Hall have saved me from a lot of red tape. Doug has also shown commendable patience whenever I've dumped incomplete travel expense forms on his desk.

Lastly, I would like to thank my supervisor, Bob Pelton. I don't think any single person will ever influence my professional career like he has. It may sound cliché, but if it weren't for him, I would not be where I am now. As an undergraduate student in 1985, I had a miserable co-op work-term in a festering pulp mill in some remote town in northern New Brunswick. After that wonderful experience, I swore never EVER to work in the pulp and paper industry again. Years later, just as I was finishing off my Master's, Bob offered me a position as a research engineer in his Pulp and Paper Group, which I accepted. This eventually led to my starting this Ph.D. I am greatful for the opportunities Bob has given me to network with industry, to attend conferences, and for the good words he has put in for me whenever a scholarship application of job ad has come up. I believe he has contributed significantly in helping me land my present job.

TABLE OF CONTENTS

TABLE OF CONTENTS (Continued) Page

TABLE OF CONTENTS (Continued) **Page**

LIST OF FIGURES

LIST OF FIGURES (Continued) **Page**

CHAPTER 4

CHAPTER 5

LIST OF FIGURES (Continued) **Page**

CHAPTER 6

APPENDIX B

LIST OF TABLES

LIST OF TABLES (Continued) **Page**

APPENDIX C

CHAPTER 1

INTRODUCTION

Pulp and paper is an important part of the Canadian economy, as it is by far Canada's largest industry and employer. In this day of dwindling forestry resources however, the source of virgin wood pulp is becoming increasingly difficult to obtain and more costly to transport to existing mills for the manufacture of paper products. Moreover, the increased efficiency of the lumber manufacture process has resulted in a reduced quantity of wood remnants and sawdust which have traditionally been a supply of pulp for many paper mills. Given these factors, along with the recent environmental concerns of preserving our forestry resources, there has been an increasing emphasis towards finding alternative sources of pulp for the manufacture of paper. One of the solutions to this problem is to include increased amounts of recycled pulp in paper products. As a result, the recycled paper industry has grown significantly over the past 15 years, and is now an essential part of the pulp and paper industry.

1.1 FUNDAMENTALS OF FLOTATION DEINKING

Recycled paper consists primarily pulp fibres (tracheids), pulp fibre fragments (fines) and various contaminants (ink, filler particles, etc.). One of the key steps in recycling paper is the deinking process. The purpose of a deinking plant is to remove any

undesirable contaminants from the pulp fibres, so that the end product approaches the properties of unprinted pulp (Dorris 1989).

In the deinking plant, the waste paper is sent to the pulper, where it is mechanically dispersed into fibres and contaminant particles. Soaps, surfactants, and dispersants are also added to the pulp to separate and remove the contaminants that adhere to the fibres. After pulping, the slurry is transferred to the screening and cleaning stages, where the larger contaminants from the pulp are removed, namely staples, paper clips, stones, plastics, and dirt particles. The next step is the ink removal stage. This can be achieved by washing or flotation stages (or combinations thereof) where the smaller contaminants (ink and filler particles) are removed. The resulting deinked pulp is then bleached and stored, or transferred to the paper machine.

In most recycled paper mills in North America, deinking is achieved by flotation. The essential steps in deinking that are related to the surface chemistry of the process are summarized by Larsson (1987):

- the removal on the ink from the fibres;
- the dispersion of the ink into small particles;
- preventing these dispersed ink particles from re-depositing on the fibres;
- the separation of the ink particles from the pulp through flotation;
- clarification of the recycled process water;

The simplified diagram of the flotation deinking process is illustrated in Figure 1-1:

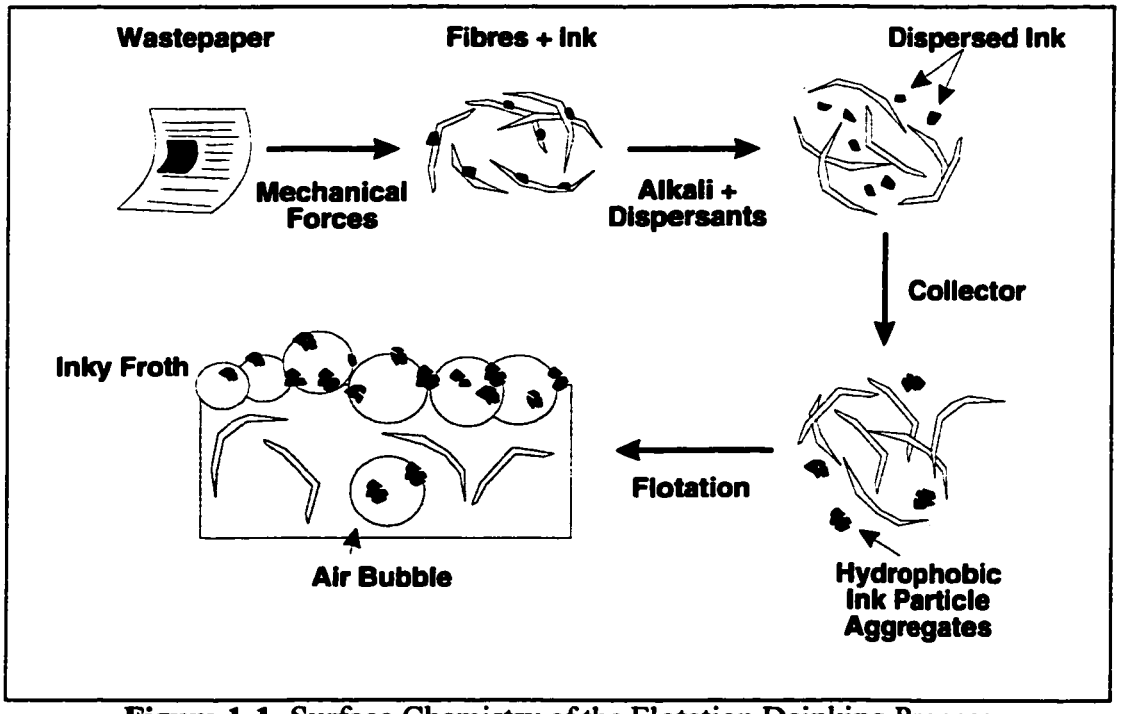

Figure 1-1. Surface Chemistry of the Flotation Deinking Process (after Larsson et al. 1982 and Fergusson 1992)

As shown in Figure 1-1, the alkali and dispersants detach the ink particles from the fibres. Surfactants and dispersants are added to make the contaminant particles more hydrophobic than the fibres. The collectors combine the finely dispersed ink particles into larger aggregates, which increases the probability of collision with the bubbles in the flotation cell. As a result, the contaminant particles aggregates adhere to the air bubbles, which migrate to the surface. The bubbles and contaminants form an inky froth on the surface, which is removed, leaving behind the relatively cleaner pulp fibres.

A simplified version of a flotation cell is shown in Figure 1-2. The three major zones in a flotation cell are described by Zabala and McCool (1988): the aeration zone, the mixing zone and the separation zone. Bubbles are dispersed into the pulp in the

aeration zone. The flotation cell is designed so that the ink-bubble collision frequency is maximized in the mixing zone, which is very turbulent. It is here that the ink particles come into contact with the bubbles and adhere. In the more quiescent separation zone, the ink-bubble complex rises to the surface and the inky froth is removed.

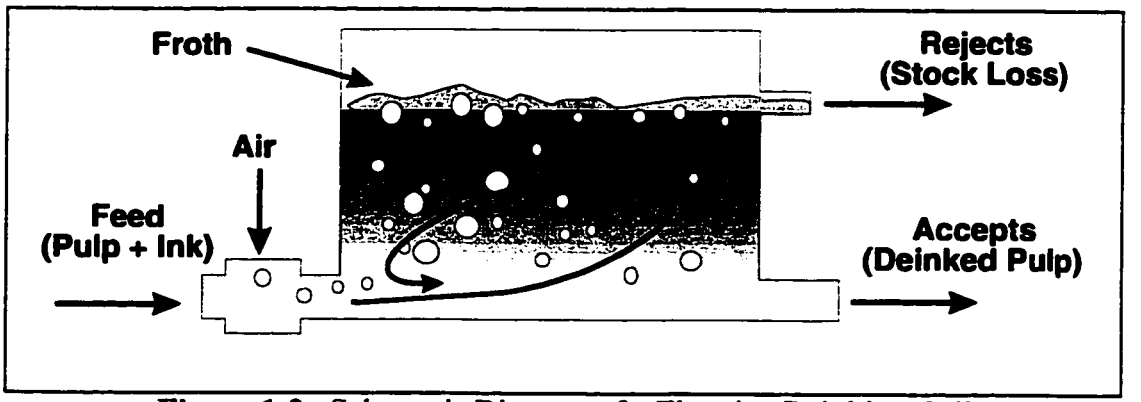

Figure 1-2. Schematic Diagram of a Flotation Deinking Cell

1.2 FLOTATION DEINKING AND PULP LOSS

In a perfect flotation system, the accepts stream shown in Figure 1-2 should consist of only pulp fibres and water and the rejects stream (froth) should consist of ink, water and the other contaminants. In practice, perfect efficiency is not feasible, since the deinked pulp will always contain some residual ink particles, and some pulp fibre always ends up in the froth.

The solid material in the froth that is removed in the rejects stream is commonly referred to as "*stock loss*". Stock losses consist of ink, fillers, fibres and fines (Turvey 1993). In paper mills, the reported amounts of pulp loss varies. For example, Zabala and McCool (1988) reported stock losses of 8% on a full-scale deinking system, of which 3%

was fibre. Linck et al.(1987) reported the total losses in two deinking plants to be 9.7 and 4.8%, with the pulp losses (fibres and fines) being between ≈1.5% and ≈0.25%, respectively. In various laboratory studies, fibre losses of 2 to 65% have been reported (Galland et al. 1977; Petri 1994; Schwinger and Dobias 1991; Liphard et al. 1993). The results are arbitrary, since they depend on experimental conditions.

In industry, it is desirable to minimize stock losses. This reduces the amount of rejects to be disposed of by landfill or incineration (Turvey 1987). More importantly, the fibre fraction of stock losses are a loss of raw material and reduce the efficiency of the recycling process (Schwinger, Dobias 1991). Preventing excessive *fibre losses* (or *pulp losses*) will reduce the required amount of feed stock for recycled paper mills.

1.3 MECHANISMS OF PULP LOSS

Previous research has shown that pulp losses are influenced by many parameters, including surfactant type, pulp furnish, consistency, paper age and the presence of calcium ions. Most of the results in the literature have been summarized by Turvey (1993) and Ajersch and Pelton (1996).

Most of the discussions in the literature on pulp loss mechanisms are based on the assumption that pulp fibres and pulp fines adhere to the air bubbles and are carried into the froth. Many authors have claimed that fibres will adhere to dispersed air bubbles (Gavelin 1954; Boadway 1956; Sedivy 1969; Isler, Widmer 1978; Larrson et al.1982; Schwinger and Dobias 1991; Schulz and Scott 1993; Turvey 1993). Despite these claims,

the theories on bubble-fibre adhesion remain speculative, as no conclusive photographic evidence of bubbles adhering to fibres has yet been published.

Besides bubbles-fibre adhesion, which is related to the surface chemistry of the air-water-fibre interface, other physically-related pulp loss mechanisms are possible. In bubble-holdup experiments, Pelton and Piette (1992) concluded that bubbles can be retained in pulp suspensions by mechanical entrapment in the fibre networks. Examination of aerated pulp suspensions in flow visualization studies led Ajersch and Pelton (1994) to propose that mechanically-trapped bubbles can levitate pulp flocs to the surface.

Another mechanism by which pulp may enter the froth is by entrainment. In this mechanism, the pulp fibres and pulp fines are hydraulically transported into the froth along with the floated water. The phenomenon of entrainment is well-documented in the literature on mineral flotation, as it explains the unwanted recovery of hydrophilic gangue in flotation cells. In deinking systems, however, the effects of entrainment on pulp loss have not been considered until relatively recently. Entrainment was briefly discussed by Schwinger and Dobias (1991) and Petri (1994). Among the first to present conclusive experimental evidence linking pulp loss to entrainment were Dorris and Pagé (1995). In laboratory-scale flotation experiments, the recovery of hydrophilic particles (fibre and fillers) was found to be correlated to the recovery of water in the flotation froth. Dorris and Pagé (1995) concluded that the fibre and filler losses were caused solely by entrainment, and not by bubble-particle adhesion.

1.4 THE SCOPE OF THIS THESIS

The three possible mechanisms by which pulp fibres and fines can be transported into the froth are bubble-fibre adhesion, mechanical entrapment and entrainment. The existing literature has identified the many parameters which affect pulp loss, but the extent to which these three pulp loss mechanisms contribute to the flotation of pulp fibres and fines remains to be quantified. The aim of this thesis is to gain a better understanding of the causes of pulp loss in flotation deinking systems, and to attempt to quantify these pulp loss mechanisms. This is achieved through a series of experiments which examine various fundamental aspects of bubble-fibre interactions in aerated pulp suspensions.

Chapter 2 addresses the theory of bubble-fibre adhesion. This chapter summarizes the results of the "bubble generation test" (BGT), in which pulp fibres and carbon black particles were placed in supersaturated solutions of carbon dioxide. The objective of this work was to determine the conditions under which new bubbles can be grown on the surface of pulp fibres and carbon black particles. These experiments provided some new insight on the mechanisms of new bubble formation in dissolved air flotation and pressurized deinking systems. A discussion is also provided on the likelihood of bubble-fibre adhesion occurring on wetted pulp fibres.

The effects of mechanical entrapment are investigated in Chapter 3, which is essentially a continuation of the bubble-holdup experiments first initiated by Pelton and Piette (1992). The objective of the present study was to determine how far spherical particles (such as bubbles) can travel through pulp suspensions before becoming

mechanically trapped. In order to make detection of the particles easier and to eliminate the possibility of bubble-fibre adhesion, the experiments were conducted using a model system. Instead of using bubbles, spherical ball-bearings were dropped into quiescent beds of settled pulp fibres. These fundamental experiments showed a link between mechanical entrapment and fibre network strength. The results have led to the conclusion that actual air bubbles escape through pulp suspensions by migrating between pulp flocs.

In Chapter 4, the entrapment and release of air bubbles is examined at a more fundamental level. This chapter summarizes a series of flow-visualization studies of bubble migration through quiescent and flowing pulp suspensions. The qualitative observations made in this work proved extremely valuable in understanding the fundamentals of three-phase flow in fibre suspensions. The results have led to the identification of several mechanisms of bubble entrapment and bubble release from pulp suspension. In addition, the observations have proven that flocculation is a key factor affecting bubble migration, which have led to important conclusions regarding the significance of mechanical entrapment as a pulp loss mechanism.

In Chapter 5, batch flotation experiments were conducted to test the hypothesis that entrainment is a dominant pulp loss mechanism. The parameters that were varied included pulp consistency, pulp type, gas flow rate and bubble size. The results gained from these flotation experiments have led to the discovery of two entrainment regimes, which are dependent on the state of flocculation of the pulp suspension.

Chapter 6 presents a mechanistic model which helps quantify the experimental pulp loss data obtained in Chapter 5. In a novel approach, the three-parameter model links the fibre content of the froth to both the extent of flocculation and independent measurements of pulp sedimentation data. Finally, a brief summary is provided in Chapter 7 which emphasize the main conclusions obtained from this work.

REFERENCES

AJERSCH, M. and PELTON, R.H. "Mechanisms of Pulp Loss in Flotation Deinking", *J. Pulp Paper Sci.* 22(9):J338-J345 (1996).

AJERSCH, M. and PELTON, R.H. "The Study of Fibre Losses in Flotation Deinking Through the Characterization of Bubble Entrapment in Flowing Pulp Suspensions", 44th Can. Chem. Eng. Conf. (List of Abstracts)., 383-384 (1994).

BOADWAY, J.D. "Gas in Papermaking Stock", *Pulp Paper Mag. Can.* 57(3):185-194 (1956).

DORRIS, G.M. "Deinking Wet End Chemistry", Recycling and the Canadian Pulp and Paper Industry: A Report to the Research Program Committee of Paprican. Sept. 5, (1989).

DORRIS, G.M. and PAGÉ, M. "Deinking of Toner-Printed Papers. Part I: Flotation Kinetics, Froth Stability and Fibre Entrainment. 3rd Research Forum on Recycling, Tech. Sect. CPPA. 215-225 (1995).

FERGUSSON, L.D. "Deinking Chemistry, Part 2", *Tappi J.* 75(8):49-57 (1992).

GALLAND, G., BERNARD, E., and SAURET, G., "Aspect physico-chimiques du desencrage", *Revue A.T.I.P.* 31(6):364-378 (1977).

GAVELIN, G. "Some Effects of Gases on Properties of Fibre Suspensions", Can. Pulp Paper Assoc. Tech. Sect. Proc. 1954:240-248 (1954).

ISLER, W. and WIDMER, F. "Creation of and Removal of Air Bubbles from Technical Paper Stock Suspensions", *Papier* 32(11):473-477 (1978).

LARRSON, A., STENIUS, P. and STROM, G. "Surface Chemistry of the Deinking Process", *Wochbl. Papierfabr.* 14:502-506 (1982)

LARSSON, A., "Surface Chemistry in Flotation Deinking", *PTI*, 388 (February, 1987).

LINCK, E., MAYR, H, MILLER, G, and SIEWERT, W. "Operating Experience with the Bird Escher Wyss Compact Flotation Deinking Plant", TAPPI Pulping Conf., 151-156 (1987).

LIPHARD, M., SCHRECK, B., and HORNFECK, K., "Surface-Chemical Aspects of Filler Flotation in Waste Paper Recycling", *Pulp Paper Can.* 94(8):T218-T222 (1993).

PELTON, R.H. and PIETTE, R., "Air Bubble-Holdup in Wood Pulp Suspension", *Can. J. Chem. Eng.* 70:660-663 (1992).

PETRI, B.M., "Deinking Newspaper in an Opened and Packed Flotation Column", M.A.Sc. Thesis, Univ. Toronto, (1994).

SCHWINGER, K. and DOBIAS, B., "The Influence of Calcium Ions on the Loss of Fibre in the Flotation Deinking Process", 1st. Res. Forum on Recycling, Tech. Sect., CPPA. 1-11 (1991).

SCHULZ, E.R. and SCOTT, W.E. "Analysis of Air Entrainment by Secondary Fibers", *Tappi J.* 76(2):147-155 (1993).

SEDIVY, O. "Air, an Important Factor in Paper Manufacture", *Zellstoff und Papier* 18:112-118 (1969).

TURVEY, R.W. "Stock Loss as a Function of Water Hardness in Deinking", *PTI* 366-368 (February, 1987).

TURVEY, R.W., "Why do Fibres Float?", *J. Pulp Paper Sci.* 19(2):J52-J57 (1993).

ZABALA, J.M. and McCOOL, M.A. "Deinking at Papelera Peninsular and the Philosophy of Deinking System Design", *Tappi J.* 71(8):62-68 (1988).

CHAPTER 2

THE GROWTH OF BUBBLES ON PULP FIBRES AND ON CARBON BLACK DISPERSED IN SUPERSATURATED CARBON DIOXIDE SOLUTION

Michael Ajersch and Robert Pelton

Published in the Nordic Pulp and Paper Research Journal 2(9):129-135 (1994).

SUMMARY

The objectives of this work were to determine the conditions under which new bubbles can be grown on the surface of wood fibers and carbon black particles dispersed in supersaturated carbon dioxide solutions. It was concluded that new bubbles cannot be grown on fully wetted fibers and carbon black surfaces under conditions likely to arise in pulp and paper mills. On the other hand, re-pulped paper can have trapped pockets of air which are active sites for bubble growth from supersaturated solutions.

The conclusions were based upon a bubble generation test in which pulps and carbon black dispersions were exposed to supersaturated carbon dioxide solutions to determine whether bubble growth (effervescence) occurred. Theoretical models and discussions in the literature were used to support our conclusions.

The significance of this work is that it is unlikely that new bubbles can be nucleated and grown on the surface of ink particles or fiber surfaces during pressurized or dissolved air flotation. Also, since no adhesion of air bubbles to fibers was observed for

the ten headbox pulps studied, bubble fiber adhesion may not be an important mechanism for fiber loss in flotation deinking.

2.1 INTRODUCTION

Many processes in the manufacture of pulp and paper involve three phase flow in which gas bubbles are dispersed in an aqueous fiber suspension. In some cases, such as in flotation deinking or gas bleaching, the gas bubbles are a key part of the process. On the other hand, the presence of air bubbles in a papermachine headbox pulp is known to be harmful (Ajersch et al. 1992a).

Usually, air is entrained in pulp suspensions by leaky pumps and valves, open channels, weirs, discharge pipes which are not submerged, etc. However, another source of entrained air is the nucleation and growth of air bubbles when a pulp is depressurized. The solubility of air in water is roughly proportional to the pressure. Thus, when a pulp is depressurized, the dissolved gases can become supersaturated. Pressurized flotation cells, dissolved air flotation, and the outflows from pressurized headboxes are locations where air bubbles possibly can be released from supersaturated solutions.

Described in this paper are the results of experiments designed to determine if new gas bubbles will grow on the surface of pulp fibers and carbon black particles (i.e. model inks) from supersaturated solutions. For example, in pressurized flotation deinking, it would be desirable to grow bubbles on the surface of hydrophobic ink particles . The results in this paper show that this is unlikely to occur.

2.2 EXPERIMENTAL

A procedure herein called the Bubble Generation Test (BGT) was developed to determine if bubbles can grow on fibers or carbon black from supersaturated solutions. The BGT consisted of mixing approximately 5 mL of pulp suspension and 30 mL of a carbonated water in a Petri dish. For most of the experiments, the carbonated water being used was bottled Perrier© water. The ability of the pulp fibers or carbon black to generate gas bubbles was determined by microscopic observation with a Wild-Leitz M420 Zoom Macroscope, using magnifications ranging from 8X to 80X. Macroscope images were videotaped and single frames were captured and digitized with an image analyzer.

The BGT was repeated at least three times for each sample. Usually the test was unequivocal; either no new bubbles formed, or the suspension boiled with new bubble generation.

The headbox pulps (samples 1 through 8, Table 2.1) were taken from four paper mills located in Quebec and Ontario, and were tested for bubble generation in the laboratory 2-3 days later. The recycled newsprint samples 10 and 11 were tested in a newsprint mill on-site.

Paper corresponding to each headbox pulp was also collected. The paper was re-pulped by tearing 2.5 g of dry paper into small pieces, adding 500 mL of distilled water and mixing at the lowest speed in an Osterizer© # 10 blender for 2 minutes to give a consistency of 0.5%.

TABLE 2.1. Bubble generation test results for headbox pulps and re-pulped paper. "Yes" and "No" denote the presence and absence of bubble generation, respectively.

Sample	Paper Grade	pH	Headbox Pulps	Re-pulped Paper
1	Pink sugar pouch	4.2	No	Yes
2	Century ledger	8.0	No	Yes
3	Registart offset 45	7.7	No	Yes
4	Oxford opaque	4.4	No	Yes
5	Coated wallstrip	4.5	No	Yes
6	Recycled newsprint	5	No	Yes
7	Recycled newsprint	5	No	Yes
8	Ream wrap	3.9	No	Yes
9[a]	Recycled newsprint (Flotation deinking feed)		No	Yes
10[a]	Recycled newsprint (Deculator feed)		No	
11[a]	Recycled newsprint (Deculator accepts.)		No	
12	Monofilament fishing line		Yes	
13	Polypropylene carpet fiber		Yes	
14	Clay-coated magazine (Pages)			Yes
15	Clay-coated magazine (Cover)			Yes
16	Filter paper			Yes
17	Wax-coated weighing paper			Yes
18	Newsprint (Hamilton Spectator)			Yes
19	Blotter paper (Control sample)			Yes
20	Blotter paper (Hydrophobized with stearyl chloride)			Yes

[a] Samples examined were tested at mill immediately upon collection.

Carbon black dispersions were tested for bubble generation (Table 2.3). The carbon black used for samples *A*, *B*, and *C* was REGAL 99I from Cabot Corporation (Waitham, Mass.). Sample *A* was dispersed in distilled, deionized water using a Branson

450 Sonifier. Sample *B* was prepared as follows: 400 mL of dilute NaOH (pH ≈ 9.5) was mixed with 0.02 g with of the carbon black, 2.0 mL of 0.01 M sodium laureate, 125 mL of 0.4 M NaCl, and dispersed with the Branson 450 Sonifier for 5 minutes. Distilled water was then added to make a total volume of 500 mL. Sample *C* was prepared by taking 250 mL of sample *B* and adding 10.0 mL of 0.1M $CaCl_2$. The flotation deinking rejects (sample *D*) were tested on-site at a newsprint paper mill.

TABLE 2.2. The influence of soaking time on the bubble generation in re-pulped papers.

Sample	Paper grade	Soaking time	Bubble generation
16	Filter paper	0	Yes
16	Filter paper	48 h	Almost No
15	Clay coated magazine cover	0	Yes
15	Clay coated magazine cover	48 h	Yes
15	Clay coated magazine cover	8 months	Yes
15	Clay coated magazine cover	8 months (plus sonification)	No

TABLE 2.3. Bubble generation test results for carbon black dispersions.

Sample	Composition	Bubble generation
A	Carbon black and distilled, de ionized water	No
B	Carbon black, sodium laureate, NaCl	No
C	Carbon black, sodium laureate, NaCl, $CaCl_2$	No
D[a]	Flotation deinking rejects	No

[a] Samples tested were tested at mill immediately upon collection.

2.3 RESULTS

The BGT experiments consisted of mixing aqueous pulp suspensions with solutions supersaturated with carbon dioxide (Perrier© water) and determining whether or not new bubble formation (effervescence) occurred. Results with various types of pulp fibers and carbon black suspensions are summarized in Tables 2.1 to 2.3. No bubble growth was seen in any of the headbox pulps. For example, Figure 2-1 shows a digitized frame of a videotaped image of a monofilament fishing line immersed in a never-dried headbox pulp. Carbon dioxide bubbles readily formed on the plastic fiber whereas no bubbles formed on the wood fibers.

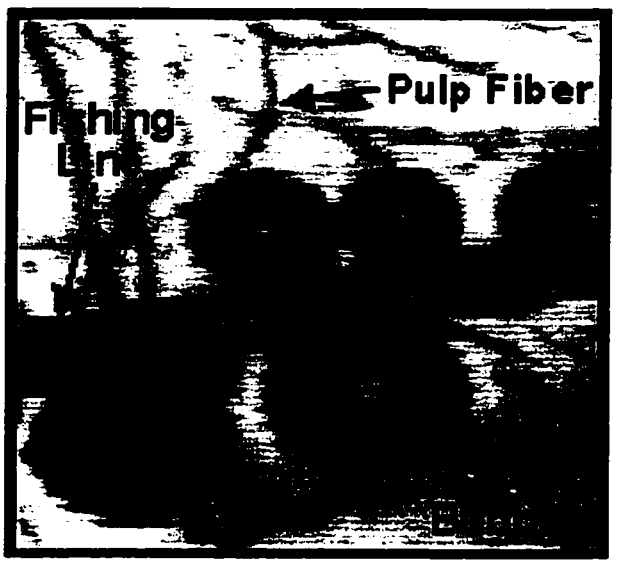

Figure 2-1. Newsprint pulp fibers and a monofilament fishing line in a supersaturated carbon dioxide solution. Bubbles grew on the fishing line and not on the pulp fibers.

The behavior of fiber suspensions from freshly re-pulped paper was different from that of never-dried headbox pulps. Bubbles continuously formed, grew and detached from the fibers for every paper tested (see Table 2.1). Figure 2-2 shows bubble formation from re-pulped paper. The arrow in frame 1 points to a small bubble originating from a fiber; the bubble diameter increased in subsequent frames. The resolution of the images directly viewed in the macroscope was much higher than those in Figure 2-2 because of limitations of videotape and image analysis. In some cases bubbles were observed to grow from the ends of fibers with gas-filled lumens. The field of view in Figure 2-2 had about 10 bubble growth sites and hundreds of fibers so only a few bubble growth sites were responsible for effervescence in supersaturated carbon dioxide.

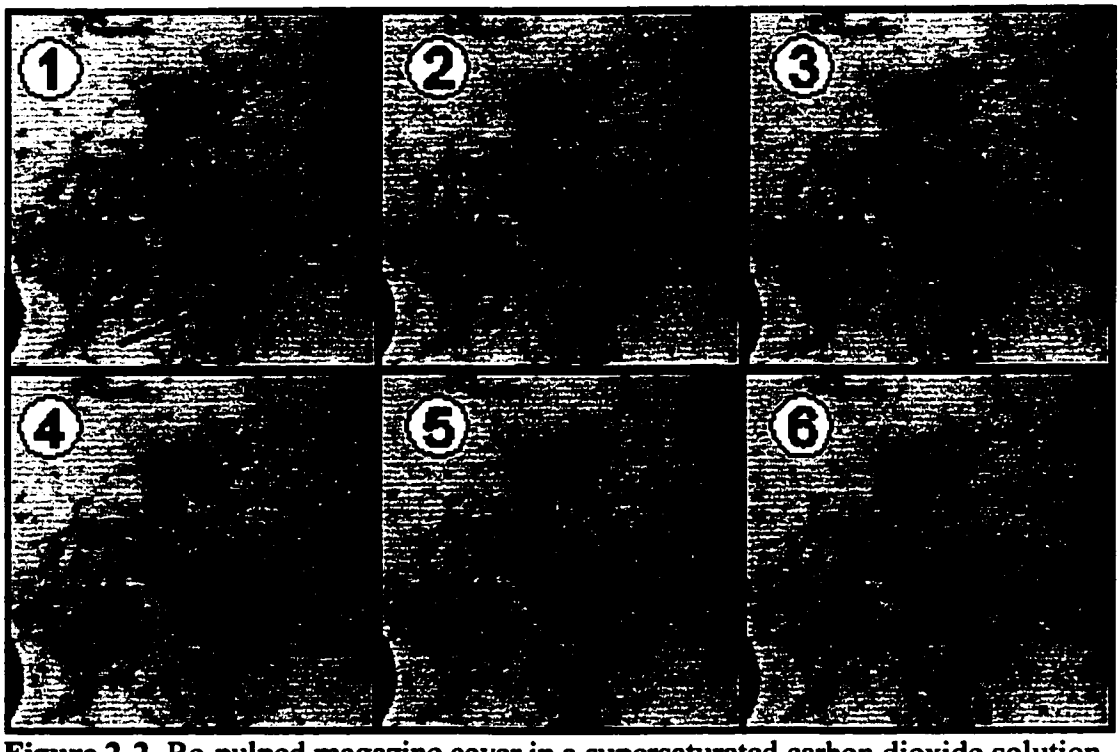

Figure 2-2. Re-pulped magazine cover in a supersaturated carbon dioxide solution. The digitized video frames are shown at 80 millisecond intervals. The arrow in frame 1 indicates a bubble growing from a site on a fiber.

The ability of re-pulped paper to effervesce in Perrier water (a positive BGT) usually decayed with soaking time. For example, the filter paper fibers (sample 16) initially tested positively, but almost no bubbles were seen to generate 48 hours after re-pulping (see Table 2.2). One exception was the clay-coated magazine cover (sample 15) which generated bubbles after eight months of soaking. On the other hand, the bubble generation sites on the re-pulped magazine cover were destroyed by exposure to ultrasonic radiation for several minutes.

No bubble growth was seen in either the carbon black dispersions or the flotation deinking rejects (Table 2.3). Figure 2-3 shows a dispersion of carbon black (sample *A*) with a hydrophobic (greasy) syringe needle in a supersaturated CO_2 solution. Bubbles vigorously formed on the needle, but no bubble generation was seen on any of the carbon particles. The carbon black particles did adhere to the fibers and existing CO_2 bubbles. Figure 2-4 shows carbon black particles adhering to a bubble stuck to the bottom of the Petri dish. Thus water had a finite receding contact angle on the carbon black particles.

Figure 2-3. Carbon black dispersed in distilled water super-saturated with carbon dioxide. Bubbles grew from the tip of a stainless steel syringe needle but not from the carbon black particles.

Figure 2-4. Carbon black particles adhering to the surface of a carbon dioxide bubble.

2.4 DISCUSSION

The key observation in this work is that new gas bubbles did not grow from wetted pulp fibers or carbon black particles. On the other hand, dried pulp, blotted pulp and plastic surfaces caused the supersaturated carbon dioxide solutions to effervesce. In the following section, these observations will be explained in terms of the many scientific studies on bubble nucleation. Finally, the significance of these observations in selected pulp and paper applications will be discussed.

The nucleation of vapor bubbles can occur through either superheating the liquid phase (ebullition), by pressure reduction (cavitation), or, as in the present case, by dissolved gas coming out of solution (effervescence) . According to theory, a newly

formed bubble nucleus will either spontaneously grow or dissolve back into the liquid, depending on whether the radius of curvature of the liquid-gas interface is greater or less than the "critical radius". The critical radius is defined as the radius of a spherical bubble which would exist in equilibrium with the surrounding liquid (Ward 1970). Bubbles larger than the critical radius spontaneously grow in supersaturated solution whereas smaller bubbles are unstable and will dissolve. The critical radius is calculated from a mechanical equilibrium balance based on the Laplace-Kelvin equation:

$$P - P_L = \frac{2\sigma}{r_c} \qquad [2.1]$$

where P is the pressure inside the bubble, P_L is the external pressure in the liquid, σ is the surface tension, and r_c is the critical bubble radius. Assuming ideal gas behavior, P is equal to the sum of the partial pressures of the solvent and solute molecules. Ward et al. (1970) have derived expressions for the critical radius in these systems.

Gas bubbles can be produced by either homogeneous or heterogeneous nucleation. In homogenous nucleation, the bubbles form within the bulk of the liquid phase, while in heterogeneous nucleation, the bubbles form at a solid-liquid interface. Homo-geneous nucleation only occurs under conditions of very large superheats or very high supersaturation levels (Harvey et al. 1944; Cole 1974; Blander, Katz 1975). Such extreme conditions were not present in our experiments. Therefore, we conclude that any bubble generation observed in the BGT was not due to homogeneous nucleation.

Heterogeneous nucleation preferentially occurs on hydrophobic surfaces because it is easier to separate liquid from a non-wetting surface than a wetting one. However, a

considerable driving force is required for heterogeneous nucleation. For a plane surface and a contact angle of 90°, the superheat required for heterogeneous nucleation is only 30% lower than the superheat required for homogeneous nucleation (Cole 1974). For milder conditions corresponding to the current work, it has been shown that heterogeneous nucleation is very unlikely to occur except in acutely angled hydrophobic cavities (Bankoff 1957; Cole 1974). For example, Wilt (1986) and Ciholas and Wilt (1988) derived expressions predicting the nucleation rates in a supersaturated water/carbon dioxide solution. The authors concluded that, homogeneous nucleation, and heterogeneous nucleation on flat surfaces, conical projections, or spherical projections, would not occur. However, heterogeneous nucleation could theoretically occur in conical pits of various shapes for contact angles ranging from 94 -135°. Only a few extremely hydrophobic substances meet this criterion. For example, the contact angle between water and paraffin is 95°.

High contact angles are not characteristic of most pulp fibers. Advancing contact angles ranging from 0° to 73° have been measured, depending on the fiber type and fiber coating (Young 1976; Klungness 1981; Hodgson, Berg 1985; Jacob, Berg 1993). Once wetted, however, pulp fibers have been shown to have receding contact angles of zero. Although it may be possible for contact angles greater than 90° to exist locally in micro-cavities on the fiber wall that would be too small to be detected by the Wilhelmy technique. We conclude that it is impossible to form new bubbles on completely wetted pulp fibers or ink particles.

The most probable explanation for effervescence in some BGT experiments was put forward by Harvey et al.(1944), who postulated that bubbles grow from pre-existing gas pockets trapped in surface cavities. In this case, the pressure in the air pocket is the sum of the partial pressures of the solvent and solute vapor, plus the partial pressure of the pre-existing gas. Thus, when a solid surface retaining an air pocket is exposed to a supersaturated solution, the dissolved gas diffuses into the air pocket, causing it to grow. A new bubble breaks off when the buoyancy forces of the growing gas pocket are greater than the surface forces holding the bubble to the solid. The work in forming a macroscopic bubble is greatly reduced when a gas pocket is already present because there is no need to overcome the surface tension forces that tend to dissolve a small nucleus. Therefore, we conclude that a positive BGT is indicative of the presence of air pockets trapped in the pulp fibers. It is of interest to consider the types of possible trapped air pockets.

Air pockets in fibers can be thermodynamically or kinetically stable. Untreated pulp fibers are completely wetted by water (i.e. receding contact angle of zero) and thus will support only kinetically stable air pockets. For example, freshly wetted fibers often have air-filled lumens. With stirring or time the lumens fill with water. Similarly, one can envisage ink-bottle-shaped pores in the fiber wall which may be slow to wet.

By contrast air pockets on hydrophobic surfaces can be thermodynamically stable. Air pockets will remain in the cavities of submerged solids if the contact angle of the liquid (θ) is greater than ($90\,^{\circ} + a$) (see Figure 2-5). Under these conditions, the liquid-

gas interface is concave on the liquid side and there is a tendency for gas to diffuse into rather than out of the air pocket. If left undisturbed, such air pockets can remain in solution indefinitely.

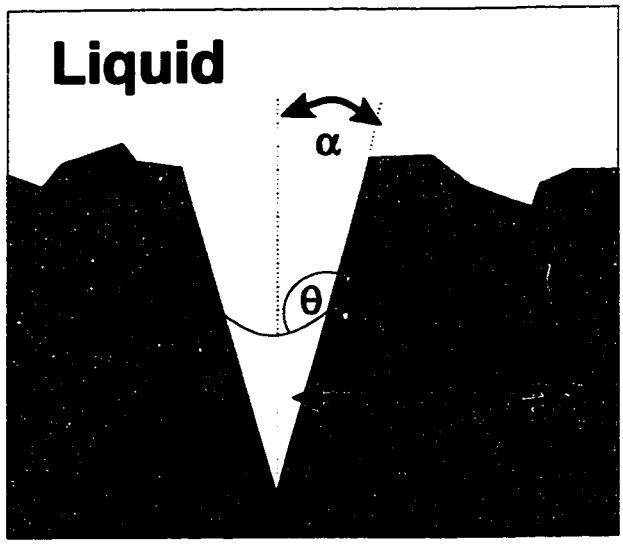

Figure 2-5. Gas pocket in a conical pit in a hydrophobic surface. The gas pocket is thermodynamically stable if the contact angle θ, is greater than 90 ° + α (Harvey et al. 1944).

Theory can be used to determine the conditions under which air pockets can be detected with the BGT. In order for the gas pocket to generate bubbles, two conditions specified by Bankoff (1957) must be met. First, the opening between the gas pocket and the bulk solution (herein called the pocket "mouth") must permit the gas water interface to have a radius of curvature equal to or greater than the critical radius. Second, the radius of curvature of the liquid-gas interface must always be greater than the critical radius as the gas pocket grows. Wilt (1986) calculated that for a supersaturation ratio of

5 (typical of an opened carbonated beverage), the critical radius is about 0.4 μm. Therefore air pockets are expected to grow spontaneously in the supersaturated carbon dioxide solutions to produce bubbles in our experiments, provided the minimum mouth radius of the air pockets is larger than 0.4 μm.

These concepts are illustrated in Figure 2-6. The hydrophobic site is a conical pit with a radius greater than r_c. An air pocket formed in this pit can be thermodynamically stable and bubble growth will occur when exposed to supersaturated carbon dioxide solution. The hydrophilic bubble growth sites consist of kinetically stable air pockets with mouths of a size large enough such that the air water interface never has a radius of curvature less than the critical radius. By contrast the kinetically stable air pocket with $r < r_c$ will not grow in supersaturated solution; such pockets are not detected in the BGT.

Our results showed that for wetted fibers, no bubble generation was observed. Two conclusions can be drawn from these observations. First, there were no acutely angled hydrophobic cavities larger than the 1 μm critical diameter, otherwise heterogeneous nucleation would have been observed. Second, no air pockets with mouth diameters larger than about 1 μm were present in the fibers at the time the pulp samples were tested.

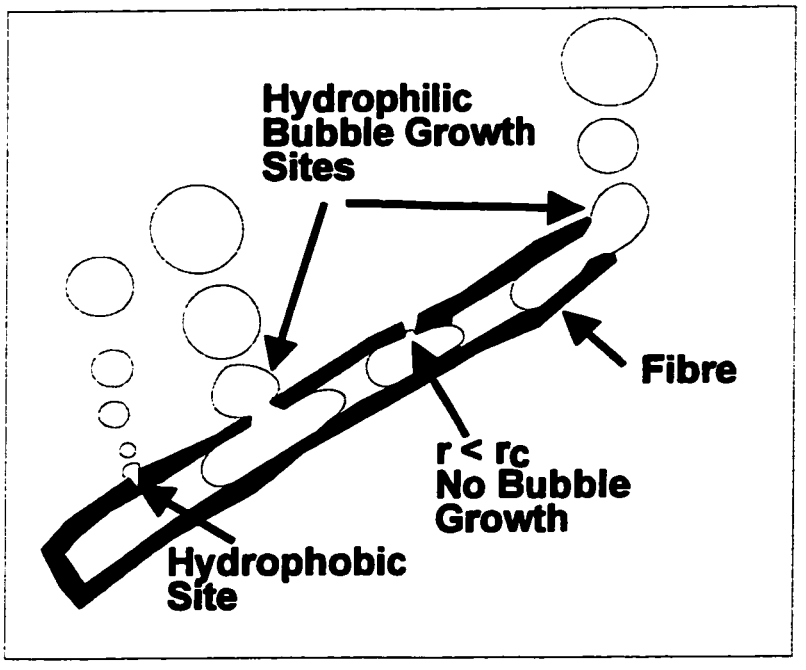

Figure 2-6. Illustration of bubble formation from different types of air pockets in a wood pulp fibre exposed to supersaturated carbon dioxide solution.

Some authors have postulated that air bubbles routinely adhere to fibers: Gavelin (1954), Sedivy (1969), Karras et al. (1988) and Turvey (1993). Adhering bubbles could cause fiber flocculation (Kerekes 1985) and fiber loss in flotation deinking (Turvey 1993). The presence of bubbles adhering to the fibers should give effervescence when mixed with supersaturated carbon dioxide solution. Pulp samples (1-8) were tested in the laboratory several days after being collected from the paper machines. Had any adhering air bubbles been present, they may have escaped or dissolved into solution.

In an attempt to observe adhering air bubbles, pulp sample 10 was examined immediately after withdrawal from the Deculator feed of a newsprint papermachine. This pulp was originally at a line pressure of 4 atm. The dispersed air content was measured at

0.5 volume percent at a pressure of 1.2 atm, as determined by density measurements (see Ajersch et al., 1992b). No adhering air bubbles were seen by visual inspection of the pulp at 1 atm under the macroscope. This conclusion was confirmed by the negative BGT.

Bubble nucleation sites (i.e. air pockets) are deactivated as a dried fiber is wetted. Conversely, when water is removed from fibers to regenerate nucleation sites, bubble generation should resume. This was demonstrated in one test, where we observed that bubble generation sites can be reactivated by blotting wetted fibers. When pulp fibers that tested negatively were placed against dry filter paper, the water was removed from the fibers by the capillary action of the dry paper. When re-immersed in the supersaturated solution, the blotted fibers generated bubbles. It is emphasized that fibers did not have to be oven-dried to produce bubble growth sites.

An indication of the stability of trapped air pockets in fibers was indicated by soaking time in water required to switch from a positive to a negative BGT. For example, filter paper 16 (Table 2.2) showed essentially no bubble generation after 48 hours whereas the magazine cover had trapped air pockets after eight months soaking in water. There are several possible explanations which could account for the long lifetime of air pockets in re-pulped magazine covers. Harvey et al. (1944) proposed that stable gas bubbles can exist in extremely hydrophobic conical cavities provided the contact angle is sufficiently large. Presumably, the latex coating on the magazine cover fibers could be sufficiently hydrophobic for this to occur. More recently, Ward and Levart

(1984) demonstrated that air pockets trapped in conical pits can remain thermodynamically stable in a closed volume of liquid, provided these nuclei are present in a sufficient number. Another possible explanation is the "organic skin" theory proposed by Fox and Herzfeld (1954). The authors hypothesized that very small bubbles are stabilized by a rigid organic skin, which mechanically prevents loss of gas by diffusion. The presence of clay, sizing and ink particles in the magazine fibers may have contributed to this effect.

Carbon dioxide bubbles no longer formed from the clay-coated magazine cover fibers (sample no. 15) once the pulp suspension had been vigorously dispersed for several minutes with the ultrasonic probe. The mechanical vibrations of the probe apparently dislodged the bubble nuclei from the fibers, thus de-activating all the nucleation sites. This perhaps demonstrates that even these air pockets exhibited kinetic stability instead of true thermodynamic stability. From a more practical perspective, these results show that significant mechanical energy is required to fully wet some types of magazine covers. This is important in laboratory flotation studies because incomplete removal of air pockets could result in an artificially high fiber loss.

The recycled newsprint contained about 50% re-pulped paper. The observation that no bubble generation occurred in the on-site mill tests indicates that during re-pulping, cleaning and deinking, air pockets were wetted.

The positive BGT results for the fishing line fibers and carpet fibers were probably due to air pockets trapped in rough areas on the plastic surface. Evidence of this

was seen in several scanning electron microscope photographs of a sample of the fishing line. Many scratches and crevices of the order of 5 to 20 μm in width were seen, which could have acted as bubble generation sites.

The carbon black dispersions were prepared in three batches: carbon black, carbon black with soap (sodium laureate) , and carbon black with soap and calcium chloride. These model inks represented various stages of the treatment of ink particles in a typical flotation deinking process. Although the carbon black particles were sufficiently hydrophobic to adhere to bubbles (Figure 2-4) and fibers, new bubbles did not grow in the presence of Perrier© water. Therefore, the suspended ink particles in these samples were not sufficiently hydrophobic or porous enough to promote heterogeneous nucleation or to support air pockets.

Dissolved air flotation is sometimes used to clarify ink-contaminated reject streams coming from flotation deinking cells. The principle is to dissolve air in water by pressurization and then release the pressure back to the atmosphere, generating small bubbles. Our experimental results and existing theory imply that new bubbles cannot nucleate on ink particles or fibers. Therefore bubble generation in dissolved air flotation is likely to originate from the growth of existing small bubbles.

Contact angle studies in the literature show that pulp fibers have a receding contact angle of zero. Thus air bubbles should not adhere to fibers immersed in water. The BGT results for never-dried pulps confirmed that there was no bubble fiber adhesion. We believe that this conclusion is general. It is generally accepted that fiber loss in

deinking results from the adhesion of bubbles to fibers causing them to float (Turvey 1993). This may not be true in many cases. Clearly, more work is required to determine the conditions under which air bubbles adhere to pulp fibers.

2.5 CONCLUSIONS

The following conclusions arise from our analysis of the bubble generation test results:

- The "BGT" detects air pockets trapped in fibers or air bubbles adhering to the external fiber surface. Theory suggests that the minimum detectable pocket mouth diameter or adhering bubble diameter in this test is approximately 1 μm.

- Experimental observations show that new bubbles cannot be grown on wetted pulp fibers and carbon black. This observation was in agreement with existing nucleation theory.

- Re-pulped paper contained air pockets which were detected by the BGT. However, the air pockets were removed by simple mixing for most pulps.

- There was no direct or BGT evidence of bubble adhesion to fibers in a commercial newsprint furnish partially based on deinked pulp. We believe that air bubble-pulp fiber adhesion rarely occurs.

Acknowledgments

This work was supported by the Mechanical and Chemimechanical Wood-pulps Network of the Canadian Network of Centers of Excellence program. The authors thank Dr. Martin Hubbe, from International Paper, for supplying the hydrophobized blotter paper.

REFERENCES

AJERSCH, M., PELTON, R.H., LOEWEN, S. and CHAN, A. "Measuring Dispersed Air in Newsprint Pulp Suspensions", *Tappi J.* 75(2):125-129 (1992a).

AJERSCH, M., PELTON, R., TOWERS, M. and LOEWEN, S. "The Characterization of Dispersed Air in Two Newsprint Paper Machines", *J. Pulp Paper Sci.* 18(4):121-126 (1992b).

BANKOFF, S.G. "Ebullition From Solid Surfaces in the Absence of a Pre-Existing Gaseous Phase", *Trans. ASME* 79:735-740 (1957).

BLANDER, M. and KATZ, J. "Bubble Nucleation in Liquids", *A.I.Ch.E. J.* 21(5):833-848 (1975).

CIHOLAS, P.A. and WILT, P.M. "Nucleation Rates in Water-Carbon Dioxide Solutions: The Spherical Cavity Case", *J. Colloid Interface Sci.* 123(1):296-298 (1988).

COLE, R. " Boiling Nucleation" Adv. Heat Transfer 10, 85-166 (1974).

FOX, F.E. and HERZFELD, K.F. "Gas Bubbles with Organic Skin as Cavitation Nuclei " (1954): *J. Acoust. Soc. Am.* 26(6):984 (1954).

GAVELIN, G. "Some Effects of Gases on Properties of Fibre Suspensions", Can. Pulp Paper Ass. Tech. Sect. Proc. 1954:240-248 (1954).

HARVEY, N.E., BARNES, D.K., McELROY, W.D., WHITELEY, A.H., PEASE, D.C. and COOPER, K.W. "Bubble Formation in Animals ", *J. Cell. Comp. Phys. 24*(1):1 (1944).

HODGSON, K.T. and BERG, J.C. (1985): "Dynamic Wettability Properties of Singe Wood Pulp Fibers and Their Relationship to Absorbency " *Wood and Fiber Sci.* 20(1):3-17 (1988).

JACOB, P. N. and BERG, J.C. (1993): "Zisman Analysis of Three Pulp Fiber Furnishes", *Tappi J.* 76(2):105-107 (1993).

KEREKES, R.J., SOSZYNSKI, R.M., and TAM DOO, P.A. (1985): "The flocculation of pulp fibers". Papermaking Raw Materials, V. Punton, Ed., Transactions of the Eighth Fundamental Research Symposium held at Oxford, Mechanical Engineering Publications Ltd., London, pp. 265-310.

KARRAS, M., PIETIKAINEN, T., KORTELAINEN, H., and TORNBERG, J. *Tappi J.* 71(1):65-69 (1988).

KLUNGNESS, J.H. "Measuring the Wetting Angle and Perimeter of Single Wood Fibers: a Modified Method", *Tappi J.* 64(12):65-66 (1981).

PELTON, R. H. and PIETTE, R. "Air Bubble Holdup in Wood Pulp Suspension", *Can. J. Chem. Eng.* 70:660-663 (1992).

SEDIVY, O. "Air, an Important Factor in Paper Manufacture", *Zellstoff und Papier* 18(4):112-118 (1969).

TURVEY, R.W. "Why do Fibres Float?", *J. Pulp Paper Sci.* 19(2):J52-J57 (1993).

WARD, C.A., BALAKRISHNAN, A. and HOOPER, F.C. "On the Thermodynamics of Nucleation in Weak Gas-Liquid Solutions", *J. Basic Eng.* 92(4):695-701 (1970).

WARD, C.A. and LEVART, E. "Conditions for Stability of Bubble Nuclei in Solid Surfaces Contacting a Liquid-Gas Solution", *J. Appl. Phys.* 56(2):491-500 (1984).

WILT, *P.M.* "Nucleation Rates and Bubble Stability in Water-Carbon Dioxide Solutions", *J. Colloid Interface Sci.* 112(2):530-538 (1986).

YOUNG, R.A. "Wettability of Wood Pulp Fibers", *Wood Fiber* 8:2:121-128 (1976).

CHAPTER 3

THE ENTRAPMENT OF SPHERICAL PARTICLES IN QUIESCENT PULP SUSPENSIONS: A MODEL SYSTEM

3.1 INTRODUCTION

The behavior of air bubbles in pulp suspensions is an important part of many processes in the pulp and paper industry. In some cases, such as in flotation deinking or multi-phase bleaching, gas bubbles are deliberately added to the pulp, and are an essential part of the process. In other areas such as paper making, excessive amounts of air are to be avoided, as gas bubbles may have undesirable effects on the product quality (May, Buckman 1975).

The efficiency of these processes depends mainly on the mechanisms controlling bubble hold-up in the pulp suspensions. While three-phase systems have been extensively studied in the literature, relatively little is understood about the properties of three-phase fibre-liquid gas systems (Taylor et al. 1994). To date, most of the studies have involved measuring bubble-hold-up in columns of pulp into which streams of gas are injected. Experimental results have demonstrated gas hold-up to be affected by various parameters such as pulp consistency and superficial gas velocity (Walmsley 1992; Went et al. 1993; Taylor et al. 1994), and pulp type and column diameter (Walmsley 1992). These studies have provided valuable insight on the behavior of bubbles streams in mixed pulp

suspensions. However, the mechanism by which individual bubbles interact and migrate through fibre suspensions still remains largely unknown.

One of the simplest explanations for bubble-hold up is bubble-fibre adhesion. Many authors have claimed that bubbles adhere to fibres: (Gavelin 1954; Sedivy 1969; Schwinger and Dobias 1991; Turvey 1993). However, the theories of bubble-fibre adhesion remain speculative. No photographs showing bubbles unequivocally adhering to fibres have yet been published. Furthermore, receding contact angle measurements of zero (implying no bubble adhesion) have been reported for a wide variety of wood fibres (Hodgson, Berg 1988; Jacob, Berg 1993; Krueger, Hodgson 1994; Krueger, Hodgson 1995). Non-zero receding contact angles have been reported in an exceptional case, involving highly-sized fibres (Krueger, Hodgson 1995). The contact angle measurements indicate that bubbles are unlikely to adhere to most types of wetted pulp fibres.

Another possible mechanism of bubble-hold, first proposed by Pelton and Piette (1992), is mechanical entrapment. In Pelton and Piette's experiments (1992), bubbles ranging from 460 μm to 9 mm in diameter were individually injected into a column of quiescent pulp with a micro-syringe, and the outcome of whether or not the bubbles reached the surface was recorded. The results were reported in terms of bubble escape probabilities: these were determined by dividing the number of bubbles which reached the surface by the total amount of bubbles injected into the pulp. Pelton and Piette (1992) concluded that the trapped bubbles were retained in the fibre network by mechanical

forces. Mechanically-trapped bubbles escaped when the buoyancy pressure of the bubbles exceeded the fibre network strength.

Pelton and Piette's (1992) results were applicable to the specific case of single bubbles rising vertically through approximately 14 cm of quiescent pulp. The pulp suspensions were too opaque to optically locate the trapped bubbles' final positions, and therefore no information was available on the total distance traveled by these bubbles. With the results, one could not differentiate between bubbles which may have only migrated a few millimeters through the pulp, or bubbles which may have almost completely traveled through the 14 cm pulp column.

The objective of this work was to determine how far spherical particles such as bubbles could travel through pulp before becoming mechanically trapped. To eliminate the possibility of bubble-fibre adhesion and to make detection in the pulp suspension easy, the experiments were conducted using a model system. Instead of injecting individual bubbles into quiescent pulp, spherical ball bearings were dropped through water at terminal velocity into uniform beds of settled pulp fibres. The parameters that were varied were the ball bearing diameter, pulp type and consistency. This paper presents the results obtained from these experiments, and discusses the relevance to bubble migration through pulp suspensions.

3.2 EXPERIMENTAL

Apparatus

The experimental apparatus consisted of 20 x 20 cm Plexiglas© optical cell with a 1 cm thickness (Figure 3-1). The ball bearings were dropped into the pulp with the aid of an insertion tube rack consisting of 6 tubes (1/4" O.D., 1/8" I.D.) spaced a distance of 1 inch (2.54 cm) apart.

The method consisted of pouring 250 ml of ≈ 0.1% consistency pulp into the optical cell, stirring the pulp and allowing it to settle. The pulp fibres settled to the bottom of the cell in a relatively uniform bed, leaving a layer of clear water above. The final height of the settled fibre bed was varied by subjecting the cell to vigorous mechanical agitating and rocking. With this method, it was possible to obtain settled fibre bed heights ranging from ≈ 3 to 8 cm.

Once the fibres bed had settled to the desired level, the insertion tube rack was lowered into water until the bottom just touched the fibre-water interface. A ball bearing was dropped into one of the insertion tubes, where it came to rest adjacent to a magnet placed outside the optical cell (Figure 3-2). The ball bearing was lowered to a minimum drop height of 5 cm above the fibre bed by moving the magnet outside the cell, and then released by pulling the magnet away from the cell. The minimum drop height was set to 5 cm to ensure that the ball bearings were falling into the fibre beds at terminal velocity. (The conditions of terminal velocity were verified by examining videotapes of the falling ball bearings).

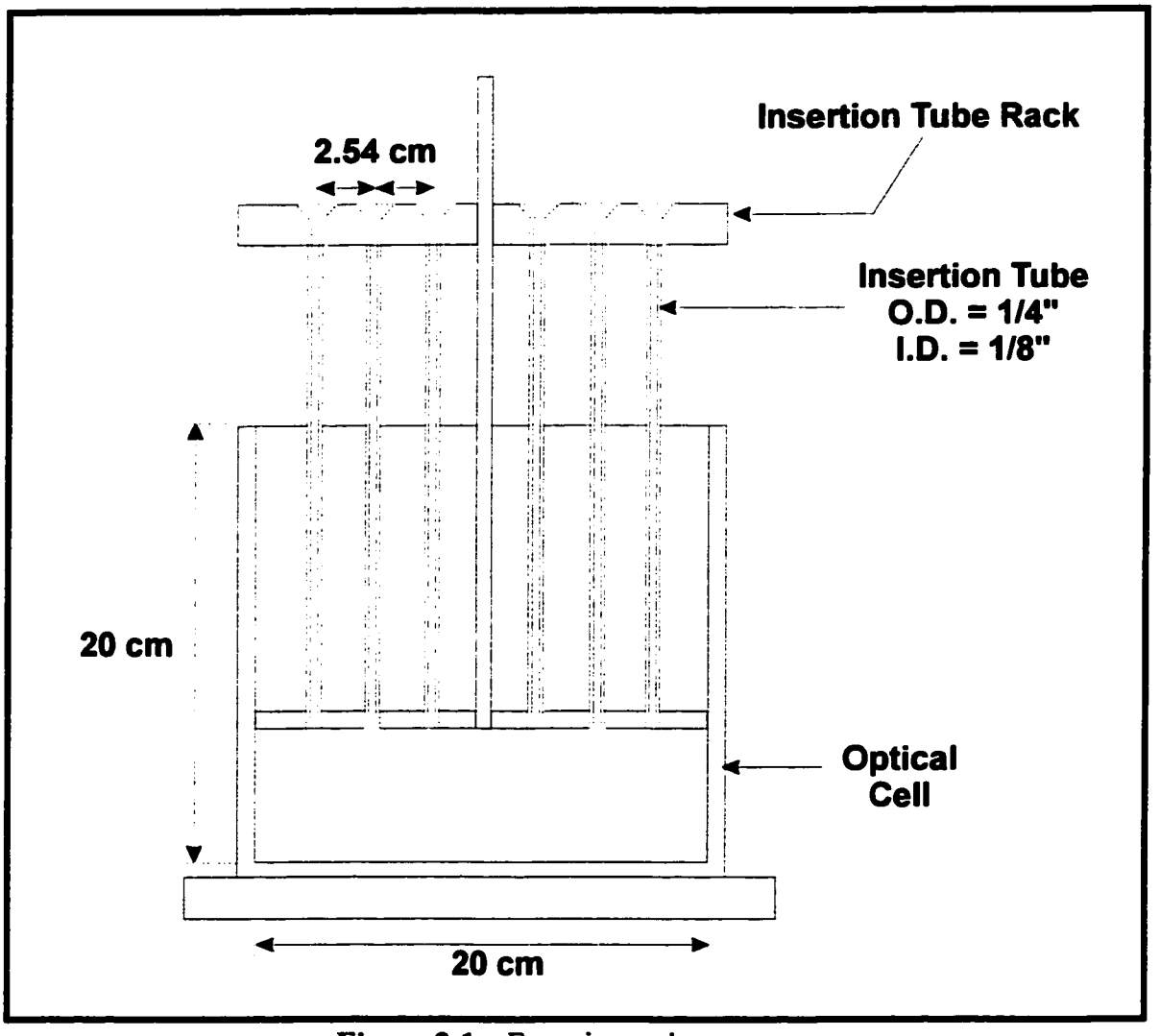

Figure 3-1. Experimental apparatus.

After the ball bearing was dropped, its final position in the fibre bed was located with the aid of a fibre-optic light source. The height of the fibre bed directly above the ball bearing and the final position of the ball bearing in the fibre bed were then recorded. This procedure was repeated until 6 ball bearings were dropped into each of the 6 insertion tubes. Usually, the pulp pad kept continually slowly setting during the experiments, and it was necessary to slightly adjust the plunger depth after each drop.

Once 6 ball bearings were dropped, they were removed from the optical cell with a magnet-tipped stirring rod. The settled pulp in the cell then re-mixed and allowed to settle again. This was repeated until 5 sets of 6 ball bearings were dropped, after which the pulp was poured out of the cell and its consistency was measured.

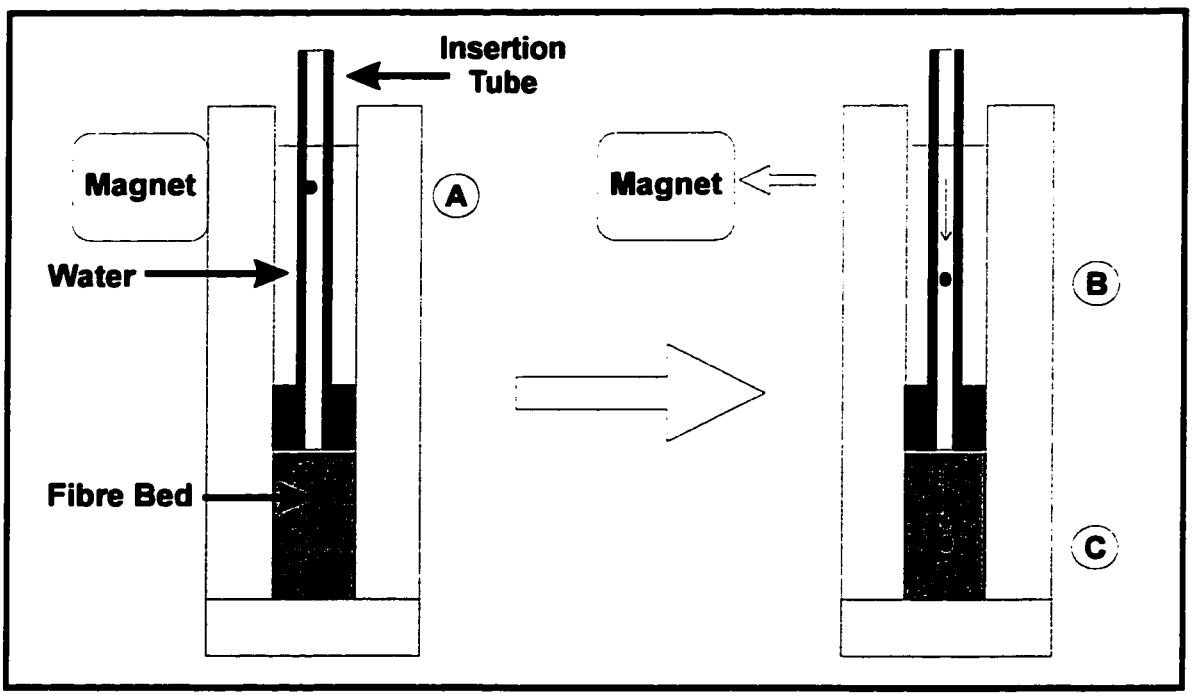

Figure 3-2. Experimental method. This diagram is a cross-section of the experimental optical cell shown in Figure 3-1. Initially, magnet placed adjacent to the cell wall retains the ball bearing in the water-filled insertion tube (A). When the magnet is removed, the ball bearing drops tube (B) and enters the fibre bed (C) at terminal velocity.

Pulp Furnishes

The Bleached Kraft Pulp (BKP) used in the experiments was obtained from a Canadian west coast mill, consisting of 40% white spruce, 40% lodgepole pine and 20% misc. (Douglas Fir, alpine fir, cedar and black spruce.) Dried sheets were disintegrated at Paprican (Pointe-Claire, Que.) and stored at 10% consistency. The mechanical pulp used

was a mixture of 60% thermomechanical pulp (TMP) and 40% stone groundwood (GWD). This TMP-GWD mix was shipped at approximately 33% consistency. The Kajaani fibre lengths and coarseness values were measured at Paprican (Pointe-Claire, Que.). The values are summarized in Table 3.1. The fines contents were measured with a Britt Drainage Jar© (Paper Materials Research Materials, Inc. N.Y.) using a 125P Ultra screen (76 μm hole-size).

Table 3.1. Physical properties of the pulp fibres. (Measured by Kajaani FS-200)

	Kajaani Fibre Lengths (mm)				
PULP FURNISH	**Arithmetic Average**	**Length-Weighted Average**	**Weight-Weighted Average**	**Coarseness (mg/ 100m)**	**Avg. Fines Content (%)**
BKP	1.21	2.47	2.98	13.8	10.7
TMP-GWD Mix	0.34	0.97	1.81	29.9	38.9

Ball Bearings:

Two different ball bearing sizes were used in the experiments. The "small" ball bearings had a diameter of (1/32"), while the "large" ball bearings had a diameter of (1/16"). The total mass of 60 ball bearings was measured to determine the average weight. The ball bearings properties are summarized in Table 3.2:

Table 3.2. Ball bearing properties

Ball Bearing Size	Diameter	Average Weight	Average Density
Small	794 μm (1/32")	2.1 mg	8.0 g/cm^3
Large	1588 μm (1/16")	16.4 mg	7.8 g/cm^3

3.3 RESULTS

Some of the terms used to describe the experimental results are shown in Figure 3-3. The 250 mL of pulp poured into the cell gave a total liquid height of 12.5 centimeters. The consistency of this unsettled pulp was defined as C_{mInit}. The height of the fibre-water interface of the settled fibre bed was defined as H_o. After being dropped into the fibre beds, the ball bearings came to rest within the fibre bed, or reached the bottom of the cell. The final position of the ball bearings, as measured from the bottom of the cell, was defined as H_f. The total distance that the ball bearings penetrated into the fibre bed was defined as ΔH, which equals the difference of $(H_o - H_f)$. Ball bearings which reached the bottom of the cell were considered as having "escaped" the fibre bed. Ball bearings were defined as "trapped" when they were retained in the fibre bed.

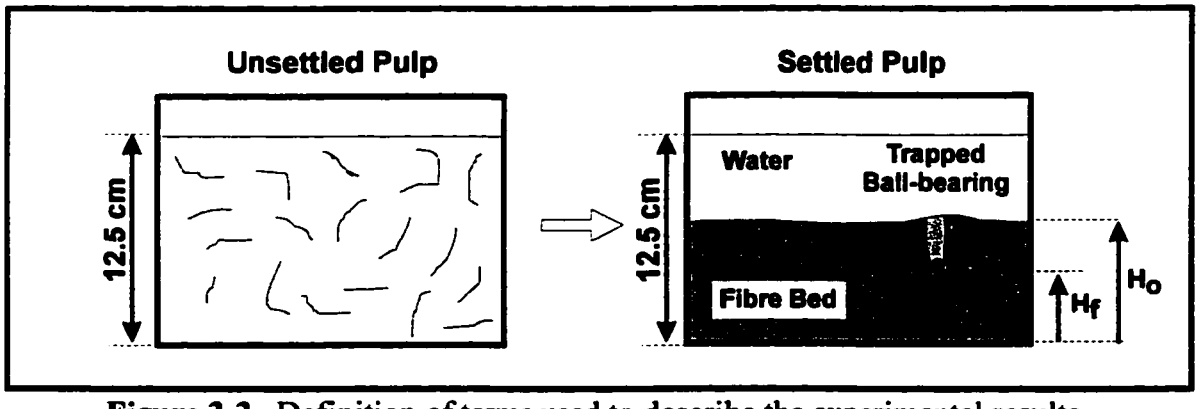

Figure 3-3. Definition of terms used to describe the experimental results.

The consistency of the settled fibres bed (C_{mo}) was estimated by assuming that the mass consistency was inversely proportional to volume occupied by the pulp fibres, according to Eq. 3.1:

$$C_{mo} = C_{mInit}\left(\frac{12.5}{H_o}\right) \qquad [3.1]$$

where the ratio (12.5/Ho) corresponds to the original liquid height of the unsettled pulp divided by the height of the settled fibre bed (H_o), where H_o is given in centimeters.

Determining the Escape Probabilities

The data were arbitrarily divided into sets according to the fibre bed consistencies, in consistency increments of 0.0005. (For example, data sets corresponding to ($0.0010 < C_{mo} < 0.0015$), ($0.0015 < C_{mo} < 0.0020$), etc.) The cumulative distributions of penetration distance (ΔH) were then determined for each group and expressed in terms of escape probabilities.

The escape probabilities of the small ball bearings as a function of the penetration depths into the BKP are shown in Figure 3-4. A value of $P_{esc} = 1$ indicates that the ball bearings had a 100% chance of breaking through the given penetration thickness and consistency. All the small ball bearings all achieved a penetration distance of 0.5 cm. The escape probabilities approached zero over shorter penetration distances for the higher consistencies. For example, for a penetration distance of $\Delta H \geq 2.5$ cm, $P_{esc} \approx 0.80$ for the (0.15-0.20%) consistency pulp, while P_{esc} was substantially lower ($\approx 5\%$) with the more concentrated (0.30-0.35%) consistency pulp. Under the same conditions, for the highest consistency measured (0.35-0.40%), P_{esc} increased to 0.15. The reason for this slight increase in escape probability with consistency is not known.

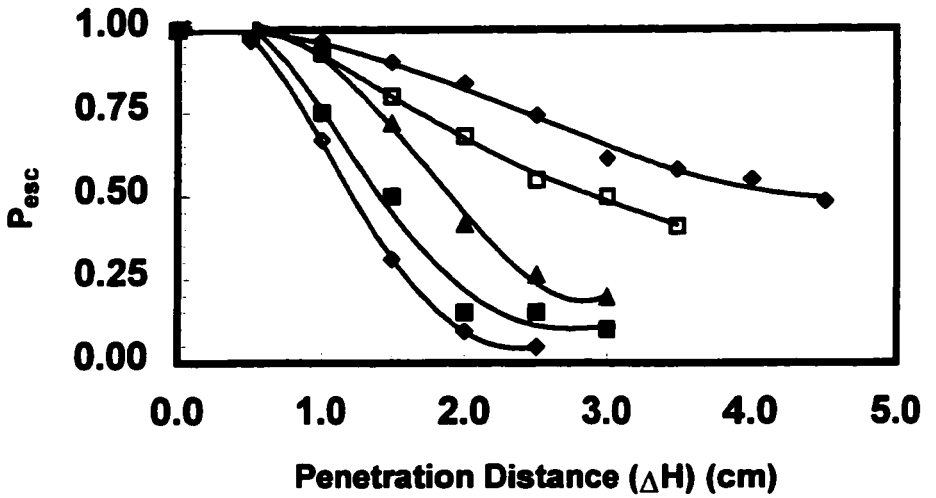

Figure 3-4. Cumulative escape probabilities for 1/32" ball bearings in BKP. The y-axis represents the fraction of ball bearings which penetrated into the fibre bed by a minimum distance of ΔH. The range of bed consistencies (C_{mo}) and the number of data for each data set (n) are denoted by the following symbols:

(◆): (0.15% < C < 0.20%), n = 31. (□) : (0.20% < C < 0.25%), n = 100.

(▲): (0.25% < C < 0.30%, n = 46. (◇): (0.30% < C < 0.35%), n = 42).

(■): (0.35% < C < 0.40%), n = 20).

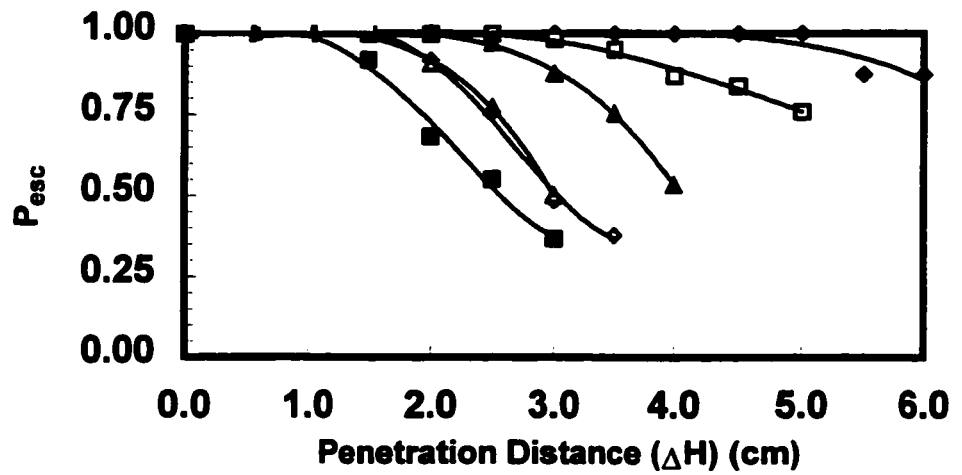

Figure 3-5. Cumulative escape probabilities for the large (1/16") ball bearings in BKP. The range of bed consistencies (C_{mo}) and the number of data for each data set (n) are denoted by the following symbols

(◆): (0.15% < C_{mo} 0.20%), n = 8. (□) : (0.20% < C_{mo} 0.25%), n = 62.

(▲): (0.25% < C_{mo} 0.30%, n = 73. (◇): (0.30% < C_{mo} 0.35%), n = 37.

(■): (0.35% < C_{mo} 0.40%, n = 38). △: (0.40% < C_{mo} 0.45%, n = 22.

There is a similar trend in the escape probability curves for the data with the large ball bearings for BKP (Figure 3-5), although the escape probabilities are somewhat increased. The more massive 1/16" ball bearings penetrated a greater distance into the fibre beds than the smaller 1/32" ball bearings. For example, the large ball bearings traveled through at least 5 cm of (0.15-0.20%) consistency pulp before P_{esc} dropped below 1. Under similar conditions, the small ball bearings could only travel through 1 cm of pulp before entrapment occurred. The escape probabilities of the large ball bearings probabilities also decreased with consistency. The lowest escape probabilities occurred with the (0.35-0.40%) pulp. For the next highest consistency data set (0.40-0.45%), the escape probabilities increased, which is contrary to what is expected. In fact, this escape curve was almost identical to the curve for the (0.30-0.35%) pulp. The reason for this is not known.

Mechanical Pulp

Only a small amount of data was collected for the TMP-GWD pulp because the ball bearings escaped in almost all the cases. Entrapment occurred in only a few rare cases with the small ball bearings with 0.6% consistency pulp. Some selected data is shown for comparison purposes in Figures 3-6 and 3-7. The data for (0.35-0.40%) pulp for the small ball bearings for both the TMP-GWD and BKP are shown in Figure 3-6. Only 8 data points were measured with the TMP-GWD, but all these ball bearings

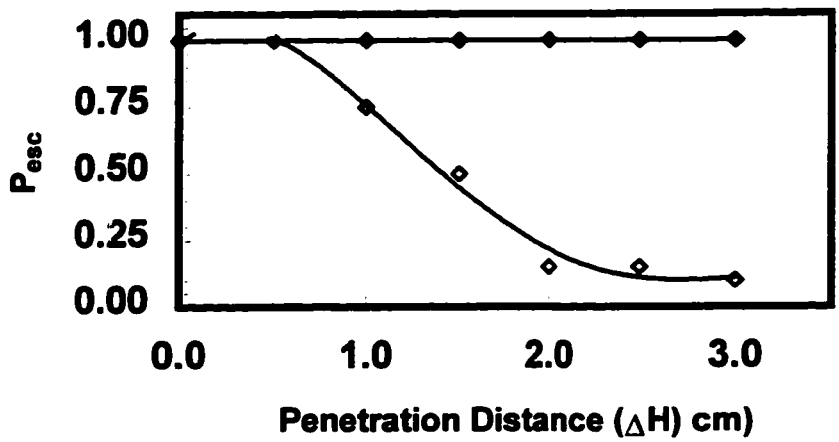

Figure 3-6: Comparison of escape probabilities between BKP and TMP-GWD, for the small (1/32") ball bearings for fibre bed consistencies ranging from ($0.35\% < C_{mo} < 0.40\%$). The following symbols denote the pulp furnish, with (n) indicating the number of data in each data set: (◆): TMP-GWD pulp, n = 8. (◇): BKP, n = 20.

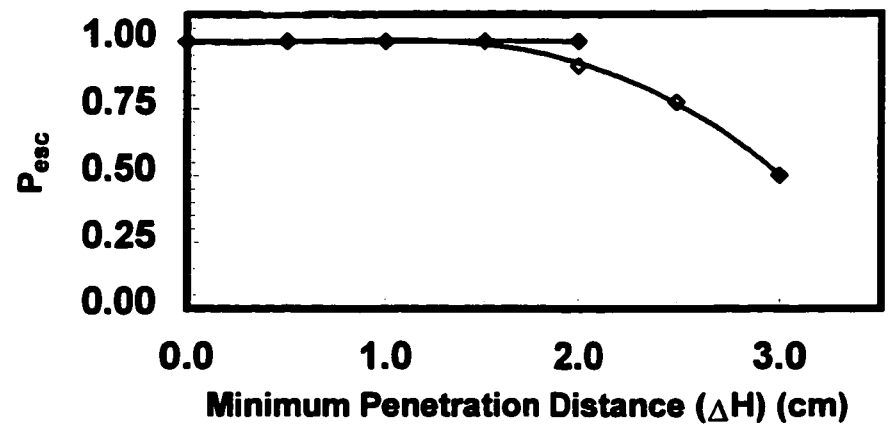

Figure 3-7. Comparison of escape probabilities between BKP and TMP-GWD, for the large (1/16") ball bearings. The range of bed consistencies (C_{mo}) and the number of data for each data set (n) are denoted by the following symbols:
(◆):TMP-GWD ($0.50\% < C_{mo} < 0.55\%$), n = 9.
(◇): BKP ($0.40 < C_{mo} < 0.45\%$), n = 22.

escaped through at least 3 centimeters of pulp. On the other hand, only about 10% of the ball bearings escaped through 3 centimeters of the BKP. A similar pattern in seen with the data for the large ball bearing in Figure 3-7. The TMP-GWD's ability to trap the ball bearings was much less than that of the BKP.

3.4 DISCUSSION

Since stainless steel does not adhere to wet pulp fibres, it is assumed that the mechanism retaining the ball bearings in fibre beds is mechanical entrapment. This discussion will focus on the results obtained with the BKP, as most of the data were obtained with this pulp.

With the dilute fibre beds approaching $C_{mo} = 0.1\%$, the ball bearings fell to the bottom of the cell, with little or no interference of the pulp fibres. For more concentrated fibre beds, two types of behavior were observed, which are illustrated in Figure 3-8. In some cases, the ball bearings appeared to randomly slip through dilute areas of the fibre bed and eventually come to rest. When this "slipping" occurred, there appeared to be little or no disruption of the fibre bed in the immediate vicinity of the ball bearing. At higher consistencies, the ball bearings appeared to penetrate the fibre bed by "plowing" into the fibre network. In this case, the ball bearings appeared to come to rest when a sufficient amount of compressed pulp had accumulated in front which could support the ball bearing weight. In some cases, a slight indentation was seen at the fibre-water

interface penetration had occurred, indicating where the fibre bed had been disrupted. This indentation seemed to be more prevalent with the large ball bearings.

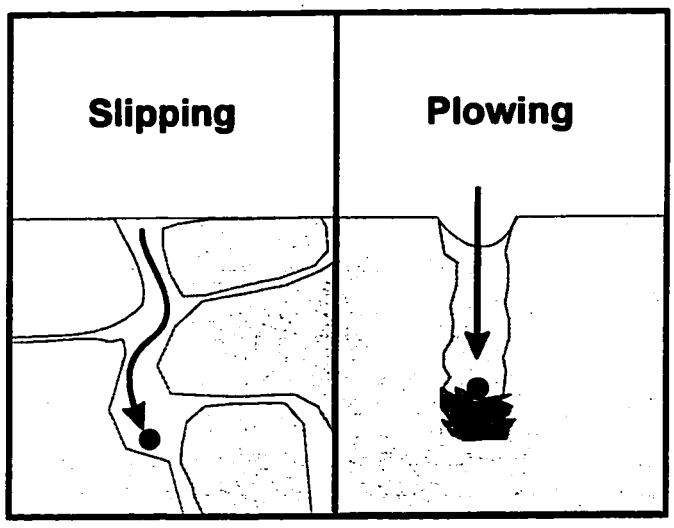

Figure 3-8. Observed mechanisms by which ball bearings migrated through settled fibre beds. With the dilute pulps, the ball bearings appeared to slip between areas of low fibre density. With the more concentrated pulps, the ball bearings appeared to plow into the fibre network, accumulating a mat of compressed fibres in front of them.

The onset of mechanical entrapment appeared to occur when the fibre beds had formed networks. The 0.1% consistency pulp initially poured into the cell was not sufficiently concentrated to form networks, as the fibres appeared completely dispersed under these conditions. During settling, however, the fibres became more concentrated and entangled until a fibre bed formed which could support its own weight. The lowest fibre bed consistencies in these experiments were of the order of $C_{mo} \approx 0.0015$, and were obtained by allowing the pulp to settle undisturbed. It is assumed that these low consistencies correspond to the "sedimentation concentration" described by Meyer and

Wahren (1964). The sedimentation concentration equals the consistency that a very dilute pulp suspension will settle to, and is a function of the fibre length-to-radius ratio. It corresponds to the state at which fibres first form a 3-dimensional network, where there are at least 3 fibre-to-fibre contact points on each fibre.

The higher fibre bed consistencies were obtained by subjecting the cell to vigorous mechanical agitation and rocking, which forced the fibres to the bottom of the optical cell. These higher consistencies were no longer representative of the sedimentation concen-tration, as the mechanical agitation was likely to have caused the caused the fibre-fibre bonds to slip or break, thus concentrating the fibre bed into a smaller volume. The maximum consistency obtainable with mechanical agitation $C_{mo} \approx$ 0.0048, giving beds which appeared very uniform and compact.

Pulp suspensions tend to form unevenly, into areas of local mass concentration called flocs (Kerekes et al. 1985). The "slipping" and "plowing" mechanisms are attributed to different regimes of flocculation. With the more dilute fibre beds, flocs which formed during settling may have left areas of relatively low consistency between the floc regions. The ball bearings may have migrated by "slipping" between these dilute inter-floc regions until coming to rest in an area where the fibre network was sufficiently strong to support ball bearings' weight. On the other hand, when "plowing" occurred, the fibre beds were sufficiently concentrated to be considered as one continuous floc. As there were no dilute inter-floc regions through which the ball bearings could slip, the only

way the ball bearings could penetrate into the fibre bed was by forcibly disrupting the fibre network directly in front of them.

Fibre network strength depends both on the consistency and fibre properties. The yield stress of a fibre network depends on the volume occupied by the fibres (Bennington et al, 1990). Meyer and Wahren (1964) demonstrated that the shear modulus of fibre network is strongly influenced by the fibre length-to-radius ratio. Furthermore, network properties depends on the fraction of "active" fibres, as described by Wahren (1979). "Active fibres" become locked into the network and give the network its strength, while "inactive fibres" do not entangle with other fibres and therefore do not contribute to the network.

Fibre network theory explains the differences in the results obtained between the BKP and TMP-GWD pulps. The fines content of the TMP-GWD pulp was 39% (by mass), as compared to the 11% fines content of the BKP. Pulp fines, in general, are considered too small to entangle and form into networks. The TMP-GWD pulp therefore a greater number of inactive fibres than the BKP. In addition, TMP-GWD had an arithmetic average fibre length of 0.34 mm, compared to 1.21 mm for the BKP. The higher fines content and lower fibre length resulting in the TMP-GWD pulp having a lower network strength. This greatly reduced the ability of the TMP-GWD pulp to trap the ball bearings, as is reflected in the results in Figures 3-6 and 3.7.

Predicting Penetration Distances

Pelton and Piette (1992) correlated the buoyancy forces for bubble escape from a pulp suspension to yield stress estimates of fibre networks. We follow this approach to estimate the maximum penetration distance of the ball bearings. The magnitude of the buoyancy force of the ball bearing acting downward on the fibre bed is given by:

$$F_b = Vg(\rho_{bb} - \rho_w) \qquad [3.2]$$

where V is the volume of the ball bearing, ρ_{bb} is the density of the ball bearing, and ρ_w is the density of water, which is assumed to be 1 g/cm^3. A buoyancy pressure can be calculated by dividing the buoyancy force divided by a surface area. Assuming the surface area of interest equals half the surface area of the spherical ball bearing, the buoyancy pressure can be given as:

$$\tau_b = \frac{1}{3} D_{bb} g(\rho_{bb} - \rho_w) \qquad [3.3]$$

where D_{bb} is the ball bearing diameter. Using Eq. 3.2 and the densities from Table 3-2, the buoyancy pressures of the ball bearings equal:

$$\tau_b(1/32") = 18.18 \text{ Pa} \qquad [3.4a]$$
$$\tau_b(1/16") = 35.47 \text{ Pa} \qquad [3.4b]$$

Neglecting the inertia of the falling ball bearings, it is assumed that the ball bearings come to rest when the buoyancy pressure of the ball bearing equals the yield stress of the pulp directly below it.

$$\tau_b = \tau_y \qquad [3.5]$$

The yield stress of pulp can be correlated in terms of the consistency (Bennington et al, 1990):

$$\tau_y = A[C]^B \qquad [3.6]$$

where A and B are empirical constants. To find the consistency at which the ball bearings come to rest, we substitute Eq. [3.5] into Eq. [3.6] and solve for the consistency:

$$C_f = \left[\frac{\tau_b}{A}\right]^{\frac{1}{B}} \qquad [3.7]$$

where C_f is the consistency of the pulp directly under the ball bearing. From the yield stress correlations reported by Bennington et al. (1990), A = 3.12 x10^6 Pa, and B = 2.79 for semi-bleached kraft pulp. Using these empirical constants and the calculated values of τ_b from Eqs. 3-4a and 3-4b, the theoretical consistencies which should support the ball bearings can be estimated:

$$C_f\,(1/32") = 0.0133 \qquad [3.8a]$$
$$C_f\,(1/16") = 0.0169 \qquad [3.8b]$$

(The detailed calculations for deriving these consistencies are shown in Appendix D-1.) The consistencies in Eqs. 3.8a and 3.8b represent estimates of the minimum consistencies which should exist below the trapped ball bearings. For consistencies lower than these critical values, the buoyancy pressure of the ball bearings would exceed the fibre network strength, and the ball bearings would disrupt the fibre network and fall to the bottom of the cell.

It is difficult to predict the total penetration distance assuming a "slipping" regime. The non-uniformity of the dilute fibre beds which are not completely flocculated give the ball bearings a random migration pattern which has yet to be quantified. The final distance achieved by the ball bearings can be estimated, however, by assuming that only "plowing" occurs. A simplified model of the plowing mechanism is shown in Figure 3-9. It is assumed that as the ball bearing penetrates the settled fibre bed, it vertically compresses the pulp directly in front of it, until a column of pulp is formed with the required of consistency of C_f.

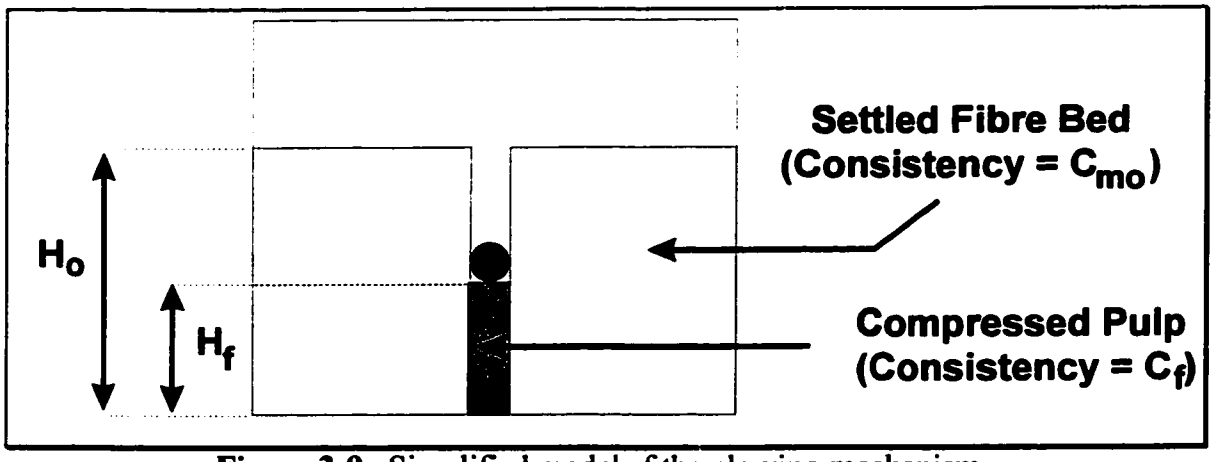

Figure 3-9. Simplified model of the plowing mechanism

Assuming that the consistencies are inversely proportional to the volume occupied by the fibres, C_f can be estimated as

$$C_f = C_{mo}\left(\frac{H_o}{H_f}\right) \qquad [3.9]$$

Rearranging Eq. 3.9 gives the final predicted height of the trapped ball bearings:

$$H_f = C_{mo}H_o/C_f \qquad [3.10]$$

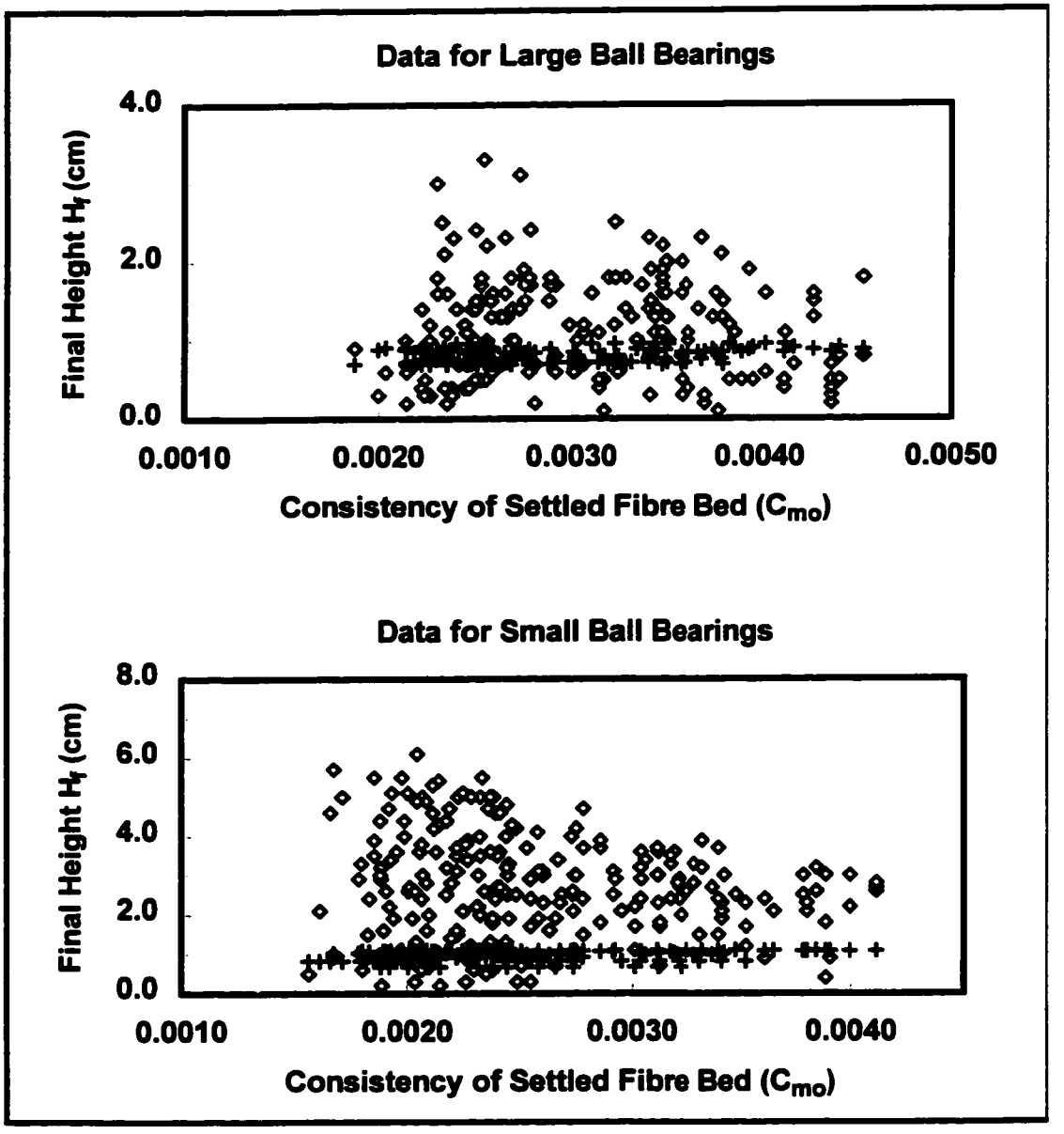

Figure 3-10. Comparison between the final positions of the trapped ball bearings in the BKP fibre beds and the predicted values. (◇): Experimental data. (+): Predicted values.

where C_{mo} is calculated from Eq. 3.1.

The final positions (H_f) of the trapped ball bearings in the BKP and the predicted values are compared in Figure 3-10. The large scatter in the experimental data at low consistencies ($C_{mo} < 0.003$) is indicative of the random nature of the slipping motion of the ball bearings between the flocs. This is especially noticeable with the data for the small ball bearings. At higher consistencies, the scatter is the data reduced and the final depths appear to level off to a constant value at $C_{mo} \approx 0.004$. This is attributed to the onset of the plowing mechanism.

A comparison between the experimental values to the predicted values is not valid at low consistencies. This is because the "slipping" in the dominant migration mechanism, and the model according to Eqs. 3-7 to 3-10 assumes that only the "plowing" occurs. At higher consistencies, there is less scatter in the data and the predicted values are in closer agreement with the experimental data. The predicted values of H_f fall roughly in the mid-range of the experimental values with the large ball bearings. However, the model underestimates the final positions for most of the data for the small ball bearings.

The predicted values of H_f in Figure 3-10 were expected to lie on a straight line. The slight scatter in the predicted values is attributed to the assumptions made in the calculations, plus experimental error. First, it was assumed that H_f was proportional to the height of the settled fibre bed (H_o). At the lower consistencies, however, the fibre-

water interface was not perfectly even, resulting is slight differences in the estimates of C_{mo}. In addition, precise measurements of H_o were not always possible, especially with dilute fibre beds which were still slowly settling while measurements were being taken. Repeated removal of the tube rack from the optical cell also introduced some error, as this reduced the total liquid height in the cell by up to 4%, which may have affected the value of C_{mo}.

A key assumption upon which Eq. 3.3 is based is that the buoyancy force of the ball bearings was distributed over half the surface area of the ball bearing. With the more dense fibre beds, the interconnected fibres may have distributed the weight of the ball bearings over a larger surface area, causing the calculated buoyancy pressure to be overestimated. In addition, the fact that the ball bearings were dropped at terminal velocity may have contributed to the total penetration depth. From the data in Figures 3-4 and 3-5, all the small ball bearings penetrated at least 0.5 cm, and all the large ball bearings penetrated at least 1 cm. These distances may be related to inertial effects and not fibre network effects.

One of the largest assumptions made was in using the yield stress data from Bennington et al. (1990). Various methods have been used to measure network strength, which have produced a wide range of results. Bennington et al. (1990) plotted network strength measurements from various sources in the literature, which showed that the range of network strength measurements typically span an order of magnitude.

Given all the errors and assumptions, , however, the predicted final ball bearing positions in Figure 3-10 are still within reasonable agreement with the experimental data. The calculations demonstrate a link between mechanical entrapment by plowing and the fibre network strength.

While penetration into the fiber bed can be accomplished by either slipping or plowing, the nature of the fundamental interactions between the ball bearings and the fibres need to considered. Were both the slipping and plowing mechanisms the result of fibre-fibre bonds in the network being broken? Or, at low consistencies, were the individual fibres in the bed sufficiently far apart to allow the ball bearings to migrate through the inter-fibre void spaces, leaving the fibre network relatively untouched?

These questions can be answered by estimating the size of the void spaces existing between the individual fibres. The inter-fibre void size distributions can be calculated from the Equation 3-11, which was derived Ogston (1958). This model is based on a random network of uniform, straight fibres of negligible thickness, with the fibre suspension having a uniform density. In order for a spherical particle to fit inside the fibre network, Ogston (1958) assumed that the center of the particle must be a distance of at least its own radius away from the nearest fibre. The volume fraction of the fibre suspension that could accommodate spherical particles of radius (r) was derived as:

$$P_D = \exp\left[-\left(2\pi\upsilon L_o r^2 + \frac{4\pi}{3}\upsilon r^3\right)\right] \qquad [3.11]$$

where P_D is the volume fraction of the fibre suspension in which the spherical particles of radius (r) can fit, ν is the average number of fibres centers per cm^3 and L_o is half the fibre length.

Assuming that the volumes of the water and pulp fibres are additive, and that the number of fibre centers per unit volume equals the number of fibres per unit volume, P_D can be re-expressed as:

$$P_D = \exp\left[\frac{-1}{12}\pi C\rho_w\rho_{pulp}D^2\frac{(3L+2D)}{(\rho_{pulp}-C\rho_{pulp}+C\rho_w)(\omega L)}\right] \qquad [3.12]$$

where C is the pulp consistency (expressed as a mass fraction), D is the particle diameter, L the fibre length and ω the fibre coarseness. The terms ρ_{pulp} and ρ_w are the densities of the pulp fibres and water, which are assumed to be 1.5 g/cm^3 and 1 g/cm^3, respectively. The detailed calculations in deriving Eq. 4-3 are summarized in Appendix D-3.

Calculated values of P_D as a function of particle diameter for various consistencies are shown in Figure 3-11. The calculations are based on the fibre properties of the BKP listed in Table 3.1, using L = 1.21 mm and ω = 13.8 mg/100 m.

The volume fraction curves in Figure 3-11 indicate that the majority of the inter-fibre void spaces in consistency range in the experiments lie in the range of 10-400 μm. P_D approaches zero at ≈ 800 μm for the 0.15% consistency BKP, and at ≈ 400 μm for 0.5% consistency BKP. For comparison, the ball bearing diameters were 793 μm (small size) and 1588 μm (large size). These dimensions are larger than most of the inter-fibre void spaces, even with the most dilute fibre beds. The calculations show that migration

between the inter-fibre void spaces was extremely unlikely. The only way the ball bearings could have penetrated the fibre bed was by disrupting the fibre-fibre bonds, regardless of whether slipping or plowing occurred.

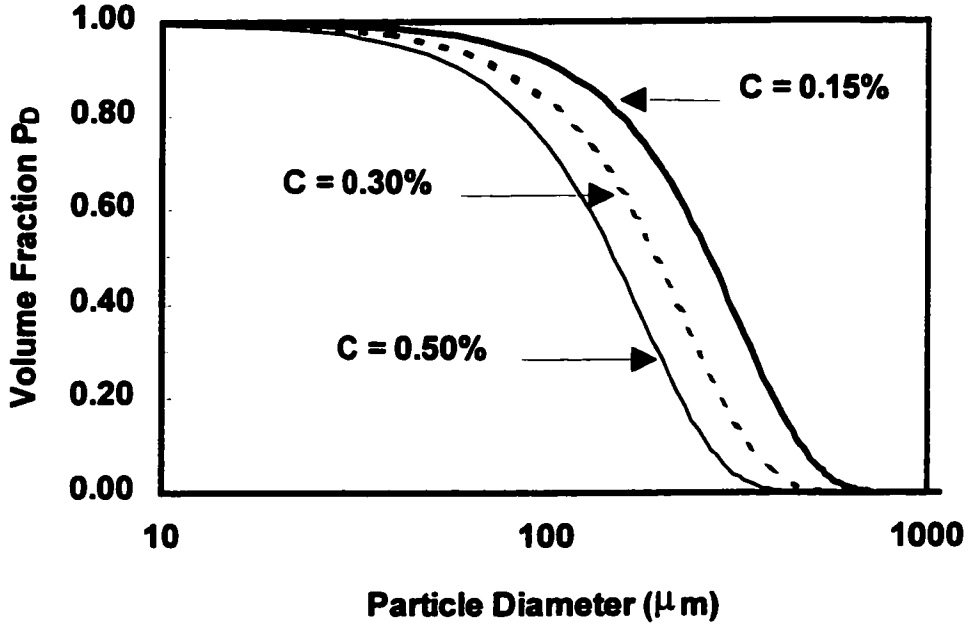

Figure 3-11. Estimates of the inter-fibre void spaces in the BKP fibre beds used in the experiments. The x-axis represents the particle diameter, and the y-axis represents the volume fraction of a uniform pulp suspension in which these particles can fit. The curves were calculated from Eq. 3-12, which is based on the model derived by Ogston (1958).

Relevance to Mechanical Entrapment of Bubbles in Pulp Suspensions

The conditions under which mechanical entrapment occurred with the ball bearings is not completely analogous to the entrapment of air bubbles in pulp suspensions. In the present study, the ball bearings penetrated downwards into the pulp, and their motion was restricted by the lower boundary of the optical cell. On the other

hand, air bubbles rising through pulp suspensions have no physical barriers restricting their upward migration, unless the pulp is placed in a closed container or in pipe flow. However, a comparison between existing bubble escape data and the present results can provide some insight on the mechanisms of bubble migration through pulp suspensions.

The data in Figures 3-4 and 3-5 show that large (1588 μm) ball bearings have a 50% probability of escaping through 3 cm of ≈ (0.3-0.35%) consistency pulp. Under similar conditions, the small (793 μm) ball-bearings only had a 10% chance escaping through distance of 2.5 cm. If bubbles of similar diameter were migrating upwards through these fibres beds, the probability of escape would be expected to be even less, because air bubbles would have a lower buoyancy pressure than the steel ball bearings.

The bubble escape data from Pelton and Piette (1992) demonstrate that air bubbles can travel greater distances through pulp than the ball bearings did in the present experiments. For example, for 0.4% consistency newsprint pulp, bubbles of ≈ 1000 μm in diameter had a 50% chance of escaping a distance of ≈ 14 cm.

The differences in these results can be explained by the nature in which the pulp suspensions were formed. In Pelton and Piette's (1992) experiments, the pulp were stirred and allowed to be approximately quiescent. It is likely that this pulp was flocculated, with relatively dilute areas existing between the flocs, unlike the pulp in the present experiments which were forcefully compacted and made uniform by vigorous mechanical agitation.

Our experimental results indicate that ball bearings are unlikely to travel more than a few centimeters through compact fibre beds. Yet the results of Pelton and Piette (1992) show that bubbles of similar diameter, with a smaller buoyancy force, can readily migrate through at least ten centimeters of pulp. A plausible explanation for these observations is that bubbles make their way to the surface by randomly migrating between the relatively dilute areas between the pulp flocs, where the network strength is relatively low. This was seen to some extent with the "slipping" migration of the ball bearing with the dilute fibre beds. If bubbles do collide with flocs of sufficient fibre density and network strength, it may be possible that bubbles penetrate inside the flocs by the "plowing" mechanism.

Whether or not this occurs needs to be verified in further experiments where bubble-floc interactions can be observed.

3.5 CONCLUSIONS

- The probabilities of escape as a function of distance were determined for ball bearings falling through uniform beds of settled pulp fibres.

- The larger (1/16" diameter) ball bearings penetrated further into the fibre beds than the smaller (1/32" diameter) ball bearings.

- The BKP had a greater ability to trap the ball bearings than the TMP-GWD pulp. This was attributed to the physical fibre properties which gave the BKP a stronger network strength.

- Two mechanisms of migration through the fibre beds were observed. With more dilute pulps, a "slipping mechanism" was observed, where the ball bearings appeared to randomly migrate within localized dilute areas in the settled fibre beds. With more concentrated pulps, a "plowing mechanism" was observed, where the ball bearings penetrated the fibre bed by compressing the fibres directly in front of them.

- Ball bearings which penetrated by the plowing mechanism came to rest within the fibre bed when buoyancy pressure equaled the network strength of the pulp directly below the ball bearing. Using existing correlations of yield stress measurements for semi-bleached kraft pulp, it was possible to estimate the final position of the trapped ball bearings.

- Ball bearings are unlikely to penetrate more than a few centimeters through compact fibre beds of consistencies of 0.3-0.5%.

- A comparison of the results to existing data for bubble hold-up experiments in quiescent pulp has led to the conclusion that bubbles escape through pulp suspensions by migrating between pulp flocs.

REFERENCES

BENNINGTION, C.P.J., KEREKES, R.J., and GRACE, J.R. "The Yield Stress of Fibre Suspensions", *Can. J. Chem. Eng.*, 68:748-757 (1990)

GAVELIN, G. "Some Effects of Gases on Properties of Fibre Suspensions", Can. Pulp Paper Assoc. Tech. Sect. Proc. 1954:240-248 (1954).

HODGSON, K.T. and BERG, J.C. "Dynamic Wettability Properties of Single Wood Pulp Fibers and Their Relationship to Absorbency" *Wood and Fiber Science* 20(1):3-17(1988).

JACOB, P.N. and BERG, J.C. "Zisman Analysis of Three Pulp Fiber Furnishes", *Tappi J.* 76(2):105-107 (1993).

KEREKES, R.J., SOSZYNSKI, R.M. and TAM DOO, P.A. "The Flocculation of Pulp Fibres", Papermaking Raw Materials, Trans. 8th Fund. Res. Symp. (Oxford), 265-309 (1985).

KRUEGER, J.J. and HODGSON, K.T. "Single-fiber Wettabiltiy of Highly Sized Pulp Fibers", *Tappi J.* 77(7):83-87 (1994).

KRUEGER, J.J. and HODGSON, K.T. "The Relationship Between Single Fibre Contact Angle and Sizing Performance", *Tappi J.* 78(2);154-161 (1995).

MAY, O.W. and BUCKMAN, S.J. "Practical Effects of Air in Papermaking", Tappi 58(2):90-94 (1975).

MEYER, R. and WAHREN, D. "On the Elastic Properties of Three-Dimensional Fibre Networks", *Svensk Papperstidn.* 67(10):432-436 (1964).

OGSTON, A.G. "The Spaces in a Uniform Random Suspension of Fibres", *Trans. Faraday Soc.* 54:1754-1757 (1958).

PELTON, R.H. and PIETTE, R., "Air Bubble-Holdup in Wood Pulp Suspensions", *Can. J. Chem. Eng.* 70:660-663 (1992)

SCHWINGER, K. and DOBIAS, B., "The Influence of Calcium Ions on the Loss of Fibre in the Flotation Deinking Process", 1st. Res. Forum on Recycling, Tech. Sect., CPPA, 1-11 (1991).

SEDIVY, O. "Air, an Important Factor in Paper Manufacture", *Zellstoff und Papier* 18:112-118 (1969).

TAYLOR, K.E., GHIAASIAN, S.M., ABDEL-KHALIK, S.I., LINDSAY, J.D. and GEORGE, J. "Macroscopic Flow Structures in a Bubbling Paper Pulp-Water Slurry", Tech. Paper Series Number 537, Inst. Paper Sci. Technol., Atlanta, GA (1994).

TURVEY, R.W., "Why do Fibres Float?", *J. Pulp Paper Sci.* 19(2):J52-J57 (1993).

WAHREN, D. "Fibre Network Structures in Papermaking Operations", Proc. Paper Sci. Tech. The Cutting Edge. Conf. 112-129 (1979).

WALMSLEY, M.R.W. "Air Bubble Motion in Wood Pulp Fibre Suspensions", *APPITA* 45:509-515 (1992).

WENT, J., JAMIALAHMADI, M. and MULLER-STEINHAGEN, H.M., "Effect of Wood Pulp Fibre Concentration on Gas Hold-up in Bubble Column", *Chem. Ing. Tech.* 65(3):306-308 (1993).

CHAPTER 4

THE BEHAVIOR OF AIR BUBBLES IN AQUEOUS WOOD PULP SUSPENSIONS

4.1 INTRODUCTION

The efficiencies of many processes in the pulp and paper industry are influenced by the presence of dispersed air bubbles in pulp suspensions (Pelton, Piette 1992). In papermaking, excessive air in pulp is something to be avoided, as it may lead to problems such as pinholes, reduced drainage on the papermachine and other undesirable paper properties (May, Buckman, 1975). In other cases, such as in flotation deinking or multi-phase bleaching, gas bubbles are deliberately added to the pulp, and are an essential part of the process. With gas-phase bleaching, gas bubbles must be uniformly mixed in the pulp in order to achieve uniform bleaching (Bennington, 1993). Bubble-fibre interactions also have a large effect on the flotation deinking process. Fibres and pulp flocs can decelerate the rise of air bubbles and cause bubble coalescence, and the increased frictional resistance of the pulp fibres can loosen adhering ink particles from the bubbles, resulting in lower ink removal efficiencies (Walmsley, 1992). Bubbles transport pulp fibres into the froth in the flotation cells, which is sent to landfill or is incinerated. In the recycled paper industry, it is desirable to minimize these pulp losses, since the cellulosic fibres in the flotation froth are a loss of raw material (Schwinger, Dobias 1991).

While three-phase systems have been extensively studied in the literature, relatively little is understood about the properties of three-phase wood fibre-liquid-gas systems (Taylor et al. 1994). This lack of knowledge is mainly due to the inherent heterogeneous nature of fibre suspensions, which makes three-phase flow difficult to predict. Unlike other two-phase systems, pulp suspensions form quasi-elastic networks (Schulze 1991; Wahren 1979) and fibres have a tendency to distribute unevenly, forming local mass concentrations, or flocs (Kerekes et al. 1985). The presence of air bubbles further complicates matters, as the flocs interfere with the upwards migration of bubbles, leading to channeling and uneven flow (Walmsley 1992; Ajersch, Pelton 1996; Went et al. 1993; Taylor et al. 1994).

The most widely-accepted mechanism of bubble hold-up in pulp suspensions is bubble-fibre adhesion. Many authors have claimed that bubbles adhere to pulp fibres (Gavelin 1954; Boadway 1956; Sedivy 1969; Kurtz 1978; Isler,Widmer 1978; Karras et al. 1988; Larsson et al.1982; Schwinger and Dobias 1991; Turvey 1993). The phenomenon of bubble-fibre adhesion, however, remains speculative. No photographs showing indisputable evidence of bubbles adhering to fibres have yet been published. Furthermore, receding contact angle measurements of zero have been reported for a wide variety of wood fibres (Hodgson, Berg 1988; Jacob, Berg 1993; Krueger, Hodgson 1994; Krueger, Hodson 1995). Non-zero receding contact angles have been reported in an exceptional case, involving highy-sized fibres (Krueger, Hodson 1995). These results imply that bubbles are unlikely to adhere to most types of wetted pulp fibres.

Other studies indicate that bubble hold-up is affected by factors other than the surface chemistry of the air-water-fibre interface. It has been shown that smaller bubbles tend to remain in pulp suspensions, while larger bubbles tend to escape and rise to the surface (Pelton, Piette 1992; Isler, Widmer 1979). Other factors affecting the retention of air in pulp include the pulp consistency (Pelton, Piette 1992; Walmsley 1992; Went et al. 1993) and the type of pulp furnish (Pelton, Piette 1992; Walmsley 1992; Schulze, Scott 1993). Flow conditions are also important, as bubbles appear to be more easily trapped in quiescent pulp suspensions than in mixed pulps (Pelton, Piette 1992; Ajersch, Pelton, 1996). Recently, it has been suggested that bubble retention in pulp suspension is a function of the strength of the fibre network (Pelton, Piette, 1992; Walmsley, 1992)

Despite the work that has been accomplished to date, very little is known about the fundamental mechanisms by which bubbles and fibres interact. The objective of the present study was to identify the physical mechanisms which affect the migration of bubbles in pulp suspension. This was accomplished by directly examining the behaviour of air bubbles in pulp suspensions in flow visualization studies. The discussion will focus on the effects of flow conditions and flocculation on bubble hold-up. A model for mechanical entrapment in quiescent pulp suspensions will also be presented.

4.2 EXPERIMENTAL

Dried sheets of bleached kraft pulp (BKP) were disintegrated with a Caframo® mixer. Pulp suspensions of $\approx$ 0.3% to 0.6% consistency were prepared. These

consistencies were sufficiently dilute to allow the bubbles in the flow cell to be observed. The pulp suspensions were poured in a Perspex® optical cell (20 cm x 20 cm x 1 cm) and circulated through the cell with a peristaltic pump. Air was entrained into the mixed pulp suspension by constricting the outlet tube above the liquid level of the pulp (Figure 4-1). Images of the circulating pulp were recorded on videotape. The images were digitized and in some cases enhanced with an IBAS (Kontron Electronics) image analysis system. The aerated pulp suspensions were also videotaped under quiescent conditions at high magnification with the aid of a Wild 240 Zoom Macroscope.

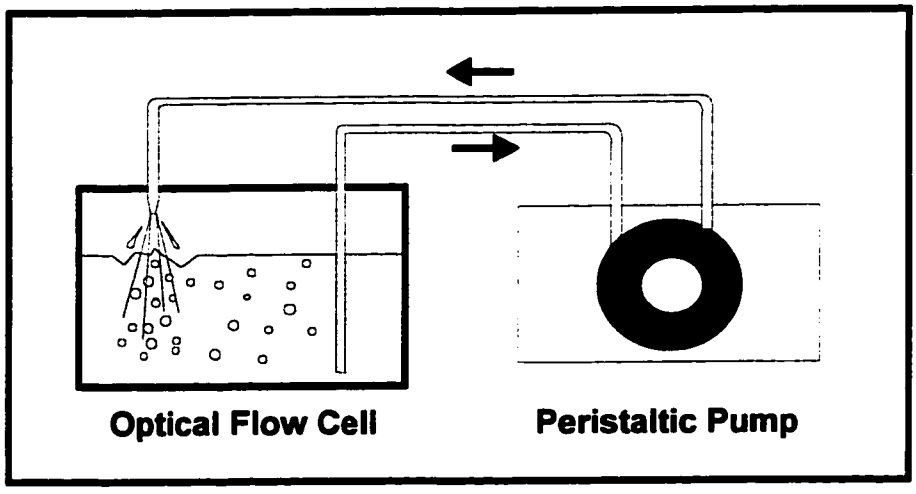

Figure 4-1. Experimental apparatus.

4.3 RESULTS

Quiescent Conditions

Bubble migration through quiescent pulp is illustrated in the high-magnification image of 0.27% consistency BKP in Figure 4-2. The two large bubbles were trapped in the fibre network because the bubble diameters were greater than the inter-fiber void

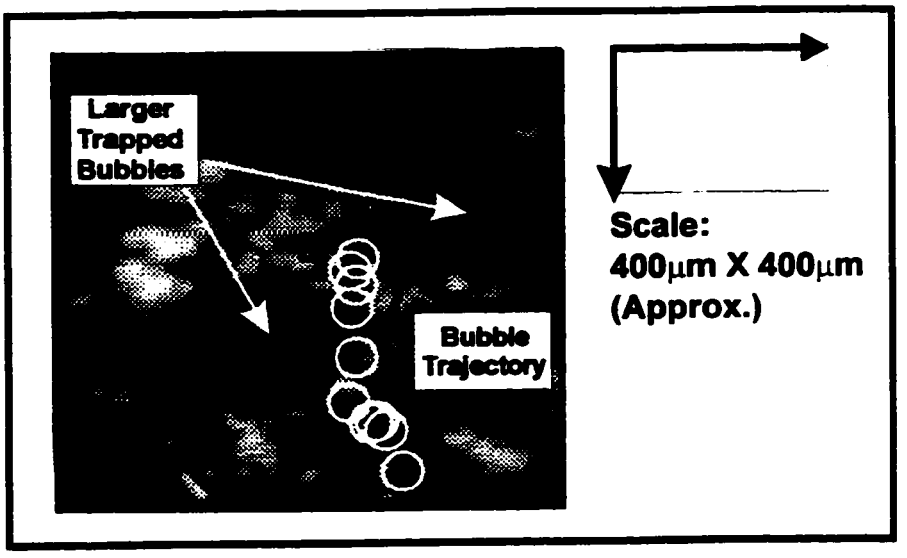

Figure 4-2. Digitzed video image of a quiescent 0.27% consistency bleached kraft pulp suspension at high magnification. The larger bubbles were trapped in the fibre network. A smaller bubble rose between the fibres, from points A to B.

spaces. A smaller bubble, approximately 80 μm in diameter, was observed to migrate from point A to B and come to rest at what appeared to be a localized region of high fibre density. The position of this bubble in each video frame is indicated by the white circles superimposed on Figure 4-2. The bubble followed a tortuous path as it collided with individual fibres and migrated around them. The bubble did not appear to adhere to the fibres.

Flowing Conditions

Figure 4-3 shows a digitized video sequence of a 0.27% consistency BKP in flow. The direction of flow is from right to left. The position of the floc and the bubble are initially outlined in frame 1, and the bubble position in subsequent frames is indicated by the arrow. The corresponding manually-traced outlines of the floc and bubble positions are shown in Figure 4- 4 for clarity.

This example illustrates a common phenomenon that was observed with flocculated pulps in flowing conditions: air bubbles migrated upwards in a series of discrete steps as these bubbles became repeatedly trapped and released from the pulp flocs. In the first few frames of the video sequence (refer to Figure 4-4, frames 1-4), the bubble had not yet contacted the floc, and continued to migrate in both a translational and vertical trajectory. The bubble then collided with the floc and became trapped inside it in (frames 5 to 9) during which time the bubble assumed the flocs' horizontal velocity. In frame 10,

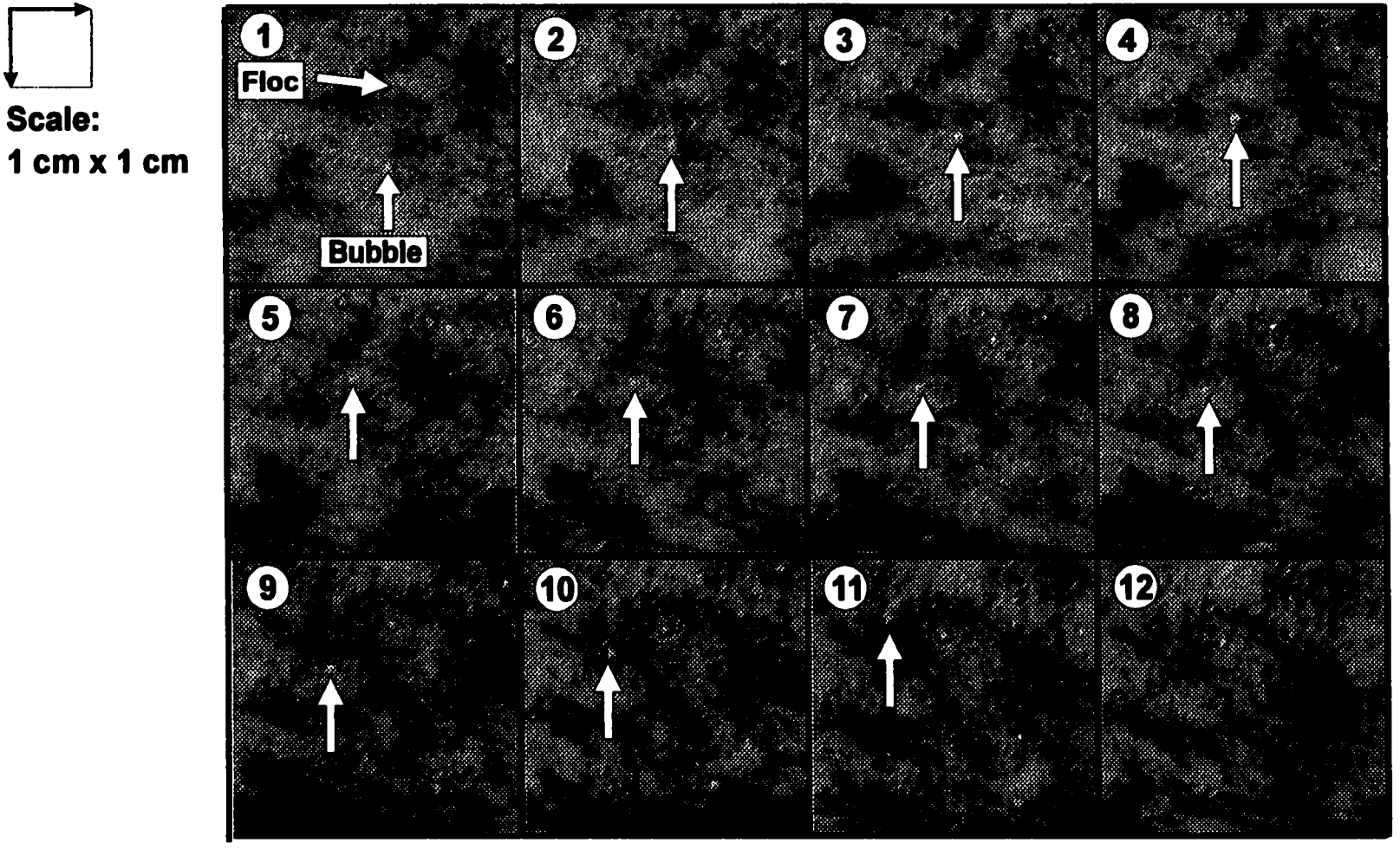

Figure 4-3. Digitized video sequence of a 0.27% consistency bleached kraft pulp in flowing conditions, in which a bubble becomes trapped in a pulp floc. The arrows in each frame indicate the bubble position.

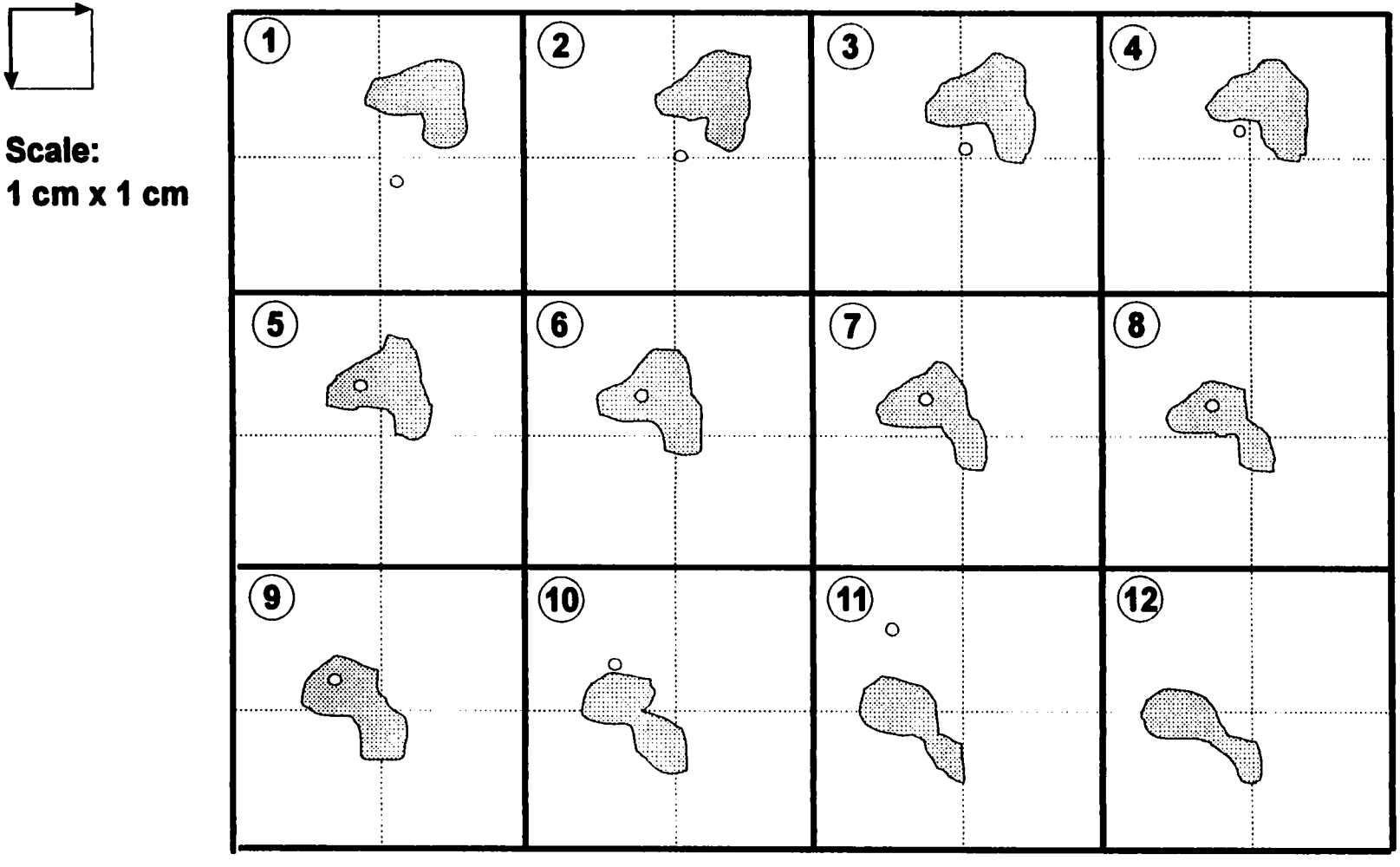

Figure 4-4. Manually-traced outlines of the bubble and floc positions from Figure 4-3. The cross-hairs in each frame indicate the center of each image.

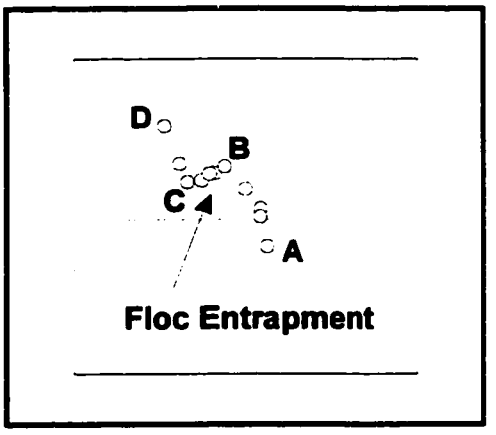

Figure 4-5. Composite image of the bubble positions from Figure 4-4, showing a typical step-like trajectory as the bubble was trapped and released from the pulp floc.

the bubble was released from the floc and continued its upward migration. The bubble positions in frames 1 through 12 are superimposed in Figure 4-5 to demonstrate the bubbles' step-like trajectory. This composite image clearly shows the bubbles' migration before contacting the floc (from A to B), while inside the floc (from B to C) and after being released (from C to D).

The floc outlines in Figure 4-4 reveals that the overall shape of the floc had changed during this entrapment-release sequence. This indicates the presence of shear forces that deformed the floc. (A similar example of floc deformation is illustrated in Figures B-1 and B-2 in Appendix B. The large floc in frame 1 (Figure B-1) gradually became dispersed by the shear forces and broke up into smaller flocs. The bubble remained trapped under this floc until frame 9, after which time the floc structure could no longer retain the bubble).

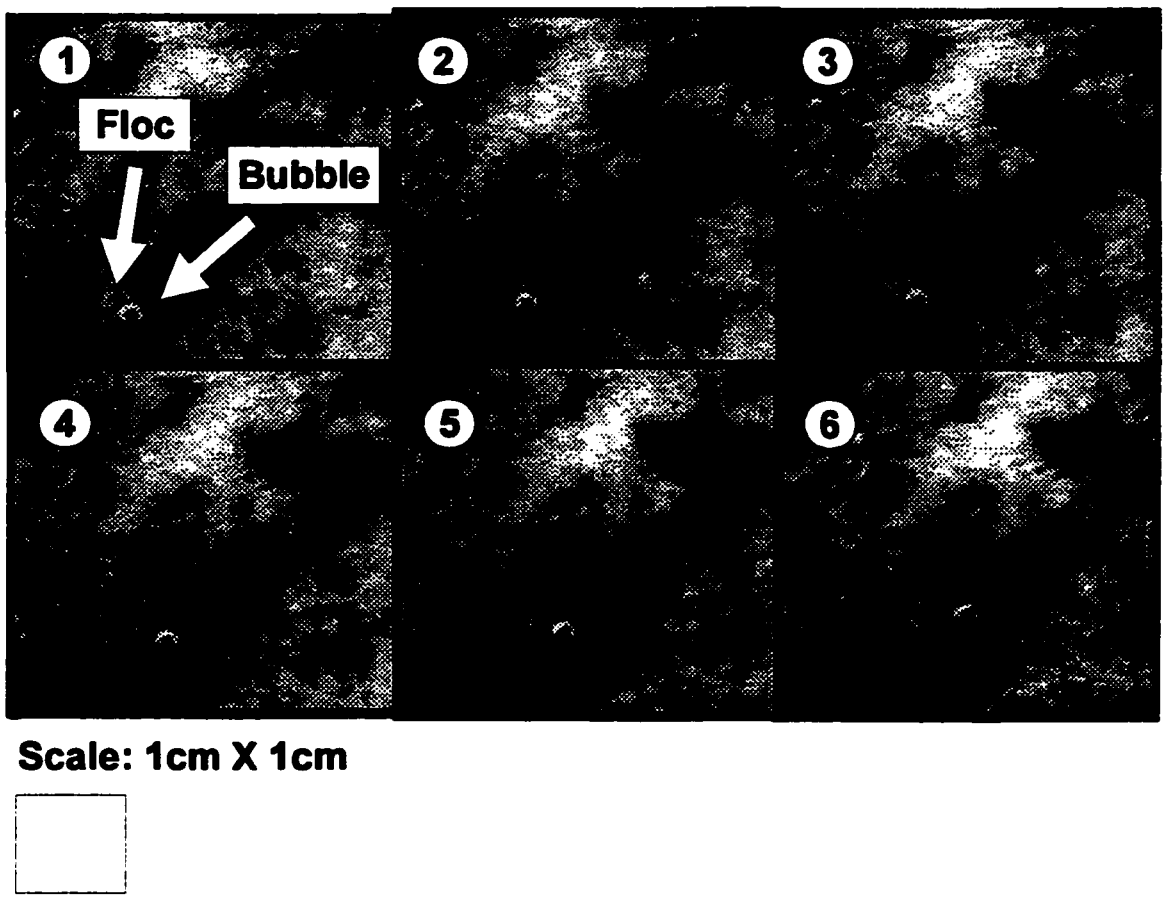

Figure 4-6. Digitally-enhanced video sequence of flowing pulp, showing a trapped bubble being swept out from under a floc.

In some cases, the flocs were strong enough to withstand the shear forces. For example, in Figure 4-6 (frame 1), the arrows indicate a pulp floc and a trapped bubble of the order of several mm in diameter. A composite image indicating the bubble positions from the original video sequence is shown in Figure 4-7. The circles between points A to B correspond to the bubble positions in frames 1 to 6 in Figure 4-6, where the bubble was trapped. From points B to C, the bubble appeared to be swept out from under the floc, during which time the floc structure remained relatively intact. From points C to D, the bubble became trapped again, and assumed the same horizontal velocity as the flowing pulp.

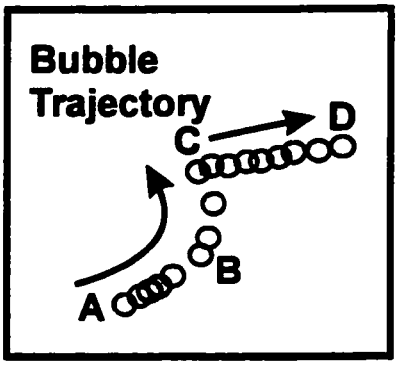

Figure 4-7. Composite image showing the bubble positions from the original video sequence used to illustrate Figure 4-6.

The digitally-enhanced video sequence in Figure 4-8 shows another example of bubble release involving a large bubble. The centimeter-sized bubble indicated by the arrow was slightly distorted as it pressed against the walls of the optical cell. This large bubble broke through the fibre network, leaving behind a channel of relatively fibre-free pulp through which smaller bubbles, of the order of 1 millimeter in diameter, were observed to follow.

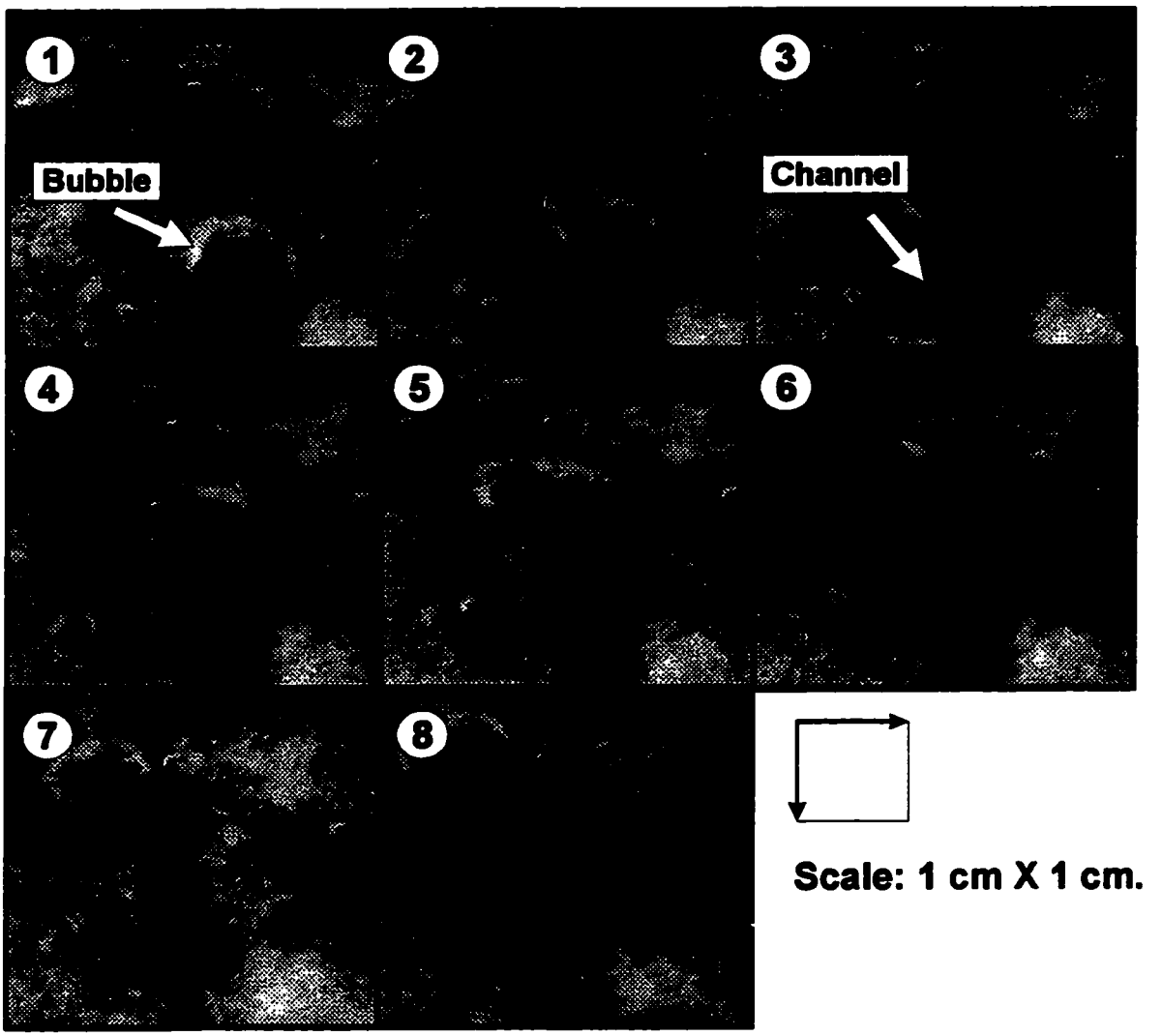

Figure 4-8. Digitally-enhanced video sequence of flowing pulp, which shows a large, cm-sized bubble escaping by breaking through the fibre network. As it migrated upwards, the bubble created a channel in the pulp, through which smaller bubbles were observed to follow.

4.4 DISCUSSION

In this study, bubble-fibre adhesion was not considered as a mechanism of bubble hold-up for the following reasons: bleached kraft pulp consists of mainly cellulose, which is a normally a hydrophilic material. Furthermore, the video sequence in Figure 4-2 shows bubbles colliding with and migrating around individual pulp fibres without adhesion occurring. The primary bubble hold-up mechanism observed in these experiments was attributed to the entangled fibres retaining the bubbles by mechanical forces. Mechanical entrapment was first referred to by Isler and Widmer (1979), who stated that small bubbles remain bound in the fiber network. Pelton and Piette (1992) also attributed bubble hold-up in their experiments with quiescent pulp to mechanical entrapment.

The following discussion will focus on various factors contributing to mechanical entrapment. First, the effects of flocculation and the dimensions of the inter-fibre void spaces will be examined, followed by a summary of the mechanisms of bubble release from flowing pulp suspensions. Two models will then be presented, in which the probabilities of mechanical entrapment are derived for both uniform and flocculated pulp suspensions under quiescent conditions. The first model will then be used to estimate the diameters of mechanically-trapped bubbles in typical headbox pulps.

Bubble Hold-up and Flocculation.

The video sequences show that flocculation plays a key role in bubble hold-up. Bubbles prefer to migrate in the relatively dilute areas between the flocs. The bubbles which do remain in the pulp are retained by mechanical entrapment in the pulp flocs. These observations are consistent with those made in previously-published work. For example, in bubble column experiments, Went et al.(1993) reported that equi-sized pulp flocs formed at 0.3% to 1% consistency. The air flow was channeled around these flocs, which forced the bubbles closer together and reduced gas hold-up. Walmsley (1992) observed that bubbles became trapped beneath flocs or rose between the flocs in the regions of low consistency. This induced flow currents, creating channels through which the majority of the bubbles flowed. At higher concentrations, when the pulp would form a continuous network, bubbles would remain in the pulp and coalesce until a critical bubble size was reached. At this point, the larger bubbles would cleave through the fibre network, forming a channel through which smaller bubbles could pass. Similar observations of this phenomenon were also reported by Taylor et al. (1994) and Ajersch and Pelton (1996). An example of this channeling effect is seen with the large centimeter-sized bubble breaking pulp suspension in Figure 4-8.

The Effect of Void Size Distributions in Pulp Suspensions on Bubble Hold-up

As shown in Figure 4-2, if a bubble is sufficiently small and the pulp sufficiently

dilute, the bubble may migrate through the pulp via the inter-fibre void spaces without disturbing the fibre network. Bubbles become mechanically trapped when they are too large to slip between the inter-fibre void spaces yet are unable to break through the fibre-fibre bonds of the network.

A bubble will continue to migrate through a pulp suspension provided it always encounters void spaces that are larger than its own diameter. The size of the void spaces can be estimated from the theory derived by Ogston (1958). Ogston's (1958) model is based on a random network of uniform, straight fibres of negligible thickness, with the density of the fibre suspension assumed to be uniform. In order for a spherical particle to fit inside the fibre network, Ogston (1958) assumed that the center of the particle must be a distance of at least its own radius away from the nearest fibre. The volume fraction of the fibre suspension that could accommodate spherical particles of radius (r) was derived as:

$$P_D = \exp\left[-\left(2\pi\upsilon L_o r^2 + \frac{4\pi}{3}\upsilon r^3\right)\right] \qquad [4.1]$$

where P_D is the volume fraction of the fibre suspension in which the spherical particles of radius (r) can fit, υ is the average number of fibres centers per cm^3 and L_o is half the fibre length.

Assuming that the volumes of the water and pulp fibres are additive, and that the number of fibre centers per unit volume equals the number of fibres per unit volume, P_D can be re-expressed as:

$$P_D = \exp\left[\frac{-1}{12}\pi C\rho_w\rho_{pulp}D^2\frac{(3L+2D)}{(\rho_{pulp}-C\rho_{pulp}+C\rho_w)(\omega L)}\right] \qquad [4.2]$$

where C is the pulp consistency (expressed as a mass fraction), D is the bubble diameter, L the fibre length and ω the fibre coarseness. The terms ρ_{pulp} and ρ_w are the densities of the pulp fibres and water, which are assumed to be 1.5 g/cm^3 and 1 g/cm^3, respectively. The detailed calculations in deriving Eq. 4.2 are summarized in Appendix D-3.

Some representative values of P_D for pulp consistencies of 0.5% and 2 % are shown in Figure 4-9, assuming fibre coarseness values of ω= 10mg/100m and 25 mg/100m, and a fibre length of L = 2 mm. As the bubble diameter (D) approaches zero, P_D approaches 1, indicating that infinitely small bubbles can fit between all the void spaces in the pulp suspensions. As the D increases, P_D decreases, as larger bubbles are less likely to fit between the fibres. P_D approaches zero for the 0.5% and 2% pulp at bubble diameters of $\approx$ 450 μm and $\approx$ 250 μm, respectively. These values are estimates of the maximum bubble diameters that can fit between the pulp fibres under these conditions.

For pulp suspensions of typical headbox consistencies of (0.5% - 1.0%), reasonable estimates of floc consistencies may fall in the range of (0.5% -2%). According to the calculations shown in Figure 4-9, the size of most of the void spaces in this consistency range are of the order of a tens of microns. This implies that only bubbles of $\approx$10-50 μm in diameter may be able to penetrate a significant distance into the flocs before encountering fibres. Once inside, these bubbles are likely to remain inside the

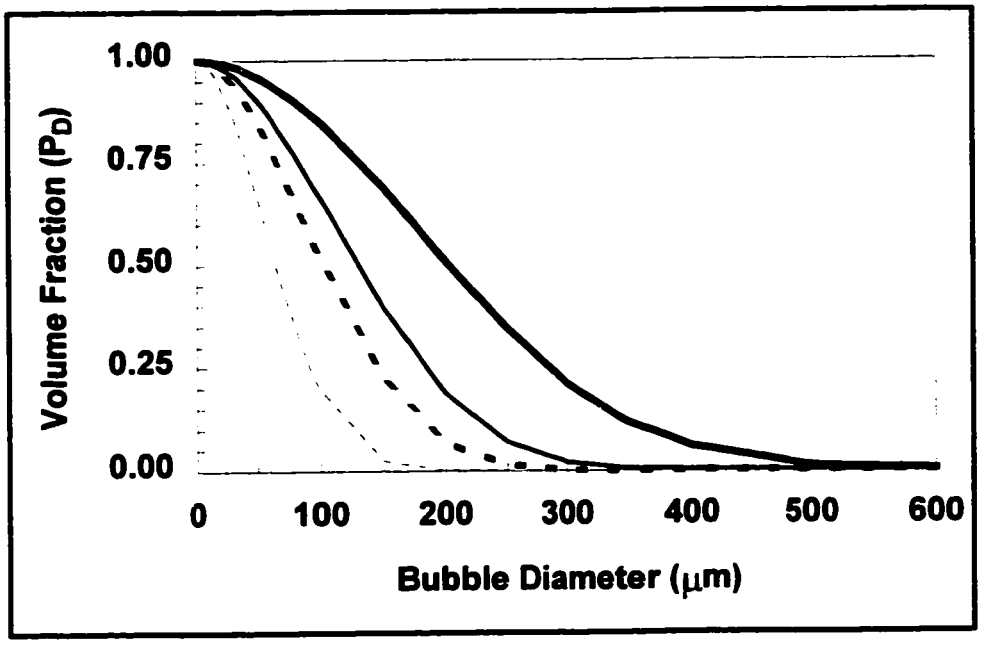

Figure 4-9. Calculated size distributions of the inter-fibre void spaces in uniform pulp suspensions. The x-axis represents the bubble diameter, and the y-axis represents the volume fraction of the pulp suspension in which these bubbles can fit. The curves were calculated from Eq. 4.2, which was derived from the theory presented by Ogston (1958). The data labels indicate the assumed pulp consistencies and fibre coarseness values as follows: [———]: C = 0.5%, ω = 25 mg/100 m. [———]: C = 0.5%, ω = 10 mg/100m; [– – –]: C = 2.0%, ω = 25 mg/100m; [·····]: C = 2.0%, ω = 10 mg/100m.

relatively quiescent fibre network within the floc, provided the floc is not dispersed by shear forces. For larger bubbles in the 100-1000 μm diameter range, the floc may act as a semi-solid sphere rather than a network of discrete fibre. These larger bubbles are more likely to remain on the exterior surface of the floc.

Mechanisms of Bubble Release from Flowing Pulp Suspensions

To date, only one model of bubble migration in flowing pulp has been presented. Isler and Widmer (1979) assumed that bubbles would migrate out of horizontal channels if the velocity of the rising bubbles exceeded the ratio of the channel height divided by the residence time in the channel. This was a simplified model where it was assumed that the fibres did not impede the upward migration of the bubbles. The present work demonstrates that bubble migration in flowing pulp is governed by flocculation. The combined mechanisms of entrapment and release from pulp flocs, which are highly dependent on flow conditions, must also be taken into account.

The various proposed mechanisms by which bubbles are released from pulp flocs are shown in Figure 4-10. These mechanisms are based on observations made from the video sequences presented in Figures 4-2 to 4-8. The simplest method that a bubble may escape is by slipping through the void spaces between individual fibres (Mechanism 1). In order for this to occur, the bubble diameter must be less than the smallest void space between the fibres. An example of this is shown with the small bubble migrating between individual fibres in Figure 4-2.

Bubble escape may also occur by disruption of the fibre network of the floc (Mechanism 2). In this mechanism, bubbles which disrupt flocs may also aid in the release of other bubbles already trapped in the floc. These bubbles may also burrow channels in the pulp, through which smaller bubbles may follow. Mechanisms 1 and 2 occur in both quiescent and flowing pulps.

In flowing pulp suspensions, the presence of shear forces results in additional bubble release mechanisms which do not occur with quiescent pulp. Lee and Brodkey (1987) observed that under turbulent flow conditions, flocs may disperse by deformation, stretching, breaking and fragmentation. These type of phenomena are illustrated in Mechanism 3: the local shear forces disperse the floc over a time interval, resulting in bubble release. An example of this is illustrated in Figures 4-3 and B.1.

Lee and Brodkey (1987) also observed that large-scale turbulence can result in translational motion of the floc, resulting in relative velocity gradients between the floc and the surrounding fluid. These shear forces acting at the bubble-floc interface can therefore cause detachment of bubbles from under a floc, as shown in Mechanism 4. The extent to which Mechanisms 3 and 4 enhance bubble release depends on both the stability of the individual pulp flocs and the relative motion between pulp flocs.

Pulp flocs can be characterized as "transient' or "coherent" (Kerekes et al. 1985). Transient flocs are of a temporary nature: these may form and re-disperse when subjected to shear. Flocs are considered to be coherent when their structure is maintained in the flow in which they are formed (Kerekes, Schell 1992). Coherent flocs form from transient flocs in conditions decaying turbulence (Kerekes 1983; Kerekes et al. 1985), which may occur downstream of pumps, in pipes leading from mixed reservoirs and in rectifier rolls in headboxes (Kerekes et al. 1985). Examples of both these types of flocs were observed in this study. The flocs in Figure 4-3 and Figure B-1 appeared to be transient because the floc shapes changed under conditions of shear. The floc in Figure

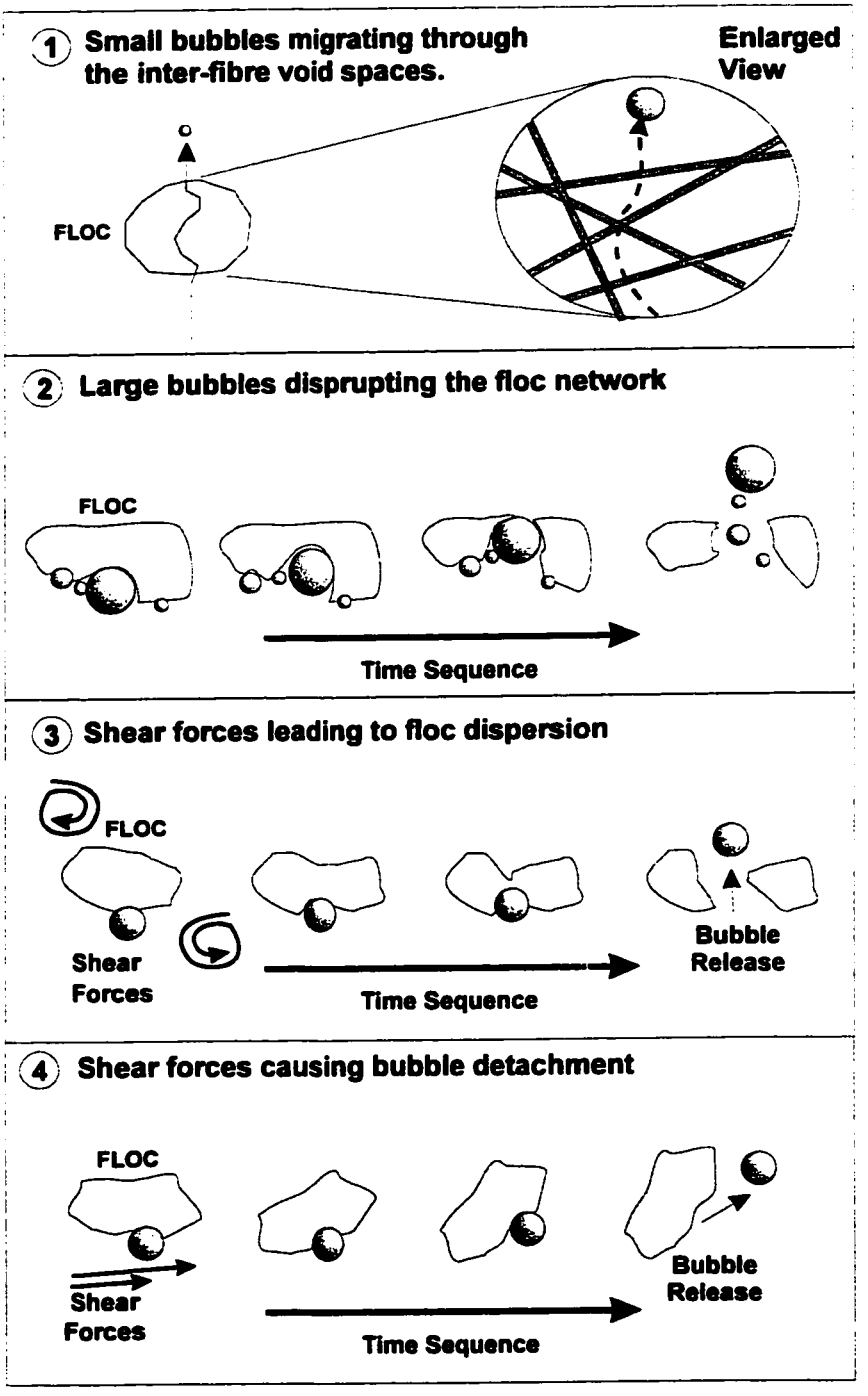

Figure 4-10. Bubble release mechanisms in flocculated pulp suspensions. Release mechanisms (1) and (2) may occur in both quiescent and flowing pulps, while release mechanisms (3) and (4) only occur in flowing pulps.

4-6 appeared to be coherent, as it remained relatively intact, even after the trapped bubble was released.

The tendency towards flocculation depends the relative proximity between individual fibres. Kerekes and Schell (1992) characterized flocculation by the "crowding factor", which corresponds to the number of fibres contained within the rotational sphere of influence of a single fibre. The crowding factor (N) can be approximated as:

$$N \approx \frac{5CL^2}{\omega} \frac{kg}{m^3} \qquad [4.3]$$

where C is the pulp consistency expressed in %, L is the fibre length expressed in meters, and ω is the fibre coarseness expressed in kg/m. Three regimes of flocculation are described by Kerekes and Schell (1992). When ($N < 1$) fibres are free to move relative to one another, and no flocculation occurs. For fibres with large length-to-diameter ratios, flocs form at ($1 < N < 60$), but these flocs are easily dispersed by hydrodynamic forces. Coherent flocs occur in the range of ($60 < N < 130$). Under these conditions, flocs adopt mechanical strength and are difficult to disperse. Mechanical entrapment is expected to occur when $N > 1$. Based on this theory, in flowing pulp, bubbles are likely to be released by Mechanisms 1, 2 and 3 when ($1 < N < 60$), and by Mechanisms 1, 2 and 4 when

($60 < N < 130$).

The relative contributions of Mechanisms 3 and 4 to bubble release also depends on the relative motion between the flocs. For pulp suspensions in pipe flow, three flow regimes are known to occur (Forgacs et al. 1958). At low flow rates, fibres migrate away

from the pipe wall and move in plug flow, and an annulus of clear water forms between the pipe wall and the pulp network surface. As the flow rate is increased, the flow is designated as "mixed". The annulus becomes turbulent and the plug structure becomes dispersed and breaks down. At higher flow rates, the plug disappears, and the pulp suspension is considered to be "turbulent". In a sufficiently turbulent pulp suspension, the individual flocs and fibres move relative to one another in a similar fashion to fluid elements: in such cases, the pulp may be termed "fluidized" (Kerekes et al. 1985).

When plug flow conditions exist in pipes, the flocs are motionless relative to one another. Mechanical entrapment can be considered to occur under "quiescent" conditions and the bubbles will likely be released by Mechanisms (1) and (2). No mechanical entrapment is expected for bubbles in the fibre-free area outside the plug flow regime. This was confirmed by Isler and Widmer (1979): in horizontal pipe flow, bubbles near the edges of the tube migrated upwards along the pipe wall.

When a bubble rises through a "fluidized" pulp suspension, Mechanisms 3 and 4 become significant. As the rising bubble contacts a floc, two outcomes are possible. In one case, the bubble becomes mechanically trapped in the floc and assumes the flocs' velocity. In the other case, the bubble escapes from the floc by one or a combination of the release mechanisms shown in Figure 4-9, and continues to rise. This process of entrapment-release repeats itself until the bubble either becomes permanently trapped in the suspension, or reaches the surface in a series of random, discrete steps, an example of which is shown in Figure 4-5.

A Model for Mechanical Entrapment in Quiescent, Uniform Pulp

It is assumed that there are two principal mechanisms by which bubbles migrate through pulp suspensions. If sufficiently small, bubbles may migrate by slipping between the inter-fibre void spaces without disrupting the fibre network. When bubbles are larger than the inter-fibre void spaces, bubble migration cannot occur unless the fibre-fibre bonds are broken. The probability of a bubble becoming mechanically trapped in given pulp suspension depends on several factors, including bubble size, the pulp consistency and the distance traveled by the bubble.

We first consider the case of bubble migration via the inter-fibre void spaces. In order for a bubble to travel through a pulp suspension by a distance equivalent to its own diameter, it must encounter a void space which are larger than itself. The probability of this occurring is assumed to equal P_D from Eq. 4.2. In order to travel a given distance (H), the bubble must pass through (H/D) equivalent diameters. The overall probability migrating through H via the inter-fibre void spaces (designated as P_S) can be approximated as:

$$P_S = P_D^{(H/D)} \qquad [4.4]$$

Next, the probability a bubble migration by breaking the fibre-fibre bonds is considered. Evidence suggests that this phenomenon is related to the buoyancy force of the bubble and the pulp network strength. For example, in bubble hold-up experiments with quiescent pulp, Pelton and Piette (1992) correlated the minimum buoyancy pressures for bubble escape to estimates of the yield stress of the fibre network. Based on

qualitative observations of bubble hold-up in a pulp column, Walmsley (1992) also proposed that bubbles remain in pulp until the buoyancy pressure equals the disruptive shear stress property of the fibre network.

The buoyancy pressure of a bubble is obtained by dividing the buoyancy force of the bubble by the surface area over which the buoyancy force is acting. The magnitude of the buoyancy force of a bubble of diameter (D) acting upward is given by:

$$F_b = \frac{\pi D^3}{6} g(\rho_w - \rho_{air}) \qquad [4.5]$$

where g is the acceleration due to gravity, ρ_w is the density of water and ρ_{air} is the density of air. Neglecting the air density (since $\rho_w >> \rho_{air}$) and assuming the surface area of interest to be half area of the spherical bubble, the bubble buoyancy pressure (τ_b) can be estimated as:

$$\tau_b = \frac{1}{3} D g \rho_w \qquad [4.6]$$

According to Pelton and Piette (1992), a bubble will escape (i.e. migrate to the surface) when the buoyancy pressure exceeds the yield stress of the pulp. Following this approach, the probability of bubble escape by breaking through (or disrupting) the fibre network (P_B) is given by:

$$P_B = (\tau_b > \tau_y) \qquad [4.7]$$

where τ_y is the yield stress of the pulp suspension. From experimental measurement, τ_y can be correlated in terms of pulp consistency (Bennington et al. 1990):

$$\tau_y = a\, C^{\,b} \qquad [4.8]$$

where a and b are empirical constants. Combining Eqs. 4.6, 4.7 and 4.8 gives:

$$P_B = (\tau_b > \tau_y) = (\frac{1}{3} D g \rho_w > a\, C^{\,b}) \qquad [4.9]$$

where P_B is assumed to be a binary probability function. P_B can only have two values, and it is independent of the distance the bubble has to travel. For example, if the buoyancy pressure exceeds the yield stress ($\tau_b > \tau_S$) the bubble will escape and $P_B = 1$. If the buoyancy pressure is less than the yield stress ($\tau_b < \tau_S$) the bubble remain trapped in the pulp suspension and $P_B = 0$.

The overall probability of bubble migrating (or "escaping") through a pulp suspension is expressed as a combination of the probabilities of migrating via the inter-fibre void spaces (P_S) and by disruption of the fibre network (P_B).

$$P_{esc}(L,D,C,\omega,a,b,H) = P_S\,(1 - P_B) + P_B \qquad [4.10]$$

where the escape probability (P_{esc}) is a function of the parameters L, D, C, ω, a, b and H. Equation 4.10 is expressed in the manner shown above because P_S and P_B are mutually exclusive. If a bubble can escape by disrupting the fibre network, the contribution of escape by slipping between the fibres is irrelevant, and P_{esc} becomes a function on P_B. On the other hand, if a bubble is unable to disrupt the fibre network, then $P_B = 0$ and P_{esc} depends only P_S. The probability of a bubble remaining in the pulp (mechanical entrapment) is equal to $(1 - P_{esc})$:

$$P_{t,q}(L,D,Cm,\omega,a,b,H) = 1 - P_{esc}(L,D,C,\omega,a,b,H) = [\,1 - (P_S\,(1- P_B) + P_B)\,] \qquad [4.11]$$

where $P_{t,q}$ is defined as the probability of mechanical entrapment in a quiescent, uniform pulp.

Mechanical Entrapment in Quiescent, Flocculated Pulp Suspensions.

Equations 4.10 and 4.11 represent a simplified case of mechanical entrapment, because they apply to a homogenous suspension of uniform pulp fibers. In actual pulp suspensions, areas of high fibre density exist within the flocs and areas of dilute pulp exist in the inter-floc regions. It is assumed that most of the mechanical entrapment occurs in the flocculated portion of the pulp suspension. The amount of mechanical entrapment in the inter-floc regions of the pulp suspension is considered to be insignificant compared to that in the flocculated regions.

Consider the probability of a bubble being trapped in the quiescent flocculated pulp suspension shown in Figure 4-11. This represents an idealized pulp suspension, where the flocs are assumed to be cubic in shape with a height of (D_{Floc}). The total height of the pulp suspension (H_{Tot}) is divided into "n" horizontal layers of thickness D_{Floc}. The flocs are considered to be randomly distributed in each horizontal layer. In order for a bubble to be trapped by the pulp suspension, it must first collide with a floc and then become trapped within it. The probability of a bubble becoming trapped in a single layer of thickness D_{Floc} equals:

$$P_{t,DFloc} = P_c P_{tFloc} \qquad [4.12]$$

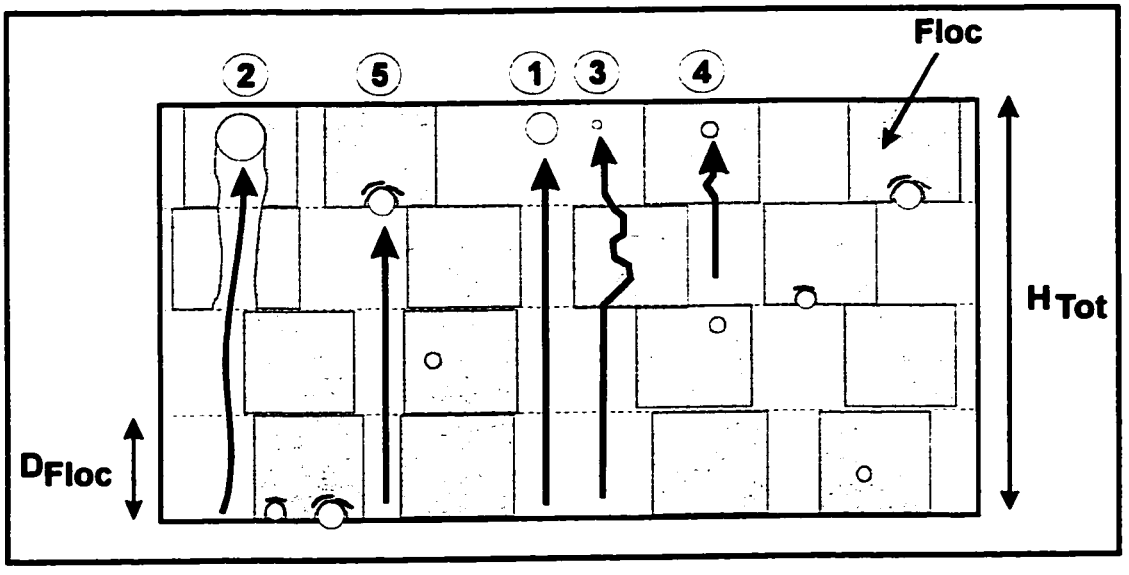

Figure 4-11. Proposed mechanisms of bubble migration through a quiescent, flocculated pulp suspension. Bubbles escape from the pulp suspension when no flocs are encountered (1), when large bubbles break through flocs (2), or when small bubbles migrate through the flocs via the inter-fibre void spaces (3). Mechanical entrapment occurs when the bubbles are too large to migrate through the flocs (4) and/or when the buoyancy pressure of the bubbles is insufficient to break through the flocs (5).

where P_c is the probability of collision with a floc, and P_{tFloc} is the probability of entrapment within a single floc. The overall probability of mechanical entrapment within the entire pulp suspension becomes $[P_{tDFloc}]^n$, where $n = (H_{Tot}/D_{Floc})$. Substituting this into Eq. 4.12 gives:

$$P_t = \left[P_c\, P_{tFloc}\right]^{\left(\frac{H_{Tot}}{D_{Floc}}\right)} \qquad [4.13]$$

In each layer, the probability of collision (P_c) is assumed to be the surface area fraction covered by the flocs. For cubic flocs, this equals the volume fraction the pulp which is flocculated (ϕ_f):

$$P_c = \phi_f = f(C) \qquad [4.14]$$

where the parameter ϕ_f is yet to be determined. However, the value ϕ_f is likely to be a function of the overall consistency of the pulp suspension (C), because no flocs exist when $C \approx 0$, and pulp suspensions are almost completely flocculated when C becomes large. The term P_{tfloc} can be estimated from Eq. 4.11:

$$P_{tfloc} = P_{t,q}(L, C_{Floc}, D, a, b\, D_{floc}) \qquad [4.15].$$

where Eq. 4.15 represents the probability of mechanical entrapment in uniform fibre suspension of thickness D_{Floc}, and of floc consistency C_{Floc}. This is based on the assumption that the consistency of the flocs is uniform and constant.

In a pulp suspension, the areas of highest fibre concentration exist, by definition, within the pulp flocs. The minimum bubble diameter required for a 100% probability of escape can be estimated by setting the buoyancy pressure of the bubble to be greater than the yield stress of the strongest pulp floc:

$$\tau_b > \tau_{Floc} \qquad [4.16]$$

Assuming that $\tau_{Floc} = aC_{Floc}^{\ b}$, and substituting in Eq. 4.6 into Eq. 4.16 and solving for D gives:

$$D_{min} = \frac{3aC_{Floc}^{\ b}}{g\rho_w} \qquad [4.17]$$

If the conditions in Eq. 4.17 are met, the probability of mechanical entrapment will always be zero. There would be 100% chance of bubble escape, regardless of a how flocculated the pulp suspension is, or distance though which the bubble must travel. This suggests that the largest bubble diameter found in aerated pulp suspensions may be an indication of the yield stress of the strongest pulp flocs.

Given the present state of knowledge, it is only possible to predict mechanical entrapment in flocculated pulp at the two extremes of flocculation. For extremely dilute pulps where the fibres are dispersed and no flocs exist, there is a 100% probability of bubble escape, because $\phi_f = P_c = 0$. At very high consistencies, the pulp suspension can be considered to be a single, large floc, with the floc consistency (C_{Floc}) approaching the overall consistency (C), with values of $\phi_f = P_c = 1$. Under these conditions, the pulp may be considered uniform, and the probability of mechanical entrapment may be approximated by Eq. 4.11.

For pulps between the two extremes of flocculation ($0 < \phi_f < 1$), bubble escape may occur by several mechanisms, such as disrupting the fibre network of the flocs, passing through void spaces in the flocs, or avoiding collision with flocs altogether (as illustrated in Figure 4-11). Predicting which of these release mechanisms is dominant requires knowledge of the floc properties. There are presently no theories or experimental results relating the floc consistencies (C_{Floc}) and floc volume fractions (ϕ_f) to

the overall pulp consistency (C_m) . This information would be valuable for predicting bubble hold-up in quiescent, flocculated pulp.

Estimating the Size Distributions of Mechanically-Trapped Bubbles.

In the literature, air bubbles in pulp suspensions are generally divided into two categories: bubbles which spontaneously migrate out of the stock and dissipate, and bubbles that remain in the pulp suspension (Gavelin 1954; Boadway 1956; Sedivy 1969; May, Buckman 1975; Kurtz 1978; Woodworth 1990). While measurements of bubble sizes in pulp suspensions have only been reported in a few cases, the results suggest that only a certain range of bubble sizes are retained in pulp suspensions. For headbox pulps, the division between bubbles which escape and those which remain trapped appears occur at bubble diameters of the order of a few hundred microns. Boadway (1956) stated that bubbles in headbox pulps larger than ≈ 800 μm rise quite rapidly to the surface, while smaller bubbles are swept down the slice. Ajersch et al. (1992) measured bubble size distributions in paper machines for 0.6-0.8% consistency newsprint. The bubbles diameters ranged from 0-400 μm, with most of the bubble diameters being within 25-200 μm. With headbox pulp from a tissue machine, Isler and Widmer (1979) reported that bubbles of 80-300 μm in diameter tended to migrate out of the pulp, while bubbles of 60-80 μm bubbles remained in the fibre network.

The approximate size range of bubbles found in headbox pulps can be explained by the mechanical entrapment model. Assuming that the majority of bubbles are trapped

by flocs, then the bubble dimensions trapped in one floc should be representative of the bubbles retained in the bulk pulp suspension. Bubble sizes can therefore be estimated from the probability of entrapment in a single, quiescent floc (P_{tFloc}) as described by Eq. 4.15.

P_{tfloc} is plotted versus bubble diameter in Figure 4.12, assuming values of L = 2 mm, ω = 25 mg/100m and for bubble diameters ranging from 1 to 1000 μm. A floc diameter of 5 mm was assumed, based on Kerekes and Schell's (1995) observations that floc diameters are approximately 2 times the fibre length. The calculations were made for semi-bleached kraft (SBK) and thermomechancial pulp (TMP), assuming floc consistencies of 0.5% and 2% consistency. The range of consistency was chosen to represent floc consistencies expected in (0.5% - 1%) headbox pulps. The empirical constants (a and b) for the SBK and TMP were taken from the experimental yield stress measurements reported by Bennington et al. (1990), with $a = 3.12 \times 10^6$ Pa and b = 2.79 for the SBK, and $a = 1.38 \times 10^7$ Pa and b = 3.56 for the TMP.

Upon examining Figure 4-12, at 2% consistency P_{tfloc} =1 for most of the range of bubble diameters, for both the SBK and TMP pulps. This implies that most bubbles will become trapped in 2% pulp flocs, with only the bubbles of the order of ≈ 10-20 μm in diameter having a finite chance of escaping. For the 0.5%, pulp, P_{tfloc} equals zero for (D > ≈ 400 μm) for the SBK, and (D > ≈ 30 μm) for the TMP. These correspond to the critical bubble escape diameters, above which all bubbles will escape from the floc. The minimum bubble escape diameter is lower for the TMP, since this pulp has a lower

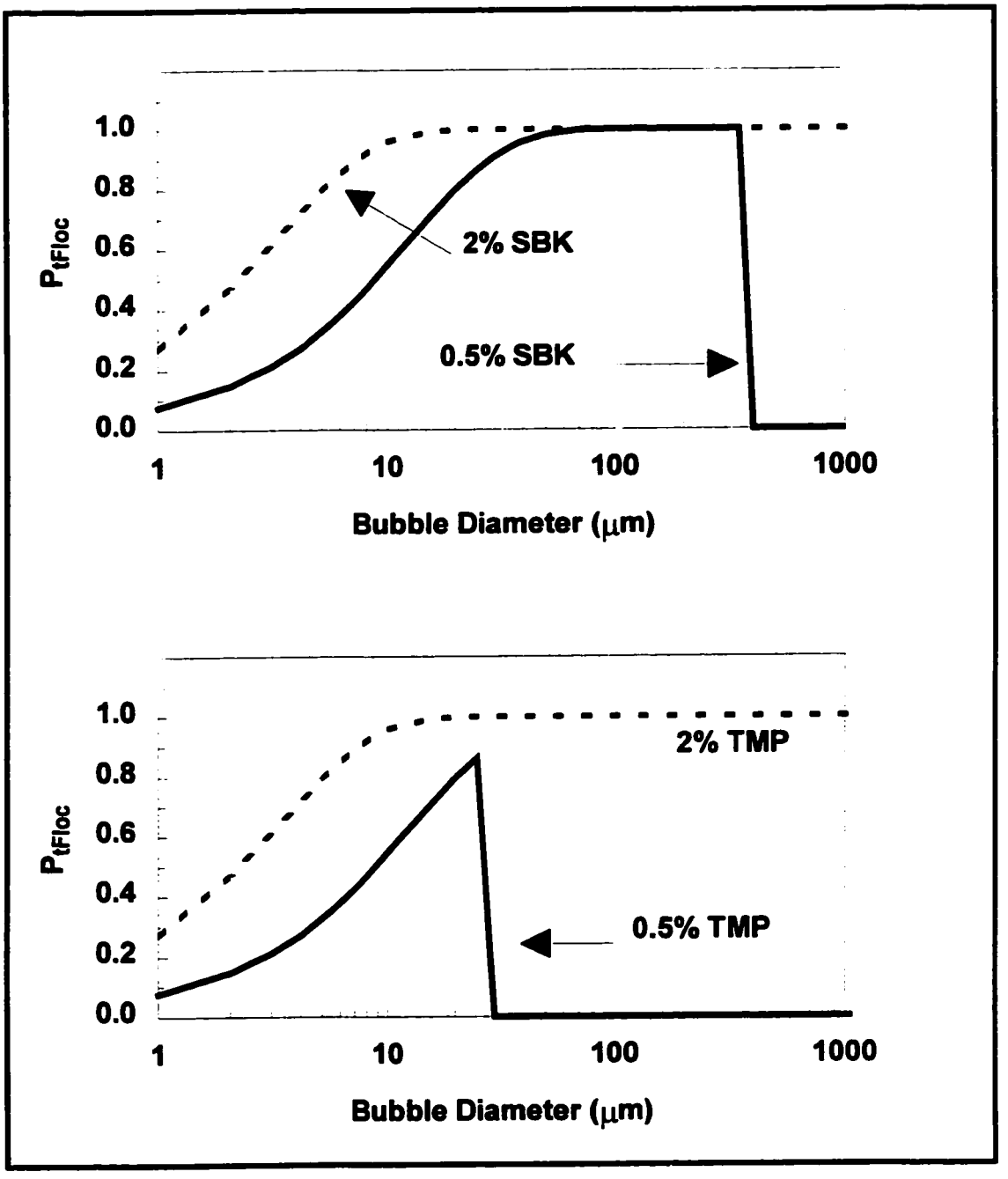

Figure 4-12. Estimated probabilities of mechanical entrapment in pulp flocs (P_{tFloc}) versus bubble diameter, for bubbles migrating through 5 mm pulp flocs of 0.5% and 2% consistency. The estimates of P_{tfloc} were calculated using experimental yield stress measurements for thermomechanical pulp (TMP) and semi-bleach kraft (SBK) reported by Bennington et al. (1990)

network strength than the SBK. In the 0.5% TMP, bubbles less than 30 μm are trapped, with the probability of entrapment being greatest with the 30 μm bubbles. For 0.5% SBK, there is an optimum range of diameters in which bubbles have a 100% probability of being trapped, corresponding to (50 μm < D < 400 μm). The estimated diameters of the trapped bubbles are in approximate agreement with reported bubbles size found in headbox pulps.

This model for mechanical entrapment is only an estimate, since it is based on several assumptions. The yield stress measurements of Bennington et al. (1990) were arbitrarily chosen for the calculations. Typical yield stress values measured by other methods may span an order of magnitude, which will affect the estimates of the trapped bubble diameters. Furthermore, yield stress measurements usually apply to the entire pulp suspension, and do not necessarily represent the yield stress of the individual pulp flocs. The present model, however, explains qualitatively why bubbles of intermediate size are the most likely to become mechanically trapped in pulp. With small bubbles having low a buoyancy pressure, the probability of escape by disrupting the fibre network may be zero, but escape may still occur by migration between the inter-fibre void spaces. Large bubbles which cannot migrate between the fibres escape by disrupting the fibre network.

4.5 CONCLUSIONS:

- Small bubbles (with diameters of a few tens of μm) can penetrate the floc by migrating between the inter-fibre void spaces within the floc to become mechanically trapped in a localized region of high fibre density within the floc.

- Large bubbles (with diameters larger than a few hundred μm) cannot penetrate flocs without disrupting the fibre-fibre bonds in the floc. These larger bubbles are more likely to become trapped at the exterior surface of pulp flocs rather than inside the flocs.

- Bubbles become mechanically trapped when the bubble diameter is greater than the dimensions of the inter-fibre void spaces, and when the buoyancy pressure of the bubble is less than the yield stress of the fibre network. The minimum requirement bubble release is that the buoyancy pressure of the bubble exceeds the yield stress of the strongest pulp floc.

- In mixed pulp suspensions, the probability of mechanical entrapment is greatly reduced by shear forces which disperse transient pulp flocs and detach trapped bubbles from coherent pulp flocs.

- In a turbulent pulp suspension, bubbles migrate upwards in random steps, as they are repeatedly trapped and released by the pulp flocs.

REFERENCES

AJERSCH, M., PELTON, R., TOWERS, M. and LOEWEN, S. "The Characterization of Dispersed Air in Two Newsprint Paper Machines", *J. Pulp Paper Sci.* 18(4):J121-J126 (1992)

AJERSCH, M. and PELTON, R.H. "The Study of Fibre Losses in Flotation Deinking Through the Characterization of Bubble Entrapment in Flowing Pulp Suspensions". *44th Canadian Chem. Eng. Conf. (List of Abstracts)* 383-384 (1994).

AJERSCH, M.J. and PELTON, R.H. "Mechanisms of Pulp Loss in Flotation Deinking", *J. Pulp Paper Sci.* 22(9):J338-J345 (1996).

BENNINGTON, C.P.J., KEREKES, R.J. and GRACE, J.R. "The Yield Stress of Fibre Suspensions", *Can. J. Chem. Eng.* 68:748-757 (1990).

BENNINGTON, C.P.J. "Mixing Gases into Medium-Consistency Pulp Suspensions Using Rotary Devices", *Tappi J.* 76(7):77-86 (1993).

BOADWAY, J.D. "Gas in Papermaking Stock". *Pulp Paper Mag. Can.* 57(3): 185-194 (1956).

FORGACS, O.L., ROBERTSON, A.A. and MASON, S.G. "The Hydrodynamic Behaviour of Paper Making Fibres", Pulp Paper Mag. Canada, 117-128 (1958).

GAVELIN, G. "Some Effects of Gases on Properties of Fibre Suspensions", *Can. Pulp Paper assoc. Tech. Sect. Proc.* 1954:240-248 (1954).

HODGSON, K.T. and BERG, J.C. "Dynamic Wettability Properties of Single Wood Pulp Fibers and Their Relationship to Absorbency" *Wood and Fiber Science* 20(1):3-17(1988).

ISLER, W. and WIDMER, F. "Creation and Removal of Air Bubbles from Technical Stock Suspensions. Part 1: Gaseous Air Content of Paper Stock Suspensions in Closed White Water Systems", *Papier* 32(11):473-477 (1978)

ISLER, W. and WIDMER, F. "Creation and Removal of Air Bubbles From Technical Paper Stock Suspensions. Part 2: Bubble Separation from Pulp Suspensions in Closed and Open Flow Channels", *Papier* 33(3):89-93 (1979).

JACOB, P.N. and BERG, J.C. "Zisman Analysis of Three Pulp Fiber Furnishes", *Tappi J.* 76(2):105-107 (1993).

KARRAS, M., PIETIKAINEN, T., KORTELAINEN, H. and TORNBERG, J. "Ultrasonic Measurement of Gaseous Air in Pulp Suspensions" *Tappi J.* 71(1):65-69 (1988).

KEREKES, R.J. "Pulp Flocculation in Decaying Turbulence: A Literature Review". *J. Pulp Paper Science*, TR88-TR91, (July, 1983).

KEREKES, R.J., SOSZYNSKI, R.M. and TAM DOO, P.A. "The Flocculation of Pulp Fibres", *Papermaking Raw Materials. Transactions of the 8th Fundamental Research Symposium (Oxford)* 265-309 (1985).

KEREKES, R.J. and SCHELL, C.J. "Characterization of Fibre Flocculation Regimes by a Crowding Factor", *J. Pulp Paper Science* 18(1):J32-J39 (1992).

KEREKES, R.J. and SCHELL, C.J. "Effects of Fiber Length and Coarseness on Pulp Flocculation", *Tappi J.* 78(2):133-139 (1995).

KRUEGER, J.J. and HODGSON, K.T. "Single-fiber Wetabiltiy of Highly Sized Pulp Fibers", *Tappi J.* 77(7):83-87 (1994).

KRUEGER, J.J. and HODGSON, K.T. "The Relationship Between Single Fibre Contact Angle and Sizing Performance", *Tappi J.* 78(2);154-161 (1995).

KURTZ K.D. "Deaeration: Some Practical Applications and Benefits for Pulp and Paper Mills" *Tappi Eng. Conf. Proc.* 349, (1978).

LARSSON, A., STENIUS, P. and STRÖM, G. "Surface Chemistry of the Deinking Process", *Wochbl. Papierfabr.* 14:502-506 (1982).

LEE, C.W. and BRODKEY, R.S. "A Visual Study of Pulp Floc Dispersion Mechanisms", *AIChE J.* 33(2):297-302 (1987).

MAY, O.T. and BUCKMAN, S.J. "Practical Effects of Air in Papermaking", *Tappi* 58(2):90-94 (1975).

OGSTON, A.G. "The Spaces in a Uniform Random Suspension of Fibres", *Trans. Faraday Soc.* 54: 1754-1757 (1958).

PELTON, R.H. and PIETTE, R. "Air Bubble Hold-up in Quiescent Wood Pulp Suspensions", *Can. J. Chem. Eng.* 70:660-663 (1992).

SCHWINGER, K. and DOBIAS, B. "The Influence of Calcium Ions on the Loss of Fibre in the Flotation Deinking Process", *1st. Research Forum on Deinking* 1-11 (1991).

SCHULZ, E.R. and SCOTT, W.E. "Analysis of Air Entrainment by Secondary Fibres", *Tappi J.* 76(2):147-155 (1993).

SCHULZE, H.J. "The Fundamentals of Flotation Deinking in Comparison to Mineral Flotation" *1st Research Forum on Recycling* 161-167 (1991).

TURVEY, R.W. "Why do Fibres Float?", *J. Pulp Paper Sci.* 19(2):J52-J57 (1993).

SEDIVY, O. "Air, an Important Factor in Paper Manufacture", *Zellstoff und Papier* 18:112-118 (1969).

TAYLOR, K.E., GHIAASIAAN, S.M., ABDEL-KHALIK, S.I., LINDSAY, J.D., and GEORGE, J. "Macroscopic Flow Structures in a Bubbling Paper Pulp-Water Slurry", *IPST Technical Paper Series Number 537. Institute of Paper Science and Technology, Atlanta, Georgia* (1994).

WAHREN, D. "Fiber Network Structures in Papermaking Operations", *Paper Science and Technology. The Cutting Edge. Conf. Proc.* 112-129 (1979).

WALMSLEY, N.N.W. "Air Bubble Motion in Wood Pulp Fibre Suspension", *APPITA* 45:509-515 (1992).

WENT, J., JAMIALAHMADI, M. and MULLER-STEINHAGEN, H. "Effect of Wood Pulp Fibre Concentration on Gas Hold-up in Bubble Columns", *Chem. Ing. Tech.* 65(3):306-308 (1993).

WOODWORTH, M.D. "Comparison of Practical Methods for Air-in-Stock Measurements" *Tappi J.* 70(11):135-138 (1990).

CHAPTER 5

MECHANISMS OF PULP LOSS IN FLOTATION DEINKING

Michael Ajersch and Robert Pelton

Published in the Journal of Pulp and Paper Science 22(9): J338-J345 (1996).

ABSTRACT

The objective of this study was to investigate the effects of pulp type, consistency and bubble size on the flotation of pulp fibres and fines. Laboratory-scale batch flotation experiments were conducted using bleached kraft and mechanical pulp in the presence of sodium dodecyl sulfate. Pulp losses were linearly dependent on the recovery of water in the foam. These pulp losses were generally greater with small bubbles (~100-400 μm) and with the mechanical pulp. With dilute pulp suspensions, the consistencies of the foam and the feed were similar. For more concentrated pulp suspensions, the consistencies of the foams were less than those of the feed, and pulp fines tended to be concentrated in the foam. The primary pulp loss mechanism was entrainment, in which pulp fibres and fines were hydraulically transported into the foam with the water. Two regimes of entrainment are possible, depending on the extent of flocculation. In the absence of flocculation, the individual loose fibres and fines from the bulk pulp suspension are carried into the foam. When the pulp is flocculated, the bubbles are

diverted around the flocs, and entrain the smaller fibres and fines from the more dilute, inter-floc regions.

5.1 INTRODUCTION

In most flotation deinking cells, between 5-12% of the pulp mass is floated in the froth (Turvey 1993), which ends up in the sludge. Depending on the furnish, between 0.5-5% of this mass is print material (pigment, oil, vehicles, binder, etc.) with the remaining mass consisting of fillers, fines and fibres (Turvey 1993). The cellulosic material (fibres and fines) comprises a fraction of the total stock losses. In a full-scale deinking system, Zabala and McCool (1988) reported stock losses of 8%, of which 3% was fibre. Linck et al. (1987) reported the total losses in two deinking plants to be 9.7% and 4.8%, with the pulp losses (fibres and fines) being ~1.5% and ~0.25%, respectively. In various laboratory studies, fibre losses ranging from 2% to 65% have been reported (Galland et al. 1977; Petri 1994; Schwinger, Dobias 1991; Liphard et al. 1993). These results are arbitrary, since they depend upon experimental conditions.

Previous research has shown that pulp losses are affected by several parameters, such as surfactant type (Hornfeck 1985; Wilson et al. 1991; Li, Muvundamina 1995; Borchardt 1993), pulp type (Schwinger, Dobias 1991; Li, Muvundamina 1995; Schwinger, Hanecker 1991), consistency (Schwinger, Dobias 1991; Li, Muvundamina 1995; Borchardt 1993), and paper age (Turvey 1993). A major factor affecting pulp loss appears to be the presence of calcium ions (Turvey 1993). A positive correlation

between fibre loss and the calcium content of the pulp has often been reported (Turvey 1993; Galland et al. 1977; Schwinger, Dobias 1991; Larsson et al. 1982; Turvey 1990; Schwinger, Hanecker 1991, Turvey 1995). This has led to several theories on how the presence of calcium affects fibre hydrophobicity. For example, Larsson et al. (1982) proposed that fibres become hydrophobic in the presence of excess calcium due to the formation of "large, soap-ink flocks" which re-precipitate on the fibres. Schwinger and Dobias (1991) suggested that fibres become hydrophobic through the adsorption of both calcium ions and surfactants. The adsorbed calcium ions reduce the negative potential energy barrier between fibre and bubble, thus enhancing flotation. Another mechanism suggested by Turvey (1993) is that the calcium forms a hydrophobic complex with the dispersed print particles.

The type of fibre is also an important factor. The work of Schwinger and Dobias (1991) and Schwinger and Hanecker (1991) demonstrated that mechanical pulps (TMP, GWD) had a greater tendency to float than chemically-treated pulps (CTMP and sulfite). The enhanced flotation of mechanical pulp fibres was attributed to the presence of hydrophobic lignin residues and resins on the fibres (Schwinger, Dobias 1991). Recent results reported by Li and Muvundamina (1995) contradict these findings: in a mixture of mechanical and chemical pulp, the authors reported that the chemical fibres had a greater tendency to float.

In the above references, most of the discussions are based on the assumption that fibres and fines adhere to the air bubbles and are carried into the froth. The theories on

bubble-fibre adhesion remain speculative, as no direct evidence of this phenomenon has yet been published. Aside from bubble-fibre adhesion, which is related to the surface chemistry of the air-water-fibre interface, other physically-related fibre loss mechanisms are possible. Based on the observation that bubbles can be mechanically trapped in fibre networks (Pelton, Piette 1992), Ajersch and Pelton (1994) proposed that bubbles in fibre flocs could carry the pulp into the froth. Entrainment, another fibre loss mechanism, occurs when fibres are hydraulically carried into the froth with the water. Entrainment was briefly discussed by Schwinger and Dobias (1991) and Petri (1994). More recently, Dorris and Pagé (1995) presented some of the first experimental evidence linking pulp loss to entrainment. In laboratory-scale flotation experiments, the recovery of hydrophilic particles (fibre and fillers) was found to be correlated to the recovery of water in the flotation froth. Dorris and Pagé (1995) concluded that the fibre and filler losses were caused solely by entrainment, and not by bubble-particle adhesion.

This paper investigates the hypothesis that entrainment is a dominant fibre loss mechanism. Hydraulic entrainment has been shown to be important in mineral flotation. Key parameters characterizing the recovery of solids by entrainment are the concentration of material in the suspension (Bisshop, White 1976; Jowett 1966) and the amount of water carried into the froth (Warren 1985), which in turn is dependent on bubble size (Lemlich 1968). Very little is known about how these parameters affect entrainment in fibre-water systems. The effects of consistency (C_m) on fibre loss remain inconclusive. Schwinger and Dobias (1991) noted a twenty-fold increase in fibre loss from C_m=0.2% to

C_m = 0.6%. On the other hand, Borchardt (1993) reported a decrease in overall yield losses when C_m was increased from 0.5% to 1.0%. It has been shown that bubble size is related to gas hold-up (Walmsley 1992; Went et al. 1993) but no quantitative work on the effects of bubble size and pulp losses has been published.

The objective of this study was to float pulp fibres in a water-fibre-surfactant suspension, and to investigate how pulp losses were affected by pulp type, consistency and bubble size.

5.2 EXPERIMENTAL

Pulp Furnishes:

Bleached kraft pulp (BKP) from a Canadian west coast mill, consisting of 40% white spruce, 40% lodgepole pine and 20% misc. (Douglas Fir, alpine fire, cedar and black spruce.) was disintegrated at Paprican (Pointe-Claire, Que.). The pulp was stored at approximately 10% consistency and had a freeness measured at 666. The mechanical pulp used was a mixture of 60% TMP and 40% stone GWD. This TMP-GWD mix was shipped at approximately 33% consistency.

The Kajaani fibre lengths and coarseness values were measured at Paprican (Pointe-Claire, Que.). The values have been summarized in Table 5.1. The fines contents were measured with a Britt Drainage Jar© (Paper Materials Research Materials, Inc. N.Y.) using a 125P Ultra screen (76 mm hole-size).

Table 5.1. Physical properties of pulp fibres (Measured by Kajaani FS-200)

	Kajaani Fibre Lengths (mm)				
PULP FURNISH	**Arithmetic Average**	**Length-Weighted Average**	**Weight-Weighted Average**	**Coarse-ness (mg/100m)**	**Avg. Fines Content (%)**
BKP	1.21	2.47	2.98	13.8	10.7
TMP-GWD Mix	0.34	0.97	1.81	29.9	38.9

Laboratory Flotation Experiments

The consistencies in the flotation experiments ranged from 0.045% to 2.2%. Samples of 1500 mL of TMP-GWD or BKP were prepared by disintegrating the concentrated pulp and diluting with appropriate amounts of distilled, deionized water. 50 ml of a 100 g/L sodium dodecyl sulfate (SDS) solution (BDH Chemicals) was added to make a total pulp volume of 1550 mL, giving an SDS concentration of approximately 3.2 g/L or 0.01 mol/L.

The experimental method is illustrated in Figure 5-1. The consistency of the feed pulp was determined from a ~ 400 mL sample. A total of 1000 mL of pulp was poured into a 1000 mL graduated cylinder and placed in a 4 L tared beaker. Nitrogen was blown into the pulp with a Tygon tube at a flow rate of 3500 mL/min. The gas flow rate was monitored with a Brooks Sho-Rate™ rotameter. The resulting foam spilled over the sides of the graduated cylinder and was collected into the beaker. After the flotation experiment, the gas dispersion tube was withdrawn from the pulp and the graduated

cylinder removed from the beaker. The wet foam was weighed, filtered, and the mass of fibres in the foam (dry basis) was measured.

The bubble size was varied by adding one of two attachments to the Tygon tube. Bubbles defined as "Large" were generated using a 1/4" (6.35 mm) (I.D.) Nalgene tube. Bubbles defined as "Small" were generated using a Pyrex©-12C 12 mm gas dispersion tube. The duration of the flotation tests varied, depending on the bubble size. The maximum amount of liquid allowed to overflow into the beaker was approximately 100 mL. Typical flotation times were 30 seconds with the small bubbles, and 5-40 min. with the large bubbles.

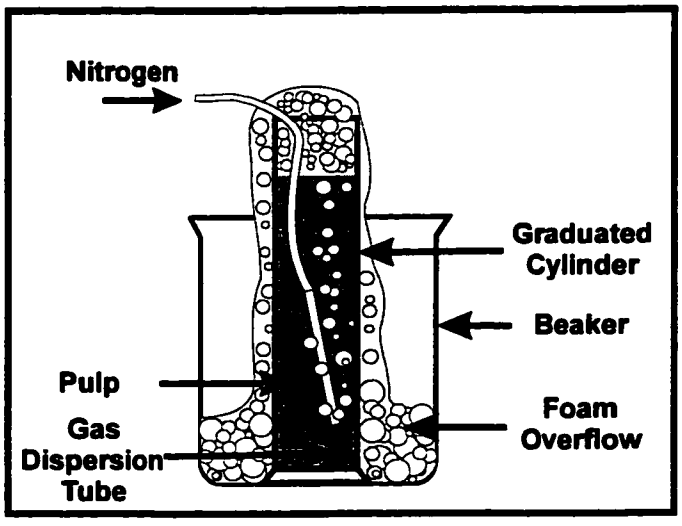

Figure 5-1. Experimental apparatus.

Bubble Size Distributions

The bubble size distributions in the foam were determined by videotaping the bubbles as close to the foam-water interface as possible: ~ 1-3 mm above the interface for the small bubbles, and ~2-5 cm for the large bubbles. The video images were digitized,

and bubble size distributions were determined using IBAS (Kontron) image analysis software.

The method of videotaping depended on the bubble size. The large bubbles were videotaped as the foam was generated. With the small bubbles, the foam spilled over the sides on the graduated cylinder, making videotaping the liquid-foam interface impossible. Videotaping occurred after the experiment was completed, as a stable foam remained at the surface of the pulp suspension. The bubbles were videotaped at approximately 90° intervals around the graduated cylinder using a video camera attached to a Wild-Leitz model M420 Zoom Macroscope. It was assumed that the bubbles videotaped in this stagnant foam were similar in size to those being generated during the flotation tests.

5.3 RESULTS

Nitrogen bubbling through a pulp-SDS suspension (see Figure 5-1) generated foam which overflowed from the graduated cylinder at a rate of ~50-225 g/min. (with the small bubbles) and ~1-10 g/min. (with the large bubbles). At dilute consistencies, pulp fibres were detected in the foam by physical touch. At higher consistencies with large bubbles, the fibres appeared to exist as macroscopic bundles several millimeters in diameter. These fibre bundles were easily visible at the junctions between the bubbles.

At lower consistencies, the pulp suspension in the graduated cylinder appeared to be uniformly mixed by the rising gas bubbles. At higher consistencies, both the BKP and TMP-GWD appeared to be quite flocculated which caused uneven mixing. Bubbles were

diverted around the flocs, forming channels. A portion of the pulp in the graduated cylinder remained stagnant, while in other areas the pulp was vigorously mixed. At higher consistencies, bubbles remained trapped in the vicinity of the gas dispersion tube, and coalesced until a critical bubble size had been reached. At this point the large bubble quickly rose to the top and subsequent smaller bubbles followed. Similar channeling effects have been reported by others (Walmsley 1992; Went et al. 1993; Taylor et al. 1994).

An example of this channeling is presented in the digitally-enhanced video image of a quiescent, 2%-consistency TMP-GWD pulp sample remaining in the graduated cylinder immediately after flotation (Figure 5-2). The pulp suspension appears quite flocculated, and bubbles are seen trapped under these flocs. Several channels which had been formed by previous bubbles' upward migration are visible. These channels are approximately 0.5 cm in diameter.

After flotation, under quiescent conditions, the pulp in the graduated cylinder would either sink or float, depending on the consistency. For low-consistency pulps (C_m ~0.1%) the pulp settled to the bottom of the graduated cylinder, leaving a fibre-free layer of clear water above it. With higher-consistency pulps ($C_m \approx 2\%$), all the fibres in the graduated cylinder floated, leaving a few centimeters of clear water at the bottom. Visual inspection of the floating pulp revealed the presence of bubbles of a few mm in diameter trapped in the fibre network. The buoyancy force of the trapped bubbles was sufficient to levitate the entire column of pulp.

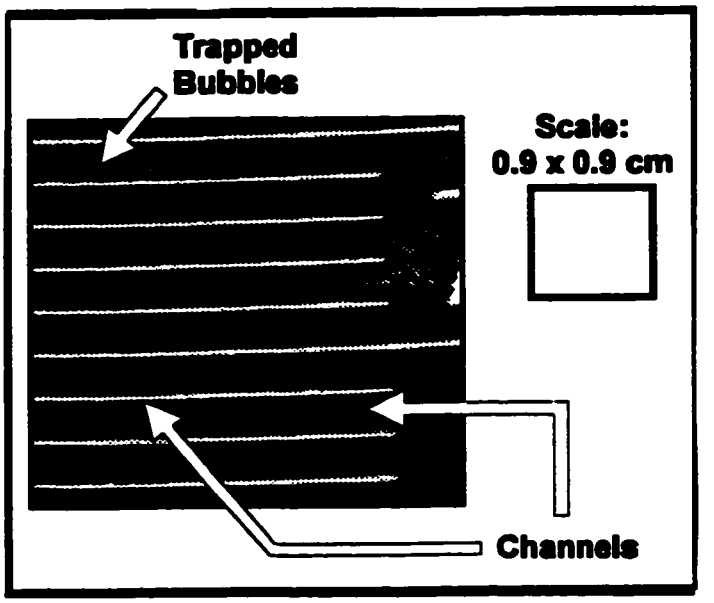

Figure 5-2. Digitally-enhanced video image of a quiescent TMP-GWD pulp immediately after a flotation experiment. The high extent of flocculation is evident. The arrows indicate channels which have been formed by the rising gas bubbles.

The bubble size distributions for samples of BKP are shown in Table 5.2. It was assumed the size distributions for the TMP-GWD pulp were similar. Possible sources of experimental error lie in the fact that bubbles were being measured at the circular glass surface. Some distortion in bubble diameters may occur for bubbles near the edge of the image. In addition, there was human error in manually tracing the bubbles' outlines with the image analysis software.

The small-bubble foam appeared to flow out of the graduated cylinder under plug flow conditions. Microscopic examination of the foam revealed that the bubbles were spherical and relatively uniform in size. The water-filled gaps between the bubbles were ~30-100 μm wide. Pulp fibres, being ~20 μm in width, could therefore fit between the

bubbles. For C_m=0.2% and C_m=2%, the mean small-bubble diameters were 118 μm to 411 μm, respectively. The increase in bubble size with consistency could be due to bubble coalescence. The average water content of the small-bubble foam (volume basis) was estimated to be 4.2%. These foams were quite stable. In one case, a foam generated from a 0.07% BKP suspension lasted indefinitely. In this case, the water eventually drained from the foam, leaving behind a dry, self-supporting fibrous structure. This indicates that the BKP fibres were hydrophilic. (Conversely, hydrophobic fibres would have caused the bubbles to coalesce as the foam drained, and the foam would have dissipated.)

Table 5.2. Bubble size distributions in the foam for BKP

BUBBLE SIZE	Consistency (%)	Number of Bubble Images	Total Number of Bubbles Counted	Mean Bubble Diameter (μm)	Standard Deviation (μm)
SMALL	0.21	4	159	118	46.4
SMALL	1.95	3	75	411	224.1
LARGE	0.22	4	140	3520	1870
LARGE	1.39	3	176	3140	1650

Since the large bubbles were videotaped at a lower magnification, the spaces between the bubbles could not be measured accurately, and the minimum detectable large bubble diameter was 0.7 mm. The size distribution of the large bubbles ranged from a few millimeters to almost 1 cm. The millimeter-sized bubbles were spherical, while the larger bubbles were polyhedral in shape. Increasing the consistency had relatively little effect on the large bubble size. For C_m=0.2% and C_m=1.4%, the mean large bubble

diameters were 3.5 mm and 3.1 mm, respectively. The large bubble foam was considerably drier, with an average water content estimated at 0.11%. Plug-flow conditions were not evident with the large bubble foam, as the drainage of water appeared uneven. Some parts of the foam appeared wetter in certain areas, especially in the vicinity of the gas dispersion tube.

Flotation experiments of varying flotation time were conducted at a constant gas flow rate of 3500 mL/min., and the mass of pulp floated is plotted in Figure 5-3 as a function of the mass of water collected in the froth. The different symbols denote differences in bubble size, pulp consistency and pulp type. Two important results are shown in Figure 5-3. First, in all cases, the data were linear, indicating constant rate processes. The pulp consistency in the foam, which is the slope of the line, can be determined from a single measurement. Second, the rate of pulp flotation is sensitive to the bubble size, pulp consistency and pulp type.

The linear trend between pulp loss and water loss for small bubbles is also evident in Figure 5-4. In this case, the pulp losses were varied by changing the gas flow rate (1800 to 5000 mL/min.) while maintaining the flotation times constant at 30 seconds. Most of the intercepts of the linear regression lines appear to approach the theoretical intercept of zero, except for the line corresponding to the BKP at 0.2% consistency, where the intercept is 0.09.

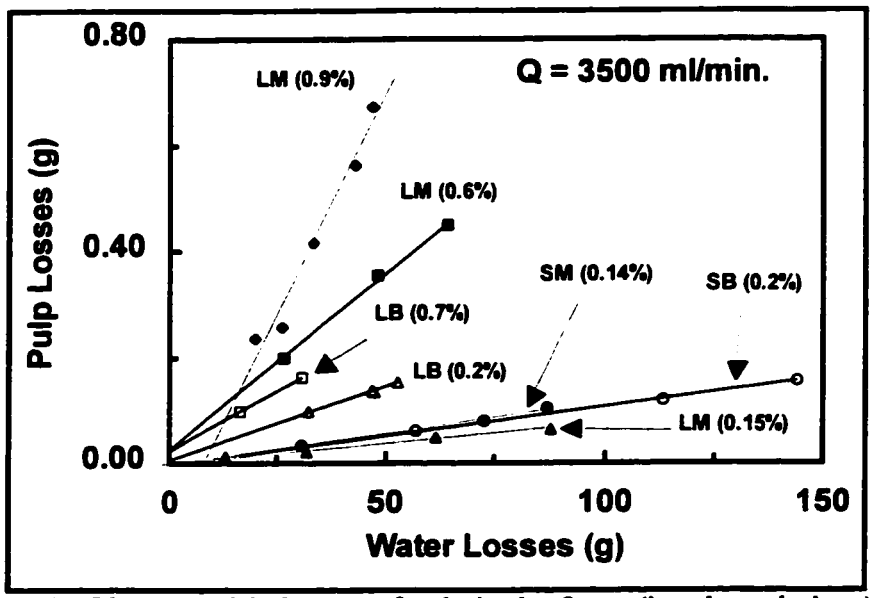

Figure 5-3. The oven-dried mass of pulp in the foam (i.e. the pulp loss) as a function of the water content of the foam. Experiments were conducted with a gas flow rate maintained at 3500 mL/min. The pulp losses were varied by changing the flotation times. The data labels indicate the bubble size (L = large, S= small) followed by the pulp type (B = BKP, M= TMP-GWD) and the average feed consistency.

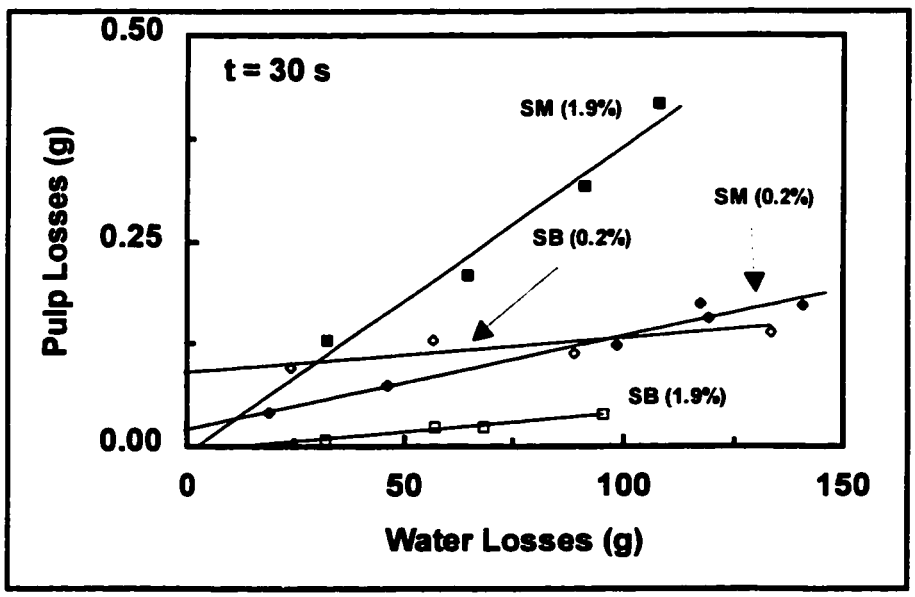

Figure 5.4. Pulp losses versus water losses for small bubbles, maintaining the flotation time constant at 30 seconds. The pulp losses were varied by changing the gas flow rates. The data labels indicate the small bubble size (S), the pulp type (B = BKP, M = TMP-GWD) and the average feed consistency.

The consistencies of the foam and feed for both types of pulp and bubble size are shown in Figure 5-5. Any data lying on the (y=x) line is an indication of the foam and feed having the same consistency. At low consistencies ($C_m < 0.0025$), the BKP data lie slightly above the y=x line while the TMP-GWD data lie slightly below it. Several of the large bubble data tended to lie above the y=x line. These data points are attributed to pulp fibres being trapped between the bubbles as the water drained out of the foam, resulting in an increased foam consistency. At higher consistencies, all of the data diverged below the y=x line, indicating that fibres were excluded from the foam. The exclusion of fibres from the foam was greatest with the small bubble data (SB, SM), especially with the BKP.

The rates of pulp transport to the froth (pulp loss) in Figure 5-6 were calculated by dividing the total mass of pulp collected (dry basis) by the duration of the flotation experiment. Pulp loss rates were dependent on the pulp type, bubble size and consistency. The data with the small bubbles (SB, SM) showed a similar pattern. That is, the rates increased with feed consistency, reached a maximum and then decreased. For $C_m < 0.2\%$, the BKP floated at a slightly higher rate than the TMP-GWD pulp. Above $C_m \approx 0.2\%$, the TMP-GWD pulp floated at a faster rate.

The rates of pulp loss were generally lower with the large bubble data (LM, LB). At low consistencies, pulp loss rates with the large bubbles were almost two orders of

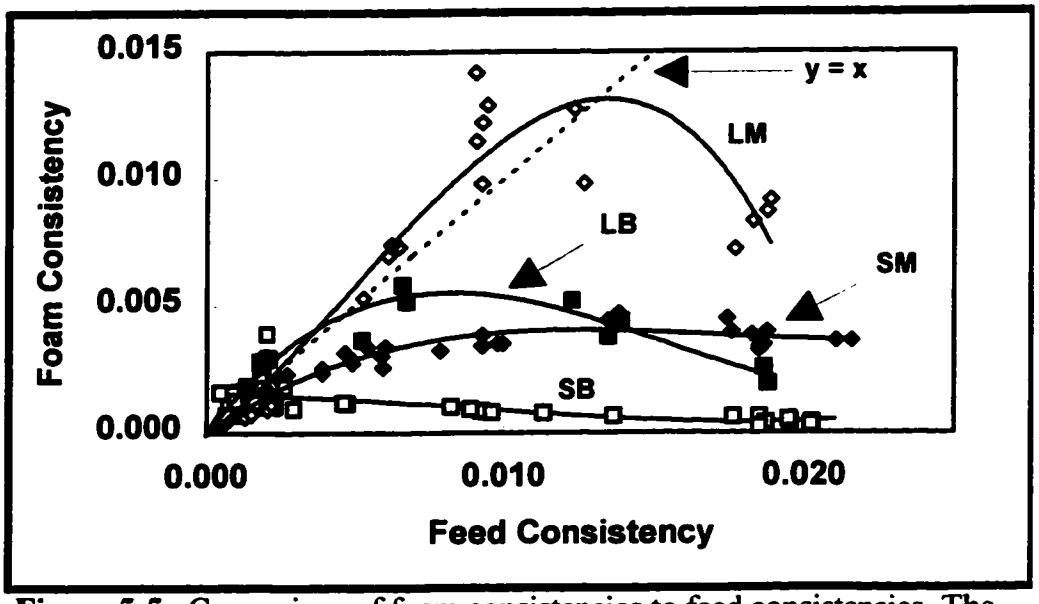

Figure 5-5. Comparison of foam consistencies to feed consistencies. The y=x line is an indication of the foam and feed consistencies being identical. The data labels correspond to the following bubble sizes and pulp types: LM = [Large bubbles, TMP-GWD], SM = [Small bubbles, TMP-GWD], LB = [Large bubbles, BKP] and SB = [Small bubbles, BKP].

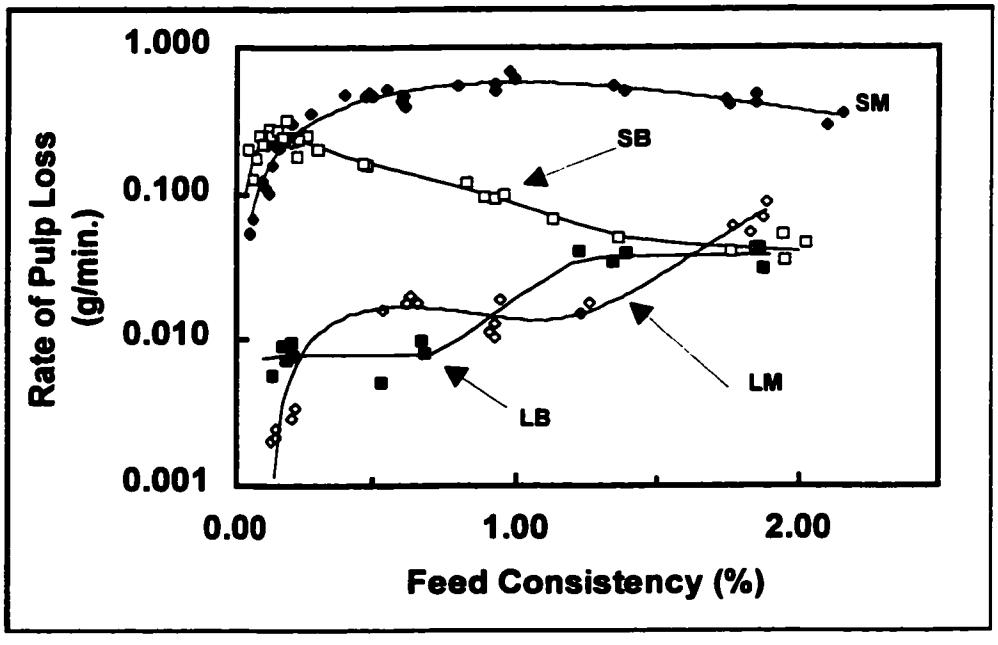

Figure 5-6. Rate of pulp losses (fibres and fines) as a function of feed consistency. The data labels correspond to the following bubble sizes and pulp types: LM = [Large bubbles, TMP-GWD], SM = [Small bubbles TMP-GWD], LB = [Large bubbles, BKP] and SB = [Small bubbles, BKP]

magnitude less than the corresponding rates with the small bubbles. Unlike the small bubble data, however, the rates of pulp loss for the (LM, LB) data increased with consistency. A sharp increase in the rate of pulp loss occurred at $C_m \approx 1.2\%$ for the TMP-GWD pulp, and at $C_m \approx 0.8\%$ for the BKP. At $C_m = 2\%$, the rates of pulp loss for the BKP for both bubble sizes (SB, LB) were identical.

Some pulps were isolated from the froths and the fines content (mass o.d. fines/total o.d. pulp mass) were measured by fractionation with the Britt Drainage Jar©. The results, summarized in Figure 5-7, indicate that in most circumstances the fines content of the foams were greater than the feed. Notable exceptions were the low consistency, large bubble data where the foam had relatively more long fibres. Explanations for these observations are given in the discussion section.

5.4 DISCUSSION

Bubble-Fibre Adhesion

The total recovery of solids in a froth occurs as a result of a combination flotation (i.e. hydrophobic particle-bubble attachment) and entrainment (Trahar 1981). In recent work (Ajersch, Pelton 1994) involving the microscopic examination of the properties of gas bubbles generated in the presence of newsprint pulp fibres, we concluded that bubble-fibre adhesion rarely occurs. Receding contact angle measurements of zero (implying no bubble adhesion) have been reported for a wide variety of wood fibres (Hodgson, Berg 1988; Jacob, Berg 1993; Krueger, Hodgson 1994) whereas finite receding contact

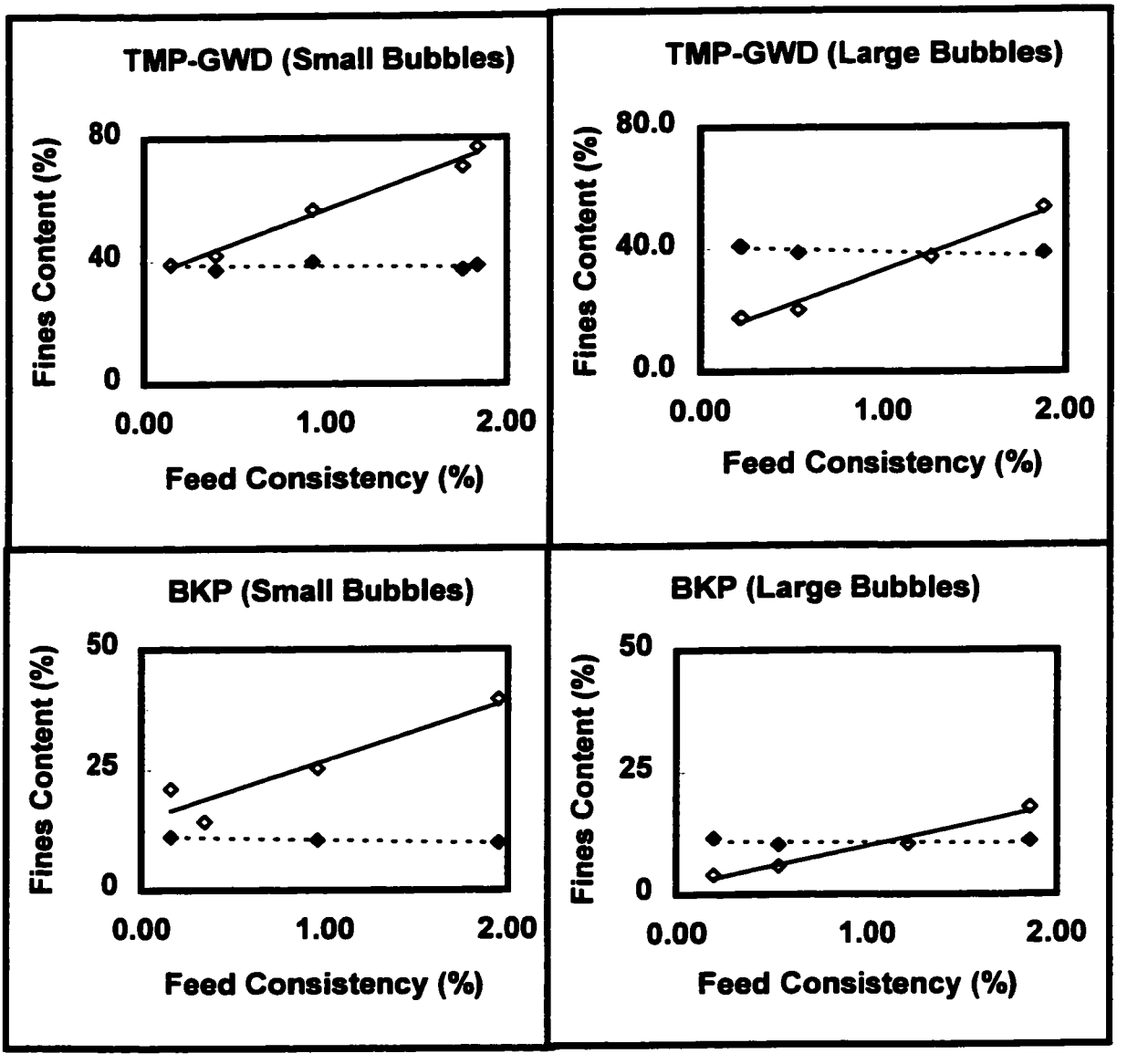

Figure 5-7. Effects of consistency on the flotation of pulp fines (< 76 μm). The black and white diamonds (◆, ◇) represent the fines contents of feed and foam, respectively. The data indicate that at higher consistencies, the relative amounts of pulp loss in the form of pulp fines increases. This effect is more prominent with the small bubbles.

angles, implying adhesion, have been reported in one exceptional case involving highly-sized fibres (Krueger, Hodgson 1995).

In the present work sizing agents were not added. Instead, SDS, an anionic surfactant was used as a foam stabilizer. The surfactant was expected to adsorb onto any hydrophobic fibre sites ensuring the fibres and fines were hydrophilic. Thus the following discussion is based on the assumption that bubble-fibre adhesion did not occur.

Pulp Loss and Entrainment

Entrainment is extensively documented in the mineral froth flotation literature (Bisshop, White 1976; Jowett 1976; Warren 1985; Trahar 1981; Maachar, Dobby 1992; Subrahmanyam, Forssberg 1988; Kawatra, Eisele 1991, Hemmings 1980). This mechanism accounts for the presence of hydrophilic gangue in the froth and for the recovery of fine particles (both hydrophobic and hydrophilic) that are too small to adhere to air bubbles. Entrainment has received little attention in flotation deinking literature. Schwinger and Dobias (1991) invoked entrainment to explain high fibre loss when excessive foam was present in laboratory batch flotation experiments. In more recent column flotation experiments, Petri (1994) also concluded that fibre losses at high gas velocities were caused by entrainment, assuming that turbulence would have minimized the effects of adhesion or mechanical entrapment.

To discriminate between entrainment and flotation, Warren (1985) plotted the recovery of mineral solids versus the recovery of water and fitted the data to straight

lines. The data from hydrophobic minerals showed finite intercepts at zero water recovery while data from hydrophilic solids gave intercepts close to zero. Warren (1985) reasoned that the slopes (or entrainment factors) represented the solids recovery by entrainment, and the intercepts represented the solids recovery by flotation.

Warren's approach (1985) was used to evaluate the contribution of flotation to the pulp losses in this work. In Figures 5-3 and 5-4, the pulp losses for both BKP and TMP-GWD appear linear with respect to water losses, with intercepts converging around the origin. This is similar to the results obtained by Dorris and Pagé (1994), who also found water losses to be linear with respect to pulp losses. In Figure 5-4, only the data set with 0.2% BKP appeared to have a non-zero origin. The reason for this is not known. The data with the same BKP at 2% consistency had an intercept close to the expected value of zero. Based on Warren's analysis, entrainment was the mechanism by which fibres and fines were transported to the foam.

Several models describing entrainment in mineral flotation systems are available (Bisshop, White 1976; Jowett 1966; Kirjavainen 1992). One of the simpler models by Bisshop and White (1976) was applied in this work. The key assumptions of their model are that the froth and bulk suspension are considered to be two perfectly mixed zones; material enters the froth by entrainment, and leaves the froth by drainage. The rate of transfer of solid component type *i* to the froth (R_i) is expressed as:

$$R_i = p_i R_w C_i \qquad [5.1]$$

where R_w is the water transfer rate, kg/m^2s.

C_i is the consistency in the liquid phase below the froth.

p_i is a transfer factor from the pulp to the froth $(0 < p_i < 1)$.

In the present work, only a small fraction of the liquid phase was transferred to the froth so C_i was nearly constant. Therefore, assuming that $p_i = 1$ for all solid components, the mass of pulp (M_{pulp}) entrained into the froth can be expressed as:

$$M_{Pulp} = M_w C_{Feed} \qquad [5.2]$$

where M_w is the mass of water in the froth and C_{Feed} is the feed consistency.

The flotation data in Figure 5-5 were plotted as a function of $M_w C_{Feed}$, the entrainment factor, in Figures 5-8 and 5-9 together with the "entrainment line" calculated from Equation 5.2. Up to a $M_w C_{Feed}$ value of 0.25 g, theory and experiment showed reasonable agreement. For $M_w C_{Feed}$ values > 0.5 g, corresponding to higher consistencies, Equation 5.2 did not fit the data: the measured masses of dried pulp in the foam under these conditions were below the entrainment line.

The Effects of Flocculation

Equation 5.2 is not valid at higher consistencies because, unlike mineral particle suspensions, the pulp fibres are not uniformly dispersed in the water. Fibres form quasi-elastic networks (Schulze 1991; Wahren 1979) and have a tendency to distribute unevenly, forming local mass concentrations called flocs (Kerekes et al. 1985). In the following paragraphs the observed negative deviation from the entrainment line in Figure

5-8 or the corresponding y=x line in Figure 5-5 are explained by the properties of flocculated fibre suspensions.

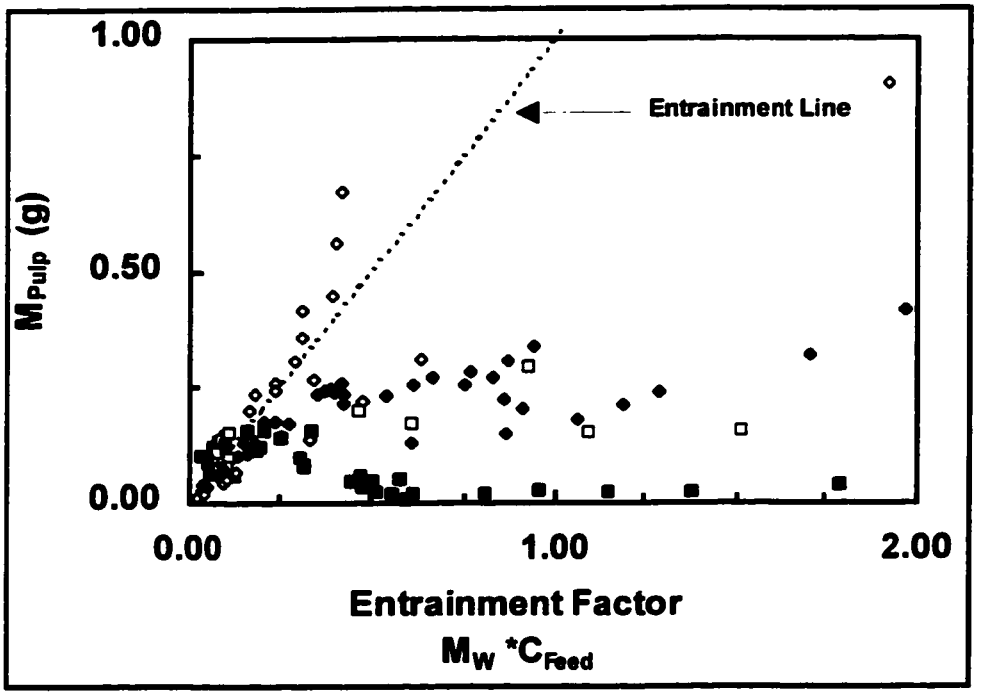

Figure 5-8. Pulp losses as a function of the entrainment factor..
(◆)TMP-GWD, small bubbles. (◇)TMP-GWD , large bubbles.
(■)BKP, small bubbles. (□)BKP, large bubbles.

Figure 5-10 is a sketch showing a magnified view of the froth/liquid pulp interface with and without flocculation. It is proposed that fibre flocs of dimensions larger than the inter-bubble spaces in froth will be excluded from the froth phase in what is essentially a filtration process. If correct, this mechanism predicts that the pulp consistency in the foam is equal to the consistency of liquid pulp between the fibre flocs. Furthermore, it follows from this argument that consistency values at which the results

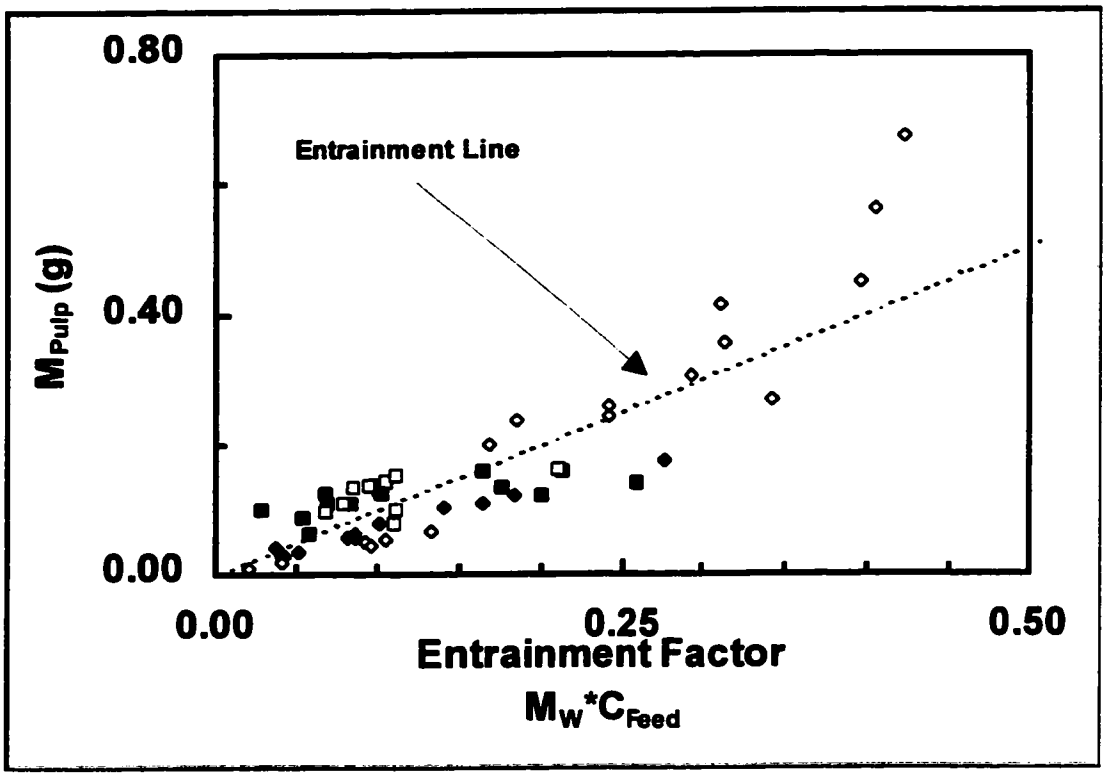

Figure 5-9. Selected pulp loss data which followed the entrainment line. Note the enlarged scale. (◆)TMP-GWD, small bubbles, C_m < 0.2%. (◇)TMP-GWD , large bubbles, C_m < 1.6%. (■)BKP, small bubbles, C_m < 0.2%. (□)BKP, large bubbles, C_m < 1.2%.

diverge from the y=x line in Figures 5-5 and 5-8 correspond to the fibre concentration at which persistent flocs first form.

Factors affecting the extent of flocculation include consistency and fibre length (Kerekes, Schell 1992; Wahren 1979) and flow conditions, such as the as the levels of shear and the shear decay (Kerekes 1983). Under similar conditions, pulp with longer fibres is more likely to flocculate. This explains the large differences in the BKP and TMP-GWD behaviors. The data diverged away from the entrainment line at a lower

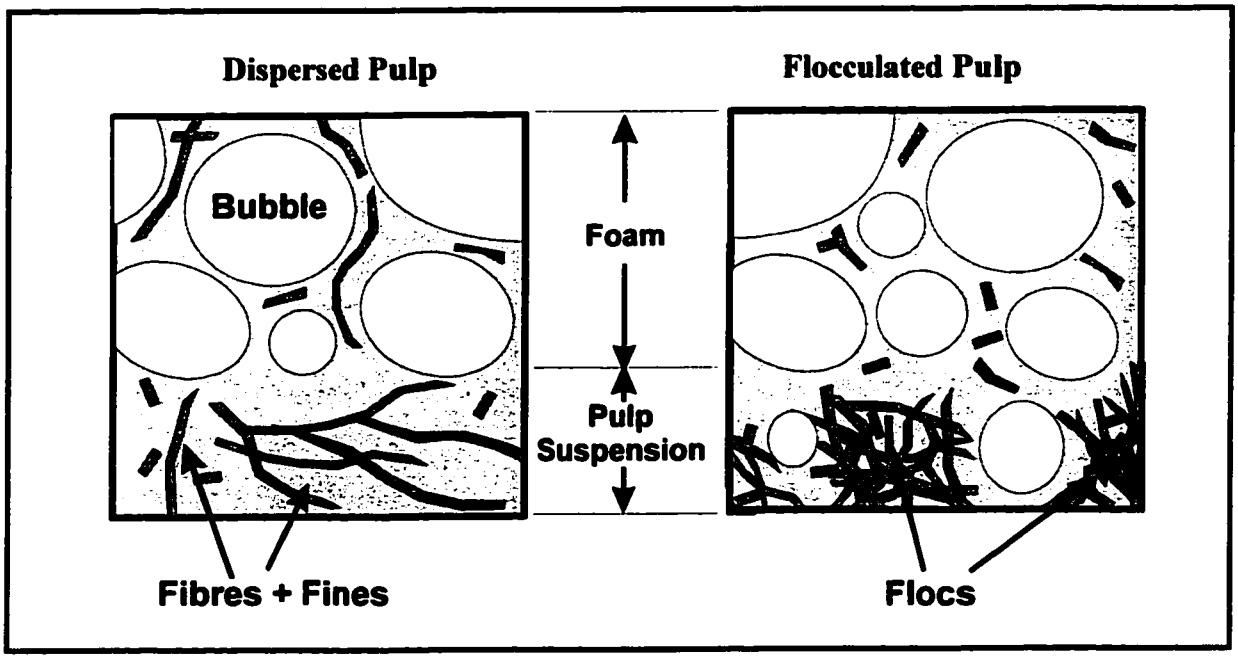

Figure 5-10. Illustration of the pulp/froth interface showing that flocs can be excluded from the froth if the floc size is comparable to the size of the inter-bubble regions in the froth. Therefore mainly inter-floc fibres will be entrained.

consistency with the BKP than with the TMP-GWD, which had a considerably shorter mean fibre length of 0.34 mm compared to 1.21 mm for BKP.

The large bubble data in Figure 5-8 followed the entrainment line for a wider range of consistency than the small-bubble data. Assuming that pulp floc diameters are 2-3 times the fibre length, the flocs in these experiments were approximately 1-4 mm in diameter. Therefore the small bubbles were an order of magnitude smaller (Table 5.2) than the flocs, whereas the large bubbles were roughly equal in size to the flocs. If the floc exclusion mechanism (Figure 5-10) is correct, it follows that higher consistencies are required to give flocs large and strong enough to be excluded from the spaces between the large bubbles in the froth.

Flocculation also explains the enhanced recovery of pulp fines observed at the higher consistencies (C_{Feed}>1.5% in Figure 5-7). The longer fibre fractions tended to concentrate within the flocs thus lowering the inter-floc concentration of long fibres. The shorter pulp fines, unable to form networks, will have less of a tendency to be depleted from the inter-floc region when flocs form. The overall effect is that the fines-to-fibre mass ratio will be greater in the inter-floc region than for the whole pulp. Since it is the inter-floc suspension which is entrained, the fines-to-fibre ratio in the foam was higher than that of the initial pulp suspension.

Drainage, the flow of water from the froth back to the liquid, complicates the interpretation of Figures 5-5, 5-7 and 5-8. The small bubble foams were wet with spherical bubbles indicating little drainage. The large bubble froths appeared more polyhedral in structure indicating that drainage may have been significant. The complication arises when fibres, because of the their size, do not drain as efficiently as water or fines. The result of impaired fibre drainage would be foam consistencies higher than the feed. Indeed, all the data significantly above the entrainment line were generated with large bubbles. An example is the LM data in Figure 5 at $C_{Feed} \approx 1\%$. Unfortunately, the same observations could be attributed to bubble/fibre adhesion so the drainage interpretation is not unequivocal.

Drainage effects also can explain some of the fines to fibre ratios shown in Figure 5-7. If fines drain more readily than do fibres, the fibre/fines ratio in the foam should be higher than the feed. With the small bubbles, in the absence of flocculation ($C_m < 0.2\%$)

the fines content of the foam and feed were similar. By contrast the large bubble froths formed from low consistency pulps had less fines relative to fibers than did the initial pulp (i.e. the feed).

Relevance to Flotation Deinking

The experimental results confirm that pulp losses can occur without bubble-fibre adhesion. In actual flotation deinking systems, however, the recovery of fibres by bubble adhesion (true flotation) cannot be entirely ruled out. In both these experiments and those of Dorris and Pagé (1994), flotation was carried out without the use of a flotation collector, and no areas of undetached ink were present on the fibre surfaces. In full-scale flotation systems, however, these factors may contribute to pulp loss. For example, Carré et al (1994), after using their hyperwashing treatment on samples from a deinking plant, found that a slightly higher level of ink fibres were removed in the froth than the noninked fibres. In agreement with Turvey (1992), they concluded that inked fibres are more hydrophobic, causing them to float. In deinking plants, therefore, the relative contributions of true flotation and entrainment to pulp loss have yet to be determined. If flotation is the dominant pulp loss mechanism, then pulp losses could be minimized by altering the surface chemistry of the pulp suspension. If entrainment is the dominant pulp loss mechanism, then reduction of pulp loss would be achieved by altering the physical parameters to minimize water recovery.

In mineral systems, it is possible to reduce entrainment by several methods. For example, water recovery can be reduced by increasing the froth residence time, which allows the hydrophilic particles to drain back into the suspension (Subrahmanyam, Forssberg (1988). In flotation columns, entrainment can be eliminated by using wash water to maintain a net downwards flow of water through the froth (Maachar, Dobby 1992). In pulp suspensions, the effects of froth washing on fibre loss were reported by Petri (1994). Petri's results (1994), however, remained inconclusive. No significant correlation between wash water and pulp losses was found.

A key parameter affecting entrainment is the rate at which fibres and fines drain from the foam back into the pulp suspension. If drainage is significant, pulp losses may be reduced by increasing the depth of the froth and removing the uppermost layer, where the froth is driest. Rinsing the froth with wash water may also reduce pulp losses. Actual pulp loss reduction by these methods is still unproved, as no information on rates of pulp fibre drainage in foams has been published. Drainage is likely to be more significant with pulp fines and the smaller fibre fractions. The results in this paper suggest that the long fibre fractions become physically trapped between the bubbles and thus, to some extent, long fibre losses are unavoidable.

Increasing the extent of flocculation caused the bubbles to be diverted around the flocs, which reduced long fibre losses. In an actual flotation cell, a highly flocculated pulp would be undesirable for effective ink recovery, as the bubbles would not contact the ink particles existing within the flocs. A possible way of optimizing long fibre loss

with ink recovery would be to alternately float and re-disperse a highly-flocculated pulp in several stages.

CONCLUSIONS

- In batch flotation experiments, BKP and TMP-GWD pulp floated in the presence of SDS. No calcium, ink or fatty-acid soap collectors were required to induce pulp losses.
- The mass of pulp collected in the foam depended upon the gas flow rate and the duration of the flotation experiment. Whether varying the gas flow rate or flotation time, the mass of pulp in the foam was linearly dependent on the mass of water in the foam.
- For $C_m < 1.4\%$, the rate at which pulp floated was lower with the large bubbles (3.1-3.5 mm diameter) than with the small bubbles (120-410 mm diameter). This was due to the diminished rate at which water was transported into the froth by the large bubbles.
- In highly-flocculated quiescent pulps, small bubbles became trapped under flocs. In sufficient quantity, these bubbles can levitate the entire mass of fibres and fines. This type of flotation is unlikely to be of any significance in conventional flotation systems, where the pulp is mixed.

- All the experimental results could be explained by entrainment. Two entrainment regimes are proposed, depending on the extent of flocculation:

    1. In the absence of flocculation, the consistency of the foam and the feed are similar.

    2. In highly-flocculated pulps, the consistency of the foam is less than that of the feed, and pulp fines tend to concentrate in the foam.

- Experimental evidence suggests that pulp fines can be washed out of the froth, while some of the longer fibre fraction remain trapped between the bubbles.

REFERENCES

AJERSCH, M., and PELTON, R.H., "The Growth of Bubbles on Pulp Fibers and on Carbon Black in Supersaturated Carbon Dioxide Solutions", Nordic Pulp and Paper Research Journal 9(2):129-135 (1994).

AJERSCH, M. and PELTON, R.H. "The Study of Fibre Losses in Flotation Deinking Through the Characterization of Bubble Entrapment in Flowing Pulp Suspensions". *44th Canadian Chem. Eng. Conf. (List of Abstracts)* 383-384 (1994).

BISSHOP, J.P. and WHITE, M.E. "Study of Particle Entrainment in Flotation Froths", *Trans. Inst. Min. Metall. (Sect. C: Mineral Process Extr. Metall.)*85:C191-C194 (1976).

BORCHARDT, J.K. "Effect of Process Variables in Laboratory Deinking Experiments", *Tappi J.* 76(11):147-154 (1993).

CARRÉ, B., GALLAND, G. and JULIEN ST. AMAND, F. "Estimation of Ink Detachment and Removal". *Prog. Paper Recycling.* 4(1):80-87 (1994).

DORRIS, G.M. and PAGÉ, M. "Deinking of Toner Printed Papers. Part I: Flotation Kinetics, Froth Stability and Fibre Entrainment. 3rd Res. Forum on Recycling, 215-225 (1995).

GALLAND, G. BERNARD, E. and SAURET, G. "Aspects Physico-Chimiques du Desencrage", *Revue A.T.I.P.* 31(6):364-378 (1977).

HEMMINGS, C.E. "An Alternative Viewpoint on Flotation Behaviour of Ultrafine Particles", *Trans. Inst .Min. Metall. (Sect. C, Mineral Process. Extr. Metall.)* 89:C113-C120 (1980).

HODGSON, K.T. and BERG, J.C. "Dynamic Wettability Properties of Single Wood Pulp Fibers and Their Relationship to Absorbency" *Wood and Fiber Science* 20(1):3-17(1988).

HORNFECK, K. "Chemie und Wirkungswiese der Tenside als Sammlerchemikalier fur Druckfarben und Fullstoff im Flotations-Deinking-Prozeb", *Woch.Papierfabr.* 17:646-649 (1985).

JACOB, P.N. and BERG, J.C. "Zisman Analysis of Three Pulp Fiber Furnishes", *Tappi J.* 76(2):105-107 (1993).

JOWETT, A. "Gangue Mineral Contamination of Froth", *Brit. Chem. Eng.* 2(5);330-333 (1966).

KAWATRA, S.K. and EISELE, T.C. "Recovery of Pyrite in Coal Flotation: Entrainment or Hydrophobicity?", *SME Annual Meeting* 1-8 (1991).

KEREKES, R.J. "Pulp Flocculation in Decaying Turbulence: A Literature Review". J. Pulp Paper Science, TR88-TR91, (July, 1983).

KEREKES, R.J., SOSZYNSKI, R.M. and TAM DOO, P.A. "The Flocculation of Pulp Fibres", *Papermaking Raw Materials. Transactions of the 8th Fundamental Research Symposium (Oxford)* 265-309 (1985).

KEREKES, R.J. and SCHELL, C.J. "Characterization of Fibre Flocculation Regimes by a Crowding Factor", *J. Pulp Paper Science* 18(1):J32-J38 (1992).

KIRJAVAINEN, V.M. "Mathematical Model for the Entrainment of Hydrophilic Particles in Froth Flotation", *Int. J. Min. Proc.* 35:1-11 (1992).

KRUEGER, J.J. and HODGSON, K.T. "Single-fiber Wettabiltiy of Highly Sized Pulp Fibers", *Tappi J.* 77(7):83-87 (1994).

KRUEGER, J.J. and HODGSON, K.T. "The Relationship Between Single Fibre Contact Angle and Sizing Performance", *Tappi J.* 78(2);154-161 (1995).

LARSSON, A., STENIUS, P. and STRÖM, G. "Surface Chemistry of the Deinking Process", *Wochbl. Papierfabr.* 14:502-506 (1982).

LEMLICH, R. "Questions and Answers on Foam Fractionation", *Chemical Engineering*, 95-102 (Dec.1968).

LI, M. and MUVUNDAMINA, M. "Fractionation of Fiber Slurries via Froth Flotation and Sedimentation", *Prog. Paper Recycling*. 32-38(May, 1995).

LINCK, E., MAYR, H., MILLER, G. and SIEWERT, W. "Operating Experience with the Bird Escher Wyss Compact Flotation Deinking Plant", *Tappi Pulping Conference* 151-156 (1987).

LIPHARD, M., SCHRECK, B. and HORNFECK, K. "Surface-Chemical Aspects of Filler Flotation in Waste Paper Recycling", *Pulp Paper Canada* 94(8):T218-T222 (1993).

MAACHAR, A. and DOBBY, G.S. "Measurement of Feed Water Recovery and Entrainment Solids Recovery in Flotation Columns", *Can. Metall. Quarterly* 31(3):167-172 (1992).

PELTON, R.H. and PIETTE, R. "Air Bubble-Holdup in Wood Pulp Suspension", *Can. J. Chem. Eng.* 70:660-663 (1992).

PETRI, B.M. "Deinking Newspaper in an Opened and Packed Flotation Column", *M.A.Sc. Thesis*, University of Toronto, (1994).

SCHULZE, H.J. "The Fundamentals of Flotation Deinking in Comparison to Mineral Flotation" *1st Research Forum on Recycling*, 161-167 (1991).

SCHWINGER, K. and DOBIAS, B. "The Influence of Calcium Ions on the Loss of Fibre in the Flotation Deinking Process", *1st. Research Forum on Deinking* 1-11 (1991).

SCHWINGER, K and HANECKER, E. "On the Flotation Tendency of Various Types of Fibre in the Deinking Process", *Woch. Papierfabr.* 21:852-854 (1991).

SUBRAHMANYAM,T.V. and FORSSBERG, E. "Froth Stability, Particle Entrainment and Drainage in Flotation - a Review", *Int. J. Min. Proc.* 23:33-53 (1988).

TAYLOR, K.E., GHIAASIAAN, S.M., ABDEL-KHALIK, S.I., LINDSAY, J.D., and GEORGE, J. "Macroscopic Flow Structures in a Bubbling Paper Pulp-Water Slurry", *IPST Technical Paper Series Number 537. Institute of Paper Science and Technology, Atlanta, Georgia* (1994).

TRAHAR, W.J. "A Rational Interpretation of the Role of Particle Size in Flotation", *Int. J. Min. Proc.* 8:289-327 (1981).

TURVEY, R.W. "The Role of Calcium Ions in Flotation Deinking". *PITA Annual Conf. "The Technology of Secondary Fibre"*, (1990).

TURVEY, R.W. "Why do Fibres Float?", *J. Pulp Paper Sci.* 19(2):J52-J57 (1993).

TURVEY, R.W. "Chemical Use in Recycling", in *Technology of Paper Recycling*, Glasglow, Blackie Academic and Professional (1995).

WAHREN, D. "Fiber Network Structures in Papermaking Operations", *Paper Science and Technology. The Cutting Edge. Conf. Proc.* 112-129 (1979).

WALMSLEY, M.R.W. "Air Bubble Motion in Wood Pulp Fibre Suspension", *APPITA* 45:509-515 (1992).

WARREN, L.J. "Determination of the Contributions of True Flotation and Entrainment in Batch Flotation Tests", *Int. J. Min. Proc.* 14:33-44 (1985).

WENT, J., JAMIALAHMADI, M. and MULLER-STEINHAGEN, H.M. "Effect of Wood Pulp Fibre Concentration on Gas Hold-up in Bubble Column", *Chem. Ing. Tech.* 65(3):306-308 (1993).

WILSON, J., PATTERSON, J. and HORNFECK, K. *Appita Conf. Proc.* 139-146 (1991).

ZABALA, J.M. and McCOOL, M.A. "Deinking at Papelera Peninsular and the Philosophy of Deinking System Design", *Tappi J.* 71(8):62-68 (1988).

CHAPTER 6

CHARACTERIZING FLOCCULATION IN PULP SUSPENSIONS FROM BATCH FLOTATION AND PULP SEDIMENTATION EXPERIMENTS

6.1 INTRODUCTION

An essential step in paper recycling is the deinking process, and in most recycled paper mills in mills North America, deinking is achieved through flotation. In typical flotation deinking cells, between 5 and 12% of the pulp mass is floated in the froth (Turvey, 1992) which ends up in the sludge. This floated mass consists of print material (pigment, oil, binder, etc.), fillers, and also includes cellulosic pulp fibres and smaller fibre fragments designated as "fines". The floated cellulosic materials (fibres and fines) are referred to as "fibre losses" or "pulp losses" and are a waste of raw material.

Over the past 15 years, much of the research has focused on identifying the various parameters affecting pulp loss. The literature has recently been reviewed by Turvey (1992) and Ajersch and Pelton (1996). In most of the literature, it is assumed that pulp fibres and fines are carried into the froth by adhering to the rising air bubbles. In addition to bubble-fibre adhesion, another mechanism by which pulp float is entrainment, in which the fibres and fines are hydraulically transported into the froth with the water. Entrainment was briefly discussed by Schwinger and Dobias (1991) and Petri (1994). More recently, Dorris and Pagé (1995) presented some of the first experimental evidence

linking pulp loss to entrainment. In laboratory-scale flotation experiments, the recovery of hydrophilic particles (fibre and fillers) was found to be correlated to the recovery of water in the flotation froth. Dorris and Pagé (1995) concluded that the fibre and filler losses were caused solely by entrainment, and not by bubble-particle adhesion. Aside from these references, however, there has been very little mention of the effects of entrainment in deinking systems.

In the previous chapter (Ajersch, Pelton 1996) we investigated the hypothesis that entrainment is a dominant pulp loss mechanism. Laboratory-scale batch flotation experiments were conducted using bleached kraft (BKP) and mechanical pulp (TMP-GWD) in the presence of sodium dodecyl sulfate. The experimental method consisted of bubbling nitrogen gas into the pulp-surfactant suspensions, and measuring the mass fraction (consistency) of pulp in both the foam and the feed. The parameters that were varied included the pulp type, feed consistency (ranging from 0.00045 to 0.022) and bubble size. "Small bubble" diameters ranged from approximately 100 to 400 μm and "large bubble" diameters ranged from approximately 3.1 to 3.5 mm.

Some of the more important results from this work are shown in Figure 5-5. One of the key findings was that at low feed consistencies, the consistency of the foam and feed were similar. This is apparent in Figure 5-5 where the data lie on the ($y = x$) line. At higher feed consistencies, the foam consistencies tended to be less than those of the feed,

and the data dropped below the (y = x) line. The extent to which this occurred depended on bubble size and pulp type.

Another important observation was that the relative amount of pulp fines (pulp fragments < 76 μm) in the foam increased with consistency. An example of this is shown with data for TMP-GWD (with small bubbles) in Figure 5-7. For feed consistencies ranging 0.0015 to 0.018, the fines fraction of the feed was measured at ≈ 0.39, while the fines fraction of the foam increased to from 0.39 to 0.77.

The difficulty in interpreting flotation results with pulp suspensions compared to other systems (i.e. mineral suspensions) is that the pulp fibres do not uniformly disperse in the water phase. The pulp fibres have a tendency to distribute unevenly, forming localized zones of concentrated fibres called "flocs" (Kerekes et al., 1985). Based on the experimental work in the previous chapter (Ajersch, Pelton 1996), we concluded that the dominant pulp loss mechanism was entrainment and that the effects of bubble-fibre adhesion were negligible. Flocculation was found to have a large effect on entrainment, and two entrainment regimes were proposed which depended on flocculation.

At lower consistencies where no flocs were present, the fibres and fines were uniformly dispersed in the feed and entrained directly into the foam. This resulted in the consistencies of the foam and feed being similar, and entrainment was described by the following expression:

$$M_{pulpEnt} = [M_{wEnt}][C_{Feed}] \qquad [6.1]$$

where $M_{pulpEnt}$ and M_{wEnt} are the mass of pulp and water entrained in the foam, respectively, and C_{Feed} is feed consistency. It was also concluded that with non-flocculated pulp (and neglecting the effects of foam drainage) the fines fraction of the foam (X_{Foam}) and the overall fines fraction of the feed (X_{Fines}) should be identical:

$$X_{Foam} = X_{Fines} \qquad [6.2]$$

At higher consistencies where flocculation was significant, Eqs. 6.1 and 6.2 were no longer considered valid, because the fibres and fines were no longer uniformly dispersed in the pulp suspension. With the flocculated pulps, the bubbles formed channels and migrated around the flocs, and it appeared that the more dilute pulp in the regions between the flocs was entrained into the foam. The consistency and fines fraction of the foam were therefore assumed to reflect the conditions existing in the "inter floc" regions of the pulp suspension, rather than the conditions within the bulk pulp suspension. Under these conditions, entrainment can be described by modifying Eq. 6.1:

$$M_{pulpEnt} = [M_{wEnt}][C_{if}] \qquad [6.3]$$

where C_{if} is the consistency of the pulp existing between the flocs. Similarly, Eq. 6.2 is can also be modified to give the fines fraction of the foam:

$$X_{Foam} = X_{if} \qquad [6.4]$$

where X_{if} is the fines fraction of the pulp between the flocs.

The hypothesis upon which Eqs. 6.3 and 6.4 are based is that foam properties from the flotation experiments represent the interfloc properties. In order to predict the entrainment of pulp fibres and fines into the foam, it is therefore essential to know the

pulp suspension's state of flocculation. Flocculation, however, is a complicated phenomenon which depends on flow conditions and fibre network properties. Presently, no published theories or models are available which can predict the interfloc consistency (C_{if}) and the fines interfloc fraction (X_{if}). This objective of this study is to develop a new model to characterize the state of flocculation and hence predict the consistency and fines fraction of the foam from the flotation experiments.

6.2 THEORY

Real pulp suspensions can be described by mass distribution functions which can depend on time, history, hydrodynamic factors, fibre properties and fibre size distributions. In this work, we reduce the complexity by considering a model pulp suspension shown in Figure 6-1.

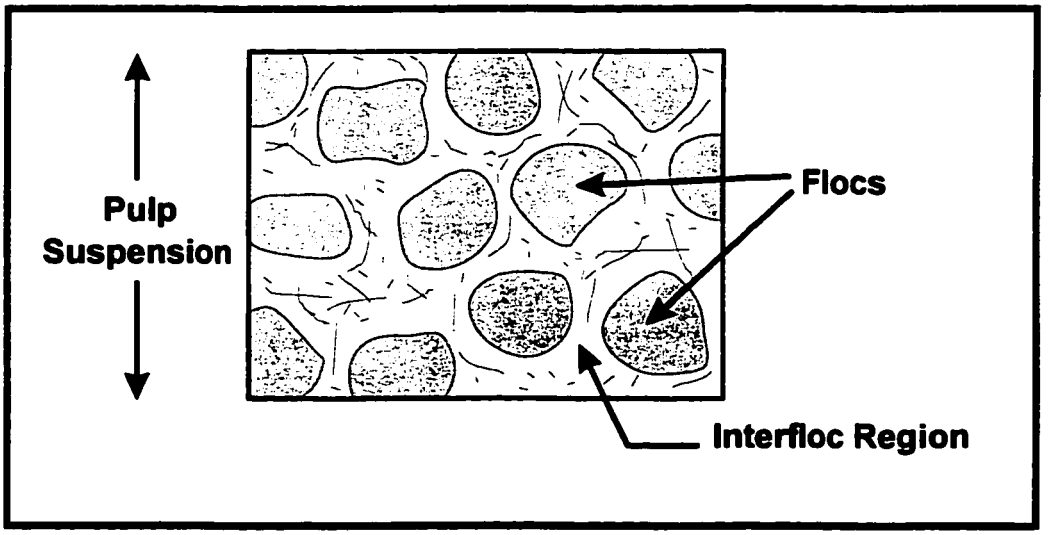

Figure 6-1. Model pulp suspension.

Some of the key terms in the model pulp suspension are defined as follows:

- Pulp Suspension: The entire system, consisting of cellulosic material and pure water.
- Pulp: The cellulosic material in the pulp suspension. The pulp consists of both long fibre fragments (fibres) and shorter fibre fragments (fines).
- Fines Fraction: The mass fraction of pulp fines in the pulp.
- Flocs: Localized regions of high pulp concentration within the pulp suspension.
- Interfloc region: The portion of the pulp suspension which is not flocculated.
- Consistency (C): The mass fraction of pulp in the pulp suspension.
- Floc consistency (C_f): The mass fraction of pulp in the flocs.
- Interfloc consistency (C_{if}): The mass fraction of pulp in the interfloc region.
- Flocculated volume fraction (ϕ_f): The volume fraction of the pulp suspension which is flocculated.

A portion of the fibres in the pulp suspension are assumed to have formed into networks in the pulp flocs, in which some of the pulp fines are embedded. It is assumed that pulp concentration within the flocs is constant, as well as the pulp concentration in the interfloc regions. The remainder of the fibres and fines are assumed to be uniformly dispersed in the interfloc region.

To date, most of the existing work on characterizing flocculation in flowing pulp suspensions has been achieved through optical methods (Bonano 1984; Hourani 1988; Kerekes, Schell 1995), where typical measurements include the floc size distributions. There is still a lack of information regarding floc consistency and the properties in the inter-floc region.

The model presented in this paper describes the interfloc properties through what is essentially a mass balance on the flocculated and non-flocculated portions of the pulp suspension. The three key parameters required to characterize the state of flocculation are the overall consistency (C) , the volume fraction of the pulp which is flocculated (ϕ_f) , and the floc consistency (C_f). For any given pulp suspension of consistency (C), an infinite number of combinations of ϕ_f and C_f can satisfy the mass balances. To reduce the number of degrees of freedom, three key assumptions have been made involving the floc volume fraction, the floc consistency and the pulp fines fractions in the flocs. Each of these assumptions will be discussed in more detail in the following sections.

Estimating the Floc Volume Fraction (ϕ_f) from Pulp Sedimentation Experiments

In this section, we present a novel approach in which the floc volume fraction (ϕ_f) can be estimated from pulp sedimentation experiments. The sedimentation experiments consisted of pouring 1000 ml of pulp suspension into 1000 ml graduated cylinders, mixing, and allowing the suspension to settle under quiescent conditions. The properties of the BKP and TMP-GWD pulp used in the sedimentation experiments are summarized in Table 5.1 in the previous chapter. The extent to which the pulp settled depended on the original consistency of the pulp and the pulp furnish. Dilute pulps tended to concentrate on the bottom and leave a large volume of water above, whereas the concentrated pulps tended to settled very little. The TMP-GWD pulp tended to settle more than the BKP.

The results of the pulp sedimentation experiments are shown in Figure 6-2. The upper graph shows the settled volume fraction (ϕ_{exp}) plotted versus the feed consistency, with ϕ_{Exp} defined as:

$$\phi_{Exp} = \frac{V_{Set}}{V_{Total}} \qquad [6.5]$$

where V_{Set} is the volume of the settled pulp, and V_{Total} = 1000 ml.

For each settled volume fraction, there is a corresponding consistency of the settled pulp, which is shown in the lower graph in Figure 6.2. The settled volume fractions (ϕ_{Exp}) can be expressed as functions of the overall consistency:

$$\phi_{Exp}(C) = [1 - e^{-139.0(C)}] \quad \text{(for TMP-GWD)} \qquad [6.6]$$

$$\phi_{Exp}(C) = [\,1 - e^{-486.5(C)}] \quad \text{(for BKP)} \qquad [6.7]$$

(These correlations were obtained using MathCad© software with the detailed calculations shown in Appendix D-6). As seen in Figure 6-2, the consistencies at which the ϕ_{Exp} values approach 1 are C ≈ 0.025 for the TMP-GWD, and C ≈ 0.009 for the BKP. A common trend is seen with both pulp furnishes: as the overall consistency increases, the settled consistency approaches the overall consistency.

Meyer and Wahren (1964) were among the first to show a link between pulp settling and fibre network properties. An equation was derived for predicting the "sedimentation concentration", which corresponded to final concentration to which a very dilute fibre suspension will settle. This equation is a function of the fibre length/fibre radius ratio, and corresponds to conditions where the fibres formed into networks with 3 contact points per fiber (Wahren 1979).

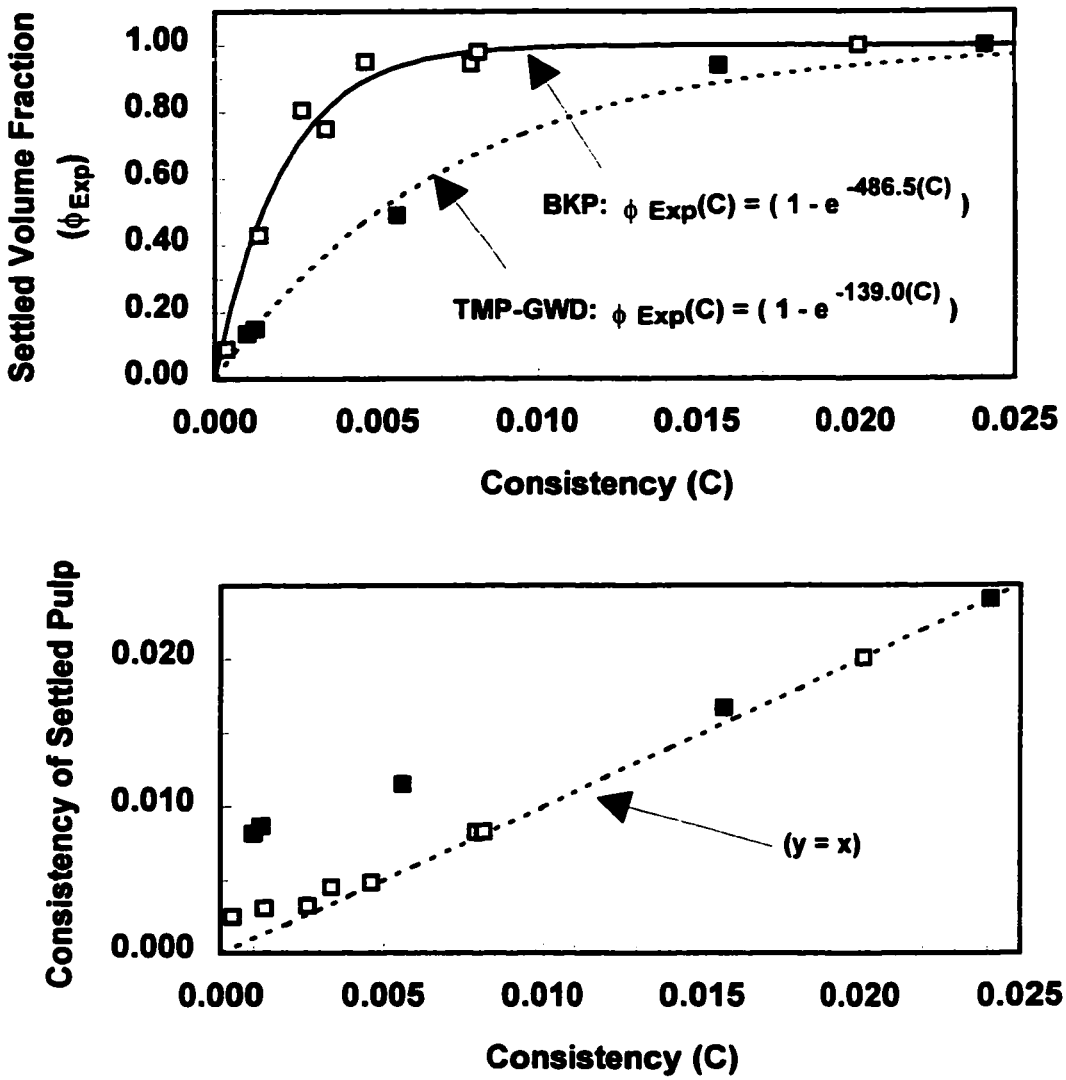

Figure 6-2. Results from the pulp sedimentation experiments. The upper graph shows ϕ_{Exp} versus the consistency. This value corresponds the volume fraction that the fibres and fines occupy in a 1000 ml graduated cylinder after settling. The lower graph indicates the mass fraction (consistency) of pulp in the sediment. The (y = x) line is an indication of the settled consistency and feed consistency being similar. (□) = data for BKP; (■) = data for TMP-GWD.

The equation predicting the sedimentation concentration, however, does not apply for concentrated pulps where flocs are present. In the case of flocculated pulp suspensions, a proposed settling mechanism is shown in Figure 6-3:

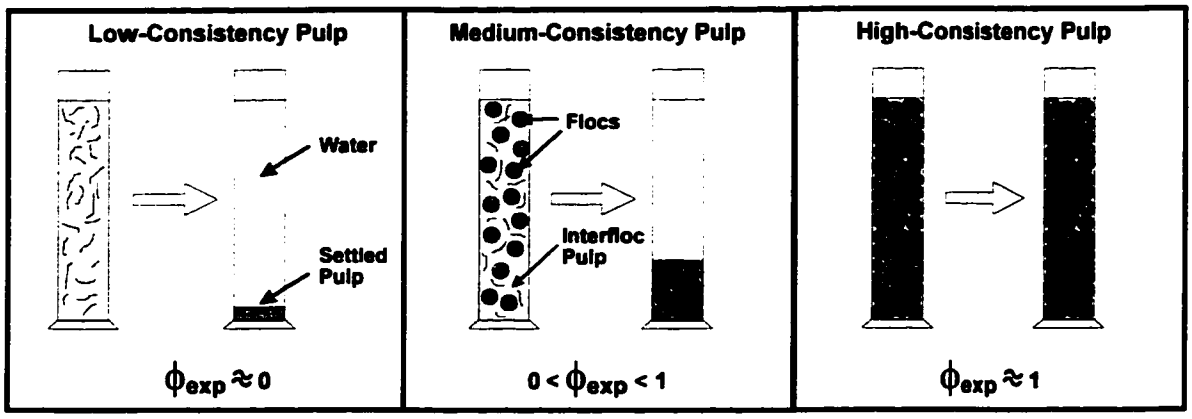

Figure 6.3 The settling of quiescent pulp as a function of consistency and flocculation. The settled volume (ϕ_{Exp}) equals the volume of the settled pulp divided by the total volume.

As illustrated above, at low consistencies, the few fibres and fines that are present concentrate on the bottom, with $\phi_{exp} \approx 0$. In this case, the consistency of the settled pulp should equal the sedimentation concentration. At intermediate consistencies, both flocs and dispersed pulp exist in the pulp suspension. The pulp settles to some intermediate value of ϕ_{Exp}, at a consistency greater than the original unsettled consistency. At high consistencies, the pulp suspension can be considered as one continuos floc. The fibres and fines have already formed into networks, and therefore the pulp no longer has the ability nor the room to settle. Under these conditions, ϕ_{exp} approaches the value of 1.

We postulate that the function $\phi_{Exp}(C)$ represents the pulp suspension's state of flocculation under idealized, quiescent conditions. For non-idealized cases (i.e. mixed

pulp suspensions) we propose that the actual floc volume fraction (ϕ_f) is related to $\phi_{Exp}(C)$ according to the following model:

$$\phi_f (C,C_{crit}, \alpha) = \alpha[\ \phi_{Exp}(C-C_{crit})\ ] \text{ for } (C > C_{crit}) \qquad \text{Eq. [6.8]}$$

$$\text{with } \phi_f = 0 \text{ for } (C < C_{crit})$$

where ϕ_f is expressed as a function of overall consistency (C) and two empirical parameters (α and C_{crit}). The physical interpretation of these parameters is illustrated in Figure 6.4.

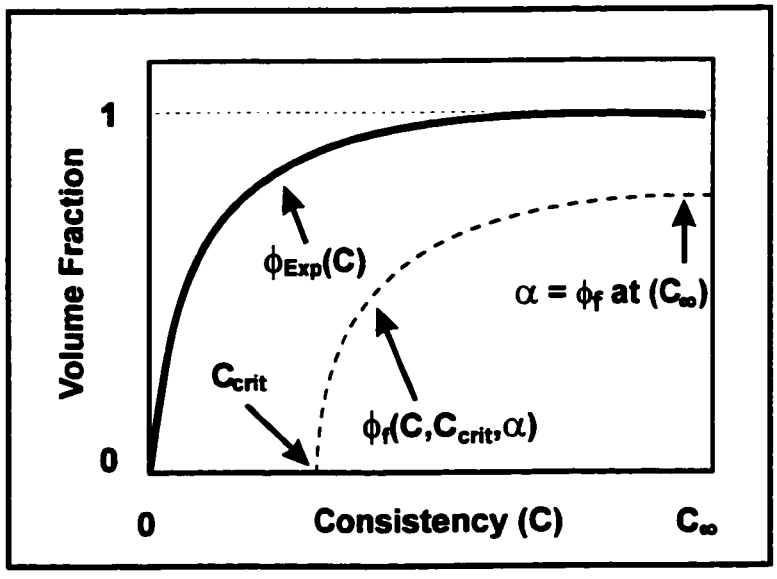

Figure 6.4 Comparison between the settled volume fraction from the pulp sedimentation experiments to actual the floc volume fraction.

The qualitative shape of typical pulp settling curve in Figure 6.4 shows $\phi_{Exp}(C)$ approaching 1 at some arbitrary large consistency (C_∞). C_{crit} is defined as the "critical consistency" and represents the consistency at which flocs first form in the pulp suspension. The value of C_{crit} shifts the $\phi_{Exp}(C)$ curve to the right and is reflection of the

fibre network properties and flow conditions. At this point, the yield stress of the first flocs formed are considered to be equal to the hydrodynamic forces. For consistencies below C_{crit}, the pulp is sufficiently dilute and/or the shear forces sufficiently high that the pulp remains dispersed, and ϕ_f remains at 0.

Had C_{crit} been the only adjustable parameter in Eq. 6.8, ϕ_f would have eventually approached the value of 1. This implies that 100% flocculation occurs at some arbitrary large consistency. In the actual flotation experiments, however, it did not appear that complete flocculation occurred. A small portion of the pulp suspension always appeared to be mixed by the rising bubbles. To compensate for these mixing effects, $\phi_{Exp}(C)$ is therefore multiplied by the parameter α to ensure that ($\phi_f < 1$). The parameter α is indicative of the maximum floc volume fraction that can exist in the pulp suspension the under the given conditions of consistency and mixing.

Estimating the Floc Consistency (C_f)

Starting with an overall volume balance, the total volume of the pulp suspension (V_{Total}) equals the volume of the pulp flocs (V_{Flocs}) plus the volume of the interfloc region (V_{if}):

$$V_{Flocs} + V_{if} = V_{Total} \qquad [6.9]$$

As derived in Appendix D-2, the pulp volume fraction in the pulp suspension (ϕ) can be expressed as a function of consistency:

$$\phi(C) = \frac{C\rho_w}{-C\rho_{pulp} + C\rho_w + \rho_{pulp}} \qquad [6.10]$$

where ρ_{pulp} is the density of the pulp, and ρ_w is the density of pure water. These are assumed to be 1.5 g/cm^3 and 1 g/cm^3, respectively. Rearranging Eq. 6.10 gives the consistency as a function of the pulp volume fraction:

$$C_m(\phi) = \frac{-\phi\rho_{pulp}}{-\phi\rho_{pulp} + \phi\rho_w - \rho_w} \qquad [6.11]$$

A volume balance on the pulp is obtained by multiplying the volumes in Eq. 6.9 by their respective pulp volume fractions:

$$\phi(C_f)V_{Flocs} + \phi(C_{if})V_{if} = \phi(C)V_{Total} \qquad [6.12]$$

where C_f is the floc consistency, C_{if} the interfloc consistency, and C the overall consistency of the pulp suspension. Substituting $V_{if} = [V_{Total} - V_{Flocs}]$ back into Eq. 6.12 gives:

$$\phi(C_f)V_{Flocs} + \phi(Cif)\,(V_{Total} - V_{Flocs}) = \phi(C)\,V_{Total} \qquad [6.13]$$

By definition, the floc volume fraction is defined as

$$\phi_f = \frac{V_{Flocs}}{V_{Total}} \qquad [6.14]$$

Rearranging Eq. 6.14 to give $V_{Flocs} = \phi_f V_{Total}$. Substituting this expression into Eq. 6.13 gives:

$$\phi(C_f)V_{Flocs} + \phi(C_{if})\,(V_{Total} - V_{Total}\,\phi f) = \phi(C)\,V_{Total} \qquad [6.15]$$

Dividing both sides by V_{Total} and solving for the floc volume consistency gives:

$$\phi(C_f) = \frac{\phi(C) - \phi(C_{if}) + \phi(C_{if})\phi_f}{\phi_f} \qquad [6.16]$$

Presently, the floc consistency (C_f) in Eq. 6.16 is unknown. However, there are theoretical limits to the range of magnitude of C_f. By definition, a floc must be more concentrated than the bulk pulp suspension. The lower limit is therefore equal to the overall consistency (C). The upper limit corresponds to the hypothetical case where all the pulp fibres and pulp fines in the pulp suspension exist in the flocs, and the interfloc region consists of only pure water. Under these conditions, $C_{if} = \phi(C_{if}) = 0$. Substituting these values into Eq. 6.16 gives the expression for the maximum theoretical volume fraction of pulp in the flocs:

$$\phi(C_{fmax}) = \frac{\phi(C)}{\phi_f} \qquad [6.17]$$

The maximum pulp volume fraction is converted into the maximum floc consistency by substituting both sides of Eq. 6.17 into 6.11:

$$C_m[\,\phi(C_{fmax})\,] = C_m\left[\frac{\phi(C)}{\phi_f}\right] \qquad [6.18]$$

The left-hand side of Eq. 6.18 simplifies down to C_{fmax}:

$$C_{fmax} = C_m\left[\frac{\phi(C)}{\phi_f}\right] \qquad [6.19]$$

The actual floc consistency lies somewhere between C and C_{fmax}. Another key assumption is now presented: we assume that the value of C_f is proportional to the floc volume fraction according to the following expression:

$$C_f = C + (C_{fmax} - C)\phi_f \qquad [6.20]$$

Substituting in C_{fmax} from Eq. 6.19 and into Eq. 6.20 gives:

$$C_f = C + \phi_f\left[C_m\left(\frac{\phi(C)}{\phi_f}\right) - C\right] \qquad [6.21]$$

The final expression for floc consistency as a function of C, Ccrit and α is obtained by substituting in the new expression for ϕ_f from Eq. 6.8 into Eq. 6.21:

$$C_f(C,C_{crit},\alpha) = C + \phi_f(C,C_{crit},\alpha)\left[C_m\left(\frac{\phi(C)}{\phi_f(C,C_{crit},\alpha)}\right) - C\right] \qquad [6.22]$$

The reasoning behind expressing the floc consistency according to Eq. [6.20] merits some discussion. Other models for floc consistency were possible, but they were discarded for various reasons. For example, one of the simplest approaches would have been to assume a constant floc consistency. Upon examining the pulp settling curves in Figure 6-2, it was observed that little or no settling occurred when ($C > 0.02$). Under these conditions, the pulp appeared highly flocculated, and the floc consistencies were assumed to be of the order of $C_f \approx 0.02$. Typical critical consistencies where flocculation, however begins, however, are of the order C = 0.003-0.008 (Walmsley, 1992). Assuming a constant floc consistency of $C_f = 0.02$ implies that the first flocs that form would have had consistencies 5-10 times greater than the overall consistency. This seemed unlikely, and therefore the constant floc consistency model was not used.

Another possible approach would have been to assume $C_f = C + \Delta C$, where ΔC is some arbitrary constant. Upon examining the settled consistency curves in Figure 6.2,

however, the difference between the initial consistency and the settled consistency decreased with the overall consistency, until the two values became identical. This led us to believe that (ΔC) was not constant. Instead, it appeared that the floc consistency was proportional to both the overall consistency and the floc volume fraction.

The use of Eq. 6.22 was purely arbitrary, but it seemed to be the most realistic, and the model fit the data well using this approach. The relation between C_f, C_{fmax} and C is shown in Figure 6.5. The curves for C_{fmax} and C_f correspond to the small-bubble data with BKP, using Eqs. 6.18 and 6.22 evaluated at $C_{crit} = 0.00155$ and $\alpha = 0.970$. At low consistencies just above C_{crit}, ϕ_f approaches zero which causes C_{fmax} to approach infinity. At higher consistencies, ϕ_f approaches 1 and C_{fmax} becomes closer to C. However, as

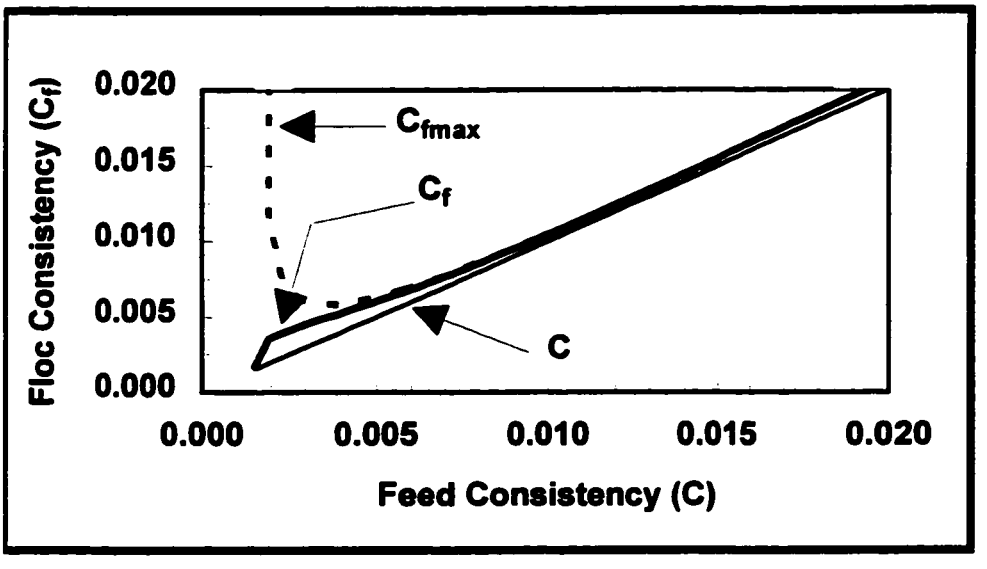

Figure 6-5 Estimated floc consistency for BKP (Small bubbles). The estimated floc consistency (C_f) lies between the actual consistency (C) and the theoretical maximum consistency (C_{fmax}).

indicated in Eq. 6.20, the model accounts for this by multiplying the difference between (C_{fmax} -C) by ϕ_f, which keeps the value of C_f finite and always slightly greater than the overall consistency (C).

Estimating the Interfloc Fines Fraction

The overall fines fraction (X_{Fines}) of the pulp suspension is defined as the mass fraction of fines within the pulp:

$$X_{Fines} = \frac{M_{fines}}{M_{pulp}} \qquad [6.23]$$

where M_{fines} is the total mass of pulp fines in the pulp suspension. In a similar fashion to the floc fines fraction is defined as:

$$X_{FinesFloc} = \frac{M_{finesFloc}}{M_{pulpFlocs}} \qquad [6.24]$$

where $M_{finesFloc}$ is the mass of pulp fines in the flocs, and $M_{pulpFlocs}$ the mass of pulp within the pulp flocs. The third key assumption is now made, in that the fines fraction in the flocs is proportional to the overall fines fraction by the following expression:

$$X_{FinesFloc} = \beta X_{Fines} \qquad [6.25]$$

where β is a proportionality constant. β is an adjustable parameter which represents the relative distribution of pulp fines between the flocs and the bulk pulp suspension. If β = 1, then there is no preferential distribution of pulp fines in the flocs, and $X_{FinesFloc} = X_{Fines}$. If $\beta < 1$, then the fibre/fines ratio in the flocs is less than that of the overall pulp suspension, indicating a preferential exclusion of pulp fines from the flocs.

Final Expressions for the Interfloc Consistency and InterFloc Fines Fraction

The expressions of the interfloc consistency (C_{if}) and the interfloc fines fraction (X_{if}) were obtained by performing mass balances on the model pulp suspension, using the assumptions described by Eqs. 6.8, 6.20 and 6.25. The final expressions are shown in Eqs. 6.26 and 6.27, with C_{if} expressed as a function of (C,C_{crit},α) and X_{if} expressed as a function of (C,C_{crit},α,β).

$$C_{if}(C,C_{crit},a) = \frac{\phi(C)\rho_{pulp} - \phi_f(C,C_{crit},\alpha)\phi[C_f(C,C_{crit},\alpha)]\rho_{pulp}}{\left\{\phi(C)\rho_{pulp} - \phi_f(C,C_{crit},\alpha)\phi[C_f(C,C_{crit},\alpha)]\rho_{pulp}\cdots \right.} \\ \left. +[1-\phi(C)]\rho_w - \phi_f(C,C_{crit},\alpha)(1-\phi[C_f(C,C_{crit},\alpha)])\rho_w\right\} \qquad [6.26]$$

$$X_{if}(C,C_{crit},\alpha,\beta) = \left[\frac{\phi(C) - \phi_f(C,C_{crit},\alpha)\phi[C_f(C,C_{crit},\alpha)]\beta}{\phi(C) - \phi_f(C,C_{crit},\alpha)\phi[C_f(C,C_{crit},\alpha]}\right]X_{Fines} \qquad [6.27]$$

The detailed calculations used in deriving Eqs. 6.26 and 6.27 are summarized in Appendix D-7.

6.3 RESULTS

The first step in fitting the model to the data involved finding the two parameters (α and C_{crit}). This was done by minimizing the sum-squared of errors between the experimental and predicted foam consistencies, with the sum-squared of errors defined as a function of α and Ccrit:

$$SSE(\alpha, C_{crit}) = \sum_i \left[C_{Foam_i} - C_{if}(C_{Feed_i}, C_{crit}, \alpha) \right]^2 \qquad [6.28]$$

where C_{Foam_i} corresponds to the experimental foam consistencies from the flotation experiments. The term $C_{if}(C_{Feed_i}, C_{crit}, \alpha)$ corresponds to the predicted interfloc consistency determined from Eq. 6.26, and is evaluated using the experimental feed consistencies (C_{Feedi}) and the parameters α and C_{crit}.

Once α and C_{crit} were determined, the parameter β was determined using a similar approach. The sum-squared of errors between the experimental and predicted fines fraction in the foam was expressed as a function of β (Eq. 6.29):

$$SSE(\beta) = \sum_j \left[X_{Foam_j} - X_{if}(C_{Feedj}, C_{crit}, \alpha, \beta) \right]^2 \text{ (for } C_{Feedj} > C_{crit}) \qquad [6.29]$$

This function was also minimized, where the feed consistency ($C_{Feed}j$) and the foam fines fraction (X_{Foam}) were obtained from the fibre fractionation experiments described in the previous chapter. (These experimental data are tabulated in Appendix C-4). The term $X_{if}(C_{Feedj}, C_{crit}, \alpha, \beta)$ corresponds to the predicted foam fines fraction from Eq. 6.27, evaluated at the experimental feed consistencies and at α, β and C_{crit}. The minima for Eqs. 6.28 and 6.29 were determined using the "minerr" function with MathCad© software. The detailed calculations are summarized in Appendix E.

The resulting values for C_{crit}, α and β are summarized in Table 6-1. The column designated "C_{max}" corresponds to the largest feed consistency for the given data set at which the experiments were conducted. The model predictions of ϕ_f, C_f, C_{if} and X_{if} are

plotted a function of the overall consistency for the range ($C_{crit} < C < C_{max}$) in Figures 6-6 to 6-9.

In the pulp sedimentation data in Figure 6-2, there was some error in the measurements taken at the higher consistencies: these pulp suspensions contained trapped air bubbles, which may have reduced the pulp's ability to settle. The data in Figure 6-2, however, appear to be reproducible and the effect of trapped air on the sedimentation curves was considered to be negligible.

Table 6-1. Calculated values for the parameters C_{crit}, α and β.

Pulp Furnish	Bubble Size	C_{crit}	α	β	C_{max}
TMP-GWD	Small	2.08×10^{-4}	0.863	0.957	0.0216
BKP	Small	0.00155	0.970	0.997	0.0202
TMP-GWD	Large	0.0116	0.892	0.913	0.0189
BKP	Large	0.0102	0.888	0.989	0.0188

For comparison purposes, the floc volume fractions in Figure 6-6 are shown with the experimental settled volume fractions. The experimental data are an indication of the state of flocculation under ideal, quiescent conditions, while the model predictions represent the conditions existing in the actual flotation experiments. The model predicts that the ϕ_f is larger for the small bubbles than with the large bubbles.

The predicted floc consistencies in Figure 6-7 are shown with the experimental data from the pulp settling experiments. The settled pulp consistencies represent the flocculation under quiescent conditions, and are only shown for comparison purposes only. The predicted floc consistencies for the mixed pulp are greater those for quiescent conditions.

The shapes of the floc consistency curves vary depending on the bubble size and pulp type. At high consistencies, it was expected that the floc consistency and the overall consistency would approach each other. This only occurs with the BKP (small bubble) data. For the TMP-GWD (small bubble) data, the difference between C_f and C appears to be constant.

There were sudden changes in slope of the floc consistency curves in Figure 6-7 when C approached C_{crit}. This was more apparent with the large-bubble data, where the floc consistencies almost doubled shortly after C_{crit}. It seems unlikely that the actual floc consistencies would follow this behavior. The shape of the floc consistency curves with the large bubbles may be due to the fact that there were fewer data to correlate the model with . In addition, the model for floc consistency from Eq. 6.20 was arbitrarily chosen. This may be an indication that the model may be more applicable for the small-bubble data.

In Figure 6-8, the data tend to lie on the (y = x) line for consistencies below C_{crit}. As discussed earlier, (Ajersch, Pelton 1996) at these low consistencies, the pulp is dispersed and the fibres and fines from the bulk pulp suspension are entrained directly into the foam. Above C_{crit}, where flocculation becomes significant, both the data and the model diverge below the y=x line. It is interesting to note the same model predicts two distinctly different curves for the small bubble data. In Figure 6.8, the TMP-GWD (small bubble) data shows that the foam consistency increases, after which it levels off to a

constant value. For the BKP (small bubble) data, the model predicts a decrease and a gradual leveling off of the foam consistency.

For values above C_{crit}, there is good agreement with the predicted interfloc consistencies and the experimental foam consistencies. This is confirmed by examining Figure 6-10, where the observed and predicted foam consistencies are plotted together. Most of the data lie on the (y=x) line in Figure 6-10, indicating a good fit.

For the large bubble data, most of the feed consistencies were below C_{crit} ; therefore there were fewer data to correlate the model with. The higher values of C_{crit} and lower α values resulted in the interfloc consistency curves decreasing, as compared to the small bubble data, where the interfloc consistencies tended to level off.

There is generally a good fit between the experimental foam fines fractions and the interfloc fines fraction (X_{if}) in Figure 6-9. A plot of the observed versus predicted values in Figure 6-11 confirm this: most of the data lie on the (y = x) line. For $C < C_{crit}$, the interfloc fines content were expected to equal the overall fines fraction (neglecting the drainage of fibres and fines from the foam). The reason some of the experimental data for the large bubbles lie below the overall fines fraction has been attributed to foam drainage effects.

The small bubble foam appeared to be wet with spherical bubbles, indicating little drainage. In the absence of flocculation, the fines content of the small bubble foam and the feed were identical. The large bubble foams, on the other hand, appeared more polyhedral in structure, indicating that drainage may have been significant. In the

absence of flocculation, the large bubble froths may have had a larger proportion of fibres since the smaller pulp fines may have drained from the foam.

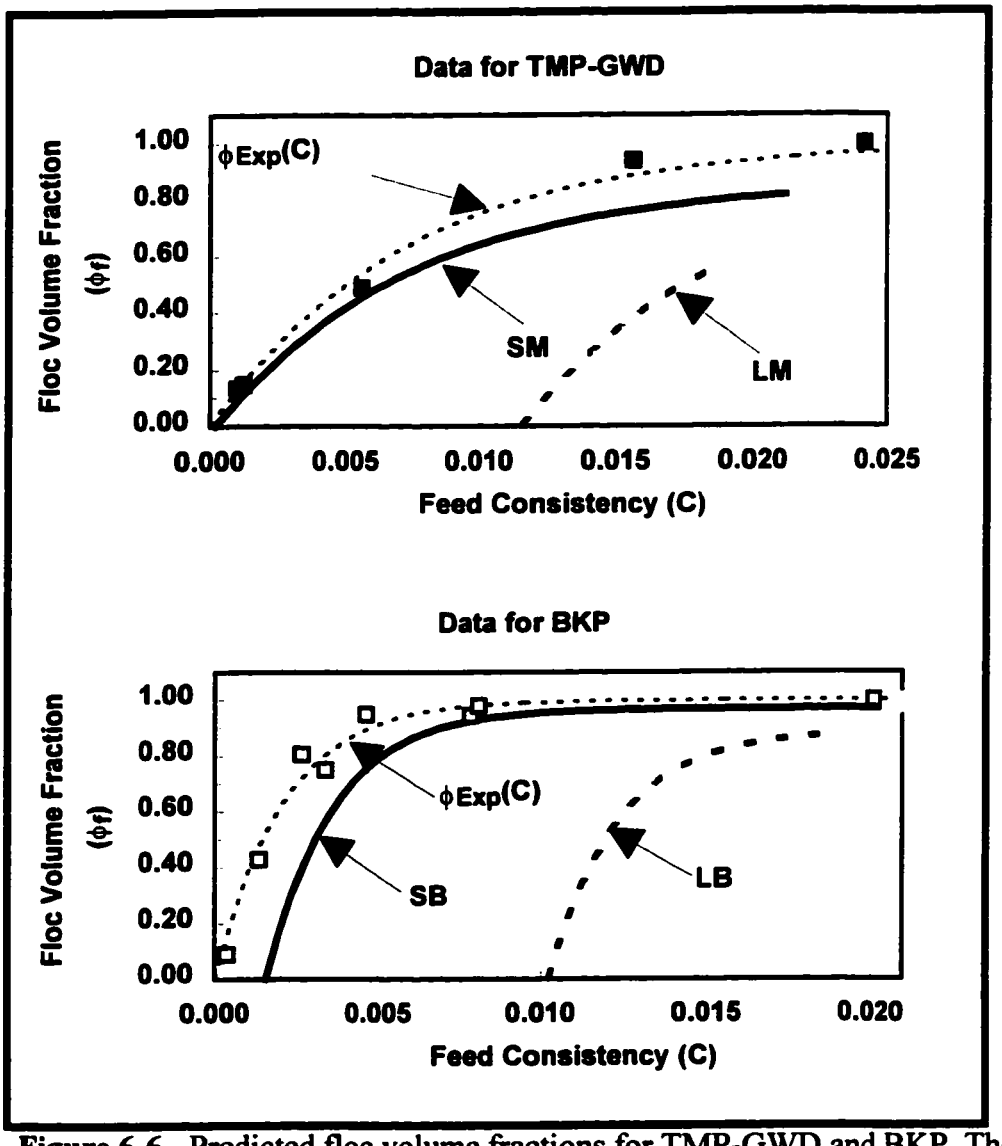

Figure 6-6. Predicted floc volume fractions for TMP-GWD and BKP. The squares (□, ■) represent the experimental settled volumes from Figure 6-2. The data labels are defined as follows: SM = TMP-GWD, small bubbles; LM = TMP-GWD, large bubbles; SB = BKP, small bubbles; LB = BKP, large bubbles.

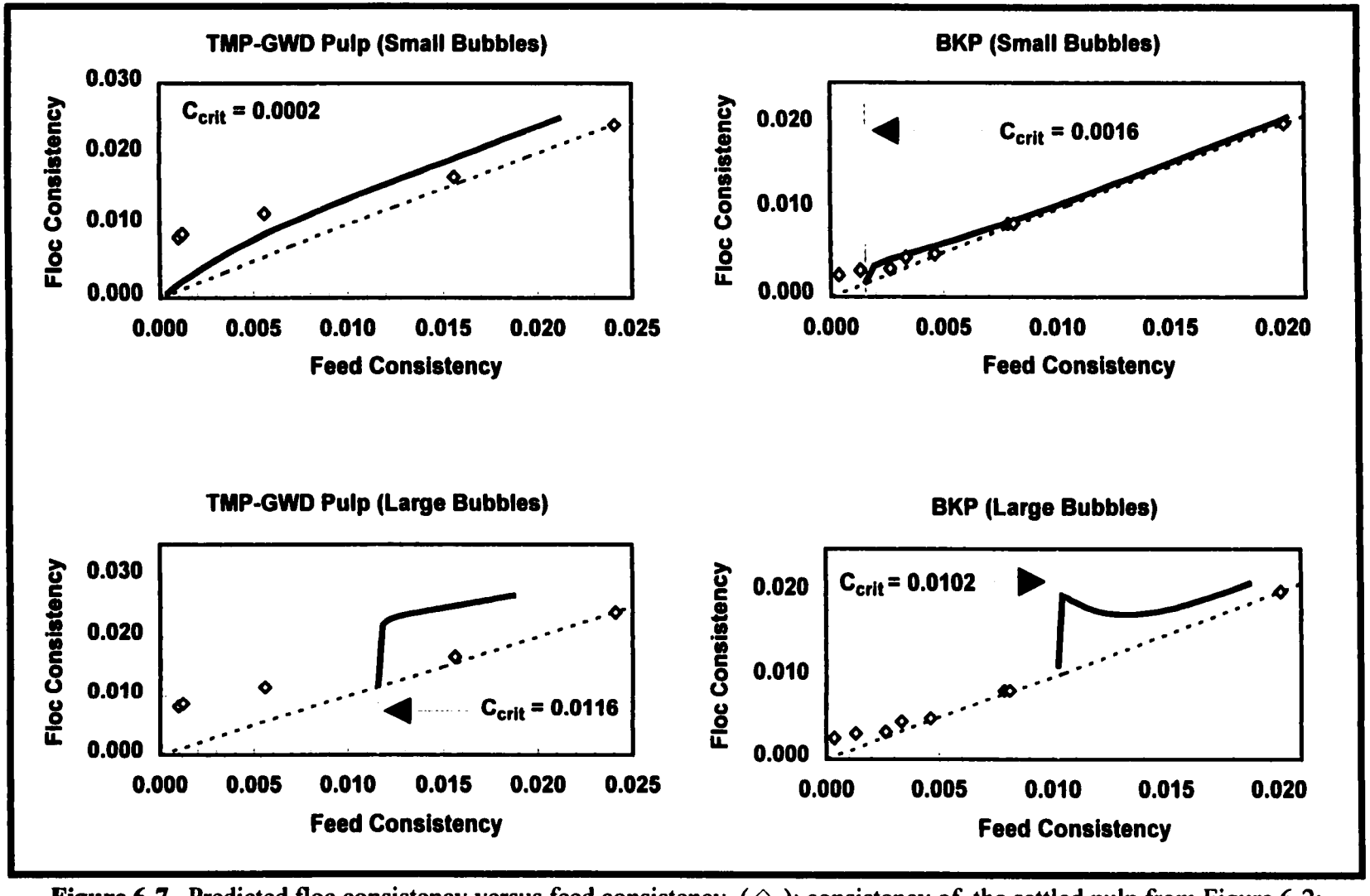

Figure 6-7. Predicted floc consistency versus feed consistency. (◇): consistency of the settled pulp from Figure 6-2; (- - -): (y=x) line. (▬): predicted floc consistency (C_f) from Eq. 6.22

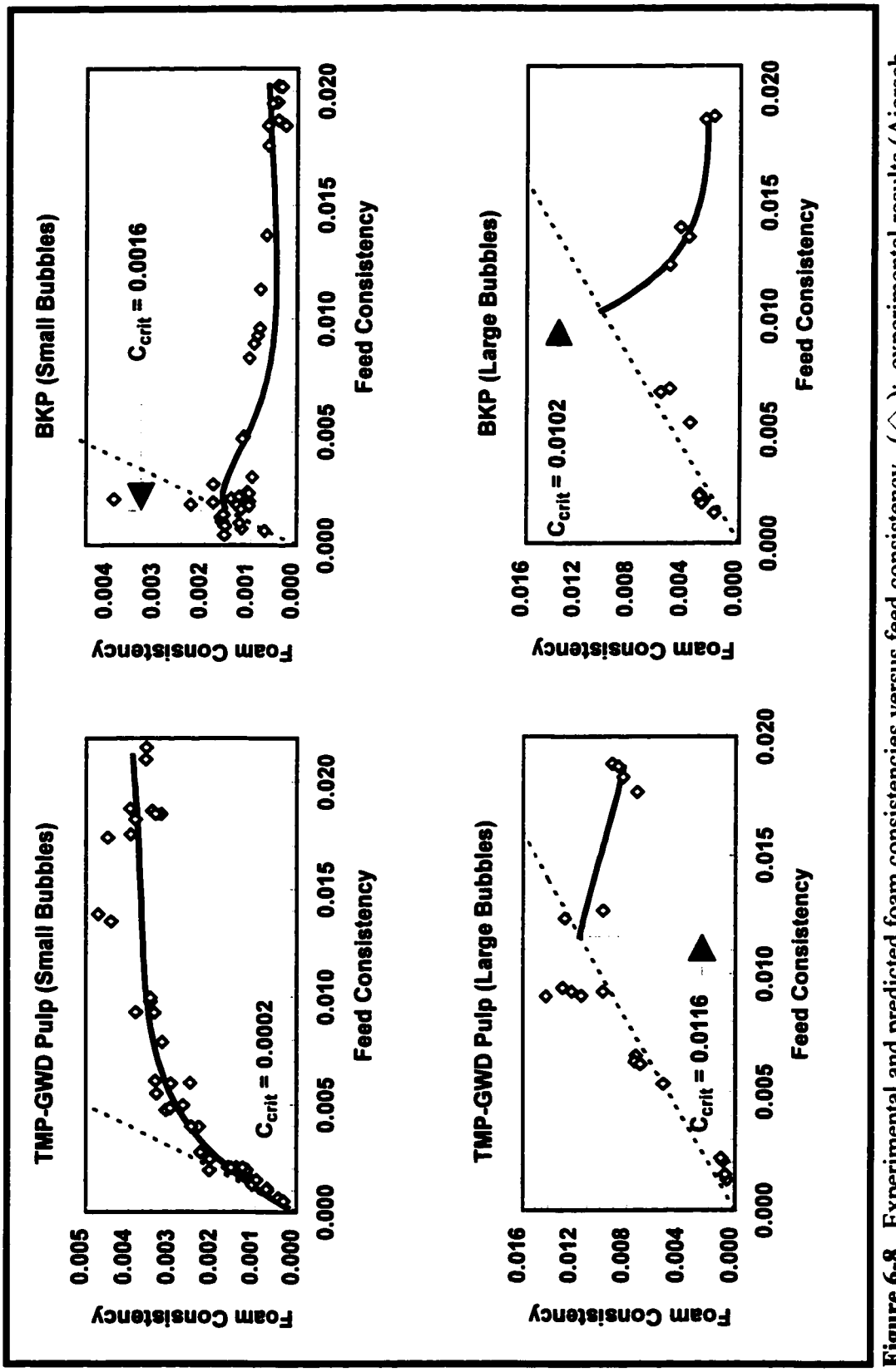

Figure 6-8. Experimental and predicted foam consistencies versus feed consistency. (◇): experimental results (Ajersch, Pelton, 1996); (- - -): (y=x) line. (———): predicted interfloc consistency (C_{if}) from Eq. 6.26. Note that the predicted values are only valid for feed consistencies greater than C_{crit}.

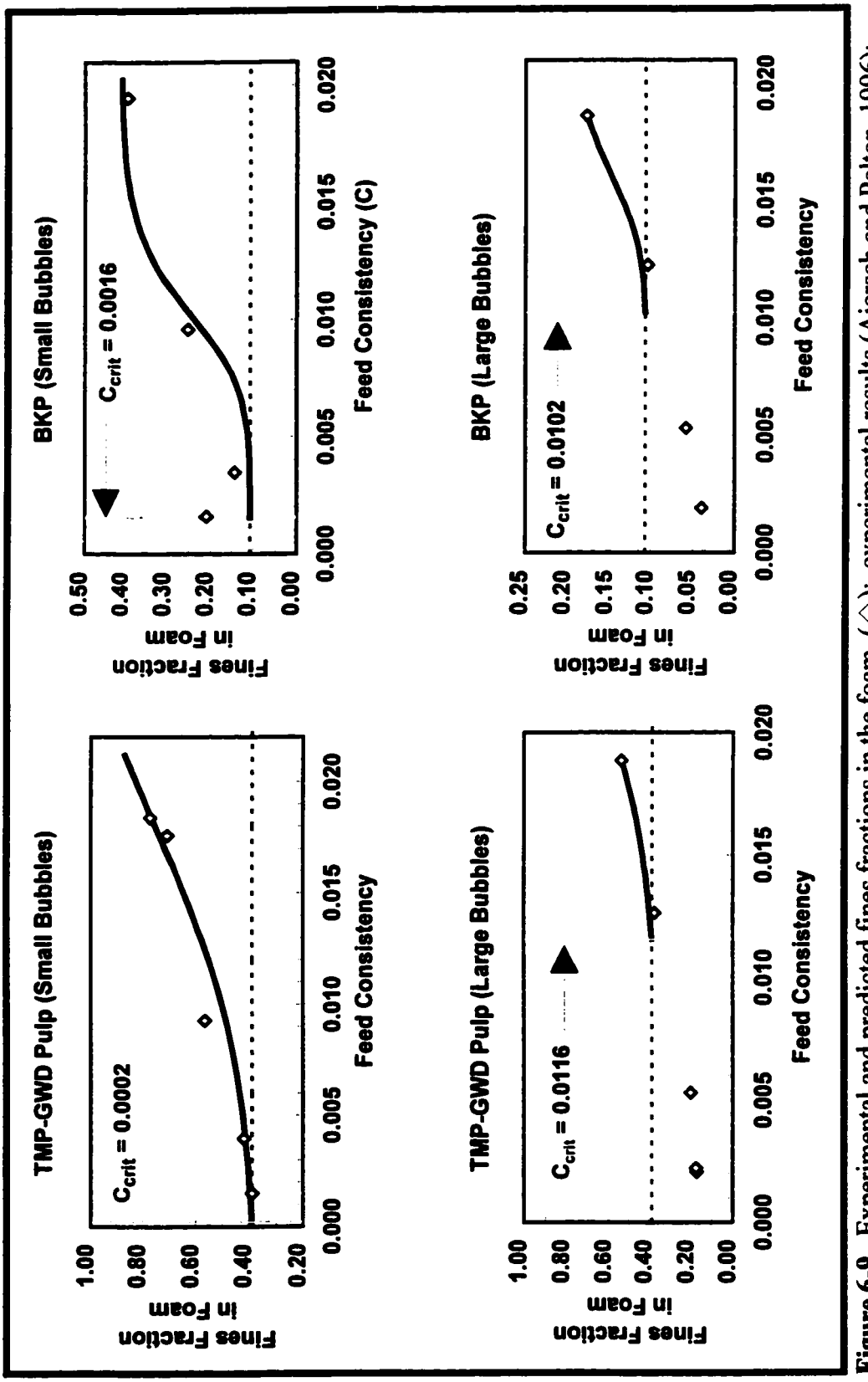

Figure 6-9. Experimental and predicted fines fractions in the foam. (◇): experimental results (Ajersch and Pelton, 1996); (- - -): average fines fraction of the pulp suspension; (———): = predicted interfloc fines fraction (X_{if}) from the Eq. 6.27.

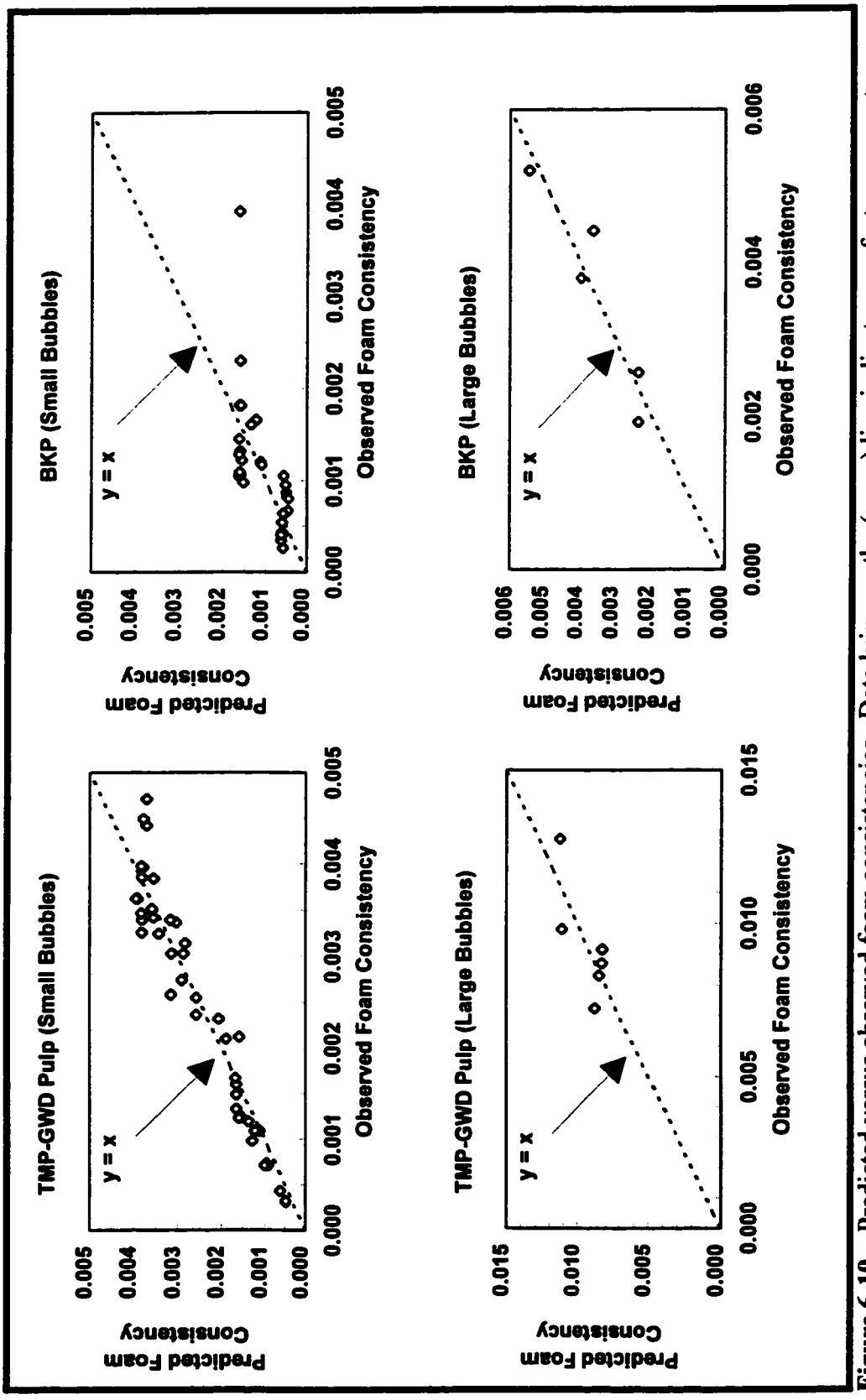

Figure 6-10. Predicted versus observed foam consistencies. Data lying on the (y = x) line indicate a perfect agreement between the model and the experimental data.

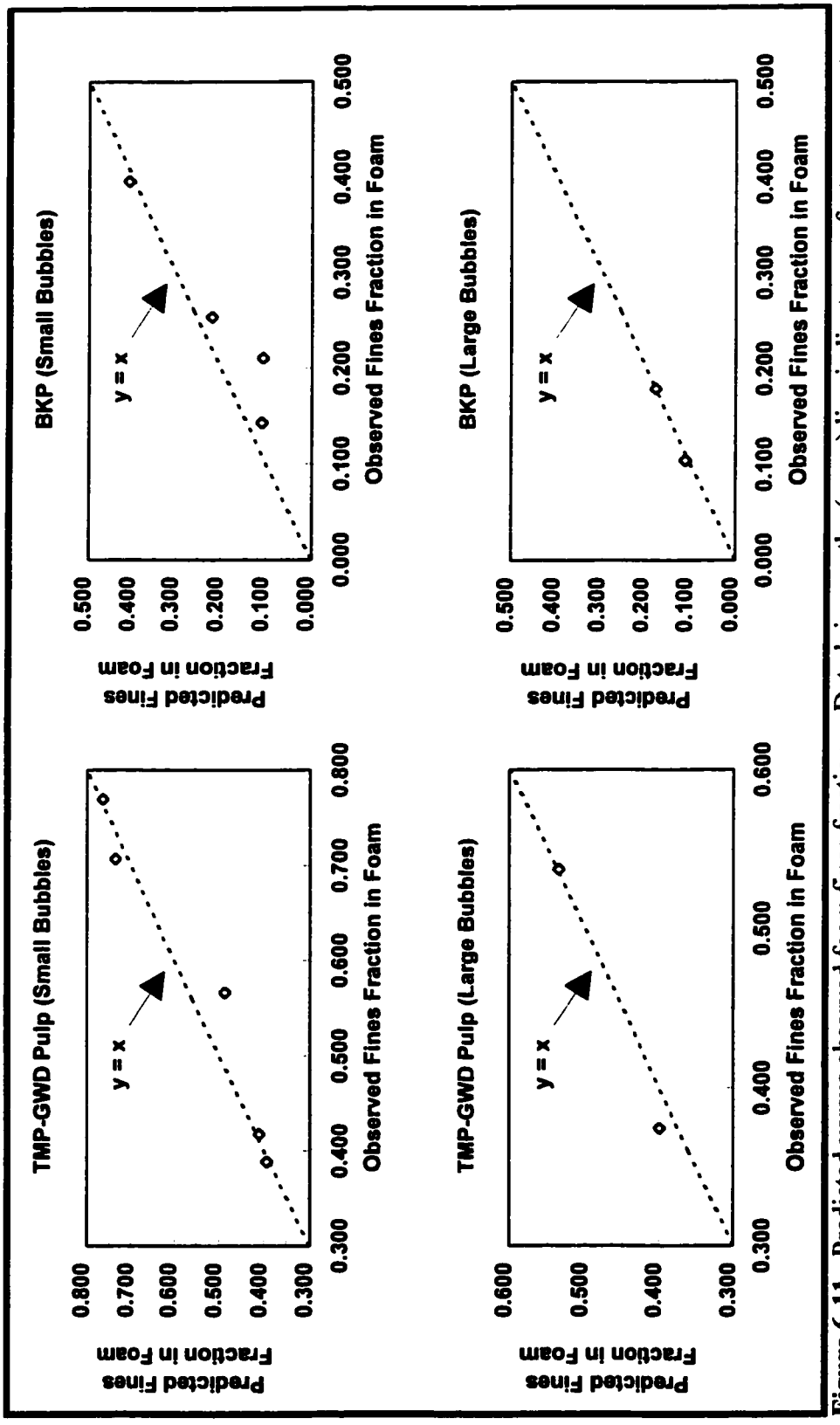

Figure 6-11. Predicted versus observed foam fines fractions. Data lying on the (y = x) line indicate a perfect agreement between the model and the experimental data.

6.4 DISCUSSION

The model presented here is based on the floc exclusion mechanism proposed in the previous chapter (Ajersch, Pelton 1996). With this mechanism, only the pulp in the interfloc regions is entrained into the foam, while the flocculated pulp remains in the pulp suspension. This mechanism was based on the qualitative observations made during the flotation experiments: most of the bubbles appeared to migrate through channels that formed between the flocs. Therefore, the pulp entrained into the foam should be the same as the pulp in these inter-floc channels. (Similar channeling effects have also been reported by others (Went et al. 1993; Taylor et al., 1994; Walmsley, 1992).

The model predictions are more applicable to the small-bubble data where channeling appears more prevalent. The small bubbles were easily diverted around the flocs, while the large bubbles tended to keep the pulp dispersed over a wider consistency range. This was attributed to the relative dimensions between the flocs and bubbles (Ajersch and Pelton, 1996). The small bubbles diameters were an order of magnitude less than the estimated floc diameters, whereas the large bubbles were roughly equal to the floc size. Providing the floc exclusion mechanism is correct, then higher consistencies may be required to provide flocs large and strong enough to enable the channeling of large bubbles to occur.

The onset of flocculation has been correlated to a parameter defined as the "crowding factor" (Kerekes, Schell, 1992). The crowding factor (N) corresponds to the number of fibres contained within the volume swept out by a single fibre:

$$N = \frac{5C_m L^2}{\omega} \qquad [6.30]$$

where C_m is the consistency expressed in %, L is the fibre length expressed in m, and ω the fibre coarseness expressed in kg/m. Eq. 6.30 is based on the assumption that the fibres are straight and uniformly suspended in the pulp suspension. When $N < 1$, fibres are free to move relative to one another. The greater the value of N, the more flocculated the pulp suspension is. When $N > 60$, fibres are considered to form a continuous network (Kerekes, Schell 1992).

The pulp fibres in the BKP in the flotation experiments were longer and had a lower coarseness than the TMP-GWD fibres. The BKP had an arithmetic-average fibre length of L = 1.21 mm and a coarseness value of ω = 13.8 mg/m, while L = 0.34 mm and ω = 29.9 mg/m for the TMP-GWD. According to Eq. 6.30, for any given consistency, the crowding factor for the BKP would be greater than that for the TMP-GWD, and therefore the BKP would have a greater tendency to flocculate. This is apparent in the pulp settling curves in Figure 6-2. The settled volume fractions (ϕ_{Exp}) approached 1 for the BKP much more rapidly than for the TMP-GWD. The quiescent BKP reached a state of 100% flocculation earlier than the TMP-GWD did.

If flocculation occurred earlier with the BKP, then the estimated values of C_{crit} for the BKP should have been lower than for the TMP-GWD. For the small bubble data, C_{crit} was 0.0002 for the TMP-GWD pulp, and 0.0016 for the BKP. This implies that flocculation occurs earlier for the TMP-GWD, which is contrary to what was expected.

The reason for this is not known. It is possible that the large scatter in the data for the BKP at low consistencies resulted in a higher estimate of C_{crit}.

For the large bubble data, the estimates of C_{crit} were 0.0102 for BKP and 0.0116 for TMP-GWD. In this case, the critical consistencies were almost identical, with the C_{crit} being slightly less for the BKP. This follows the expected trend, but it is difficult to conclude whether the lower estimate of C_{crit} for the BKP data is significant. More information is needed, as no data points were available for the BKP-large bubble data between ($0.007 < C < 0.012$).

The estimates of C_{crit} for the large-bubble data were an order of magnitude greater than those for the small bubble data. One possible explanation for this is that the increased turbulence and mixing effects of the large bubbles kept the pulp more dispersed and retarded the onset of flocculation. The predicted floc volume fractions in Figure 6-6 tend to support this hypothesis: with the large bubbles were used, the estimated floc volume fractions were lower than with the small bubbles.

Another possible explanation for the increased values of C_{crit} with the large bubbles involves the different mechanisms by which fibres and fines are transported into the foam at the fibre-water interface. Examining video images of the small-bubble foam revealed spherical bubbles of relatively uniform diameters, with the inter-bubble spaces being of the order of $\approx$ (50 μm to 100 μm). Individual pulp fibres and fines are of the order of 20-30 μm in diameter. Based on the inter-bubble dimensions, this implies that

individual fibres and fines are more likely to be entrained between the bubbles, with the larger flocs being excluded from the foam (Figure 6.12).

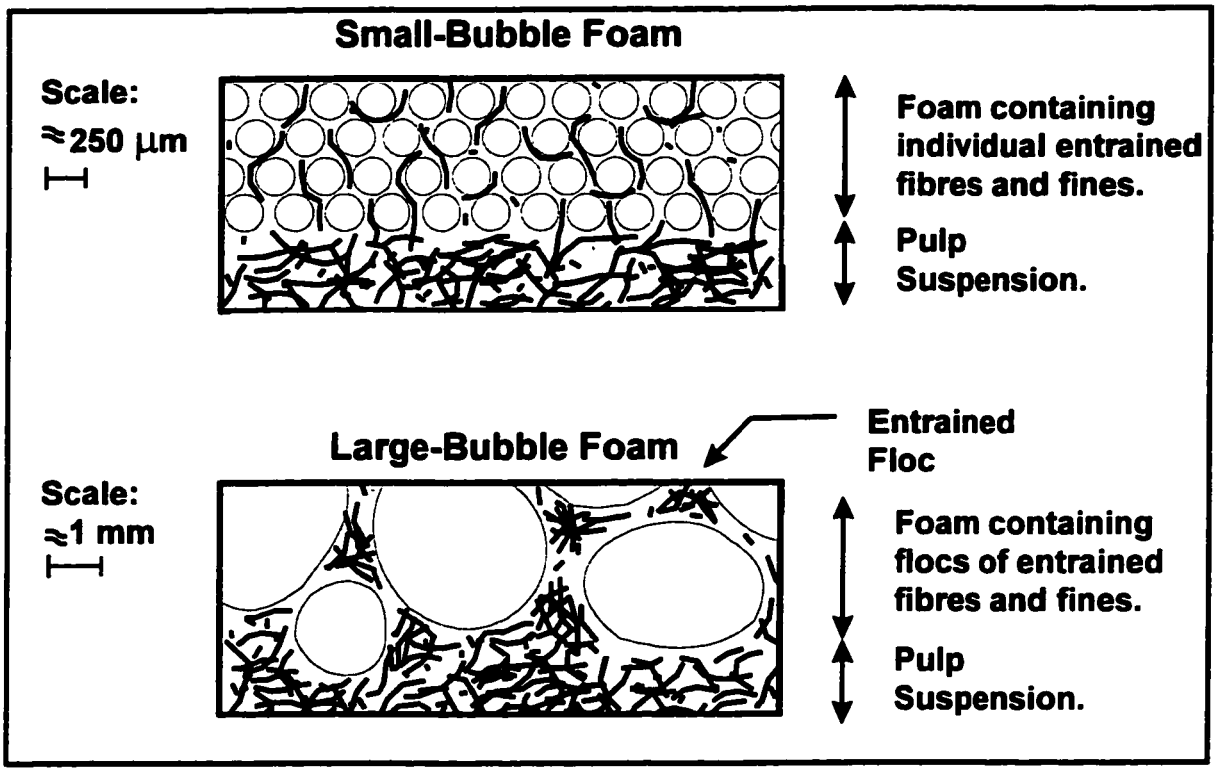

Figure 6-12. Transport of pulp into the foam at the fibre-water interface. With the small bubbles, only individual fibres and fines can be entrained into the foam. With the large bubbles, individual fibres, fines and pulp flocs can all be entrained.

The inter-bubble spaces in large-bubble foams may have been sufficiently large to permit the entrainment of not only individual fibres and fines but small flocs as well (Figure 6.12). This hypothesis is supported by observations at high consistencies with the large-bubble foams: macroscopic fibre bundles of several millimeters in diameter were found at the junctions between the bubbles (Ajersch, Pelton 1996). The entrained

flocs may have resulting in the foam properties to be similar to that of the bulk pulp suspension over a wider range of feed consistencies.

Other Approaches to Modeling

Other approaches were attempted to fit the data to a model but were discarded for various reasons. For example, Kerekes and Schell (1992) first suggested that for a pulp suspensions with a crowding factors (N), zones may exist around the flocs with a crowding factor of N_o. In one of our first attempts, we assumed that that flocs would form such that the crowding factor between the flocs (N_o) remained constant. This was designated the "critical flocculation model". Since pulp fines are generally considered too small to form into networks and flocculate, the crowding factor was re-defined to take into account the presence of pulp fines:

$$N_{fibre} = \left[\frac{\rho_{pulp}\rho_w}{(\rho_{pulp} - \rho_w)C - \rho_{pulp}}\right]\left[\frac{-\pi L^2 C(1 - X_{Fines})}{6\omega}\right] \qquad \text{Eq. [6.31]}$$

N_{fibre} corresponds to the number of long fibres contained in the volume swept by a single fibre, and is a function of consistency and fines fraction. (When $X_{Fines} = 0$, Eq. 6.31 is approximately equal to Eq. 6.30). The detailed calculations in deriving Eq. 6.31 are shown in Appendix D-5.

In the critical flocculation model, the flocs were assumed to be spherical, with a diameter of twice the fibre length (2L). The adjustable parameters were the floc consistency and the total number of flocs. The floc volume fractions were determined by multiplying the number of flocs times the volume of a single floc. The method consisted

of calculating the individual crowding factors of the foam with Eq. 6.31, using the experimental data where the both the foam consistencies and fines fraction were known. An average foam crowding factor ($N_{FoamAvg}$) was determined from theses values and a value of β was then specified. The floc consistency and number of flocs were determined numerically by forcing the equations for the interfloc consistencies (C_{if}) to equal the experimental foam consistencies, and the interfloc crowding factors to equal $N_{FoamAvg}$.

This critical flocculation model was tested on the small bubble data, but did not prove suitable. The model was very sensitive to estimates of β, and the numerical solutions only converged for when $\beta > \approx 0.9$. In addition, the model showed an inverse relation between the floc volume fraction and overall consistency, which is contrary to what was observed in the pulp settling experiments.

In a second approach, no restrictions were placed on the interfloc crowding factor. Instead, a floc consistency was specified. The number of flocs and β were solved numerically by forcing the experimental foam consistencies and fines fractions to equal the equations for C_{if} and X_{if}. The problem with this method was that there were too many degrees of freedom. The mass balances worked for an infinite number of combinations of C_f, β and ϕ_f. In order to characterize the pulp suspensions flocculation, it was necessary to reduce the degrees of freedom, or have an independent measurements of some floc property. This led us to relate C_f and ϕ_f to the experimental settled volumes with in Eqs. 6.8 and 6.20.

The interfloc fines fraction (X_{if}) was very sensitive to the parameter β. For example, for the small bubble data with TMP-GWD, β = 0.957. This caused the X_{if} curve in Figure 6-9 to increase from 0.39 to 0.77. However, changing β changed slightly to the value of 1 would have changed the estimate of X_{if} to the constant value of the overall TMP-GWD fines fraction of 0.39.

As shown in Table 6-1, the fines fraction parameter (β) was always less than 1, which implies that the pulp fines were selectively excluded from the pulp flocs. This is attributed to the longer fibres concentrating in the flocs. Pulp fines, which were too small to entangle and form networks, tended to stay outside the flocs. This exclusion of pulp fines from the flocs was not very great, because in most cases, β is close to 1.

The fact that $\beta \approx 1$ led us to question whether or not this parameter was significant. In another approach, β was eliminated by assuming that the mass of pulp fines per unit mass of water remained constant throughout the pulp suspension. With this assumption, the pulp fines were merely present in the water phase, but did not contribute to flocculation. This eliminated β and reduced the number of adjustable parameters down to α and Ccrit. However, this method tended to overestimate the interfloc consistencies and the mass balances were valid only for a small consistency range. We therefore returned to the original assumption that $X_{FinesFloc} = \beta X_{Fines}$.

Another important assumption in this model was that the pulp density equaled the density of pure cellulose. The value of $\rho_{pulp} = 1.5$ g/cm^3 was arbitrary chosen, because this was close to reported densities of cellulose in the literature. (The Cleveland Rubber

Co.(1968) states that crystalline cellulose has a specific gravity of 1.27 to 1.61. In another source, the density of cellulose found in wood was reported to be 1.535-1.547 g/cm3 (Brandrup, Immercut 1966)). In reality, pulp fibres absorb water, and the wet fibre density is likely to be less than that of pure cellulose. To test the model's sensitivity to ρ_{pulp}, we recalculated the parameters for the small bubble data assuming $\rho_{pulp} = 1.2$ g/cm^3 instead of 1.5 g/cm^3. The results are summarized in Table 6-2. The estimates for C_{crit}, α and β are essentially the same, which indicates that the model is relatively insensitive to the assumed value of ρ_{pulp}.

Table 6-2: Calculated parameters for the small-bubble data using different estimates of pulp density.

Pulp Type	ρ_{pulp}	C_{crit}	α	β
TMP-GWD	1.5 g/cm3	2.075×10^{-4}	0.8630	0.9570
TMP-GWD	1.2 g/cm3	2.094×10^{-4}	0.8623	0.9567
BKP	1.5 g/cm3	0.00155	0.9695	0.9974
BKP	1.2 g/cm3	0.00155	0.9694	0.9973

Implications

The original purpose of the flotation experiments (Ajersch, Pelton 1996) was to determine the extent to which entrainment contributed to pulp loss. This present work demonstrates that additional information can be gained from bench-top flotation experiments. By combining the data from flotation tests along with pulp sedimentation data, the pulp suspensions' state of flocculation under mixed conditions can be estimated. This method may prove useful when optical methods for measuring flocculation are not convenient nor available.

This work represents the first step toward quantifying pulp loss in flotation deinking systems. Once a pulp suspensions' interfloc properties can be measured, the next step is to develop a model to predict the amount of water which is entrained into the foam. This involves modeling 3-phase flow in heterogeneous systems, and is recommended as a subject of further research.

6.5 CONCLUSIONS

- A three-parameter model was derived to predict the foam consistencies and fines fractions from flotation experiments with mixed pulp suspensions.

- Using bench-top flotation experiments combined with pulp settling experiments, the model can be used to characterize a pulp suspensions state of flocculation in terms of floc volume fraction, floc consistency and the relative distribution of pulp fines between the flocs and non-flocculated regions.

- The model is based on three key assumptions. First, the floc volume fractions in mixed pulp are proportional to the settled pulp volumes measured under quiescent conditions. Second, the floc consistencies were related to a theoretical maximum and minimum floc consistency, and were also proportional to the floc volume fractions. Finally, the pulp fines fractions in the flocs were directly proportional to the overall fines fraction of the pulp suspension.

- The model is most applicable when the flow conditions are such that small bubbles are channeled around the pulp flocs.

- The model indicates that pulp fines tend to be excluded from pulp flocs.

LIST OF SYMBOLS

C = Overall consistency, defined as the mass fraction of pulp in the pulp suspension.

C_{crit} = Adjustable parameter, corresponding to the consistency at which pulp flocs first form.

C_f = Floc consistency.

C_{Feed} = Feed consistency from the pulp flotation experiments.

C_{fmax} = Maximum floc consistency. This corresponds to the hypothetical case where all the pulp exists in flocs, and the interfloc region contains only water.

C_{Foam} = Foam consistency.

C_{if} = Interfloc consistency.

$C_m(\phi)$ = Consistency, defined as a function of the pulp volume fraction (ϕ).

M_{fines} = Total mass of pulp fines (g).

$M_{finesFlocs}$ = Mass of pulp fines within the flocs (g).

M_{pulp} = Total mass of pulp in the pulp suspension (g).

$M_{pulpFlocs}$ = Mass of pulp within the flocs (g).

M_{pulpif} = Mass of pulp in the interfloc region (g).

$M_{pulpEnt}$ = Mass of pulp entrained into the foam (g).

M_{wEnt} = Mass of water entrained into the foam (g).

V_{Flocs} = Volume of the flocs (ml).

V_{Pulp} = Total volume of the pulp in the pulp suspension (ml).

$V_{pulpFlocs}$ = Volume of pulp within the flocs (ml).

V_{Set} = Final volume to which the pulp fibres and fines settle under quiescent conditions. V_{Set} is determined from the pulp settling experiments (ml).

V_{Total} = Total volume (ml).

X_{Fines} = Overall fines fraction of the pulp suspension, which is defined as the mass fraction of fines in the pulp.

$X_{FinesFloc}$ = Fines fraction within the flocs.

X_{Foam} = Fines fraction in the foam.

X_{if} = Fines fraction in the interfloc region.

Greek Symbols:

α: = Adjustable parameter, relating the floc volume fraction (f_f) to $f_{Exp}(C)$.

β: = Adjustable parameter, relating the overall fines fraction to the fines fraction in the flocs (where $X_{FinesFloc} = bX_{Fines}$).

$\phi = \phi(C)$ = Volume fraction of pulp in the pulp suspension.

$\phi(C_f)$ = Volume fraction of pulp in the flocs.

$\phi(C_{fmax})$ = Volume fraction of pulp at the maximum floc consistency.

$\phi(C_{if})$ = Volume fraction of pulp in the interfloc region.

$\phi_{Exp}(C)$ = Experimental settled pulp volume fraction, defined as a function of C. $\phi_{Exp}(C)$ is defined as (V_{Set}/V_{Total}).

ϕ_f = Floc volume fraction (cm^3).

ρ_{pulp} = Density of the cellulosic material (pulp). (Assumed to be 1.5 g/cm^3).

ρ_w = Density of pure water (Assumed to be 1 g/cm^3).

REFERENCES

AJERSCH, M. and PELTON, R.H. "Mechanisms of Pulp Loss in Flotation Deinking", *J. Pulp Paper Sci.* 22(9):J338-J344 (1996).

BRANDRUP, J and IMMERCUT, E.H. (Editors). *Polymer Handbook.* Interscience Publishers. John Wiley & Sons, Inc. (USA) (1966).

BONANO, E.J. "A Study of Floc Breakup and Formation in Flowing Concentrated Fibre Suspensions", *Int. J. Multiphase Flow.* 10(5):623-633 (1984).

CLEVELAND RUBBER CO. *Handbook of Chemistry and Physics 49th Ed.*, Cleveland Rubber Co. Cleveland, Ohio (1968).

HOURANI, M.J. "Fibre Flocculation in Pulp Suspensions Flow. Part 2: Experimental Results", *Tappi J.* June:186-189 (1988).

KEREKES, R.J. and SCHELL, C.J. "Characterization of Fibre Flocculation Regimes by a Crowding Factor", *J. Pulp Paper Sci.* 18(1):J32-J38 (1992).

KEREKES, R.J. and SCHELL, C.J. "Effects of Fiber Length and Coarseness on Pulp Flocculation", *Tappi J.* 78(2):133-139 (1995).

KEREKES, R.J., SOZYNSKI, R.M. and TAM DOO, P.A., "The Flocculation of Pulp Fibres", Papermaking Raw Materials, Trans. 8th. Fund. Res. Symp. (Oxford), 265-309 (1985).

MEYER, R. and WAHREN, D. "On the Elastic Properties of Three-Dimensional Fibre Networks", *Svensk Papperstidn.* 67(10):432-436 (1964).

PETRI, B.M. "Deinking Newspaper in an Opened and Packed Flotation Column', M.A.Sc.Thesis, Univ. Toronto (1994).

SCHWINGER, K and DOBIAS, B., "The Influence of Calcium Ions of the Loss of Fibre in the Flotation Deinking Process", 1st Res. Forum on Recycling, Tech. Sect., CPPA, 1-11 (1991).

TAYLOR, K.E., GHIAASIAAN, S.M., ABDEL-KHALIK, S.I., LINDSAY, J.D. and GEORGE, J., "Macroscopic Flow Structures in a Bubbling Paper Pulp-Water Slurry", Tech. Paper series Number 537, Inst. Paper Sci. Technol., Altanta, GA (1994).

TURVEY, R.W. "Why do Fibres Float?", *J. Pulp Paper Sci.* 19(2):J52-J57 (1993).

WAHREN, D. "Fiber Network Structures in Papermaking Operations", Proc. Paper Sci. Tech. The Cutting Edge. Conf, 112-129 (1979).

WALMSLEY, M.R.W., "Air Bubble Motion in Wood Pulp Fibre Suspension" *APPITA* 45:509-515 (1992).

WENT, J. JAMIALAHMADI, M. and MULLER-STEINHAGEN, H.M., "Effect of Wood Pulp Fibre Concentration on Gas Hold-up in Bubble Column", *Chem. Ing. Tech.* 65(3):306-308 (1993).

CHAPTER 7

SUMMARY

This purpose of this thesis was to investigate the factors contributing to pulp loss in flotation deinking systems. Three pulp loss mechanisms were proposed in the introductory chapter. In bubble-fibre adhesion, air bubbles adhere to the hydrophobic areas of pulp fibers and fines and cause the pulp to float. In mechanical entrapment, bubbles are physically retained in fibre networks by mechanical forces. Flotation occurs when a sufficient number of trapped bubbles are present in the fibre networks and/or pulp flocs. In entrainment, on the other hand, no direct contact is made between the bubbles and pulp. Instead, the fibres and fines are hydraulically transported into the froth along with the water.

In the literature on flotation deinking, the most widely-accepted mechanism of pulp loss to date has been bubble-fibre adhesion. Other researchers, however, have reported receding contact angles of zero (implying no adhesion) for a wide variety of fibres. The observations made in Chapters 2 and 4 confirm that bubble adhesion is unlikely to occur. In the bubble generation tests in Chapter 2, no evidence of bubble adhesion was found with fibers in a commercial newsprint pulp which contained deinked pulp. Nor were trapped air pockets detected in headbox pulps or in flotation deinking

rejects. In the flow visualization studies in Chapter 4, bubbles were seen to migrate around and between individual fibres of bleached kraft pulp instead of adhering to them.

The primary mechanism of bubble hold-up in pulp suspensions was therefore attributed to mechanical entrapment. The parameters affecting mechanical entrapment were evaluated in Chapters 3 and 4. In Chapter 3, the fundamental experiments in which ball bearings were dropped into quiescent pulp were used as a model for bubble migration through pulp suspensions. Using existing correlations of the yield stress measurements of the pulp, it was possible to estimate the total distance that the ball bearings could penetrate into quiescent fibre beds. When comparing the experimental results with existing published data on bubble hold-up in quiescent pulp, an important fact was noted: air bubbles could migrate further through a quiescent, flocculated pulp suspension than ball bearings of similar size could migrate through uniform, settled fibre beds. To explain the differences between these two sets of results, it was concluded that air bubbles must migrate through pulp via the dilute areas between the flocs.

The flow visualization studies in Chapter 4 provided visual proof that bubble migration occurred predominantly in the inter-floc regions in pulp suspensions. The video sequences of pulp suspensions under flow conditions showed bubbles migrating upwards in a series of random steps, as they were repeatedly mechanically trapped and released from pulp flocs. A preliminary model was presented to describe mechanical entrapment in uniform and flocculated pulp suspensions in quiescent conditions. In

mixed pulp suspensions, it was determined that the likelihood of mechanical entrapment was greatly reduced, as compared to quiescent conditions. Under turbulent conditions, shear forces tended to detach trapped bubbles from beneath pulp flocs, or disperse transient pulp flocs and release any bubbles trapped inside. Mechanical entrapment was not therefore not considered to be a significant pulp loss mechanism in conventional flotation deinking cells in which the pulp is vigorously mixed.

In the experimental flotation tests in Chapter 5, the use of a surfactant combined with the mixing action of the rising bubbles rendered the effects of bubble-fibre adhesion and mechanical entrapment negligible. The results proved that significant amounts of pulp could be floated without the use of deinking chemicals, The dominant pulp loss mechanism in the experiments was attributed to entrainment, whereby pulp fibres and fines were hydraulically transported into the foam with the water. Flocculation was found to have a large effect on the amount of pulp entrained into the froth; therefore two entrainment regimes were proposed which depended on flocculation. When the pulp was sufficiently dilute and mixed such that no flocs were present, the fibre content of the foam was similar to that of the feed. When flocs were present, bubbles were channeled around the pulp flocs, resulting in conditions where the properties of the foam represented the properties of the pulp existing in the dilute area between the flocs.

The conclusions derived from Chapter 5 implied that in order to predict pulp losses in mixed pulp suspension, it was necessary to characterize the pulp suspensions' state of flocculation. This was achieved in Chapter 6: a three-parameter model was

derived which predicted the consistencies and pulp fines fraction in the foam from the flotation experiments. By combining the bench-top flotation results with independently-measured pulp sedimentation curves, the model could characterize a pulp suspensions state of flocculation in terms the floc volume fraction, floc consistency and the relative distribution of fibres and fines between the flocs and non-flocculated regions. The model was more applicable when the bubbles were sufficiency small to be channeled around the pulp flocs, and the model predicted that pulp fines tend to be excluded from pulp flocs. .

The experimental results from this thesis confirm that pulp loss can occur without bubble-fibre adhesion. In an actual flotation deinking plant, the relative contributions of bubble adhesion and entrainment to pulp loss have yet to be quantified. Although it is considered unlikely to occur, if bubble adhesion is the dominant pulp loss mechanism, then pulp losses could be minimized by altering the surface chemistry of the air-fibre-water interface. If entrainment is the dominant pulp loss mechanism, then reduction of pulp loss can be achieved by altering the physical parameters to minimize water recovery. Investigating methods to reduce the up-take of water in flotation froths would be of interest for the next research topic on pulp loss in deinking systems.

APPENDIX A

Raw Data from the Ball-Bearing Entrapment Experiments from Chapter 3.

Table A.1. Data for BKP, Large B.B.'s.

Note: For pulp type, BKP = Bleached kraft pulp; TMP-GWD = Mechanical Pulp.
For B.B. size, L = 1/16" diameter. S = 1/32" diameter.

Pulp Type	B.B. Size	Initial Height of Fibre Bed H_o (cm)	Final Height of B.B. H_f (cm)	Initial Pulp Consistency (C_{mInit})	Distance Travelled by B.B. ΔH (cm)	Estimated Consistency of Settled Fibre Bed (C_{mo})
Data for ($0.0015 < C_{mo} < 0.0020$)						
BKP	L	6.3	0.0	0.00094	6.3	0.00187
BKP	L	6.3	0.9	0.00094	5.4	0.00187
BKP	L	6.4	0.0	0.00098	6.4	0.00191
BKP	L	6.9	0.0	0.00094	6.9	0.00171
BKP	L	6.9	0.0	0.00094	6.9	0.00171
BKP	L	7.4	0.0	0.00109	7.4	0.00184
BKP	L	7.5	0.0	0.00094	7.5	0.00157
BKP	L	7.5	0.0	0.00116	7.5	0.00193
Data for ($0.0020 < C_{mo} < 0.0025$)						
BKP	L	5.0	0.2	0.00094	4.8	0.00236
BKP	L	5.0	1.1	0.00094	3.9	0.00236
BKP	L	5.0	1.6	0.00094	3.4	0.00236
BKP	L	5.0	0.0	0.00098	5.0	0.00245
BKP	L	5.0	0.4	0.00098	4.6	0.00245
BKP	L	5.0	1.2	0.00098	3.8	0.00245
BKP	L	5.2	1.2	0.00094	4.0	0.00227
BKP	L	5.3	0.0	0.00094	5.3	0.00223
BKP	L	5.3	0.9	0.00094	4.4	0.00223
BKP	L	5.3	1.4	0.00094	3.9	0.00223
BKP	L	5.4	2.3	0.00103	3.1	0.00239
BKP	L	5.5	0.0	0.00098	5.5	0.00222
BKP	L	5.5	0.4	0.00098	5.1	0.00222
BKP	L	5.5	0.8	0.00103	4.7	0.00235
BKP	L	5.6	1.8	0.00103	3.8	0.00231
BKP	L	5.6	3.0	0.00103	2.6	0.00231
BKP	L	5.7	0.0	0.00098	5.7	0.00215

Table A.1 (Cont'd.)

Pulp Type	B.B. Size	Initial Height of Fibre Bed H_o (cm)	Final Height of B.B. H_f (cm)	Initial Pulp Consistency (C_{mInit})	Distance Travelled by B.B. ΔH (cm)	Estimated Consistency of Settled Fibre Bed (C_{mo})
BKP	L	5.7	0.2	0.00098	5.5	0.00215
BKP	L	5.7	0.0	0.00103	5.7	0.00226
BKP	L	5.8	0.4	0.00103	5.4	0.00223
BKP	L	5.8	0.0	0.00109	5.8	0.00235
BKP	L	6.0	0.0	0.00094	6.0	0.00197
BKP	L	6.0	0.0	0.00109	6.0	0.00227
BKP	L	6.0	1.0	0.00109	5.0	0.00227
BKP	L	6.0	0.0	0.00116	6.0	0.00241
BKP	L	6.1	0.0	0.00109	6.1	0.00223
BKP	L	6.1	0.0	0.00109	6.1	0.00223
BKP	L	6.2	0.0	0.00109	6.2	0.00220
BKP	L	6.2	2.5	0.00116	3.7	0.00233
BKP	L	6.2	0.7	0.00120	5.5	0.00242
BKP	L	6.2	0.7	0.00120	5.5	0.00242
BKP	L	6.3	0.0	0.00116	6.3	0.00229
BKP	L	6.3	0.0	0.00120	6.3	0.00238
BKP	L	6.3	0.4	0.00120	5.9	0.00238
BKP	L	6.3	0.3	0.00120	6.0	0.00238
BKP	L	6.4	0.4	0.00120	6.0	0.00235
BKP	L	6.5	0.0	0.00109	6.5	0.00209
BKP	L	6.5	1.6	0.00120	4.9	0.00231
BKP	L	6.5	0.0	0.00124	6.5	0.00238
BKP	L	6.6	0.7	0.00116	5.9	0.00219
BKP	L	6.6	0.3	0.00120	6.3	0.00227
BKP	L	6.6	0.0	0.00124	6.6	0.00234
BKP	L	6.6	2.1	0.00124	4.5	0.00234
BKP	L	6.7	0.0	0.00120	6.7	0.00224
BKP	L	6.7	0.0	0.00120	6.7	0.00224
BKP	L	6.7	0.3	0.00120	6.4	0.00224
BKP	L	6.7	1.4	0.00129	5.3	0.00241
BKP	L	6.8	0.0	0.00109	6.8	0.00200
BKP	L	6.9	0.0	0.00124	6.9	0.00224
BKP	L	6.9	0.5	0.00124	6.4	0.00224
BKP	L	7.0	1.0	0.00120	6.0	0.00214
BKP	L	7.0	0.7	0.00120	6.3	0.00214

Table A.1 (Cont'd.)

Pulp Type	B.B. Size	Initial Height of Fibre Bed H_o (cm)	Final Height of B.B. H_f (cm)	Initial Pulp Consistency (C_{minit})	Distance Travelled by B.B. ΔH (cm)	Estimated Consistency of Settled Fibre Bed (C_{mo})
BKP	L	7.2	0.0	0.00116	7.2	0.00201
BKP	L	7.2	0.0	0.00120	7.2	0.00209
BKP	L	7.2	0.6	0.00124	6.6	0.00215
BKP	L	7.2	0.0	0.00129	7.2	0.00224
BKP	L	7.3	0.0	0.00120	7.3	0.00205
BKP	L	7.3	0.0	0.00124	7.3	0.00212
BKP	L	7.5	0.3	0.00120	7.2	0.00200
BKP	L	7.5	0.0	0.00120	7.5	0.00200
BKP	L	7.6	0.0	0.00124	7.6	0.00204
BKP	L	7.6	0.6	0.00124	7.0	0.00204
Data for ($0.0025 < C_{mo} < 0.0030$)						
BKP	L	4.1	1.5	0.00094	2.6	0.00288
BKP	L	4.2	0.7	0.00094	3.5	0.00281
BKP	L	4.2	0.6	0.00098	3.6	0.00291
BKP	L	4.2	0.8	0.00098	3.4	0.00291
BKP	L	4.2	1.7	0.00098	2.5	0.00291
BKP	L	4.4	1.0	0.00094	3.4	0.00268
BKP	L	4.4	1.8	0.00094	2.6	0.00268
BKP	L	4.4	1.7	0.00098	2.7	0.00278
BKP	L	4.4	2.4	0.00098	2.0	0.00278
BKP	L	4.5	0.0	0.00094	4.5	0.00262
BKP	L	4.5	1.3	0.00094	3.2	0.00262
BKP	L	4.6	0.8	0.00094	3.8	0.00257
BKP	L	4.6	1.3	0.00098	3.3	0.00266
BKP	L	4.7	0.9	0.00094	3.8	0.00251
BKP	L	4.7	1.8	0.00103	2.9	0.00275
BKP	L	4.7	1.9	0.00103	2.8	0.00275
BKP	L	4.8	1.1	0.00094	3.7	0.00246
BKP	L	4.8	0.9	0.00098	3.9	0.00255
BKP	L	4.8	0.0	0.00103	4.8	0.00269
BKP	L	4.8	0.8	0.00103	4.0	0.00269
BKP	L	4.8	1.4	0.00103	3.4	0.00269
BKP	L	4.9	0.7	0.00103	4.2	0.00263
BKP	L	4.9	1.3	0.00103	3.6	0.00263

Table A.1 (Cont'd.)

Pulp Type	B.B. Size	Initial Height of Fibre Bed H_o (cm)	Final Height of B.B. H_f (cm)	Initial Pulp Consistency (C_{mInit})	Distance Travelled by B.B. ΔH (cm)	Estimated Consistency of Settled Fibre Bed (C_{mo})
BKP	L	4.9	0.0	0.00115	4.9	0.00292
BKP	L	5.0	1.3	0.00103	3.7	0.00258
BKP	L	5.1	0.5	0.00103	4.6	0.00253
BKP	L	5.1	1.5	0.00103	3.6	0.00253
BKP	L	5.1	1.7	0.00103	3.4	0.00253
BKP	L	5.1	1.8	0.00103	3.3	0.00253
BKP	L	5.1	0.2	0.00115	4.9	0.00281
BKP	L	5.2	0.8	0.00103	4.4	0.00248
BKP	L	5.2	0.8	0.00103	4.4	0.00248
BKP	L	5.2	1.4	0.00103	3.8	0.00248
BKP	L	5.2	1.5	0.00115	3.7	0.00275
BKP	L	5.2	1.7	0.00115	3.5	0.00275
BKP	L	5.2	1.7	0.00120	3.5	0.00289
BKP	L	5.2	1.8	0.00120	3.4	0.00289
BKP	L	5.3	0.0	0.00109	5.3	0.00257
BKP	L	5.3	0.8	0.00115	4.5	0.00270
BKP	L	5.3	1.0	0.00115	4.3	0.00270
BKP	L	5.4	1.6	0.00115	3.8	0.00265
BKP	L	5.4	2.3	0.00115	3.1	0.00265
BKP	L	5.4	0.6	0.00120	4.8	0.00278
BKP	L	5.4	1.8	0.00120	3.6	0.00278
BKP	L	5.5	0.0	0.00109	5.5	0.00247
BKP	L	5.5	0.0	0.00109	5.5	0.00247
BKP	L	5.5	0.0	0.00115	5.5	0.00260
BKP	L	5.5	1.4	0.00120	4.1	0.00273
BKP	L	5.5	3.1	0.00120	2.4	0.00273
BKP	L	5.6	0.5	0.00115	5.1	0.00256
BKP	L	5.7	0.5	0.00115	5.2	0.00251
BKP	L	5.8	0.4	0.00115	5.4	0.00247
BKP	L	5.8	0.6	0.00120	5.2	0.00259
BKP	L	5.8	0.7	0.00120	5.1	0.00259
BKP	L	5.8	1.6	0.00120	4.2	0.00259
BKP	L	5.9	3.3	0.00120	2.6	0.00254
BKP	L	5.9	0.0	0.00124	5.9	0.00262
BKP	L	6.0	0.5	0.00120	5.5	0.00250

Table A.1 (Cont'd.)

Pulp Type	B.B. Size	Initial Height of Fibre Bed H_o (cm)	Final Height of B.B. H_f (cm)	Initial Pulp Consistency (C_{mInit})	Distance Travelled by B.B. ΔH (cm)	Estimated Consistency of Settled Fibre Bed (C_{mo})
BKP	L	6.0	1.0	0.00120	5.0	0.00250
BKP	L	6.0	1.4	0.00120	4.6	0.00250
BKP	L	6.0	0.8	0.00120	5.2	0.00250
BKP	L	6.0	1.5	0.00120	4.5	0.00250
BKP	L	6.0	2.4	0.00120	3.6	0.00250
BKP	L	6.0	0.0	0.00124	6.0	0.00258
BKP	L	6.0	0.0	0.00124	6.0	0.00258
BKP	L	6.0	1.5	0.00124	4.5	0.00258
BKP	L	6.1	0.7	0.00120	5.4	0.00246
BKP	L	6.2	0.0	0.00124	6.2	0.00250
BKP	L	6.2	0.0	0.00124	6.2	0.00250
BKP	L	6.2	0.0	0.00129	6.2	0.00260
BKP	L	6.3	1.0	0.00129	5.3	0.00256
BKP	L	6.3	2.2	0.00129	4.1	0.00256
BKP	L	6.5	0.7	0.00129	5.8	0.00248
Data for ($0.0030 < C_{mo} < 0.0035$)						
BKP	L	3.6	1.4	0.00094	2.2	0.00328
BKP	L	3.6	1.8	0.00094	1.8	0.00328
BKP	L	3.6	1.4	0.00098	2.2	0.00340
BKP	L	3.7	1.8	0.00094	1.9	0.00319
BKP	L	3.7	1.3	0.00098	2.4	0.00331
BKP	L	3.7	1.3	0.00098	2.4	0.00331
BKP	L	3.8	1.2	0.00098	2.6	0.00322
BKP	L	3.8	2.3	0.00103	1.5	0.00340
BKP	L	3.9	1.1	0.00098	2.8	0.00314
BKP	L	4.0	0.7	0.00098	3.3	0.00306
BKP	L	4.0	1.1	0.00098	2.9	0.00306
BKP	L	4.0	1.2	0.00098	2.8	0.00306
BKP	L	4.0	1.8	0.00103	2.2	0.00323
BKP	L	4.0	1.8	0.00103	2.2	0.00323
BKP	L	4.0	0.3	0.00109	3.7	0.00340
BKP	L	4.0	0.3	0.00109	3.7	0.00340
BKP	L	4.1	1.2	0.00098	2.9	0.00298
BKP	L	4.2	0.6	0.00109	3.6	0.00324

Table A.1 (Cont'd.)

Pulp Type	B.B. Size	Initial Height of Fibre Bed H_o (cm)	Final Height of B.B. H_f (cm)	Initial Pulp Consistency (C_{minit})	Distance Travelled by B.B. ΔH (cm)	Estimated Consistency of Settled Fibre Bed (C_{mo})
BKP	L	4.2	1.5	0.00115	2.7	0.00341
BKP	L	4.2	0.0	0.00116	4.2	0.00344
BKP	L	4.2	1.1	0.00116	3.1	0.00344
BKP	L	4.2	1.4	0.00116	2.8	0.00344
BKP	L	4.3	0.1	0.00109	4.2	0.00317
BKP	L	4.3	0.5	0.00109	3.8	0.00317
BKP	L	4.4	1.5	0.00120	2.9	0.00341
BKP	L	4.4	1.9	0.00120	2.5	0.00341
BKP	L	4.5	1.0	0.00109	3.5	0.00302
BKP	L	4.5	1.0	0.00120	3.5	0.00334
BKP	L	4.6	0.4	0.00116	4.2	0.00314
BKP	L	4.6	0.5	0.00116	4.1	0.00314
BKP	L	4.7	1.1	0.00129	3.6	0.00343
BKP	L	4.7	1.3	0.00129	3.4	0.00343
BKP	L	4.8	0.6	0.00116	4.2	0.00301
BKP	L	4.8	0.6	0.00116	4.2	0.00301
BKP	L	4.8	1.7	0.00129	3.1	0.00336
BKP	L	5.0	2.5	0.00129	2.5	0.00322
BKP	L	5.2	1.6	0.00129	3.6	0.00310
Data for (0.0035 < Cmo < 0.0040)						
BKP	L	3.1	1.5	0.00094	1.6	0.00381
BKP	L	3.3	0.8	0.00094	2.5	0.00358
BKP	L	3.4	1.1	0.00094	2.3	0.00347
BKP	L	3.4	1.6	0.00094	1.8	0.00347
BKP	L	3.4	1.7	0.00094	1.7	0.00347
BKP	L	3.4	1.8	0.00094	1.6	0.00347
BKP	L	3.4	1.9	0.00094	1.5	0.00347
BKP	L	3.4	2.2	0.00094	1.2	0.00347
BKP	L	3.4	1.7	0.00098	1.7	0.00360
BKP	L	3.4	2.1	0.00103	1.3	0.00380
BKP	L	3.5	1.3	0.00098	2.2	0.00350
BKP	L	3.5	2.0	0.00098	1.5	0.00350
BKP	L	3.5	2.3	0.00103	1.2	0.00369
BKP	L	3.5	0.0	0.00109	3.5	0.00389
BKP	L	3.6	0.1	0.00109	3.5	0.00378

Table A.1 (Cont'd.)

Pulp Type	B.B. Size	Initial Height of Fibre Bed H_o (cm)	Final Height of B.B. H_f (cm)	Initial Pulp Consistency (C_{mInit})	Distance Travelled by B.B. ΔH (cm)	Estimated Consistency of Settled Fibre Bed (C_{mo})
BKP	L	3.7	2.0	0.00103	1.7	0.00349
BKP	L	3.7	0.5	0.00116	3.2	0.00391
BKP	L	3.8	0.3	0.00109	3.5	0.00358
BKP	L	3.8	0.5	0.00109	3.3	0.00358
BKP	L	3.8	1.6	0.00115	2.2	0.00377
BKP	L	3.8	1.3	0.00116	2.5	0.00380
BKP	L	3.8	1.9	0.00120	1.9	0.00395
BKP	L	3.9	1.4	0.00115	2.5	0.00367
BKP	L	3.9	0.2	0.00116	3.7	0.00371
BKP	L	3.9	0.3	0.00116	3.6	0.00371
BKP	L	4.0	1.6	0.00115	2.4	0.00358
BKP	L	4.0	2.0	0.00115	2.0	0.00358
BKP	L	4.0	0.4	0.00116	3.6	0.00361
BKP	L	4.0	1.0	0.00116	3.0	0.00361
BKP	L	4.0	1.1	0.00116	2.9	0.00361
BKP	L	4.0	1.3	0.00120	2.7	0.00375
BKP	L	4.0	1.1	0.00124	2.9	0.00387
BKP	L	4.1	0.0	0.00116	4.1	0.00352
BKP	L	4.2	0.5	0.00129	3.7	0.00384
BKP	L	4.2	1.2	0.00129	3.0	0.00384
BKP	L	4.3	1.3	0.00120	3.0	0.00349
BKP	L	4.3	1.6	0.00120	2.7	0.00349
BKP	L	4.6	1.0	0.00129	3.6	0.00351
Data for ($0.0040 < C_{mo} < 0.0045$)						
BKP	L	3.3	0.0	0.00116	3.3	0.00438
BKP	L	3.3	0.2	0.00116	3.1	0.00438
BKP	L	3.3	0.3	0.00116	3.0	0.00438
BKP	L	3.3	0.3	0.00116	3.0	0.00438
BKP	L	3.3	0.4	0.00116	2.9	0.00438
BKP	L	3.3	0.5	0.00116	2.8	0.00438
BKP	L	3.3	0.7	0.00116	2.6	0.00438
BKP	L	3.3	0.8	0.00120	2.5	0.00454
BKP	L	3.3	1.8	0.00120	1.5	0.00454
BKP	L	3.5	0.4	0.00116	3.1	0.00413

Table A.1 (Cont'd.)

Pulp Type	B.B. Size	Initial Height of Fibre Bed H_o (cm)	Final Height of B.B. H_f (cm)	Initial Pulp Consistency (C_{mInit})	Distance Travelled by B.B. ΔH (cm)	Estimated Consistency of Settled Fibre Bed (C_{mo})
BKP	L	3.5	0.5	0.00116	3.0	0.00413
BKP	L	3.5	1.3	0.00120	2.2	0.00429
BKP	L	3.5	1.5	0.00120	2.0	0.00429
BKP	L	3.5	1.6	0.00120	1.9	0.00429
BKP	L	3.5	0.5	0.00124	3.0	0.00442
BKP	L	3.5	0.8	0.00124	2.7	0.00442
BKP	L	3.7	0.7	0.00124	3.0	0.00418
BKP	L	3.9	0.5	0.00124	3.4	0.00397
BKP	L	3.9	0.0	0.00129	3.9	0.00413
BKP	L	3.9	1.1	0.00129	2.8	0.00413
BKP	L	4.0	0.6	0.00129	3.4	0.00403
BKP	L	4.0	1.6	0.00129	2.4	0.00403

Table A.2. Data for BKP, Small B.B.'s.

Pulp Type	B.B. Size	Initial Height of Fibre Bed H_o (cm)	Final Height of B.B. H_f (cm)	Initial Pulp Consistency (C_{mInit})	Distance Travelled by B.B. ΔH (cm)	Estimated Consistency of Settled Fibre Bed (C_{mo})
Data for ($0.0015 < C_{mo} < 0.0020$)						
BKP	S	4.7	2.2	0.00072	2.5	0.00192
BKP	S	4.8	2.9	0.00072	1.9	0.00188
BKP	S	4.8	3.2	0.00072	1.6	0.00188
BKP	S	5.2	0.0	0.00072	5.2	0.00174
BKP	S	5.7	4.7	0.00087	1.0	0.00192
BKP	S	5.8	0.2	0.00087	5.6	0.00188
BKP	S	5.9	3.9	0.00087	2.0	0.00185
BKP	S	5.9	5.5	0.00087	0.4	0.00185
BKP	S	6.1	1.0	0.00087	5.1	0.00179
BKP	S	6.1	3.3	0.00087	2.8	0.00179
BKP	S	6.3	1.9	0.00098	4.4	0.00194
BKP	S	6.4	5.0	0.00087	1.4	0.00171
BKP	S	6.5	3.0	0.00098	3.5	0.00188
BKP	S	6.6	4.6	0.00087	2.0	0.00165
BKP	S	6.6	3.5	0.00098	3.1	0.00185
BKP	S	6.7	1.5	0.00098	5.2	0.00182
BKP	S	6.8	2.1	0.00087	4.7	0.00161
BKP	S	7.0	0.5	0.00087	6.5	0.00156
BKP	S	7.0	4.4	0.00105	2.6	0.00188
BKP	S	7.1	5.1	0.00110	2.0	0.00193
BKP	S	7.2	0.0	0.00110	7.2	0.00190
BKP	S	7.2	2.6	0.00110	4.6	0.00190
BKP	S	7.3	1.0	0.00098	6.3	0.00167
BKP	S	7.5	0.0	0.00087	7.5	0.00146
BKP	S	7.5	0.9	0.00114	6.6	0.00190
BKP	S	7.5	3.4	0.00116	4.1	0.00193
BKP	S	7.6	1.6	0.00115	6.0	0.00189
BKP	S	7.7	2.9	0.00110	4.8	0.00178
BKP	S	7.8	2.4	0.00114	5.4	0.00183
BKP	S	8.0	0.6	0.00115	7.4	0.00180
BKP	S	8.2	5.7	0.00110	2.5	0.00167

Table A.2 (Cont'd.)

Pulp Type	B.B. Size	Initial Height of Fibre Bed H_o (cm)	Final Height of B.B. H_f (cm)	Initial Pulp Consistency (C_{minit})	Distance Travelled by B.B. ΔH (cm)	Estimated Consistency of Settled Fibre Bed (C_{mo})
Data for ($0.0020 < C_{mo} < 0.0025$)						
BKP	S	3.7	2.5	0.00072	1.2	0.00244
BKP	S	3.8	0.6	0.00072	3.2	0.00238
BKP	S	3.8	1.8	0.00072	2.0	0.00238
BKP	S	3.8	1.9	0.00072	1.9	0.00238
BKP	S	3.9	2.2	0.00072	1.7	0.00231
BKP	S	3.9	3.0	0.00072	0.9	0.00231
BKP	S	4.1	0.0	0.00072	4.1	0.00220
BKP	S	4.2	0.2	0.00072	4.0	0.00215
BKP	S	4.2	1.0	0.00072	3.2	0.00215
BKP	S	4.3	2.0	0.00072	2.3	0.00210
BKP	S	4.5	2.6	0.00072	1.9	0.00201
BKP	S	4.5	2.6	0.00087	1.9	0.00243
BKP	S	4.7	0.0	0.00087	4.7	0.00233
BKP	S	4.8	0.8	0.00087	4.0	0.00228
BKP	S	4.8	1.2	0.00087	3.6	0.00228
BKP	S	5.0	3.0	0.00098	2.0	0.00244
BKP	S	5.2	0.0	0.00087	5.2	0.00210
BKP	S	5.2	0.7	0.00087	4.5	0.00210
BKP	S	5.2	0.5	0.00098	4.7	0.00235
BKP	S	5.4	1.9	0.00087	3.5	0.00202
BKP	S	5.4	0.3	0.00098	5.1	0.00226
BKP	S	5.4	1.0	0.00105	4.4	0.00243
BKP	S	5.4	4.0	0.00105	1.4	0.00243
BKP	S	5.5	4.0	0.00087	1.5	0.00199
BKP	S	5.5	4.4	0.00087	1.1	0.00199
BKP	S	5.5	1.5	0.00098	4.0	0.00222
BKP	S	5.5	1.6	0.00098	3.9	0.00222
BKP	S	5.5	3.1	0.00098	2.4	0.00222
BKP	S	5.5	3.5	0.00098	2.0	0.00222
BKP	S	5.5	3.7	0.00098	1.8	0.00222
BKP	S	5.5	2.4	0.00105	3.1	0.00239
BKP	S	5.5	4.6	0.00105	0.9	0.00239
BKP	S	5.6	3.6	0.00087	2.0	0.00195

Table A.2 (Cont'd.)

Pulp Type	B.B. Size	Initial Height of Fibre Bed H_o (cm)	Final Height of B.B. H_f (cm)	Initial Pulp Consistency (C_{mInit})	Distance Travelled by B.B. ΔH (cm)	Estimated Consistency of Settled Fibre Bed (C_{mo})
BKP	S	5.6	3.3	0.00110	2.3	0.00245
BKP	S	5.7	4.3	0.00098	1.4	0.00214
BKP	S	5.7	2.2	0.00105	3.5	0.00231
BKP	S	5.7	3.6	0.00110	2.1	0.00240
BKP	S	5.9	5.0	0.00098	0.9	0.00207
BKP	S	5.9	5.0	0.00105	0.9	0.00223
BKP	S	5.9	2.0	0.00110	3.9	0.00232
BKP	S	5.9	3.5	0.00110	2.4	0.00232
BKP	S	5.9	5.0	0.00110	0.9	0.00232
BKP	S	5.9	3.2	0.00115	2.7	0.00244
BKP	S	5.9	4.8	0.00115	1.1	0.00244
BKP	S	5.9	1.9	0.00116	4.0	0.00245
BKP	S	6.0	0.0	0.00098	6.0	0.00203
BKP	S	6.0	0.3	0.00098	5.7	0.00203
BKP	S	6.0	0.0	0.00110	6.0	0.00228
BKP	S	6.0	1.9	0.00114	4.1	0.00238
BKP	S	6.0	5.0	0.00114	1.0	0.00238
BKP	S	6.0	2.7	0.00115	3.3	0.00240
BKP	S	6.0	3.5	0.00115	2.5	0.00240
BKP	S	6.0	2.7	0.00116	3.3	0.00241
BKP	S	6.0	4.6	0.00116	1.4	0.00241
BKP	S	6.0	1.3	0.00117	4.7	0.00244
BKP	S	6.1	5.1	0.00098	1.0	0.00200
BKP	S	6.1	5.1	0.00110	1.0	0.00225
BKP	S	6.1	2.6	0.00114	3.5	0.00234
BKP	S	6.1	1.3	0.00116	4.8	0.00237
BKP	S	6.1	3.6	0.00116	2.5	0.00237
BKP	S	6.1	5.0	0.00116	1.1	0.00237
BKP	S	6.2	1.1	0.00098	5.1	0.00197
BKP	S	6.2	4.2	0.00105	2.0	0.00212
BKP	S	6.2	5.5	0.00116	0.7	0.00233
BKP	S	6.2	4.7	0.00117	1.5	0.00236
BKP	S	6.3	2.8	0.00105	3.5	0.00209
BKP	S	6.3	4.9	0.00105	1.4	0.00209
BKP	S	6.3	2.5	0.00110	3.8	0.00218

Table A.2 (Cont'd.)

Pulp Type	B.B. Size	Initial Height of Fibre Bed H_o (cm)	Final Height of B.B. H_f (cm)	Initial Pulp Consistency (C_{mInit})	Distance Travelled by B.B. ΔH (cm)	Estimated Consistency of Settled Fibre Bed (C_{mo})
BKP	S	6.3	4.4	0.00110	1.9	0.00218
BKP	S	6.3	3.4	0.00114	2.9	0.00227
BKP	S	6.3	3.9	0.00114	2.4	0.00227
BKP	S	6.3	0.6	0.00116	5.7	0.00229
BKP	S	6.3	4.0	0.00117	2.3	0.00232
BKP	S	6.4	5.4	0.00110	1.0	0.00214
BKP	S	6.4	2.1	0.00115	4.3	0.00225
BKP	S	6.4	3.8	0.00116	2.6	0.00226
BKP	S	6.4	1.2	0.00117	5.2	0.00228
BKP	S	6.4	5.0	0.00117	1.4	0.00228
BKP	S	6.5	0.0	0.00105	6.5	0.00202
BKP	S	6.5	1.4	0.00114	5.1	0.00220
BKP	S	6.5	2.8	0.00114	3.7	0.00220
BKP	S	6.6	3.2	0.00115	3.4	0.00218
BKP	S	6.6	4.7	0.00116	1.9	0.00219
BKP	S	6.7	0.0	0.00110	6.7	0.00205
BKP	S	6.7	4.9	0.00110	1.8	0.00205
BKP	S	6.7	6.1	0.00110	0.6	0.00205
BKP	S	6.7	3.6	0.00114	3.1	0.00213
BKP	S	6.8	4.6	0.00115	2.2	0.00212
BKP	S	6.8	5.3	0.00115	1.5	0.00212
BKP	S	6.9	3.0	0.00114	3.9	0.00207
BKP	S	7.0	1.0	0.00114	6.0	0.00204
BKP	S	7.0	1.3	0.00114	5.7	0.00204
BKP	S	7.0	3.6	0.00115	3.4	0.00205
BKP	S	7.0	0.6	0.00116	6.4	0.00206
BKP	S	7.0	2.4	0.00116	4.6	0.00206
BKP	S	7.0	3.8	0.00116	3.2	0.00206
BKP	S	7.0	1.6	0.00117	5.4	0.00209
BKP	S	7.1	2.7	0.00114	4.4	0.00201
BKP	S	7.1	2.6	0.00116	4.5	0.00203
BKP	S	7.4	5.5	0.00117	1.9	0.00197
Data for ($0.0025 < C_{mo} < 0.0030$)						
BKP	S	3.3	0.9	0.00072	2.4	0.00274
BKP	S	3.4	0.7	0.00072	2.7	0.00266

Table A.2 (Cont'd.)

Pulp Type	B.B. Size	Initial Height of Fibre Bed H_o (cm)	Final Height of B.B. H_f (cm)	Initial Pulp Consistency (C_{mInit})	Distance Travelled by B.B. ΔH (cm)	Estimated Consistency of Settled Fibre Bed (C_{mo})
BKP	S	3.4	1.9	0.00072	1.5	0.00266
BKP	S	3.5	1.9	0.00072	1.6	0.00258
BKP	S	4.0	2.5	0.00087	1.5	0.00273
BKP	S	4.0	2.5	0.00087	1.5	0.00273
BKP	S	4.0	2.6	0.00087	1.4	0.00273
BKP	S	4.0	2.1	0.00087	1.9	0.00273
BKP	S	4.1	3.4	0.00087	0.7	0.00266
BKP	S	4.1	3.4	0.00087	0.7	0.00267
BKP	S	4.2	3.0	0.00087	1.2	0.00260
BKP	S	4.2	2.3	0.00087	1.9	0.00260
BKP	S	4.3	2.9	0.00087	1.4	0.00254
BKP	S	4.4	0.3	0.00087	4.1	0.00248
BKP	S	4.4	2.4	0.00098	2.0	0.00277
BKP	S	4.7	3.0	0.00098	1.7	0.00260
BKP	S	4.7	3.1	0.00098	1.6	0.00260
BKP	S	4.8	0.3	0.00098	4.5	0.00254
BKP	S	4.8	1.7	0.00098	3.1	0.00254
BKP	S	4.8	2.4	0.00098	2.4	0.00254
BKP	S	4.8	2.9	0.00098	1.9	0.00254
BKP	S	4.8	1.1	0.00105	3.7	0.00274
BKP	S	4.8	3.0	0.00105	1.8	0.00274
BKP	S	4.9	2.5	0.00105	2.4	0.00268
BKP	S	4.9	2.5	0.00114	2.4	0.00291
BKP	S	4.9	3.1	0.00114	1.8	0.00291
BKP	S	5.0	1.6	0.00105	3.4	0.00263
BKP	S	5.0	1.8	0.00114	3.2	0.00285
BKP	S	5.0	3.7	0.00114	1.3	0.00285
BKP	S	5.0	3.9	0.00114	1.1	0.00285
BKP	S	5.0	2.9	0.00117	2.1	0.00292
BKP	S	5.1	4.1	0.00105	1.0	0.00258
BKP	S	5.1	4.1	0.00105	1.0	0.00258
BKP	S	5.2	3.7	0.00105	1.5	0.00253
BKP	S	5.2	3.0	0.00114	2.2	0.00275
BKP	S	5.2	4.2	0.00114	1.0	0.00275
BKP	S	5.2	1.5	0.00116	3.7	0.00278

Table A.2 (Cont'd.)

Pulp Type	B.B. Size	Initial Height of Fibre Bed H_o (cm)	Final Height of B.B. H_f (cm)	Initial Pulp Consistency (C_{mInit})	Distance Travelled by B.B. ΔH (cm)	Estimated Consistency of Settled Fibre Bed (C_{mo})
BKP	S	5.2	3.7	0.00116	1.5	0.00278
BKP	S	5.2	4.7	0.00116	0.5	0.00278
BKP	S	5.3	2.5	0.00105	2.8	0.00248
BKP	S	5.3	4.2	0.00105	1.1	0.00248
BKP	S	5.3	4.0	0.00116	1.3	0.00273
BKP	S	5.4	2.3	0.00116	3.1	0.00268
BKP	S	5.6	3.1	0.00116	2.5	0.00258
BKP	S	5.7	0.7	0.00114	5.0	0.00250
BKP	S	5.8	4.3	0.00114	1.5	0.00246
Data for ($0.0030 < C_{mo} < 0.0035$)						
BKP	S	2.8	2.0	0.00072	0.8	0.00322
BKP	S	2.8	2.0	0.00072	0.8	0.00322
BKP	S	2.9	2.3	0.00072	0.6	0.00311
BKP	S	3.0	1.1	0.00072	1.9	0.00301
BKP	S	3.0	1.7	0.00072	1.3	0.00301
BKP	S	3.0	2.2	0.00072	0.8	0.00301
BKP	S	3.2	1.0	0.00087	2.2	0.00342
BKP	S	3.2	1.9	0.00087	1.3	0.00342
BKP	S	3.2	2.1	0.00087	1.1	0.00342
BKP	S	3.2	2.3	0.00087	0.9	0.00342
BKP	S	3.3	1.5	0.00087	1.8	0.00331
BKP	S	3.4	2.4	0.00087	1.0	0.00321
BKP	S	3.4	2.9	0.00087	0.5	0.00321
BKP	S	3.4	2.7	0.00087	0.7	0.00321
BKP	S	3.5	0.7	0.00087	2.8	0.00312
BKP	S	3.5	1.7	0.00087	1.8	0.00312
BKP	S	3.5	1.8	0.00087	1.7	0.00312
BKP	S	3.6	2.4	0.00087	1.2	0.00303
BKP	S	3.6	3.2	0.00087	0.4	0.00303
BKP	S	3.7	2.1	0.00087	1.6	0.00295
BKP	S	3.9	2.7	0.00105	1.2	0.00337
BKP	S	4.0	2.8	0.00105	1.2	0.00329
BKP	S	4.0	3.3	0.00105	0.7	0.00329
BKP	S	4.0	3.0	0.00110	1.0	0.00343

Table A.2 (Cont'd.)

Pulp Type	B.B. Size	Initial Height of Fibre Bed H_o (cm)	Final Height of B.B. H_f (cm)	Initial Pulp Consistency (C_{mInit})	Distance Travelled by B.B. ΔH (cm)	Estimated Consistency of Settled Fibre Bed (C_{mo})
BKP	S	4.1	2.8	0.00105	1.3	0.00321
BKP	S	4.3	3.4	0.00105	0.9	0.00306
BKP	S	4.3	3.6	0.00110	0.7	0.00319
BKP	S	4.3	1.5	0.00117	2.8	0.00340
BKP	S	4.3	2.4	0.00117	1.9	0.00340
BKP	S	4.3	3.7	0.00117	0.6	0.00340
BKP	S	4.4	3.0	0.00110	1.4	0.00311
BKP	S	4.4	3.6	0.00110	0.8	0.00311
BKP	S	4.4	3.2	0.00117	1.2	0.00332
BKP	S	4.4	3.9	0.00117	0.5	0.00332
BKP	S	4.5	2.4	0.00114	2.1	0.00317
BKP	S	4.5	3.3	0.00114	1.2	0.00317
BKP	S	4.5	3.5	0.00114	1.0	0.00317
BKP	S	4.5	2.6	0.00117	1.9	0.00325
BKP	S	4.7	2.9	0.00114	1.8	0.00304
BKP	S	4.7	3.6	0.00114	1.1	0.00304
BKP	S	4.7	3.0	0.00117	1.7	0.00311
BKP	S	4.7	3.7	0.00117	1.0	0.00311
Data for ($0.0035 < C_{mo} < 0.0040$)						
BKP	S	3.1	2.3	0.00087	0.8	0.00352
BKP	S	3.1	1.2	0.00087	1.9	0.00353
BKP	S	3.1	1.7	0.00087	1.4	0.00353
BKP	S	3.6	2.2	0.00115	1.4	0.00400
BKP	S	3.6	3.0	0.00115	0.6	0.00400
BKP	S	3.7	0.4	0.00115	3.3	0.00389
BKP	S	3.7	1.8	0.00115	1.9	0.00389
BKP	S	3.7	3.0	0.00115	0.7	0.00389
BKP	S	3.7	0.9	0.00116	2.8	0.00390
BKP	S	3.8	2.5	0.00115	1.3	0.00379
BKP	S	3.8	2.5	0.00115	1.3	0.00379
BKP	S	3.8	3.0	0.00115	0.8	0.00379
BKP	S	3.8	2.1	0.00116	1.7	0.00380
BKP	S	3.8	2.3	0.00116	1.5	0.00380
BKP	S	3.8	2.6	0.00117	1.2	0.00384

Table A.2 (Cont'd.)

Pulp Type	B.B. Size	Initial Height of Fibre Bed H_o (cm)	Final Height of B.B. H_f (cm)	Initial Pulp Consistency (C_{mInit})	Distance Travelled by B.B. ΔH (cm)	Estimated Consistency of Settled Fibre Bed (C_{mo})
BKP	S	3.8	3.2	0.00117	0.6	0.00384
BKP	S	4.0	0.9	0.00116	3.1	0.00361
BKP	S	4.0	2.4	0.00116	1.6	0.00361
BKP	S	4.0	2.1	0.00117	1.9	0.00365
BKP	S	4.2	2.5	0.00117	1.7	0.00348

Table A.3. Data for TMP-GWD Pulp, Large B.B.'s.

Pulp Type	B.B. Size	Initial Height of Fibre Bed H_o (cm)	Final Height of B.B. H_f (cm)	Initial Pulp Consistency (C_{mInit})	Distance Travelled by B.B. ΔH (cm)	Estimated Consistency of Settled Fibre Bed (C_{mo})
Data for ($0.0025 < C_{mo} < 0.0030$)						
TMP-GWD	L	4.5	0.0	0.00099	4.5	0.00274
TMP-GWD	L	4.3	0.0	0.00099	4.3	0.00287
TMP-GWD	L	4.4	0.0	0.00102	4.4	0.00290
TMP-GWD						
Data for ($0.0030 < C_{mo} < 0.0035$)						
TMP-GWD	L	4.0	0.0	0.00099	4.0	0.00308
TMP-GWD	L	3.8	0.0	0.00099	3.8	0.00325
TMP-GWD	L	3.8	0.0	0.00102	3.8	0.00336
Data for ($0.0035 < C_{mo} < 0.0040$)						
TMP-GWD	L	3.5	0.0	0.00099	3.5	0.00353
TMP-GWD	L	3.5	0.0	0.00102	3.5	0.00365
Data for ($0.0040 < C_{mo} < 0.0045$)						
TMP-GWD	L	3.1	0.0	0.00102	3.1	0.00412
TMP-GWD	L	3.0	0.0	0.00102	3.0	0.00426
TMP-GWD	L	3.0	0.0	0.00102	3.0	0.00426

Table A.3 (Cont'd.)

Pulp Type	B.B. Size	Initial Height of Fibre Bed H_o (cm)	Final Height of B.B. H_f (cm)	Initial Pulp Consistency (C_{mInit})	Distance Travelled by B.B. ΔH (cm)	Estimated Consistency of Settled Fibre Bed (C_{mo})
Data for ($0.0045 < C_{mo} < 0.0050$)						
TMP-GWD	L	2.8	0.0	0.00102	2.8	0.00456
TMP-GWD	L	2.7	0.0	0.00102	2.7	0.00473
TMP-GWD	L	2.7	0.0	0.00102	2.7	0.00473
TMP-GWD	L	2.5	0.0	0.00099	2.5	0.00494
TMP-GWD	L	2.5	0.0	0.00099	2.5	0.00494
Data for ($0.0050 < C_{mo} < 0.0055$)						
TMP-GWD	L	2.5	0.0	0.00102	2.5	0.00511
TMP-GWD	L	2.5	0.0	0.00102	2.5	0.00511
TMP-GWD	L	2.5	0.0	0.00102	2.5	0.00511
TMP-GWD	L	2.4	0.0	0.00099	2.4	0.00514
TMP-GWD	L	2.4	0.0	0.00099	2.4	0.00514
TMP-GWD	L	2.4	0.0	0.00099	2.4	0.00514
TMP-GWD	L	2.4	0.0	0.00102	2.4	0.00532
TMP-GWD	L	2.3	0.0	0.00099	2.3	0.00537
TMP-GWD	L	2.3	0.0	0.00099	2.3	0.00537
Data for ($0.0055 < C_{mo} < 0.0060$)						
TMP-GWD	L	2.3	0.0	0.00102	2.3	0.00556
TMP-GWD	L	2.2	0.0	0.00099	2.2	0.00561
TMP-GWD	L	2.2	0.0	0.00099	2.2	0.00561
TMP-GWD	L	2.2	0.0	0.00099	2.2	0.00561
TMP-GWD	L	2.2	0.0	0.00099	2.2	0.00561
TMP-GWD	L	2.2	0.0	0.00102	2.2	0.00581
TMP-GWD	L	2.2	0.0	0.00102	2.2	0.00581
TMP-GWD	L	2.2	0.0	0.00102	2.2	0.00581
TMP-GWD	L	2.1	0.0	0.00099	2.1	0.00588
Data for ($0.0060 < C_{mo} < 0.0065$)						
TMP-GWD	L	2.1	0.0	0.00102	2.1	0.00608
TMP-GWD	L	2.0	0.0	0.00099	2.0	0.00617
TMP-GWD	L	2.0	0.0	0.00099	2.0	0.00617
TMP-GWD	L	2.0	0.0	0.00102	2.0	0.00639
TMP-GWD	L	2.0	0.0	0.00102	2.0	0.00639
TMP-GWD	L	1.9	0.0	0.00099	1.9	0.00649

Table A.3 (Cont'd.)

Pulp Type	B.B. Size	Initial Height of Fibre Bed H_o (cm)	Final Height of B.B. H_f (cm)	Initial Pulp Consistency (C_{mInit})	Distance Travelled by B.B. ΔH (cm)	Estimated Consistency of Settled Fibre Bed (C_{mo})
Data for ($0.0070 < C_{mo} < 0.009$)						
TMP-GWD						
TMP-GWD	L	1.8	0.0	0.00102	1.8	0.00710
TMP-GWD	L	1.7	0.0	0.00102	1.7	0.00752
TMP-GWD	L	1.7	0.0	0.00102	1.7	0.00752
TMP-GWD	L	1.6	0.0	0.00102	1.6	0.00799
TMP-GWD	L	1.4	0.0	0.00099	1.4	0.00881
TMP-GWD	L	1.4	0.0	0.00099	1.4	0.00881

Table A.4. Data for TMP-GWD Pulp, Small B.B.'s.

Pulp Type	B.B. Size	Initial Height of Fibre Bed H_o (cm)	Final Height of B.B. H_f (cm)	Initial Pulp Consistency (C_{mInit})	Distance Travelled by B.B. ΔH (cm)	Estimated Consistency of Settled Fibre Bed (C_{mo})
Data for ($0.0030 < C_{mo} < 0.0035$)						
TMP-GWD	S	4.0	0.0	0.00099	4.0	0.00310
TMP-GWD	S	4.0	0.0	0.00100	4.0	0.00313
TMP-GWD	S	4.0	0.0	0.00100	4.0	0.00313
TMP-GWD	S	3.9	0.0	0.00099	3.9	0.00318
TMP-GWD	S	3.9	0.0	0.00100	3.9	0.00321
TMP-GWD	S	3.8	0.0	0.00099	3.8	0.00327
TMP-GWD	S	3.8	0.0	0.00099	3.8	0.00327
TMP-GWD	S	3.8	0.0	0.00100	3.8	0.00330
TMP-GWD	S	3.7	0.0	0.00100	3.7	0.00339
Data for ($0.0035 < C_{mo} < 0.0040$)						
TMP-GWD	S	3.5	0.0	0.00099	3.5	0.00355
TMP-GWD	S	3.5	0.0	0.00099	3.5	0.00355
TMP-GWD	S	3.5	0.0	0.00099	3.5	0.00355
TMP-GWD	S	3.5	0.0	0.00099	3.5	0.00355
TMP-GWD	S	3.5	0.0	0.00099	3.5	0.00355
TMP-GWD	S	3.5	0.0	0.00100	3.5	0.00358
TMP-GWD	S	3.4	0.0	0.00100	3.4	0.00368

Table A.4 (Cont'd.)

Pulp Type	B.B. Size	Initial Height of Fibre Bed H_o (cm)	Final Height of B.B. H_f (cm)	Initial Pulp Consistency (C_{mInit})	Distance Travelled by B.B. ΔH (cm)	Estimated Consistency of Settled Fibre Bed (C_{mo})
TMP-GWD	S	3.3	0.0	0.00099	3.3	0.00376
TMP-GWD	S	3.2	0.0	0.00099	3.2	0.00388
Data for ($0.0040 < C_{mo} < 0.0045$)						
TMP-GWD	S	2.9	0	0.00100	2.9	0.00432
TMP-GWD	S	2.8	0	0.00099	2.8	0.00443
Data for ($0.0045 < C_{mo} < 0.0070$)						
TMP-GWD	S	2.7	0	0.00100	2.7	0.00464
TMP-GWD	S	2.2	0	0.00100	2.2	0.00569
TMP-GWD	S	2	0	0.00100	2	0.00626
TMP-GWD	S	2	0.5	0.00100	1.5	0.00626
TMP-GWD	S	1.9	0.3	0.00100	1.6	0.00659

Table A.5. Ball Bearing Escape Probabilties Derived From Tables A.1 to A.4.

Pulp Type	B.B. Size	Consis-tency Range of Fibre Bed (C_{mo})	Maxi-mum Fibre Bed Height H_{oMax}	Min-imum Fibre Bed Height H_{oMin}	Number of Data (n)	Escape Probabilties (Given as the fraction of ball bearings which penetrate through the fibre bed by a given distance ΔH)												
						ΔH ≥ 0)	ΔH ≥ 0.5	ΔH ≥ 1.0	ΔH ≥ 1.5)	ΔH ≥ 2.0	ΔH ≥ 2.5	ΔH ≥ 3.0	ΔH ≥ 3.5	ΔH ≥ 4.0	ΔH ≥ 4.5	ΔH ≥ 5.0	ΔH ≥ 5.5	ΔH ≥ 6.0)
BKP	L	0.0015 - 0.0020	7.5	6.3	8	1.000	1.000	1.000	1.000	1.000	1.000	1.000	1.000	1.000	1.000	1.000	0.875	0.875
BKP	L	0.0020 - 0.0025	7.6	5.0	62	1.000	1.000	1.000	1.000	1.000	1.000	0.984	0.952	0.871	0.839	0.758	n/a	n/a
BKP	L	0.0025 - 0.0030	6.5	4.1	73	1.000	1.000	1.000	1.000	1.000	0.973	0.877	0.753	0.534	n/a	n/a	n/a	n/a
BKP	L	0.0030 - 0.0035	5.2	3.6	37	1.000	1.000	1.000	1.000	0.919	0.757	0.486	0.378	n/a	n/a	n/a	n/a	n/a
BKP	L	0.0035 - 0.0040	4.6	3.1	38	1.000	1.000	1.000	0.921	0.684	0.553	0.368	n/a	n/a	n/a	n/a	n/a	n/a
BKP	L	0.0040 - 0.0045	4.0	3.3	22	1.000	1.000	1.000	1.000	0.909	0.773	0.500	n/a	n/a	n/a	n/a	n/a	n/a
BKP	S	0.0015 - 0.0020	8.2	4.7	31	1.000	0.968	0.968	0.903	0.839	0.742	0.613	0.581	0.548	0.484	n/a	n/a	n/a
BKP	S	0.0020 - 0.0025	7.4	3.7	100	1.000	1.000	0.930	0.800	0.680	0.550	0.500	0.410	n/a	n/a	n/a	n/a	n/a
BKP	S	0.0025 - 0.0030	5.8	3.3	46	1.000	1.000	0.935	0.717	0.413	0.261	0.196	n/a	n/a	n/a	n/a	n/a	n/a
BKP	S	0.0030 - 0.0035	4.7	2.8	42	1.000	0.976	0.667	0.310	0.095	0.048	n/a	n/a	n/a	n/a	n/a	n/a	n/a
BKP	S	0.0035 - 0.0040	4.2	3.1	20	1.000	1.000	0.750	0.500	0.150	0.150	0.100	n/a	n/a	n/a	n/a	n/a	n/a
TMP-GWD	L	0.0050 - 0.0055	2.5	2.3	9	1.000	1.000	1.000	1.000	1.000	n/a	n/a	n/a	n/a	n/a	n/a	n/a	n/a
TMP-GWD	S	0.0035 - 0.0040	3.5	3.2	8	1.000	1.000	1.000	1.000	1.000	1.000	1.000	n/a	n/a	n/a	n/a	n/a	n/a

(*) Espace probablities were only determined for values of ($\Delta H < H_{oMin}$).

APPENDIX B

Additional Video Images of Aerated Pulp Suspensions from the Flow Visualization Studies from Chapter 4.

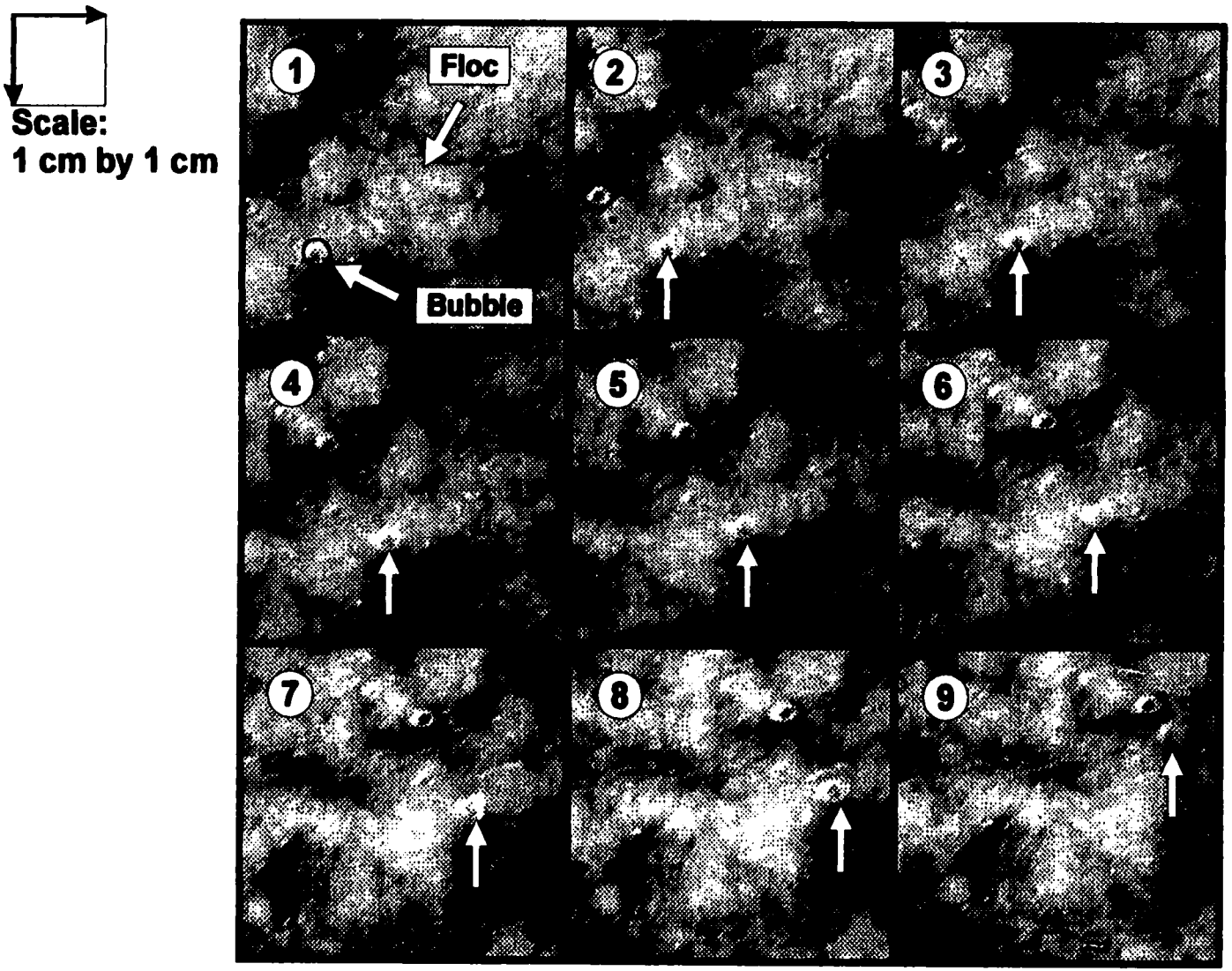

Figure B-1. Contrast-enhanced digitized video sequence of bleached kraft pulp in flowing conditions, in which a pulp flocs disperses, resulting in the release of a trapped bubble. The arrows in each frame indicate the bubble position.

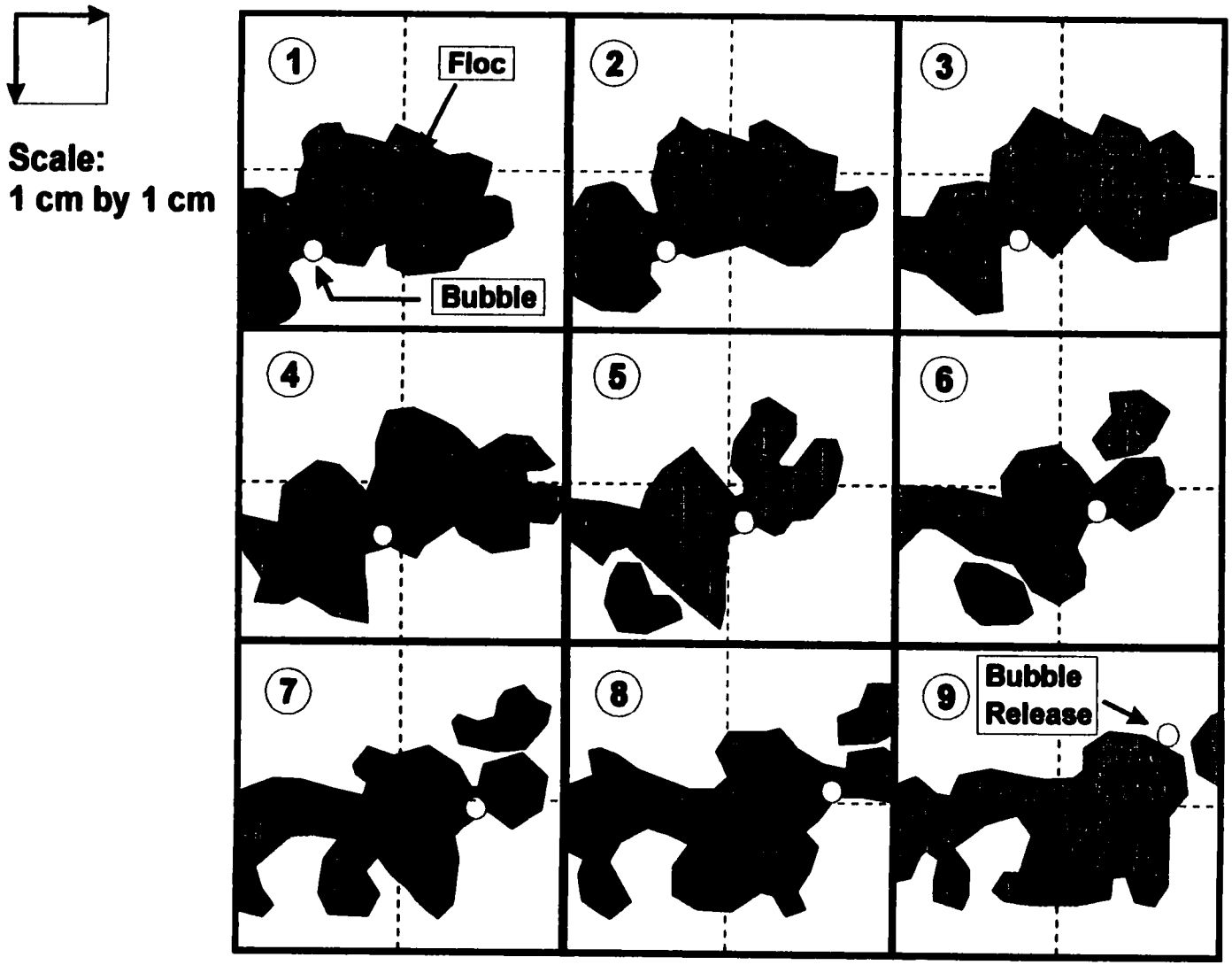

Figure B-2. Manually-traced outlines of the bubble and floc positions from Figure B-1. The cross-hairs in each frame indicate the center of each image. The shear forces dispersed the floc, and the bubble was released in Frame 9.

APPENDIX C

Raw Data from the Pulp Flotation Experiments from Chapter 5.

Table C.1. Data for TMP-GWD Pulp (Small Bubbles).

Data File #	Rotameter Reading	Flotation Time (min.)	Feed Consistency	Foam Consistency	Mass of Water Floated (g)	Mass of Pulp Floated (g)
90-100	40	0.50	0.00162	0.00119	87.09	0.1036
90-101	40	0.50	0.00050	0.00032	83.21	0.0271
90-102	40	0.50	0.00978	0.00350	96.22	0.3382
90-103	40	0.50	0.00398	0.00236	101.35	0.2399
90-104	41	0.50	0.00995	0.00351	87.40	0.3075
90-105	39	0.50	0.00602	0.00258	89.59	0.2314
90-108	38-39	0.50	0.00791	0.00324	83.58	0.2716
90-109	38-40	0.50	0.00065	0.00043	78.34	0.0336
90-111	~40	0.50	0.00278	0.00232	75.58	0.1757
90-112	~40	0.50	0.00928	0.00384	66.09	0.2548
90-116	~40	0.50	0.00550	0.00336	76.69	0.2586
90-122	40	0.50	0.00473	0.00314	75.04	0.2366
90-138	40	0.50	0.02158	0.00362	49.43	0.1794
90-140	40	0.50	0.02103	0.00362	40.99	0.1489
90-141	40	0.50	0.00110	0.00071	77.91	0.0557
90-142	40	0.50	0.01742	0.00449	49.43	0.2229
90-146	40	0.50	0.01385	0.00471	54.22	0.2568
90-147	40	0.50	0.01350	0.00442	61.26	0.2721
90-165	~40	0.50	0.00141	0.00109	72.54	0.0791
90-166	~40	0.33	0.00127	0.00109	30.85	0.0337
90-167	~40	0.50	0.00598	0.00303	71.31	0.2168
90-168	~40	0.37	0.00611	0.00339	42.43	0.1443
90-90	42	0.50	0.00485	0.00303	80.81	0.2460
90-91	41-42	0.50	0.00049	0.00031	87.40	0.0268
90-92	40	0.50	0.00246	0.00210	62.10	0.1308
90-97	40	0.50	0.00497	0.00274	85.53	0.2351
90-98	40	0.50	0.00099	0.00071	87.46	0.0618
95-120	40	0.50	0.00185	0.00124	98.63	0.1229
95-123	50	0.50	0.00197	0.00123	141.03	0.1732
95-124	45	0.50	0.00207	0.00149	117.38	0.1747
95-125.	40	0.50	0.01851	0.00325	64.35	0.2101
95-126	50	0.50	0.01866	0.00346	91.41	0.3178
95-127	60	0.50	0.01824	0.00385	107.84	0.4170

Table C.1 (Cont'd.)

Data File #	Rotameter Reading	Flotation Time (min.)	Feed Consistency	Foam Consistency	Mass of Water Floated (g)	Mass of Pulp Floated (g)
95-159	~40	0.33	0.00210	0.00167	44.83	0.0752
95-161	40	0.67	0.00207	0.00133	151.02	0.2006
95-162	30	0.50	0.00206	0.00160	46.35	0.0745
95-163	20	0.50	0.00193	0.00212	19.34	0.0411
95-164	30	0.50	0.01875	0.00397	32.48	0.1295
95-41	40	0.50	0.01756	0.00396	51.72	0.2054
95-43	~40	0.50	0.00105	0.00073	77.91	0.0572
95-88	40	0.50	0.01849	0.00339	69.89	0.2377
95-89	40	0.50	0.00927	0.00342	82.80	0.2839
95-90	40	0.50	0.00149	0.00098	109.89	0.1074
95-91	40	0.50	0.00398	0.00255	94.72	0.2422

Table C.2. Data for BKP (Small Bubbles).

Data File #	Rotameter Reading	Flotation Time (min.)	Feed Consistency	Foam Consistency	Mass of Water Floated(g)	Mass of Pulp Floated (g)
90-113	40	0.50	0.00824	0.00105	57.44	0.0604
90-114	40	0.50	0.00104	0.00164	65.79	0.1079
90-115	40	0.50	0.00480	0.00117	66.52	0.0778
90-117	40	0.50	0.00189	0.00182	86.70	0.1585
90-118	40	0.50	0.00123	0.00166	82.90	0.1379
90-119	40	0.50	0.00267	0.00182	68.34	0.1246
90-120	40	0.50	0.00074	0.00122	72.10	0.0880
90-123	40	0.50	0.00134	0.00161	77.11	0.1244
90-124	40	0.50	0.00925	0.00087	54.69	0.0475
90-125	40	0.50	0.00468	0.00120	68.08	0.0819
90-126	40	0.50	0.00065	0.00071	88.60	0.0626
90-127	40	0.50	0.01849	0.00064	33.05	0.0211
90-135	40	0.50	0.01367	0.00067	37.75	0.0252
90-136	40	0.50	0.01131	0.00080	42.43	0.0340
90-137	40	0.50	0.00086	0.00158	77.97	0.1235
90-148	~40	0.50	0.01761	0.00063	31.65	0.0200
90-149	~40	0.50	0.00045	0.00159	63.35	0.1010
90-150	~40	0.50	0.00890	0.00095	50.21	0.0478
95-100	~40	0.50	0.00098	0.00127	85.91	0.1089
95-102	~40	0.50	0.00206	0.00145	84.04	0.1220
95-104	~40	0.50	0.01952	0.00043	41.43	0.0178
95-144	40	0.50	0.00212	0.00128	88.85	0.1137
95-145	45	0.50	0.00177	0.00132	119.46	0.1574
95-146	20	0.50	0.00204	0.00392	24.32	0.0957
95-147	30	0.50	0.00181	0.00230	56.34	0.1297
95-148	50	0.50	0.00194	0.00104	133.44	0.1395
95-149	50	0.50	0.01872	0.00041	95.46	0.0393
95-150	30	0.50	0.01849	0.00026	32.10	0.0084
95-151	40	0.50	0.02025	0.00040	56.79	0.0230
95-152	55	0.50	0.02020	0.00034	68.20	0.0229
95-64	~40	0.67	0.00236	0.00109	144.30	0.1569
95-65	~40	0.50	0.00176	0.00106	113.59	0.1201
95-66	~40	0.33	0.00229	0.00105	56.64	0.0597
95-92	~40	0.50	0.01947	0.00054	49.05	0.0266
95-93	~40	0.50	0.00958	0.00082	59.93	0.0493
95-94	~40	0.50	0.00302	0.00098	101.83	0.0996
95-95	~40	0.50	0.00160	0.00122	109.70	0.1345

Table C.3. Data for TMP-GWD Pulp (Large Bubbles).

Data File #	Rotameter Reading	Flotation Time (min.)	Feed Consistency	Foam Consistency	Mass of Water Floated(g)	Mass of Pulp Floated (g)
90-157	~40	20.00	0.00654	0.00733	48.13	0.3556
90-158	~40	10.00	0.00630	0.00739	26.73	0.1991
90-160	~40	20.00	0.00151	0.00080	61.25	0.0491
90-161	~40	10.00	0.00129	0.00063	31.81	0.0202
90-162	~40	5.00	0.00151	0.00080	13.46	0.0107
90-163	~40	30.00	0.00151	0.00074	88.03	0.0649
90-164	~40	25.00	0.00620	0.00697	63.78	0.4478
90-169	~40	21.00	0.00908	0.01146	20.31	0.2356
90-170	~40	40.00	0.00926	0.01219	33.66	0.4156
95-154	~40	15.00	0.00207	0.00093	46.70	0.0434
95-155	~40	3.50	0.01887	0.00915	33.64	0.3107
95-157	~40	15.00	0.01269	0.00980	27.00	0.2673
95-158	~40	15.00	0.00222	0.00108	47.60	0.0516
95-160	~40	15.00	0.00535	0.00532	45.33	0.2423
95-35	~40	12.85	0.01876	0.00870	102.58	0.9004
95-54	~40	4.00	0.01831	0.00831	26.22	0.2198
95-55	~40	2.25	0.01767	0.00723	18.92	0.1378
95-56	~40	20.00	0.00924	0.00978	26.09	0.2578
95-57	~40	30.00	0.00942	0.01290	42.95	0.5612
95-58	~40	20.00	0.01236	0.01274	23.75	0.3066
95-59	~40	?	0.00904	0.01417	46.79	0.6723

Table C.4. Data for BKP (Large Bubbles).

Data File #	Rotameter Reading	Flotation Time (min.)	Feed Consistency	Foam Consistency	Mass of Water Floated(g)	Mass of Pulp Floated (g)
95-117	~40	15.00	0.00202	0.00289	47.01	0.1364
95-128	~40	20.00	0.00215	0.00292	52.39	0.1533
95-129	~40	7.53	0.01392	0.00441	66.51	0.2949
95-153	~40	15.00	0.00191	0.00266	41.42	0.1103
95-166	~40	15.00	0.00531	0.00367	20.81	0.0767
95-167	~40	5.00	0.01226	0.00520	38.20	0.1998
95-168	~40	3.50	0.01865	0.00257	58.70	0.1510
95-60	~40	25.00	0.00136	0.00185	77.46	0.1433
95-61	~40	15.00	0.00179	0.00283	47.33	0.1342
95-63	~40	10.00	0.00208	0.00297	32.47	0.0966
95-76	~40	10.00	0.00666	0.00582	16.80	0.0983
95-77	~40	5.00	0.01350	0.00380	44.92	0.1713
95-78	~40	20.00	0.00679	0.00520	30.98	0.1619
95-99	~40	5.00	0.01879	0.00193	80.53	0.1554

Table C.5
Conversion of Rotameter Readings to Gas Flow Rates.

Rotameter Reading	Gas Flow Rate (std. cc /min)
20	1888
30	2679
40	3465
45	3861
50	4243
60	4989
80	6248

Table C.6. Data with Varying Gas Flow Rates (Flotation time constant at 30 s).

Data File #	Pulp Type	Bubble Size	Feed Consistency	Foam Consistency	Mass of Water Floated (g)	Mass of Pulp Floated (g)	Gas Flow Rate (cc/min.)
95-163	TMP-GWD	Small	0.00193	0.00212	19.34	0.0411	1888
95-162	TMP-GWD	Small	0.00206	0.00160	46.35	0.0745	2679
95-120	TMP-GWD	Small	0.00185	0.00124	98.63	0.1229	3465
95-123	TMP-GWD	Small	0.00197	0.00123	141.03	0.1732	4243
95-124	TMP-GWD	Small	0.00207	0.00149	117.38	0.1747	3861
95-164	TMP-GWD	Small	0.01875	0.00397	32.48	0.1295	2679
95-125.	TMP-GWD	Small	0.01851	0.00325	64.35	0.2101	3465
95-126	TMP-GWD	Small	0.01866	0.00346	91.41	0.3178	4243
95-127	TMP-GWD	Small	0.01824	0.00385	107.84	0.4170	4989
95-144	BKP	Small	0.00212	0.00128	88.85	0.1137	3465
95-145	BKP	Small	0.00177	0.00132	119.46	0.1574	3861
95-146	BKP	Small	0.00204	0.00392	24.32	0.0957	1888
95-147	BKP	Small	0.00181	0.00230	56.34	0.1297	2679
95-148	BKP	Small	0.00194	0.00104	133.44	0.1395	4243
95-149	BKP	Small	0.01872	0.00041	95.46	0.0393	4243
95-150	BKP	Small	0.01849	0.00026	32.10	0.0084	2679
95-151	BKP	Small	0.02025	0.00040	56.79	0.0230	3465
95-152	BKP	Small	0.02020	0.00034	68.20	0.0229	4621

Table C.7. Data with Varying Flotation Times (Gas flow rate = constant = 3465 cc/min.).

Data File #	Pulp Type	Bubble Size	Feed Consistency	Foam Consistency	Mass of Water Floated (g)	Mass of Pulp Floated (g)	Flotation Time (min.)
90-165	TMP-GWD	Small	0.00141	0.00109	72.54	0.07915	0.50
90-166	TMP-GWD	Small	0.00127	0.00109	30.85	0.03365	0.33
90-100	TMP-GWD	Small	0.00162	0.00119	87.09	0.10355	0.50
90-167	TMP-GWD	Small	0.00598	0.00303	71.31	0.21675	0.50
90-168	TMP-GWD	Small	0.00611	0.00339	42.43	0.14425	0.37
90-105	TMP-GWD	Small	0.00602	0.00258	89.59	0.2314	0.50
90-160	TMP-GWD	Large	0.00151	0.00080	61.25	0.04905	20.00
90-161	TMP-GWD	Large	0.00129	0.00063	31.81	0.02015	10.00
90-162	TMP-GWD	Large	0.00151	0.00080	13.46	0.01075	5.00
90-163	TMP-GWD	Large	0.00151	0.00074	88.03	0.0649	30.00
90-157	TMP-GWD	Large	0.00654	0.00733	48.13	0.3556	20.00
90-158	TMP-GWD	Large	0.00630	0.00739	26.73	0.1991	10.00
90-164	TMP-GWD	Large	0.00620	0.00697	63.78	0.44775	25.00
90-169	TMP-GWD	Large	0.00908	0.01146	20.31	0.2356	21.00
90-170	TMP-GWD	Large	0.00926	0.01219	33.66	0.41555	40.00
95-56	TMP-GWD	Large	0.00924	0.00978	26.09	0.2578	20.00
95-57	TMP-GWD	Large	0.00942	0.01290	42.95	0.5612	30.00
95-59	TMP-GWD	Large	0.00904	0.01417	46.79	0.6723	?
95-35	TMP-GWD	Large	0.01876	0.00870	102.58	0.90035	12.85
95-54	TMP-GWD	Large	0.01831	0.00831	26.22	0.2198	4.00
95-55	TMP-GWD	Large	0.01767	0.00723	18.92	0.1378	2.25
95-65	BKP	Small	0.00176	0.00106	113.59	0.12005	0.50
95-66	BKP	Small	0.00229	0.00105	56.64	0.05965	0.33
95-64	BKP	Small	0.00236	0.00109	144.30	0.1569	0.67
95-61	BKP	Large	0.00179	0.00283	47.33	0.13415	15.00
95-117	BKP	Large	0.00202	0.00289	47.01	0.13635	15.00
95-63	BKP	Large	0.00208	0.00297	32.47	0.0966	10.00
95-128	BKP	Large	0.00215	0.00292	52.39	0.1533	20.00

Table C.7 (Cont'd.)

Data File #	Pulp Type	Bubble Size	Feed Consistency	Foam Consistency	Mass of Water Floated (g)	Mass of Pulp Floated (g)	Flotation Time (min.)
95-76	BKP	Large	0.00666	0.00582	16.80	0.0983	10.00
95-78	BKP	Large	0.00679	0.00520	30.98	0.1619	20.00
95-77	BKP	Large	0.01350	0.00380	44.92	0.1713	5.00
95-129	BKP	Large	0.01392	0.00441	66.51	0.2949	7.53

Table C.8. Pulp Settling Data

Data File #	Pulp Type	Initial Pulp Consistency	Consistency of Settled Pulp	Settled Volume Fraction (ϕf)
99-42	BKP	0.00035	0.00253	0.090
99-41	BKP	0.00131	0.00308	0.430
99-37	BKP	0.00262	0.00325	0.805
99-44	BKP	0.00335	0.00452	0.750
99-40	BKP	0.00461	0.00485	0.950
99-38	BKP	0.00787	0.00831	0.945
99-43	BKP	0.00811	0.00833	0.980
99-39	BKP	0.02010	0.02010	1.000
99-47	TMP-GWD	0.00097	0.00820	0.135
99-49	TMP-GWD	0.00121	0.00868	0.150
99-46	TMP-GWD	0.00559	0.01154	0.490
99-48	TMP-GWD	0.01562	0.01672	0.940
99-45	TMP-GWD	0.02409	0.02409	1.000

Note: The settling experiments were performed in 1000 mL graduated cylinders. The settled volume fractions (ϕ_f) were determined by dividing the volume of the settled pulp by the original 1000 mL volume.

Table C.9. Raw Data for the Fibre Fractionation-Flotation Experiments

Data File #	Pulp Type	Bubble Size	Flotation Time (min.)	Feed Consistency	Foam Consistency	Fines Fraction in Feed	Fines Fraction in Foam	Total Mass of Foam Collected (g)	Mass of Pulp in the Foam (g)
95-90	TMP-GWD	Small	0.5	0.00149	0.00098	0.3904	0.3883	110.00	0.1074
95-91	TMP-GWD	Small	0.5	0.00398	0.00255	0.3709	0.4177	94.96	0.2422
95-89	TMP-GWD	Small	0.5	0.00927	0.00342	0.3980	0.5660	83.08	0.2839
95-41	TMP-GWD	Small	0.5	0.01756	0.00396	0.3695	0.7067	51.93	0.2054
95-88	TMP-GWD	Small	0.5	0.01836	0.00339	0.3840	0.7692	70.13	0.2377
95-154	TMP-GWD	Large	15	0.00207	0.00093	0.4106	0.1730	46.74	0.0434
95-158	TMP-GWD	Large	15	0.00221	0.00108	0.4086	0.1756	47.65	0.0516
95-160	TMP-GWD	Large	~ 15?	0.00531	0.00532	0.3883	0.2014	45.57	0.2423
95-157	TMP-GWD	Large	15	0.01266	0.00980	0.3775	0.3743	27.27	0.2673
95-155	TMP-GWD	Large	3.5	0.01885	0.00915	0.3881	0.5372	33.95	0.3107
95-95	BKP	Small	0.5	0.00160	0.00123	0.1116	0.2105	109.53	0.1345
95-94	BKP	Small	0.5	0.00347	0.00098	0.0000	0.1431	101.63	0.0996
95-93	BKP	Small	0.5	0.00958	0.00082	0.1057	0.2535	59.98	0.0493
95-92	BKP	Small	0.5	0.01947	0.00054	0.0995	0.3955	49.08	0.0266
95-153	BKP	Large	15	0.00191	0.00265	0.1156	0.0395	41.53	0.1103
95-166	BKP	Large	15	0.00530	0.00367	0.1027	0.0580	20.89	0.0767
95-167	BKP	Large	5	0.01224	0.00520	0.1034	0.1039	38.40	0.1998
95-168	BKP	Large	3	0.01861	0.00257	0.1100	0.1785	58.85	0.1510

APPENDIX D

Derivations of the Equations and Models Used in Chapters 3 to 6.

APPENDIX D-1

Determining Densities and Buoyancy Pressures of Ball Bearings (From Chapter 3)

Given the two ball bearing diameters used in the experiments:

$D_{Small} := \frac{1}{32} \cdot in$ $\quad D_{Small} = 793.75 \cdot \mu m$

$D_{Large} := \frac{1}{16} \cdot in$ $\quad D_{Large} = 1.588 \cdot 10^{3} \cdot \mu m$

B.B. Weights:

From Lab Book 85-137, the average weight of the b.b.'s were taken by measuring the total weight of 60 b.b.'s, and dividing by 60:

$W_{Small} := \frac{0.1258}{60} \cdot gm$ $\quad W_{Small} = 2.097 \cdot mg$

$W_{Large} := \frac{0.9847}{60} \cdot gm$ $\quad W_{Large} = 16.412 \cdot mg$

$\frac{W_{Large}}{W_{Small}} = 7.828$ The ratio should be 8, if b.b.'s are the same density.

B.B. Volumes:

$V_{Small} := \frac{\pi \cdot D_{Small}^{3}}{6}$ $\quad V_{Small} = 2.618 \cdot 10^{-4} \cdot mL$

$V_{Large} := \frac{\pi \cdot D_{Large}^{3}}{6}$ $\quad V_{Large} = 0.002 \cdot mL$

B.B. Densities:

$\rho_{Small} := \frac{W_{Small}}{V_{Small}}$ $\quad \rho_{Small} = 8.007 \cdot \frac{gm}{cm^{3}}$

$\rho_{Large} := \frac{W_{Large}}{V_{Large}}$ $\quad \rho_{Large} = 7.835 \cdot \frac{gm}{cm^{3}}$

Determining Buoyancy Pressure:

Define the buoyancy pressure as the buoyancy force per unit area:

$$\tau_b = \frac{F_b}{A}$$

where the magnitude of the buoyancy force acting downward is given by:

$$F_b = V \cdot g \cdot (\rho_{bb} - \rho_{water})$$

$$\rho_{water} = 1 \cdot \frac{gm}{cm^3}$$

A is assumed to be the half-area of a sphere of diameter D.

$$A = \frac{\pi \cdot D^2}{2}$$

Substituting in the buoyancy force and area into the buoyancy pressure (τb) gives:

$$\tau_b = \frac{1}{3} \cdot D \cdot g \cdot (\rho_{bb} - \rho_{water})$$

$$\tau_{bLarge} = \frac{1}{3} \cdot D_{Large} \cdot g \cdot (\rho_{Large} - \rho_{water}) \qquad \tau_{bLarge} = 35.467 \cdot Pa$$

$$\tau_{bSmall} = \frac{1}{3} \cdot D_{Small} \cdot g \cdot (\rho_{Small} - \rho_{water}) \qquad \tau_{bSmall} = 18.181 \cdot Pa$$

The yield stress for BKP is given by:

$\tau_y = 3.12 \cdot 10^6 \cdot Pa \cdot C^{2.79}$ (From Bennington et al., *Can. J. Chem. Eng.* 68:748-757 (1990)

To find the consistency required to support the ball bearing, set the buoyancy pressure equ to the yield stress, and solve for the consistency.

$$\tau_{bLarge} = 3.12 \cdot 10^6 \cdot Pa \cdot C_{Large}^{2.79} \qquad \tau_{bSmall} = 3.12 \cdot 10^6 \cdot Pa \cdot C_{Small}^{2.79}$$

$$C_{Large} := \left(\frac{\tau_{bLarge}}{3.12 \cdot 10^6 \cdot Pa} \right)^{\frac{1}{2.79}} \qquad C_{Small} := \left(\frac{\tau_{bSmall}}{3.12 \cdot 10^6 \cdot Pa} \right)^{\frac{1}{2.79}}$$

$$C_{Large} = 0.0169 \qquad C_{Small} = 0.0133$$

APPENDIX D-2

Deriving Equations Relating the Mass and Volume Consistencies.

Consider a pulp suspension with a total volume V_{Total} under isothermal conditions. Assume that pulp suspension consists of only pulp (fibres and fines) and pure water. The volumes of the pulp and water are assumed to be additive. The density of the pulp is designated as ρ_{pulp}, and the density of water is designated ρ_w.

Define the variables and their units:

$V_{Total} := cm^3$ $V_{pulp} := cm^3$ $V_w := cm^3$

Total volume of the pulp suspension | Volume of the pulp (fibres + fines) | Volume of the water.

Let V_{Total} be arbitrarily set to 1000 mL

$V_{Total} = 1000 \cdot mL$

$M_{Total} := gm$ $M_{pulp} := gm$ $M_w := gm$

Total mass | Total mass of pulp. | Total mass of water.

$\rho := \frac{gm}{cm^3}$ $\rho_{pulp} \equiv 1.5 \cdot \frac{gm}{cm^3}$ $\rho_w \equiv 1 \cdot \frac{gm}{cm^3}$

Density of the pulp suspension | Density of the pulp. | Density of the water.

ϕ ϕ_w Volume fractions of pulp and water, respectively

$C := 0.01$ Pulp consistency (Mass fraction of fibres per unit mass of pulp).

Equations:

$V_{Total} \equiv V_{pulp} + V_w$ Eq. (1) Overall volume balance.

$M_{Total} \equiv M_{pulp} + M_w$ Eq. (2) Overall mass balance.

$$\phi_w = \frac{V_w}{V_{Total}} \qquad \text{Eq. (3a)} \qquad V_{Total} = 0.001 \cdot m^3$$

$$\phi = \frac{V_{pulp}}{V_{Total}} \qquad \text{Eq. (3b)}$$

By definition: $\phi + \phi_w = 1$

Eqs. (4a, 4b, 4c): Mass = volume times density.

$$M_{pulp} = V_{pulp} \cdot \rho_{pulp} \qquad \text{Eq. (4a)}$$

$$M_w = V_w \cdot \rho_w \qquad \text{Eq. (4b)}$$

$$M_{Total} = V_{Total} \cdot \rho \qquad \text{Eq. (4c)}$$

The mass consistency is defined as:

$$C = \frac{M_{pulp}}{M_{Total}} \qquad \text{Eq. (5)}$$

Solving for M_{pulp} gives:

$$M_{pulp} = C \cdot M_{Total} \qquad \text{Eq (6)}$$

The overall pulp density is defined as:

$$\rho = \frac{M_{Total}}{V_{Total}} \qquad \text{Eq. (7)}$$

Substitute M_{Total} from Eq. (2) into Eq. (7):

$$\rho = \frac{(M_{pulp} + M_w)}{V_{Total}} \qquad \text{Eq. (8)}$$

Substitute M_{pulp} from Eq. (6) into Eq. (8).

$$\rho = \frac{(C \cdot M_{Total} + M_w)}{V_{Total}} \qquad \text{Eq. (9)}$$

Substitute $M_{Total} = V_{Total} * \rho$ from Eq. (4c) into Eq. (9).

$$\rho = \frac{(C \cdot V_{Total} \cdot \rho + M_w)}{V_{Total}} \qquad \text{Eq. (10)}$$

Substitute M_w from Eq. (4b) into Eq. (10)

$$\rho = \frac{\left(C \cdot V_{Total} \cdot \rho + V_w \cdot \rho_w\right)}{V_{Total}} \qquad \text{Eq. (11)}$$

From Eq. (3a): $V_w = \phi_w \cdot V_{Total}$ Substitute this into Eq.(11)

$$\rho = \frac{\left(C \cdot V_{Total} \cdot \rho + \phi_w \cdot V_{Total} \cdot \rho_w\right)}{V_{Total}} \qquad \text{Eq. (12)}$$

Solve for ϕ_w

$$\phi_w = \frac{(\rho - C \cdot \rho)}{\rho_w} \qquad \text{Eq. (13)}$$

Recall Eq. (8):

$$\rho = \frac{\left(M_{pulp} + M_w\right)}{V_{Total}} \qquad \text{Eq. (8)}$$

Substitute M_{pulp} and M_w from Eqs. (4a) and (4b) into Eq. (8):

$$\rho = \frac{\left(V_{pulp} \cdot \rho_{pulp} + V_w \cdot \rho_w\right)}{V_{Total}} \qquad \text{Eq. (14)}$$

From volume balance (Eq. 1), substitute in $V_{pulp} = (V_{Total} - V_w)$ into Eq. (14)

$$\rho = \frac{\left[\left(V_{Total} - V_w\right) \cdot \rho_{pulp} + V_w \cdot \rho_w\right]}{V_{Total}} \qquad \text{Eq. (15)}$$

Substitute $V_w = \phi_w \cdot V_{Total}$ from Eq. (3a) into Eq. (15)

$$\rho = \frac{\left[\left(V_{Total} - \phi_w \cdot V_{Total}\right) \cdot \rho_{pulp} + \phi_w \cdot V_{Total} \cdot \rho_w\right]}{V_{Total}} \qquad \text{Eq. (16)}$$

Sub ϕ_w from Eq. (13) into Eq. (16)

$$\rho = \frac{\left[\left[V_{Total} - \frac{(\rho - C \cdot \rho)}{\rho_w} \cdot V_{Total}\right] \cdot \rho_{pulp} + (\rho - C \cdot \rho) \cdot V_{Total}\right]}{V_{Total}} \qquad \text{Eq. (17)}$$

Solve for C and simplify

$$C = \frac{-\left(-\rho_{pulp} + \frac{\rho_{pulp}}{\rho_w}\cdot\rho\right)}{\left(\frac{-\rho_{pulp}}{\rho_w}\cdot\rho + \rho\right)} \qquad \text{Eq. [18]}$$

$$C = \rho_{pulp}\cdot\frac{(\rho_w - \rho)}{(\rho\cdot(-\rho_{pulp} + \rho_w))} \qquad \text{Eq. [19]}$$

Solving for the overall pulp density ρ gives:

$$\rho = \rho_{pulp}\cdot\frac{\rho_w}{\left(-C\cdot\rho_{pulp} + C\cdot\rho_w + \rho_{pulp}\right)} \qquad \text{Eq. [20]}$$

Converting Mass Consistency to Volume Consistency

The volume consistency is defined as ϕ, which is the volume fraction of pulp in the pulp suspension.

ϕ_w where, from Eq. (3b): $\phi = \frac{V_{pulp}}{V_{Total}}$

Recall Eq. (13):

$$\phi_w = \frac{(\rho - C\cdot\rho)}{\rho_w} \qquad \text{Eq. (13)}$$

Substitute in $\phi_w = 1 - \phi$ into Eq. (13).

$$1 - \phi = \frac{(\rho - C\cdot\rho)}{\rho_w} \qquad \text{Eq. (22)}$$

Substitute ρ from Eq. (20) into Eq. (22).

$$1 - \phi = \frac{\left[\rho_{pulp}\cdot\frac{\rho_w}{\left(-C\cdot\rho_{pulp} + C\cdot\rho_w + \rho_{pulp}\right)} - C\cdot\rho_{pulp}\cdot\frac{\rho_w}{\left(-C\cdot\rho_{pulp} + C\cdot\rho_w + \rho_{pulp}\right)}\right]}{\rho_w} \qquad \text{Eq. [23]}$$

Solve for ϕ and simplify.

$$\phi = 1 - \frac{\rho_{pulp}}{(-C\cdot\rho_{pulp} + C\cdot\rho_{w} + \rho_{pulp})} + C\cdot\frac{\rho_{pulp}}{(-C\cdot\rho_{pulp} + C\cdot\rho_{w} + \rho_{pulp})} \qquad \text{Eq. [24]}$$

$$\phi = C\cdot\frac{\rho_{w}}{(-C\cdot\rho_{pulp} + C\cdot\rho_{w} + \rho_{pulp})}$$

Eq. (25). This relates the volume consistency to the mass consistency.

Rearranging Eq. [26] and solving for C gives:

$$C = -\phi\cdot\frac{\rho_{pulp}}{(-\phi\cdot\rho_{pulp} + \phi\cdot\rho_{w} - \rho_{w})}$$

Eq. [26] This relates the mass consistency in terms of volume consistency.

APPENDIX D-3

Deriving a Model for the Mechanical Entrapment of Bubbles in a Uniform Fibre Network

Part I. Calculating the size of the void spaces in a fibre network.

Reference: Ogston, A.G. "The Spaces in a Uniform Random Suspensions of Fibres. *Trans. Faraday Soc.* Vol. 54: 1754-1757 (1958).

Parameters:

$\rho_{pulp} := 1.5 \cdot \frac{gm}{cm^3}$ Pulp fibre density.

$\rho_w := 1 \cdot \frac{gm}{cm^3}$ Water density.

$L_o := mm$ Half-length of a fiber (where $2*L_o = L$).

$L := 2 \cdot mm$ Fibre length.

$r := mm$ Radius of a given spherical particle.

$D := mm$ Diameter of a spherical particle.

$\omega := 25 \cdot \frac{mg}{100 \cdot m}$ Fibre coarseness.

$\phi := \frac{mL}{mL}$ Volume fraction of fibres in the pulp suspension.

$C := \frac{gm}{gm}$ Mass fraction of fibres in the pulp suspension (consistency).

$\nu := cm^{-3}$ Average number of fibre centers per cm^3.

From Ogston (1958), the fraction of the total volume of a uniform fibre suspension that can accommodate spherical particles of radius "r" is given by:

$$P_D := \exp\left[-\left(2 \cdot \pi \cdot \nu \cdot L_o \cdot r^2 + \frac{4 \cdot \pi}{3} \cdot \nu \cdot r^3\right)\right] \qquad \text{Eq. (1)}$$

Substitute $L_o := \frac{L}{2}$ into Eq. (1).

$$P_D = \exp\left(-\pi \cdot \nu \cdot L \cdot r^2 - \frac{4}{3} \cdot \pi \cdot \nu \cdot r^3\right) \quad \text{Eq. (2)}$$

Substitute $r = \frac{D}{2}$ into Eq. (2):

$$P_D = \exp\left(\frac{-1}{4} \cdot \pi \cdot \nu \cdot L \cdot D^2 - \frac{1}{6} \cdot \pi \cdot \nu \cdot D^3\right) \quad \text{Eq. (3)}$$

Define the mass of one fibre as the coarseness times the fibre length.

$$M_{OneFibre} = \omega \cdot L \quad \text{Eq. (4)}$$

Define the volume of a single fibre as the fibre mass divided by density.

$$V_{OneFibre} = \frac{M_{OneFibre}}{\rho_{pulp}} \quad \text{Eq. (5)}$$

Substituting Eq. [4] into Eq. (5) gives $V_{OneFibre} = \omega \cdot \frac{L}{\rho_{pulp}}$ Eq. (6)

Determine the number of fibres per unit volume: Arbitrarily select a unit volume of (V_{Tot}):

$$V_{Tot} = 1 \cdot cm^3$$

To get the total volume pulp fibres in V_{Tot}, multiply by the volume fraction of pulp fibres (ϕ):

$$V_{Fibres} = V_{Tot} \cdot \phi \quad \text{Eq. (7)}$$

The total number of fibres equals the fibre volume divided by the volume of a single fibre:

$$NumFibres = \frac{V_{Fibres}}{V_{OneFibre}} \quad \text{Eq. (8).}$$

Substitute V_{Fibres} from Eq. (7) into Eq. (8).

$$NumFibres = V_{Tot} \cdot \frac{\phi}{V_{OneFibre}} \quad \text{Eq. (9)}$$

Substitute $V_{OneFibre}$ from Eq. (5) into Eq. (9)

$$NumFibres = V_{Tot} \cdot \frac{\phi}{(\omega \cdot L)} \cdot \rho_{pulp} \quad \text{Eq. (10)}$$

Ogston (1958) defines ν as the average number of fibre centers per cm^3. We **assume** that this is equivalent to the number of actual fibres per unit volume.

By definition: $$\nu = \frac{\text{NumFibres}}{V_{Tot}} \qquad \text{Eq. (11)}$$

Substituting Eq. (10) into Eq. (11) gives:

$$\nu = \frac{\phi}{(\omega \cdot L)} \cdot \rho_{pulp} \qquad \text{Eq. (12)}$$

From Appendix D-2, the volume fraction of pulp (ϕ) is defined as:

$$\phi = C \cdot \frac{\rho_w}{\left(-C \cdot \rho_{pulp} + C \cdot \rho_w + \rho_{pulp}\right)} \qquad \text{Eq. (13)}$$

Substituting Eq. (13) into Eq. (12) gives:

$$\nu = C \cdot \frac{\rho_w}{\left[\left(-C \cdot \rho_{pulp} + C \cdot \rho_w + \rho_{pulp}\right) \cdot (\omega \cdot L)\right]} \cdot \rho_{pulp} \qquad \text{Eq. (14)}$$

Substituting Eq. (14) into Eq. (3) and simplifying gives:

$$P_D = \exp\left[\frac{-1}{12} \cdot \pi \cdot C \cdot \rho_w \cdot \rho_{pulp} \cdot D^2 \cdot \frac{(3 \cdot L + 2 \cdot D)}{\left[\left(-C \cdot \rho_{pulp} + C \cdot \rho_w + \rho_{pulp}\right) \cdot (\omega \cdot L)\right]}\right] \qquad \text{Eq. (15)}$$

Define Eq. (15) as a function of D,C, L and ω and plot it to see what it looks like:

$$P_D(D,C,L,\omega) = \exp\left[\frac{-1}{12} \cdot \pi \cdot C \cdot \rho_w \cdot \rho_{pulp} \cdot D^2 \cdot \frac{(3 \cdot L + 2 \cdot D)}{\left[\left(-C \cdot \rho_{pulp} + C \cdot \rho_w + \rho_{pulp}\right) \cdot (\omega \cdot L)\right]}\right] \qquad \text{Eq. (15a)}$$

Assume typical values for L and ω: $L = 2 \cdot mm$ $D = 1 \cdot \mu m, 5 \cdot \mu m .. 1000 \cdot \mu m$

$$\omega_1 = 25 \cdot \frac{mg}{100 \cdot m} \quad \omega_2 = 10 \cdot \frac{mg}{100 \cdot m}$$

Plot of void size distribution in a uniform fibre network

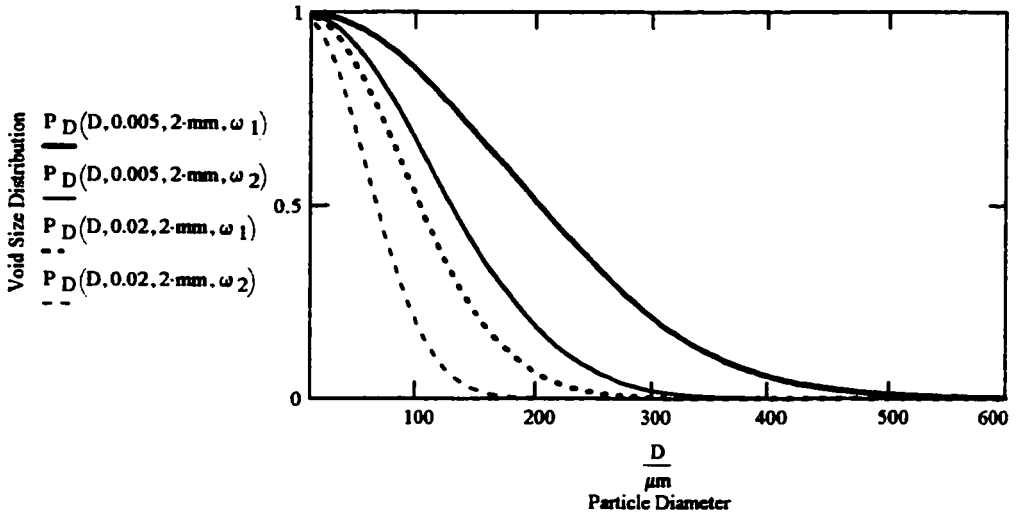

Part II. Estimating the Probability Bubble Migration Through a Given Distance in a Fibre Suspension.

$H = 1 \cdot mm$ Let "H" be the distance through with a bubble has to migrate through a uniform pulp suspension.

$D = 10 \cdot \mu m$ Let "D" be the bubble diameter.

Consider two mechanisms by which the bubble can escape the pulp suspension.
i) by slipping through the void spaces between the fibres
ii) by breaking through through the fibre network.

Let the probability of escaping by the slipping [Mechanism (i)] be P_S. Let the probability of escaping by breaking through the fibre network [Mechanism (ii)] be P_B.

First, we consider P_B.
P_B depends only on the buoyancy pressure and the pulp yield stress. It is independent of the distance the bubble has to travel. We assume a bubble will escape when the buoyancy pressure of the bubble exceeds the yield stress of the pulp. The probability of escape by breaking through is therefore given by:

$$P_B = (\tau_b > \tau_y) \qquad \text{Eq. (16)}$$

where τ_b is the buoyancy pressure, and τ_y is the yield stress of the pulp.

The magnitude of the buoyancy pressure of a bubble of diameter D in water is given by:

$$\tau_b = \frac{1}{3} \cdot D \cdot g \cdot (\rho_w - \rho_{air}) \qquad \text{Eq. (17)}$$

Neglecting the density of air (since ρair << ρwater) gives

$$\tau_b = \frac{1}{3} \cdot D \cdot g \cdot \rho_w \qquad \text{Eq. (18)}$$

The yield stress of pulp is commonly correlated in terms of consistency:

$$\tau_y = a \cdot C^b \qquad \text{Eq. (19)}$$

Substituting Eqs. (18) and (19) into Eq. (16) gives:

$$P_B(D,C,a,b) = \left(\frac{1}{3} \cdot D \cdot g \cdot \rho_w > a \cdot C^b \right) \qquad \text{Eq. (20)}$$

where P_B is expressed as a function of D,C,a and b. Note that P_B is a binary function, and has the values of either 1 or 0. If the buoyancy pressure exceeds the fibres network yield stress, $P_B = 1$. If the buoyancy pressure is less than the network yield stress, then $P_B = 0$.

Next, consider the probability of slipping through the void spaces (P_S). P_S depends on the probability of the bubble always encountering void spaces larger than the actual bubble diameter. This, in turn, depends on the distance the bubble has to travel.

Define the probability of a bubble slipping through fibres by a distance of it's own diameter (P_{SD}). We **assume** that this is equal to volume fraction of pulp with void spaces large enough to accommodate it.

Therefor, P_{SD} should equal P_D, as defined by Eq. (15).

Recall Eq. (15): $$P_D = \exp\left[\frac{-1}{12} \cdot \pi \cdot C \cdot \rho_w \cdot \rho_{pulp} \cdot D^2 \cdot \frac{(3 \cdot L + 2 \cdot D)}{\left[\left(-C \cdot \rho_{pulp} + C \cdot \rho_w + \rho_{pulp} \right) \cdot (\omega \cdot L) \right]} \right]$$

We set $P_{SD} = P_D$.

$$P_{SD} = P_D \qquad \text{Eq. (21)}$$

To migrate through a distance H, the bubble has slip through through the fibre network by (H/D) equivalent diameters. The overall probability of slipping through P_S is therefore given by:

$$P_S = P_D^{\frac{H}{D}} \qquad \text{Eq. (22)}$$

Substituting Eq. (15) in Eq. (22) gives:

$$P_S(D,C,L,\omega,H) = \exp\left[\frac{-1}{12}\cdot\pi\cdot C\cdot\rho_w\cdot\rho_{pulp}\cdot D^2\cdot\frac{(3\cdot L+2\cdot D)}{\left[\left(-C\cdot\rho_{pulp}+C\cdot\rho_w+\rho_{pulp}\right)\cdot(\omega\cdot L)\right]}\right]^{\left(\frac{H}{D}\right)} \qquad \text{Eq. (23).}$$

where P_S is expressed as a function of D,C,L,ω and H.

The overall probability of escaping is given by:

$$P_{esc} = P_s\cdot\left(1-P_B\right)+P_B \qquad \text{Eq. (24)}$$

Eq. (24) is based on the binary nature of the probability of breaking through a fibre network. According to Eq. (24), if the bubble can break through the fibre network ($P_B = 1$) and $P_{esc} = 1$, and the contribution of escaping by slipping (P_S) through is zero. If the bubble cannot break through , $P_B = 0$ and P_{esc} depends only on P_S.

To get the final probability of escape, substitute Eq. (20) and (23) into Eq. (24)

$$P_{esc}(D,C,L,\omega,a,b,H) = P_S(D,C,L,\omega,H)\cdot\left(1-P_B(D,C,a,b)\right)+P_B(D,C,a,b) \qquad \text{Eq. (25)}$$

The probability of mechanical entrapment equals ($1 - P_{esc}$):

$$P_{trap}(D,C,L,\omega,a,b,H) = 1-P_{esc}(D,C,L,\omega,a,b,H) \qquad \text{Eq. (26)}$$

To estimate the probability of mechanical entrapment, we need values of the empirical con: a and b. We refer to the yield stress correlations derived by Bennington et al. (1990).

Reference: Bennington, C.P.J., Kerekes, R.J. and Grace, J.R. "The Yield Stress of Fibres Suspensions", *Can. J. Chem. Eng.* Vol. 68:748-757 (1990).

From the yields stress measurements of Bennington et al. (1990):

SBK: $\tau_y = 312000C_m^{2.79}$ (Semi-bleached Kraft, $C < 0.05$)

SBW: $\tau_y = 1100000C_m^{2.99}$ (Stone Groundwood)

TMP: $\tau_y = 13800000C_m^{3.56}$ (Thermomechanical Pulp)

$a_{SBK} := 3.12\cdot10^6\cdot Pa$ $b_{SBK} := 2.79$

$a_{TMP} := 1.38\cdot10^7\cdot Pa$ $b_{TMP} := 3.56$

Plot the probabilities to see what the functions look like:

Assume: $L = 2 \cdot mm$ $\omega = 25 \cdot \frac{mg}{100 \cdot m}$ $H = 5 \cdot mm$ $D = 1 \cdot \mu m, 5 \cdot \mu m .. 2000 \cdot \mu m$

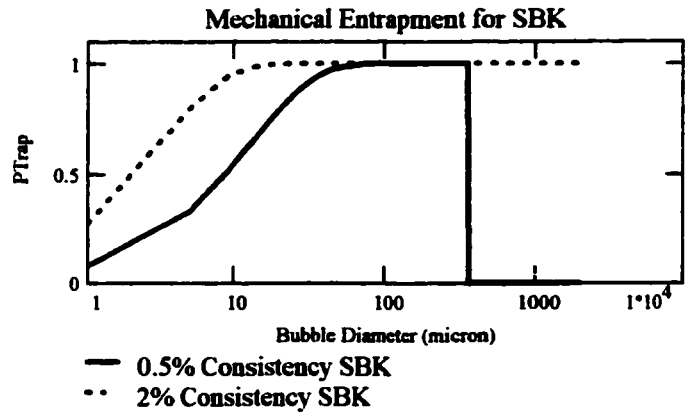

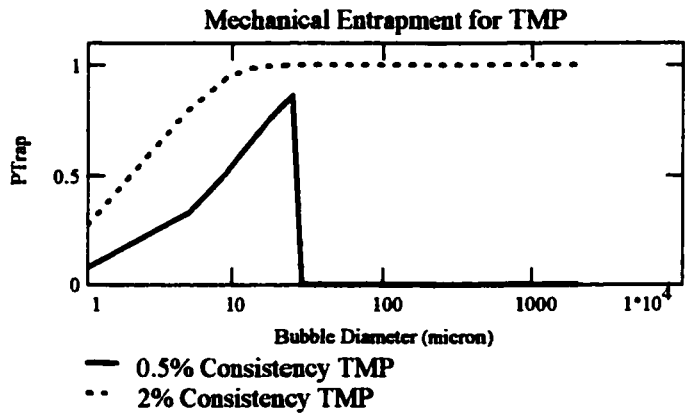

APPENDIX D-4

Determining the Void Size Distributions of the Bleached Kraft Pulp used in the Ball-Bearing Entrapment Experiments from Chapter 3.

Given the Bleached Kraft Pulp properties (from Table 3.1):

$L := 1.21 \cdot mm$ Arithmetic average fiber length.

$\omega := 13.8 \cdot \frac{mg}{100 \cdot m}$ Fibre coarseness.

$\rho_w \equiv 1 \cdot \frac{gm}{cm^3}$ Assumed density of pure water.

$\rho_{pulp} \equiv 1.5 \cdot \frac{gm}{cm^3}$ Assumed pulp fibre density.

From Appendix D-3, the void size distribution in a uniform fibre network was derived as:

$$P_D(D,C,L,\omega) := \exp\left[\frac{-1}{12} \cdot \pi \cdot C \cdot \rho_w \cdot \rho_{pulp} \cdot D^2 \cdot \frac{(3 \cdot L + 2 \cdot D)}{\left[\left(-C \cdot \rho_{pulp} + C \cdot \rho_w + \rho_{pulp}\right) \cdot (\omega \cdot L)\right]}\right]$$

Plot P_D versus diameter for various consistencies:

$C_1 := 0.0015$ $C_3 := 0.003$ $C_5 := 0.005$ $D := 1 \cdot \mu m, 5 \cdot \mu m .. 2000 \cdot \mu m$

Void Size Distribution Vs. Particle Diameter

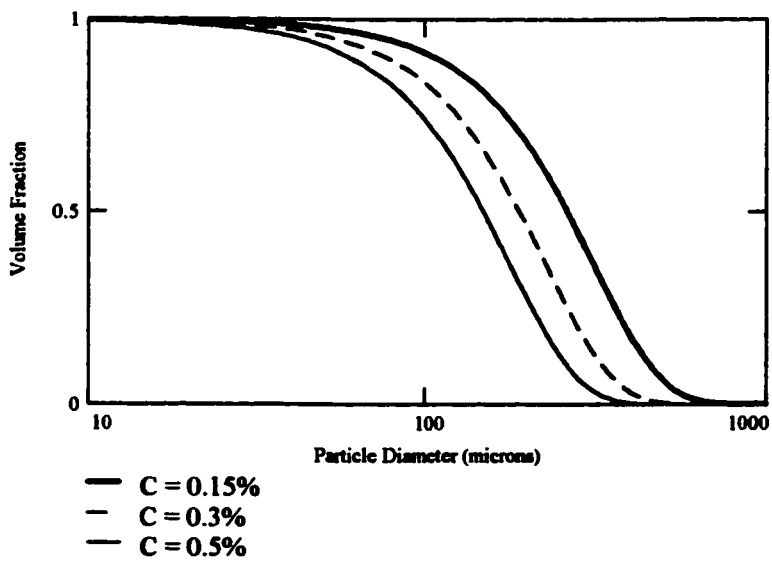

The calculations show that most of the void spaces in the BKP suspensions are less than 1000 microns.

APPENDIX D-5
Deriving an Expression for the Crowding Factor from First Principles (which takes into account the presence of pulp fines).

Parameters:

$\rho_{pulp} \equiv 1.5 \cdot \frac{gm}{cm^3}$ Pulp Fibre Density.

$\rho_w \equiv 1 \cdot \frac{gm}{cm^3}$ Water Density.

For the purposes of the present calculations, we will use the physical properties of the BKP pulp used in Chapters 3 and 5. (Refer to Table 3.1)

$L := 1.21 \cdot mm$ Arithmetic average fibre length. .

$\omega := 0.138 \cdot \frac{mg}{m}$ Fibre Coarseness.

$X_F := 0.107$ The fines content of the TMP-GWD pulp.

$C := .02$ Consistency of the pulp suspension (arbitrarily set to 0.02).

Recall from Appendix D-2, Eq. (20), the density of the pulp suspension (ρ) is given by:

$$\rho := \rho_{pulp} \cdot \frac{\rho_w}{\left(-C \cdot \rho_{pulp} + C \cdot \rho_w + \rho_{pulp}\right)} \qquad \text{Eq. (1)}$$

The crowding factor is defined expressed as the number of fibres contained within the spherical volume of rotation of a single fibre (Kerekes, R.J. and Schell, C.J. "Characterization of Fibre Flocculation Regimes by a Crowding Factor" *JPPS*. 18(1) J32-J38 (1992).

Assume the pulp fibres and pulp fines are uniformly dispersed in the pulp suspension. The spherical volume swept by one fibre is $4/3\pi R^3$, where $R = L/2$:

$$V_{FibSweep} := \frac{4}{3} \cdot \pi \cdot \left(\frac{L}{2}\right)^3 \qquad \text{Eq. (2)} \qquad V_{FibSweep} = 9.276 \cdot 10^{-4} \cdot cm^3$$

The total mass of this swept volume equals the volume times the overall density:

$$M_{Sweep} := V_{FibSweep} \cdot \rho \qquad \text{Eq. (3)} \qquad M_{Sweep} = 0.934 \cdot mg$$

The mass of cellulosic material (fibres and fines) equals the total mass times the consistency

$M_{PulpSweep} := M_{Sweep} \cdot C$ Eq. (4) $M_{PulpSweep} = 0.019 \cdot mg$

Divide the cellulosic mass is into long fibres and fines by multiplying by X_F and $(1 - X_F)$, respectively.

$M_{FibreSweep} := M_{PulpSweep} \cdot (1 - X_F)$ Eq. (5) $M_{FibreSweep} = 0.017 \cdot mg$

$M_{FinesSweep} := M_{PulpSweep} \cdot X_F$ Eq. (6) $M_{FinesSweep} = 0.002 \cdot mg$

The mass of a single long fibre equals the length times the coarseness:

$M_{OneFibre} := L \cdot \omega$ Eq. (7) $M_{OneFibre} = 1.67 \cdot 10^{-4} \cdot mg$

The total number of long fibres within the spherical volume or rotation equals the total mass long fibres divided by the mass of a single long fibre:

$$NumFibres := \frac{M_{FibreSweep}}{M_{OneFibre}}$$ Eq. (8) $NumFibres = 99.88$

Only the long fibres contribute to flocculation, since pulp fines are considered to be to short to entangle and form networks. When calculating the crowding factor, we therefore ignore the number of fines within the spherical volume of rotation of a pulp fibre.

Therefore, by definition, "NumFibres" also equals to the "Crowding Factor".

$$N := \frac{M_{FibreSweep}}{M_{OneFibre}}$$ Eq. (9)

Substituting in $M_{FibreSweep}$ from Eq. (5) and $M_{OneFibre}$ from Eq. (7) into Eq. (9) gives:

$$N := M_{PulpSweep} \cdot \frac{(1 - X_F)}{(L \cdot \omega)}$$ Eq. (10).

Substituting in $M_{PulpSweep}$ from Eq. (4) into Eq. (10) gives:

$$N := M_{Sweep} \cdot C \cdot \frac{(1 - X_F)}{(L \cdot \omega)}$$ Eq. (11)

Substituting M_{Sweep} from Eq. (3) into Eq. (11) gives:

$$N = V_{FibSweep} \cdot \rho \cdot C \cdot \frac{(1 - X_F)}{(L \cdot \omega)} \qquad \text{Eq. (12)}$$

Substituting in $V_{FibSweep}$ from Eq. (2) and ρ from Eq. (1) into Eq. (12) gives the final expression for the crowding factor:

$$N = \frac{1}{6} \cdot \pi \cdot L^2 \cdot \rho_{pulp} \cdot \frac{\rho_w}{(-C \cdot \rho_{pulp} + C \cdot \rho_w + \rho_{pulp})} \cdot C \cdot \frac{(1 - X_F)}{\omega} \qquad \text{Eq. (13)}$$

where Eq. (13) is our definition of crowding factor, which corresponds to the number of "long fibres" within the spherical volume of rotation of a single fibre.

Compare this with the definition of crowding factor presented by Kerekes (1996) which doesn't take into account the pulp fines:

$$N_{Ker} = \frac{500 \cdot C \cdot \left(\frac{L}{m}\right)^2}{\left[\frac{\omega}{\left(\frac{kg}{m}\right)}\right]} \quad \text{which simplifies to} \quad N_{Ker} = \frac{500 \cdot C \cdot L^2}{\omega} \cdot \frac{kg}{m^3} \qquad \text{Eq. (14)}$$

Reference: Kerekes, R.J. "Characterizing Fibre Suspensions", *Tappi Engineering Conf. Proc.* 21-28 (1996).

Define our crowding factor [Eq. (13)] as a function of C and X_F, and compare to the crowding factor from Kerekes [Eq. (14)].

$$N(C, X_F) := \frac{1}{6} \cdot \pi \cdot L^2 \cdot \rho_{pulp} \cdot \frac{\rho_w}{(-C \cdot \rho_{pulp} + C \cdot \rho_w + \rho_{pulp})} \cdot C \cdot \frac{(1 - X_F)}{\omega}$$

$$N_{Ker}(C) := \frac{500 \cdot C \cdot L^2}{\omega} \cdot \frac{kg}{m^3}$$

Plot the crowding factors:

C := 0, 0.0005 .. 0.02

Crowding Factor Vs. Consistency
(Comparison between present model and Kerekes' equation)

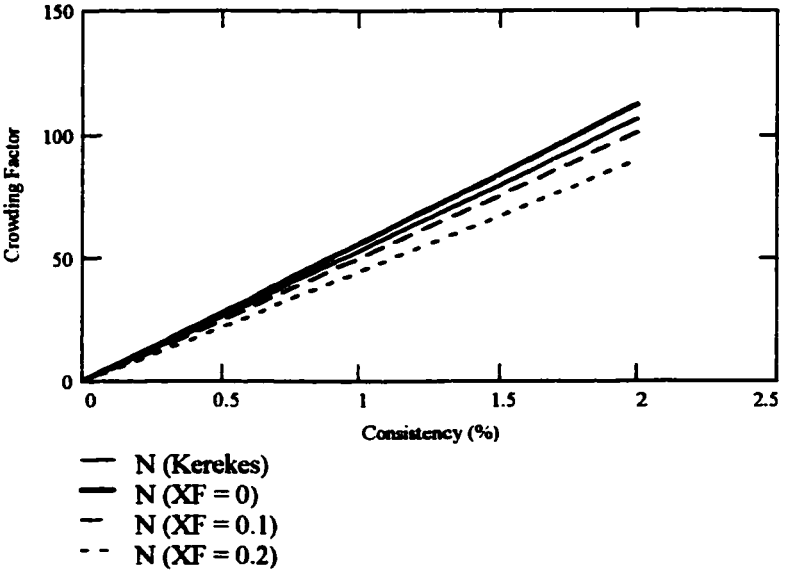

Note: Our crowding factor (N) agrees closely with Kerekes crowding factor when $X_F = 0$. As the fines content increases, N becomes less than Kerekes' crowding factor. This is because for a given consistency, the presence of pulp fines reduces the number of long fibres found within a given volume of pulp.

APPENDIX D-6
Correlating the Pulp Settling Data

Data for BKP (From Table C-8):

Initial Pulp Consistency	Settled Pulp Consistency	Volume Fraction of Settled Pulp
C_{BKP}	C_{BKPSet}	ϕ_{BKPSet}
0.00035	0.00253	0.09
0.00131	0.00308	0.43
0.00262	0.00325	0.805
0.00335	0.00452	0.75
0.00461	0.00485	0.95
0.00787	0.00831	0.945
0.00811	0.00833	0.98
0.0201	0.0201	1.0

Data for TMP-GWD Pulp (From Table C-8):

Initial Pulp Consistency	Settled Pulp Consistency	Volume Fraction of Settled Pulp
C_{MECH}	$C_{MECHSet}$	$\phi_{MECHSet}$
0.00097	0.0082	0.135
0.00121	0.00868	0.15
0.00559	0.01154	0.49
0.01562	0.01672	0.94
0.02409	0.02409	1.0

We wish to correlate the data in the form: $\phi = (1 - e^{KC})$.

Initialize values:

$j := 0..4 \quad i := 0..7$

$K_1 := 1 \quad K_2 := 1$

Define the function for the BKP data as follows:

$$\phi_{BKPFit}(C, K_1) := \left(1 - e^{K_1 C}\right)$$

Define the sum squared of errors as:

$$SSE_{BKP}(K_1) := \sum_{i=0}^{7} \left(\phi_{BKPSet_i} - \phi_{BKPFit}\left(C_{BKP_i}, K_1\right)\right)^2$$

Plot the function $SSE_{BKP}(K)$ to make an initial guess on K_1.

$K := -1000, -990 .. 200$

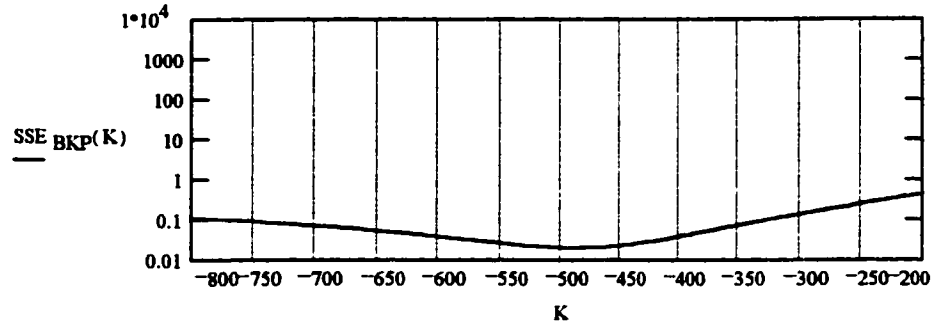

$SSE_{BKP}(K)$ has a minimum around -480. Set the initial guess for $K_1 := -480$

Use MathCad's Solve Block Function to find K_1 more precisely:

$TOL := 0.00001$

Given

$SSE_{BKP}(K_1) = 0$

$K_1 := \text{minerr}(K_1)$

$1 = 1$

$K_1 = -486.4652$

Similarly, for the TMP-GWD pulp, define:

$$\phi_{MECHFit}(C, K_2) := \left(1 - e^{K_2 \cdot C}\right)$$

$$SSE_{MECH}(K_2) := \sum_{j=0}^{4} \left(\phi_{MECHSet_j} - \phi_{MECHFit}\left(C_{MECH_j}, K_2\right)\right)^2$$

Plot $SSE_{MECH}(K)$ to make an initial guess on K_2.

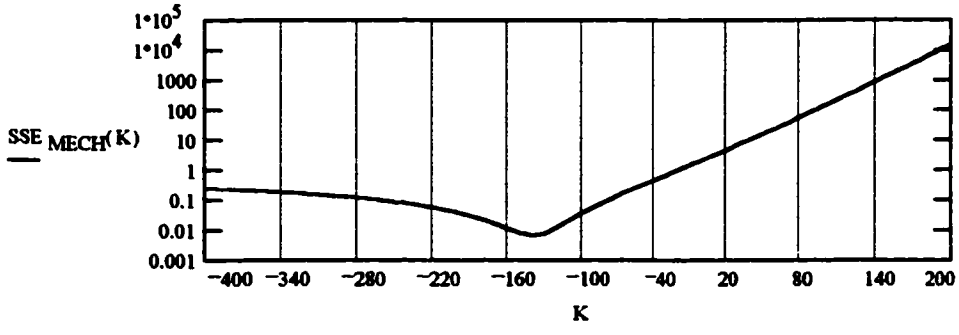

The plot of $SSE_{MECH}(K)$ shows that the initial guess for K2 is: $K_2 := -140$

Use the Solve Block function to find K_2 more precisely:

Given $\quad TOL = 1 \cdot 10^{-5}$

$SSE_{MECH}(K_2) = 0$

$1 = 1$

$K_2 := \text{minerr}(K_2)$

$K_2 = -138.9636$

Summarizing:

The BKP pulp settling data is correlated by: $\phi_{BKPFit}(C) := \left(1 - e^{K_1 \cdot C}\right)$ where $K_1 = -486.4652$

The TMP-GWD pulp settling data is correlated by: $\phi_{MECHFit}(C) := \left(1 - e^{K_2 \cdot C}\right)$ where $K_2 = -138.9636$

Plot the data to see what it looks like: $\quad C := 0, 0.001 .. 0.025$

Settled Consistency Data Vs. Original Consistency.

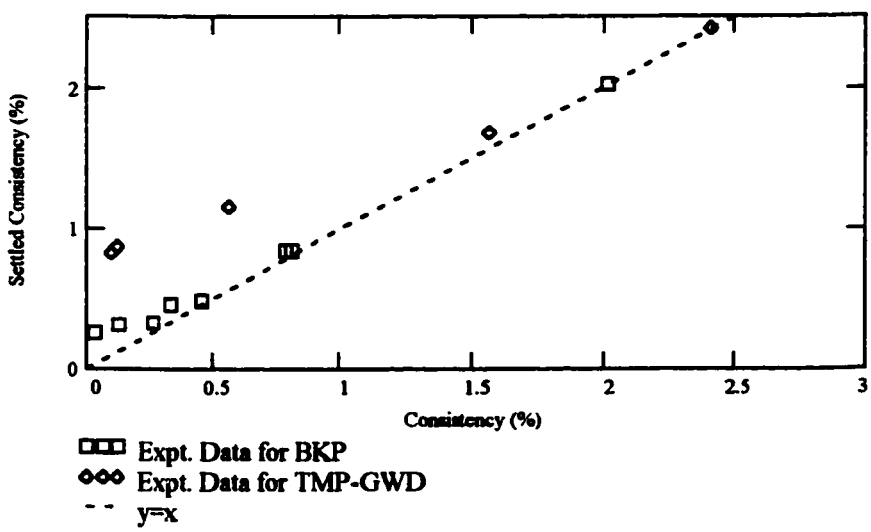

Settled Volume Fractions Vs. Original Consistency

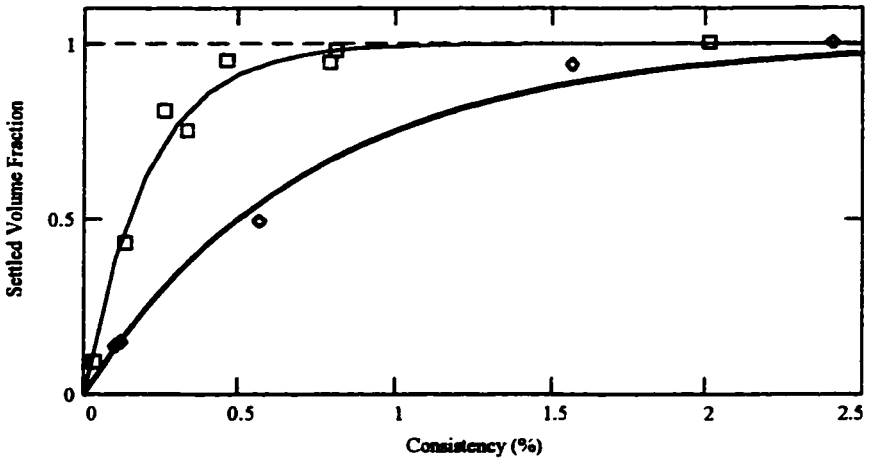

Expt. Settling Data (BKP)
Expt. Settling Data (TMP-GWD)
Correlation for BKP Data
Correlation for TMP-GWD Data
Settled Vol. Frac. = 1

APPENDIX D-7
Deriving the Model for the Interfloc Consistency and the Interfloc Fines Fraction.

Definitions:

PULP SUSPENSION: The combined mixture of pulp fibres, pulp fines and water.

PULP: The cellulosic material in the pulp suspension. The pulp consists of FIBRES and FINES.

FLOCS: Localized regions of high consistency in the pulp suspension.

FLOCCULATED REGION: The portion of the pulp suspension which is made up of flocs

INTERFLOC REGION: The portion of the pulp suspension which is not made up of flocs By definition, the interfloc region is more dilute than the flocculated region.

Measurable Parameters:

$v_{Total} = 1000 \cdot mL$	Total volume of the pulp suspension. For now, we arbitrarily set this to be 1000 mLs.
$c_m = 0.01$	Overall consistency (this equals the mass fraction of pulp in the pulp suspension).
$x_{Fines} = 0.389$	Overall fines content. This equals the mass fraction of fines in the pulp.

Assumed Parameters

c_f	Consistency of the pulp flocs.
c_{if}	Consistency of the interfloc region.
ϕ_f	Volume fraction of the pulp suspension which is flocculated.
$\phi(c)$	Volume fraction of pulp in the pulp suspension.
$\phi(c_f)$	Volume fraction of pulp in the flocs.
$\phi(c_{if})$	Volume fraction of pulp in the interfloc region

Assumed Parameters (cont'd.)

$\beta := 0.85$ Empirical constant to be defined later. β relates the fines content in the pulp flocs to the overall fines content by the expression:

$$X_{FinesFloc} := \beta \cdot X_{Fines}$$

$\rho_{pulp} \equiv 1.5 \cdot \frac{gm}{cm^3}$ $\rho_w \equiv 1 \frac{gm}{cm^3}$ Density of oven-dry pulp fibres and fines, and density of water. (ρ_{pulp} and ρ_w assumed to be constant)

Equations:

$$\phi(C) := \frac{C \cdot \rho_w}{(-C \cdot \rho_{pulp} + C \cdot \rho_w + \rho_{pulp})}$$ Eq. [1]. Volume consistency. This represents the volume fraction of pulp in the pulp suspension.

PART 1. General Mass Balance

$C := 0.01$ To start, for now we arbitrarily set the consistency to C = 0.01.

$\phi(C) = 0.007$ Overall volume fraction of cellulosic material in the pulp suspension.

$V_{pulp} := \phi(C) \cdot V_{Total}$ Eq. [2] Total volume of cellulose material in the suspension.

$V_w := (1 - \phi(C)) \cdot V_{Total}$ Eq. [3] Total volume of water in the suspension.

The sum of V_w and V_{pulp} should add up to the total volume of 1000 mLs.

$V_{pulp} = 6.689 \cdot mL$ $V_w = 993.311 \cdot mL$ $V_{pulp} + V_w = 1 \cdot 10^3 \cdot mL$

The total mass of cellulosic material (fibres and fines) in the pulp suspension:

$M_{pulp} := V_{pulp} \cdot \rho_{pulp}$ Eq. [4] $M_{pulp} = 10.033 \cdot gm$

Break this up into fibres and fines:

$M_{fines} := M_{pulp} \cdot X_{Fines}$ Eq. [5] $M_{fines} = 3.903 \cdot gm$

$M_{fibre} := M_{pulp} \cdot (1 - X_{Fines})$ Eq. [6] $M_{fibre} = 6.13 \cdot gm$

Substitute Eq. [2] into Eq. [4]:

$M_{pulp} := \phi(C) \cdot V_{Total} \cdot \rho_{pulp}$ Eq. [7] $M_{pulp} = 10.033 \cdot gm$

The total mass water in the pulp suspension is given by:

$M_w := V_w \rho_w$ Eq. [8] $M_w = 993.311 \cdot gm$

Substitute in Eq. [3] into Eq. [8]:

$M_w = (1 - \phi(C)) \cdot V_{Total} \cdot \rho_w$ Eq. [9] $M_w = 993.311 \cdot gm$

Checking the math:

$\frac{M_{pulp}}{M_{pulp} + M_w} = 0.01$ should equal the overall consistency. $C = 0.01$

Volume Balance on the Flocculated Portion of the Pulp Suspension

$\phi(C_f)$ is defined as the volume fraction of pulp in a floc.

For the time being, we arbitrarily $sec_f = 0.012$ which gives $\phi(C_f) = 0.00803$

Define the volume fraction of the pulp suspension which is flocculated as ϕ_f.

where $\phi_f =$ Total Volume of all the pulp flocs / Total Volume of the pulp suspension For now, arbitrarily set $\phi_f = 0.7$

The total volume occupied by the pulp flocs, defined as V_{Flocs}, is therefore given by:

$V_{Flocs} = V_{Total} \cdot \phi_f$ Eq. [10] $V_{Flocs} = 700 \cdot mL$

Total volume of the dispersed (i.e. non-flocculated) pulp in the "INTERFLOC" region is the difference between the total volume and V_{Flocs}.

$V_{if} = V_{Total} - V_{Flocs}$ Eq. [11] where the subscript "if" designates the "InterFloc" region.

Substitute Eq. [10] into Eq. [11]:

$V_{if} = V_{Total} \cdot (1 - \phi_f)$ Eq. [12]

The total floc volume is broken up into water and pulp as follows:

$V_{pulpFlocs} = V_{Flocs} \cdot \phi(C_f)$ Eq. [13] Total volume of pulp in the flocs (including fibres and fines).

$V_{wFlocs} = V_{Flocs} \cdot (1 - \phi(C_f))$ Eq. [14] Total volume of water in the flocs.

Checking the math:

The sum of V_{wFlocs} and $V_{pulpFlocs}$ should equal V_{Flocs}:

$V_{wFlocs} + V_{pulpFlocs} = 700 \cdot mL$

$V_{Flocs} = 700 \cdot mL$

Also, by definition, $V_{pulpFlocs}$ should be less than V_{pulp}.

$V_{pulpFlocs} = 5.622 \cdot mL$ $V_{pulp} = 6.689 \cdot mL$

Convert the volumes to masses by multiplying by the respective densities:

$M_{wFlocs} = V_{wFlocs} \cdot \rho_w$ Eq. [15] Total mass of water in the flocs. $M_{wFlocs} = 694.378 \cdot gm$

$M_{pulpFlocs} = V_{pulpFlocs} \cdot \rho_{pulp}$ Eq. [16] Total mass of pulp in the flocs. $M_{pulpFlocs} = 8.434 \cdot gm$

Substitute $V_{PulpFlocs}$ from Eq. [13] into Eq. [16]:

$M_{pulpFlocs} = V_{Flocs} \cdot \phi(C_f) \cdot \rho_{pulp}$ Eq [17]

Substitute V_{Flocs} from Eq. [10] into Eq. [17]:

$M_{pulpFlocs} = V_{Total} \cdot \phi_f \phi(C_f) \cdot \rho_{pulp}$ Eq. [18] $M_{pulpFlocs} = 8.434 \cdot gm$

Multiply Eq. [18] by $X_{FinesFloc}$ and (1 - $X_{FinesFloc}$) to get total mass of fines and fibres in the flocs, respectively.

$M_{finesFlocs} = V_{Total} \cdot \phi_f \phi(C_f) \cdot \rho_{pulp} \cdot X_{FinesFloc}$ Eq. [19] $M_{finesFlocs} = 2.789 \cdot gm$

$M_{fibreFlocs} = V_{Total} \cdot \phi_f \phi(C_f) \cdot \rho_{pulp} \cdot (1 - X_{FinesFloc})$ Eq. [20] $M_{fibreFlocs} = 5.645 \cdot gm$

Key Assumption #1: The fines content in the flocs is related to the overall fines as follows

$X_{FinesFloc} = \beta \cdot X_{Fines}$ Eq. [21] (where β is an adjustable parameter).

Substitute Eq. [21] into Eqs. [19] and [20]:

$M_{finesFlocs} = V_{Total} \cdot \phi_f \phi(C_f) \cdot \rho_{pulp} \cdot \beta \cdot X_{Fines}$ Eq. [22] $M_{finesFlocs} = 2.789 \cdot gm$

$M_{fibreFlocs} = V_{Total} \cdot \phi_f \phi(C_f) \cdot \rho_{pulp} \cdot (1 - \beta \cdot X_{Fines})$ Eq. [23] $M_{fibreFlocs} = 5.645 \cdot gm$

To determine how much pulp (i.e. fibres and fines) is present in the interfloc region, subtra the mass of pulp in the flocs from the total mass of pulp.

$M_{pulpif} = M_{pulp} - M_{pulpFlocs}$ Eq. [24] $M_{pulpif} = 1.6 \cdot gm$

Repeat with water, pulp fibres, and pulp fines.

$M_{wif} = M_w - M_{wFlocs}$ Eq. [25] $M_{wif} = 298.934 \cdot gm$

$M_{fineif} = M_{fines} - M_{finesFlocs}$ Eq. [26] $M_{fineif} = 1.114 \cdot gm$

$M_{fibreif} = M_{fibre} - M_{fibreFlocs}$ Eq. [27] $M_{fibreif} = 0.485 \cdot gm$

(Note: none of the values of M_{pulpif}, M_{wIf}, M_{fineif} or $M_{fibreif}$ should be negative!)

Checking the mass balances:

$M_{wif} + M_{wFlocs} = 993.311 \cdot gm$ should equal the total mass of water. $M_w = 993.311 \cdot gm$

$M_{pulpif} + M_{pulpFlocs} = 10.033 \cdot gm$ should equal the total mass of pulp. $M_{pulp} = 10.033 \cdot gm$

$M_{finesif} + M_{fibreif} = 1.6 \cdot gm$ should equal the total mass of interfloc pulp $M_{pulpif} = 1.6 \cdot gm$

PART 2. The Interfloc Consistency

By definition, the interfloc consistency equals the mass fraction of pulp in the interfloc region:

$$C_{if} = \frac{M_{pulpif}}{M_{pulpif} + M_{wif}} \qquad \text{Eq. [28]}$$

Substitute M_{pulpif} from Eq. [24] into Eq. [28]:

$$C_{if} = \frac{(M_{pulp} - M_{pulpFlocs})}{(M_{pulp} - M_{pulpFlocs} + M_{wif})} \qquad \text{Eq. [29]}$$

Substitute M_{wif} from Eq [25] into Eq. [29]:

$$C_{if} = \frac{(M_{pulp} - M_{pulpFlocs})}{(M_{pulp} - M_{pulpFlocs} + M_w - M_{wFlocs})} \qquad \text{Eq. [30]}$$

Substitute $M_{pulpflocs}$ from Eq. [18] into Eq. [30].

$$C_{if} = \frac{(M_{pulp} - V_{Total} \cdot \phi_f \phi(C_f) \cdot \rho_{pulp})}{(M_{pulp} - V_{Total} \cdot \phi_f \phi(C_f) \cdot \rho_{pulp} + M_w - M_{wFlocs})} \qquad \text{Eq. [31]}$$

Substitute M_{pulp} from Eq. [7] into Eq. [31]:

$$C_{if} = \frac{(\phi(C) \cdot V_{Total} \cdot \rho_{pulp} - V_{Total} \cdot \phi_f \phi(C_f) \cdot \rho_{pulp})}{(\phi(C) \cdot V_{Total} \cdot \rho_{pulp} - V_{Total} \cdot \phi_f \phi(C_f) \cdot \rho_{pulp} + M_w - M_{wFlocs})} \qquad \text{Eq. [32]}$$

Substitute M_{wFlocs} from Eq. [15] into Eq. [32] .

$$C_{if} = \frac{(\phi(C) \cdot V_{Total} \cdot \rho_{pulp} - V_{Total} \cdot \phi_f \phi(C_f) \cdot \rho_{pulp})}{(\phi(C) \cdot V_{Total} \cdot \rho_{pulp} - V_{Total} \cdot \phi_f \phi(C_f) \cdot \rho_{pulp} + M_w - V_{wFlocs} \cdot \rho_w)} \qquad \text{Eq. [33]}$$

Substitute V_{wFlocs} from Eq. [14] into Eq. [33].

$$C_{if} = \frac{(\phi(C) \cdot V_{Total} \cdot \rho_{pulp} - V_{Total} \cdot \phi_f \phi(C_f) \cdot \rho_{pulp})}{\left[\phi(C) \cdot V_{Total} \cdot \rho_{pulp} - V_{Total} \cdot \phi_f \phi(C_f) \cdot \rho_{pulp} + M_w - V_{Flocs} \cdot (1 - \phi(C_f)) \cdot \rho_w\right]} \qquad \text{Eq. [34]}$$

Substitute V_{Flocs} from Eq. [10] into Eq. [34] .

$$C_{if} = \frac{(\phi(C)\cdot V_{Total}\cdot\rho_{pulp} - V_{Total}\cdot\phi_f\phi(C_f)\cdot\rho_{pulp})}{\left[\phi(C)\cdot V_{Total}\cdot\rho_{pulp} - V_{Total}\cdot\phi_f\phi(C_f)\cdot\rho_{pulp} + M_w - V_{Total}\cdot\phi_f\left(1-\phi(C_f)\right)\cdot\rho_w\right]} \quad \text{Eq. [35]}$$

Substitute M_w for Eq. [9] into Eq. [35].

$$C_{if} = \frac{(\phi(C)\cdot V_{Total}\cdot\rho_{pulp} - V_{Total}\cdot\phi_f\phi(C_f)\cdot\rho_{pulp})}{\left[\begin{array}{l}\phi(C)\cdot V_{Total}\cdot\rho_{pulp} - V_{Total}\cdot\phi_f\phi(C_f)\cdot\rho_{pulp} \cdots \\ + (1-\phi(C))\cdot V_{Total}\cdot\rho_w - V_{Total}\cdot\phi_f\left(1-\phi(C_f)\right)\cdot\rho_w\end{array}\right]} \quad \text{Eq. [36]}$$

Simplifying gives the final expression for the interfloc consistency in terms of C, C_f and ϕ_f:

$$C_{if} = \frac{(\phi(C)\cdot\rho_{pulp} - \phi_f\phi(C_f)\cdot\rho_{pulp})}{\left[\phi(C)\cdot\rho_{pulp} - \phi_f\phi(C_f)\cdot\rho_{pulp} + (1-\phi(C))\cdot\rho_w - \phi_f\left(1-\phi(C_f)\right)\cdot\rho_w\right]} \quad \text{Eq. [37]}$$

PART 3. The Interfloc Fines Fraction.

Define the interfloc fines fraction as the mass of pulp fines in the interfloc region, divided by the total mass of pulp in the interfloc region:

$$X_{if} = \frac{M_{finesif}}{M_{pulpif}} \quad \text{Eq. [38]}$$

Substitute $M_{finesif}$ from Eq. [26] and M_{pulpif} from Eq. [24] into Eq. [38].

$$X_{if} = \frac{(M_{fines} - M_{finesFlocs})}{(M_{pulp} - M_{pulpFlocs})} \quad \text{Eq. [39]}$$

Substitute M_{fines} from Eq. [5] into Eq. [39].

$$X_{if} = \frac{(M_{pulp}\cdot X_{Fines} - M_{finesFlocs})}{(M_{pulp} - M_{pulpFlocs})} \quad \text{Eq. [40]}$$

Substitute $M_{finesfloc}$ from Eq. [19] into Eq. [40].

$$X_{if} = \frac{(M_{pulp}\cdot X_{Fines} - V_{Total}\cdot\phi_f\phi(C_f)\cdot\rho_{pulp}\cdot X_{FinesFloc})}{(M_{pulp} - M_{pulpFlocs})} \quad \text{Eq. [41]}$$

Substitute in $M_{pulpFlocs}$ from Eq. [18] into Eq. [41]

$$X_{if} = \frac{(M_{pulp}\cdot X_{Fines} - V_{Total}\cdot\phi_f\phi(C_f)\cdot\rho_{pulp}\cdot X_{FinesFloc})}{(M_{pulp} - V_{Total}\cdot\phi_f\phi(C_f)\cdot\rho_{pulp})} \quad \text{Eq. [42]}$$

Substitute M_{pulp} from Eq. [7] into Eq. [42].

$$X_{if} = \frac{(\phi(C)\cdot V_{Total}\cdot \rho_{pulp}\cdot X_{Fines} - V_{Total}\cdot \phi_f \phi(C_f)\cdot \rho_{pulp}\cdot X_{FinesFloc})}{(\phi(C)\cdot V_{Total}\cdot \rho_{pulp} - V_{Total}\cdot \phi_f \phi(C_f)\cdot \rho_{pulp})} \qquad \text{Eq. [43]}$$

Substitute $X_{FinesFloc} = \beta \cdot X_{Fines}$ into Eq. [43].

$$X_{if} = \frac{(\phi(C)\cdot V_{Total}\cdot \rho_{pulp}\cdot X_{Fines} - V_{Total}\cdot \phi_f \phi(C_f)\cdot \rho_{pulp}\cdot \beta \cdot X_{Fines})}{(\phi(C)\cdot V_{Total}\cdot \rho_{pulp} - V_{Total}\cdot \phi_f \phi(C_f)\cdot \rho_{pulp})} \qquad \text{Eq. [44]}$$

Simplifying gives the final expression for the interfloc fines content in terms of C, C_f, β and ϕ_f:

$$X_{if} = \frac{(\phi(C) - \phi_f \phi(C_f)\cdot \beta)}{(\phi(C) - \phi_f \phi(C_f))} \cdot X_{Fines} \qquad \text{Eq. [45]}$$

Note: the parameter β represents the relative distribution of pulp fines between the pulp suspension and the flocs. If ($\beta = 1$), then there is no preferential distribution of pulp fines between the pulp flocs, and $X_{FinesFloc} = X_{Fines}$.

PART 4. Deriving Mass Balance Equations to Verify Estimates of the Interfloc Properties.

The values of C_{if} and X_{if} are functions of C, C_{if} and ϕ_f and β. For any given value of C_{if} or X_{if}, an infinite number of combinations C, $\phi(C_f)$, β and ϕ_f are mathematically possible. Many combinations, however, are not physically realizable: mass balance restrictions forbid negative consistencies or floc volumes. The purpose of this section is to derive mass balance equations to verify the validity of the estimated values of C_f, ϕ_f and β are valid

Pulp Mass Balance: We begin with an overall balance on the pulp. Set the criterion that the total mass of pulp in the suspension must be greater or equal to the mass of pulp in the flocs.

Define the Boolean expression:

$M_{pulp} \geq M_{pulpFlocs}$ Eq. [46]. This Boolean expression equals "1" if the pulp mass balance is valid, and "0" the pulp mass balance does not work.

Verify:

$$M_{pulp} \geq M_{pulpFlocs} = 1 \qquad \frac{M_{pulp}}{M_{pulpFlocs}} = 1.19 \qquad \text{Eq. [47]}$$

Substitute M_{pulp} from Eq. [7] into Eq. [46].

$$M_{pulpFlocs} \le \phi(C) \cdot V_{Total} \cdot \rho_{pulp} \qquad \text{Eq. [48]}$$

Substitute $M_{pulpFlocs}$ from Eq. [18] into Eq. [48].

$$V_{Total} \cdot \phi_f \phi(C_f) \cdot \rho_{pulp} \le \phi(C) \cdot V_{Total} \cdot \rho_{pulp} \qquad \text{Eq. [49]}$$

Divide both sides by V_{Total} and ρ_{pulp}.

$$\frac{V_{Total} \cdot \phi_f \phi(C_f) \cdot \rho_{pulp}}{V_{Total} \cdot \rho_{pulp}} \le \frac{\phi(C) \cdot V_{Total} \cdot \rho_{pulp}}{V_{Total} \cdot \rho_{pulp}} \qquad \text{Eq. [50]}$$

Simplifying gives

$$\phi_f \phi(C_f) \le \phi(C) \qquad \text{Eq. [51]}$$

Define $F_1(C, C_f, \phi_f) := \phi_f \phi(C_f) \le \phi(C)$ Eq. [52]

$F_1(C, C_f, \phi_f) = 1$

Check the math by comparing the ratios from Eqs [47] and [52]:

$$\frac{\phi(C)}{(\phi_f \phi(C_f))} = 1.19 \quad \text{equals} \quad \frac{M_{pulp}}{M_{pulpFlocs}} = 1.19$$

Water Mass Balance. Criterion: The total mass of water in the pulp suspension must be greater or equal to the the mass of water in the flocs.

Define the Boolean expression:

$$M_w \ge M_{wFlocs} \qquad \text{Eq. [53].}$$

Verify

$$M_w \ge M_{wFlocs} = 1 \qquad \frac{M_w}{M_{wFlocs}} = 1.431 \qquad \text{Eq. [54]}$$

Substitute M_w from Eq. [9] into Eq. [53].

$$M_{wFlocs} \le (1 - \phi(C)) \cdot V_{Total} \cdot \rho_w \qquad \text{Eq. [55]}$$

Substitute M_{wFlocs} from Eq. [15] into Eq. [55].

$$V_{wFlocs} \cdot \rho_w \le (1 - \phi(C)) \cdot V_{Total} \cdot \rho_w \qquad \text{Eq. [56]}$$

Substitute V_{wFlocs} from Eq. [14] into Eq. [56].

$$V_{Flocs} \cdot (1 - \phi(C_f)) \cdot \rho_w \le (1 - \phi(C)) \cdot V_{Total} \cdot \rho_w \qquad \text{Eq. [57]}$$

Substitute V_{Flocs} from Eq. [10] into Eq. [57].

$$V_{Total}\cdot\phi_f\left(1-\phi(C_f)\right)\cdot\rho_w \le (1-\phi(C))\cdot V_{Total}\cdot\rho_w \qquad \text{Eq. [58]}$$

Divide by $[V_{Total}]^*[\rho_w]$ and simplify:

$$\frac{V_{Total}\cdot\phi_f\left(1-\phi(C_f)\right)\cdot\rho_w}{V_{Total}\cdot\rho_w} \le \frac{(1-\phi(C))\cdot V_{Total}\cdot\rho_w}{V_{Total}\cdot\rho_w} \qquad \text{Eq. [59]}$$

$$-\phi_f\left(-1+\phi(C_f)\right) \le 1-\phi(C) \qquad \text{Eq. [60]}$$

Define $F_2(C,C_f,\phi_f) := -\phi_f\left(-1+\phi(C_f)\right) \le 1-\phi(C)$ Eq. [61]

$F_2(C,C_f,\phi_f) = 1$

Check the math by comparing the ratios $\frac{1-\phi(C)}{-\phi_f\left(-1+\phi(C_f)\right)} = 1.431$ equals $\frac{M_w}{M_{wFlocs}} = 1.431$ from Eqs [54] and [61]:

The overall pulp and water balance can be expressed as a combination of the two functions F_1 and F_2.

$F_1(C,C_f,\phi_f) := \phi_f\phi(C_f) \le \phi(C)$ Eq. [52]

$F_2(C,C_f,\phi_f) := -\phi_f\left(-1+\phi(C_f)\right) \le 1-\phi(C)$ Eq. [61]

$PulpCheck(C,C_f,\phi_f) := F_1(C,C_f,\phi_f)\cdot F_2(C,C_f,\phi_f)$ Eq. [62]

$PulpCheck(C,C_f,\phi_f) := (\phi_f\phi(C_f) \le \phi(C))\cdot\left[-\phi_f\left(-1+\phi(C_f)\right) \le 1-\phi(C)\right]$

If PulpCheck is equal to 1, then mass balances of the pulp and water are valid.
If PulpCheck is equal to 0, then the pulp and water mass balances do not work, and the estimates of C_f, ϕ_f are invalid.

Pulp Fines Mass Balance (#1). Criterion: The total mass of pulp fines must be greater or equal to the mass of pulp fines in the inter-floc regions.

Define the Boolean expression:

$M_{fines} \ge M_{finesif}$ Eq. [63]

Verify:

$M_{fines} \ge M_{finesif} = 1$ $\frac{M_{fines}}{M_{finesif}} = 3.502$ Eq. [64]

Substitute $M_{finesif}$ from Eq. [26] into Eq. [63].

$$M_{fines} - M_{finesFlocs} \leq M_{fines} \qquad \text{Eq. [65]}$$

Substitute M_{fines} from Eq. [5] into Eq. [65]

$$M_{pulp} \cdot X_{Fines} - M_{finesFlocs} \leq M_{pulp} \cdot X_{Fines} \qquad \text{Eq. [66]}$$

Substitute $M_{finesFlocs}$ from Eq. [19] into Eq. [66].

$$M_{pulp} \cdot X_{Fines} - V_{Total} \cdot \phi_f \phi(C_f) \cdot \rho_{pulp} \cdot X_{FinesFloc} \leq M_{pulp} \cdot X_{Fines} \qquad \text{Eq. [67]}$$

Substitute M_{pulp} from Eq. [7] into Eq. [67].

$$\phi(C) \cdot V_{Total} \cdot \rho_{pulp} \cdot X_{Fines} - V_{Total} \cdot \phi_f \phi(C_f) \cdot \rho_{pulp} \cdot X_{FinesFloc} \leq \phi(C) \cdot V_{Total} \cdot \rho_{pulp} \cdot X_{Fines} \qquad \text{Eq. [68]}$$

Substitute $X_{FinesFloc} := \beta \cdot X_{Fines}$ into Eq. [68]

$$\phi(C) \cdot V_{Total} \cdot \rho_{pulp} \cdot X_{Fines} - V_{Total} \cdot \phi_f \phi(C_f) \cdot \rho_{pulp} \cdot \beta \cdot X_{Fines} \leq \phi(C) \cdot V_{Total} \cdot \rho_{pulp} \cdot X_{Fines} \qquad \text{Eq. [69]}$$

Divide both sides by $[V_{Total}][\rho_{pulp}][X_{Fines}]$ and simplify

$$\frac{\phi(C) \cdot V_{Total} \cdot \rho_{pulp} \cdot X_{Fines} - V_{Total} \cdot \phi_f \phi(C_f) \cdot \rho_{pulp} \cdot \beta \cdot X_{Fines}}{V_{Total} \cdot \rho_{pulp} \cdot X_{Fines}} \leq \frac{\phi(C) \cdot V_{Total} \cdot \rho_{pulp} \cdot X_{Fines}}{V_{Total} \cdot \rho_{pulp} \cdot X_{Fines}} \qquad \text{Eq. [70]}$$

$$\phi(C) - \phi_f \phi(C_f) \cdot \beta \leq \phi(C) \qquad \text{Eq. [71]}$$

Define $F_3(C, C_f, \phi_f, \beta) := \phi(C) - \phi_f \phi(C_f) \cdot \beta \leq \phi(C)$ Eq. [72]

$F_3(C, C_f, \phi_f, \beta) = 1$

Check the math by comparing the ratios from Eqs [64] and [72]: $\frac{\phi(C)}{(\phi(C) - \phi_f \phi(C_f) \cdot \beta)} = 3.502$ equals $\frac{M_{fines}}{M_{finesif}} = 3.502$

Pulp Fines Mass Balance (#2). Criterion: The mass of pulp in the interfloc region must be greater or equal to the mass of pulp fines in the interfloc region.

Define the Boolean expression:

$$M_{pulpif} \geq M_{finesif} \qquad \text{Eq. [73]}$$

Verify:

$$M_{pulpif} \geq M_{finesif} = 1 \qquad \frac{M_{pulpif}}{M_{finesif}} = 1.435 \qquad \text{Eq. [74]}$$

Substitute $M_{finesif}$ from Eq. [26] and M_{pulpif} from Eq. [24] into Eq. [73]

$$M_{fines} - M_{finesFlocs} \leq M_{pulp} - M_{pulpFlocs} \qquad \text{Eq. [75]}$$

Substitute $M_{finesFlocs}$ from Eq. [20] into Eq. [75]

$$M_{fines} - V_{Total} \cdot \phi_f \phi(C_f) \cdot \rho_{pulp} \cdot X_{FinesFloc} \leq M_{pulp} - M_{pulpFlocs} \qquad \text{Eq. [76]}$$

Substitute $M_{pulpFlocs}$ from Eq. [18] into Eq. [76].

$$M_{fines} - V_{Total} \cdot \phi_f \phi(C_f) \cdot \rho_{pulp} \cdot X_{FinesFloc} \leq M_{pulp} - V_{Total} \cdot \phi_f \phi(C_f) \cdot \rho_{pulp} \qquad \text{Eq. [77]}$$

Substitute M_{fines} from Eq. [5] into Eq. [77].

$$M_{pulp} \cdot X_{Fines} - V_{Total} \cdot \phi_f \phi(C_f) \cdot \rho_{pulp} \cdot X_{FinesFloc} \leq M_{pulp} - V_{Total} \cdot \phi_f \phi(C_f) \cdot \rho_{pulp} \qquad \text{Eq. [78]}$$

Substitute M_{pulp} from Eq. [7] into Eq. [78].

$$\phi(C) \cdot V_{Total} \cdot \rho_{pulp} \cdot X_{Fines} - V_{Total} \cdot \phi_f \phi(C_f) \cdot \rho_{pulp} \cdot X_{FinesFloc} \leq \phi(C) \cdot V_{Total} \cdot \rho_{pulp} - V_{Total} \cdot \phi_f \phi(C_f) \cdot \rho_{pulp} \qquad \text{Eq. [79]}$$

Substitute $X_{FinesFloc} = \beta \cdot X_{Fines}$ into Eq. [79]

$$\phi(C) \cdot V_{Total} \cdot \rho_{pulp} \cdot X_{Fines} - V_{Total} \cdot \phi_f \phi(C_f) \cdot \rho_{pulp} \cdot \beta \cdot X_{Fines} \leq \phi(C) \cdot V_{Total} \cdot \rho_{pulp} - V_{Total} \cdot \phi_f \phi(C_f) \cdot \rho_{pulp} \qquad \text{Eq. [80]}$$

Divide both sides of Eq. [81] by $[V_{Total}][\rho_{pulp}]$ and simplify.

$$\frac{\phi(C) \cdot V_{Total} \cdot \rho_{pulp} \cdot X_{Fines} - V_{Total} \cdot \phi_f \phi(C_f) \cdot \rho_{pulp} \cdot \beta \cdot X_{Fines}}{V_{Total} \cdot \rho_{pulp}} \leq \frac{\phi(C) \cdot V_{Total} \cdot \rho_{pulp} - V_{Total} \cdot \phi_f \phi(C_f) \cdot \rho_{pulp}}{V_{Total} \cdot \rho_{pulp}} \qquad \text{Eq. [81]}$$

$$-X_{Fines} \cdot \left(-\phi(C) + \phi_f \phi(C_f) \cdot \beta\right) \leq \phi(C) - \phi_f \phi(C_f) \qquad \text{Eq. [82]}$$

Define this as $F_4(C, C_f, \phi_f, \beta) = -X_{Fines} \cdot \left(-\phi(C) + \phi_f \phi(C_f) \cdot \beta\right) \leq \phi(C) - \phi_f \phi(C_f)$ Eq. [83]

$$F_4(C, C_f, \phi_f, \beta) = 1$$

Verify the math by comparing the ratios from Eqs. [74] and [83]

$$\frac{\phi(C) - \phi_f \phi(C_f)}{-X_{Fines} \cdot \left(-\phi(C) + \phi_f \phi(C_f) \cdot \beta\right)} = 1.435 \qquad \text{equals} \qquad \frac{M_{pulpif}}{M_{finesif}} = 1.435$$

Pulp Fines Mass Balance (#3). Criterion: The total mass of pulp must be greater or equa to mass of pulp fines in the flocs

Define the Boolean expression:

$$M_{pulp} \geq M_{finesFlocs} \qquad \text{Eq. [84]}$$

Verify:

$$M_{pulp} \geq M_{finesFlocs} = 1 \qquad \frac{M_{pulp}}{M_{finesFlocs}} = 3.598 \qquad \text{Eq. [85]}$$

Substitute $M_{finesfloc}$ from Eq. [19] into Eq. [84]

$$V_{Total} \cdot \phi_f \phi(C_f) \cdot \rho_{pulp} \cdot X_{FinesFloc} \leq M_{pulp} \qquad \text{Eq. [86]}$$

Substitute M_{pulp} for Eq. [7] into Eq. [86]

$$V_{Total} \cdot \phi_f \phi(C_f) \cdot \rho_{pulp} \cdot X_{FinesFloc} \leq \phi(C) \cdot V_{Total} \cdot \rho_{pulp} \qquad \text{Eq. [87]}$$

Substitute $X_{FinesFloc} = \beta \cdot X_{Fines}$ into Eq. [87]

$$V_{Total} \cdot \phi_f \phi(C_f) \cdot \rho_{pulp} \cdot \beta \cdot X_{Fines} \leq \phi(C) \cdot V_{Total} \cdot \rho_{pulp} \qquad \text{Eq. [88]}$$

Divide both sides of Eq. [88] by $[V_{Total}][\rho_{pulp}]$ and simplify.

$$\frac{V_{Total} \cdot \phi_f \phi(C_f) \cdot \rho_{pulp} \cdot \beta \cdot X_{Fines}}{V_{Total} \cdot \rho_{pulp}} \leq \frac{\phi(C) \cdot V_{Total} \cdot \rho_{pulp}}{V_{Total} \cdot \rho_{pulp}} \qquad \text{Eq. [89]}$$

$$\phi_f \phi(C_f) \cdot \beta \cdot X_{Fines} \leq \phi(C) \qquad \text{Eq. [90]}$$

Define $F_5(C, C_f, \phi_f, \beta) := \phi_f \phi(C_f) \cdot \beta \cdot X_{Fines} \leq \phi(C)$ Eq. [91]

$F_5(C, C_f, \phi_f, \beta) = 1$

Verify the math by comparing ratios of Eqs. [85] and [90]

$$\frac{\phi(C)}{\phi_f \phi(C_f) \cdot \beta \cdot X_{Fines}} = 3.598 \text{ equals } \frac{M_{pulp}}{M_{finesFlocs}} = 3.598$$

The overall pulp fines mass balance can be expressed as a combination of the three functions F_3, F_4 and F_5.

$$F_3(C, C_f, \phi_f, \beta) := \phi(C) - \phi_f \cdot \phi(C_f) \cdot \beta \le \phi(C) \quad \text{Eq. [72]}$$

$$F_4(C, C_f, \phi_f, \beta) := -X_{Fines} \cdot (-\phi(C) + \phi_f \cdot \phi(C_f) \cdot \beta) \le \phi(C) - \phi_f \cdot \phi(C_f) \quad \text{Eq. [83]}$$

$$F_5(C, C_f, \phi_f, \beta) := \phi_f \cdot \phi(C_f) \cdot \beta \cdot X_{Fines} \le \phi(C) \quad \text{Eq. [91]}$$

$$FinesCheck(C, C_f, \phi_f, \beta) := F_3(C, C_f, \phi_f, \beta) \cdot F_4(C, C_f, \phi_f, \beta) \cdot F_5(C, C_f, \phi_f, \beta) \quad \text{Eq. [92]}$$

PART 5. Relating the Floc Volume (ϕ_f) and Floc Consistency to the Experimental Pulp Settling Data

Estimating the Floc Consistency (C_f)

Start off with a general volume balance on the flocculated and non-flocculated region:

$V_{Flocs} + V_{if} = V_{Total}$ Eq. [93] where V_{Floc} is the total volume of the flocs,
V_{if} is the volume of the interfloc region.

To do a volume balance on the pulp, multiply the volumes in Eq. [93] by the respective pu volume fractions:

$$\phi(C_f) \cdot V_{Flocs} + \phi(C_{if}) \cdot V_{if} = \phi(C) \cdot V_{Total} \quad \text{Eq. [94]}$$

Check the math. LS = RS:

$\phi(C_f) \cdot V_{Flocs} + \phi(C_{if}) \cdot V_{if} = 6.689 \cdot mL$

$\phi(C) \cdot V_{Total} = 6.689 \cdot mL$

Substitute $V_{if} = V_{Total} - V_{Flocs}$ into Eq. [94]

$$\phi(C_f) \cdot V_{Flocs} + \phi(C_{if}) \cdot (V_{Total} - V_{Flocs}) = \phi(C) \cdot V_{Total} \quad \text{Eq. [95]}$$

From the definition of floc volume fraction: $\phi_f = \frac{V_{Flocs}}{V_{Total}}$

Rearranging gives: $V_{Flocs} := \phi_f V_{Total}$ Substitute this in Eq. [95].

$$V_{Total} \cdot \phi_f \cdot \phi(C_f) + \phi(C_{if}) \cdot (V_{Total} - V_{Total} \cdot \phi_f) = \phi(C) \cdot V_{Total} \quad \text{Eq. [96]}$$

Divide both sides by V_{Total} and simplify.

$$\frac{\phi(C_f)\cdot V_{Total}\cdot\phi_f+\phi(C_{if})\cdot(V_{Total}-V_{Total}\cdot\phi_f)}{V_{Total}}=\frac{\phi(C)\cdot V_{Total}}{V_{Total}} \qquad \text{Eq. [97]}$$

$$\phi(C_f)\cdot\phi_f+\phi(C_{if})-\phi(C_{if})\cdot\phi_f=\phi(C) \qquad \text{Eq. [98]}$$

(Eq. [98] is a rigorous volume balance on the pulp, with no approximations.)

Solving for $\phi(C_f)$ from Eq. [98] gives:

$$\phi(C_f)=\frac{\phi(C)-\phi(C_{if})+\phi(C_{if})\cdot\phi_f}{\phi_f} \qquad \text{Eq. [99]}$$

Key Assumption #2: Assume a MAXIMUM floc consistency corresponding to the theoretical maximum consistency the flocs can have. This represents the hypothetical case of all the fibres and fines existing only in the flocs, with the interfloc region consisting of only pure water. In this hypothetical case, $C_{if} = 0$ and $\phi(C_{if})= 0$. Using these criteria, Eq. [99] can be rewritten as:

$\phi(C_{fmax}) = \frac{\phi(C)}{\phi_f}$ Eq. [100] where C_{fmax} is the maximum floc consistency.

Next, convert the pulp volume fractions in Eq. [100] into pulp mass fractions.

Recall Eq. [1]:

$$\phi(C) := \frac{C\cdot\rho_w}{(-C\cdot\rho_{pulp}+C\cdot\rho_w+\rho_{pulp})}$$

Rearranging Eq. [1] gives the pulp mass consistency in terms of volume fraction:

$$C_m(\phi) := \frac{-\phi\rho_{pulp}}{(-\phi\rho_{pulp}+\phi\rho_w-\rho_w)} \qquad \text{Eq. [101]}$$

where $\phi(C)$ is the volume pulp volume fraction, and is a function of the consistency (C)

$C_m(\phi)$ is the pulp mass fraction, and is a defined as a function of the volume fraction (ϕ)

By definition, $C_m(\phi(C))\equiv C$

Substitute Eq. [101] on Eq. [100]:

$$C_m(\phi(C_{fmax}))\equiv C_m\left(\frac{\phi(C)}{\phi_f}\right)$$

The LHS simplifies to C_{fmax} since by definition $C_m[\ \phi(C_{fmax})\ ] = C_{fmax}$.

$$C_{fmax} = C_m\left(\frac{\phi(C)}{\phi_f}\right) \qquad \text{Eq. [102]}$$

Key Assumption #3: The floc consistency is given by Eq. [103]

$$C_f = C_{fmin} + (C_{fmax} - C_{fmin})\cdot\phi_f \qquad \text{Eq. [103]}$$

Here, it is assumed that the actual floc consistency lies somewhere between a theoretical minimum and a theoretical maximum value. It is also assumed that the floc consistency is proportional to the floc volume fraction.

By definition, the lowest possible floc consistency (C_{fmin}) equals the overall consistency (C). Substitute this into Eq. [103]

$$C_f = C + \phi_f (C_{fmax} - C) \qquad \text{Eq. [104]}$$

Substitute C_{fmax} from Eq. [102] into Eq. [104], to give the general expression for floc consistency:

$$C_f = C + \phi_f\left(C_m\left(\frac{\phi(C)}{\phi_f}\right) - C\right) \qquad \text{Eq. [105]}$$

where ϕ_f is the yet-to-be determined volume fraction of flocs in the pulp suspension.

5.2 Estimating the Floc Volume Fraction

It is assumed that the floc volume fractions in the flotation experiments are proportional to settled pulp volumes in the experimental pulp settling experiments.

Consider the settling data for the mechanical (TMP-GWD) pulp used in the experiments:

Initial Pulp Consistency	Settled Pulp Consistency	Volume Fraction of Settled Pulp
C_{MECH}	$C_{MECHSet}$	$\phi_{MECHSet}$
0.00097	0.0082	0.135
0.00121	0.00868	0.15
0.00559	0.01154	0.49
0.01562	0.01672	0.94
0.02409	0.02409	1.0

The first column represents the initial consistency of the pulp in the graduated cylinder, prior to settling. The second column represents the consistency of the pulp after settling. The third column represents the volume fraction of the settled pulp, which is defined as $\phi_{MECHSet}$ = (Final volume of pulp-water interface) / (Initial Volume of pulp-water interface)

In this specific case, the experimental settled volumes were correlated by:

$\phi_{Exp}(C) := \left(1 - e^{-138.9636 \cdot C}\right)$ (See Appendix D-6)

Key Assumption #4: We assume that the actual floc volume fraction is related to the experimental settled volume fraction as follows:

$\phi_f(C, C_{crit}, \alpha) := \alpha \cdot \phi_{Exp}(C - C_{crit}) \cdot (C > C_{crit})$ Eq. [106] (where α and C_{crit} are adjustable parameters).

Physical Significance:

The experimental pulp settling curve is shifted to the right by C_{crit}, which represents the critical consistency at which flocs firsts form. For $C < C_{crit}$, no flocs are presents and $\phi_f = 0$. The experimental pulp settling curve gives values of $\phi_{Exp}(C) = 1$, which implies 100% flocculation. In the flotation experiments, it is assumed that there is always some dispersed pulp. Therefore, the pulp settling curve is multiplied by the parameter α, where ($0 < \alpha < 1$), to take into account that 100% flocculation is unlikely to occur in the experiments.

Plot the settling data to see what it looks like: $c := 0, 0.0001 .. 0.025$

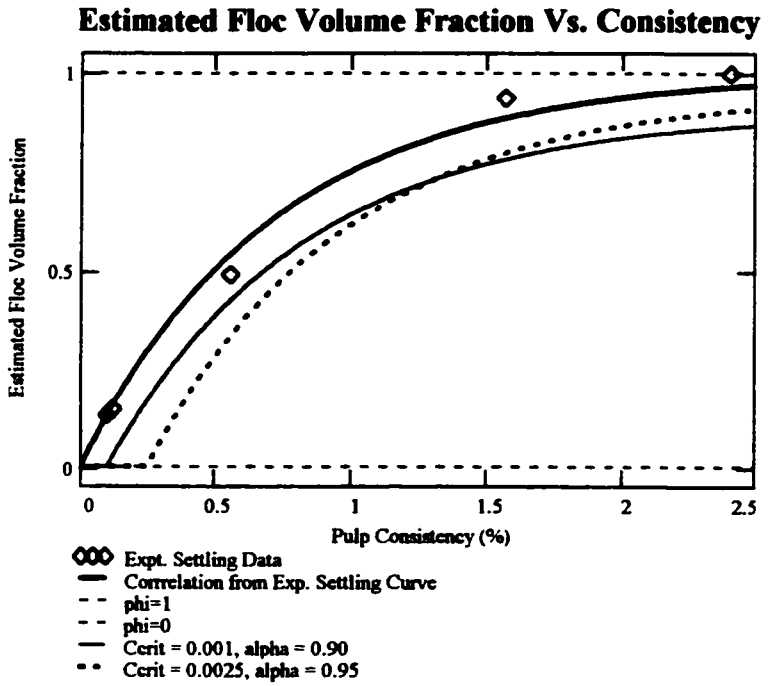

PART 6: Substituting the Estimates ϕ_f and C_f into the Equations for the Interfloc Consistencies and Fines Fractions.

Substitute $\phi_f(C,Ccrit,\alpha)$ from Eq. [106] into Eqs. [104] and [105].

$$C_{fmax}(C,C_{crit},\alpha) := C_m\left(\frac{\phi(C)}{\phi_f(C,C_{crit},\alpha)}\right) \qquad \text{Eq. [107]}$$

$$C_f(C,C_{crit},\alpha) := C + \phi_f(C,C_{crit},\alpha)\cdot\left(C_m\left(\frac{\phi(C)}{\phi_f(C,C_{crit},\alpha)}\right) - C\right) \qquad \text{Eq. [108]}$$

Repeat for C_{if} (Eq.[37]) and X_{if} (Eq. [45]):

$$C_{if}(C,C_{crit},\alpha) := \frac{(\phi(C)\cdot\rho_{pulp} - \phi_f(C,C_{crit},\alpha)\cdot\phi(C_f(C,C_{crit},\alpha))\cdot\rho_{pulp})}{\left[\begin{array}{l}\phi(C)\cdot\rho_{pulp} - \phi_f(C,C_{crit},\alpha)\cdot\phi(C_f(C,C_{crit},\alpha))\cdot\rho_{pulp}\cdots \\ +(1-\phi(C))\cdot\rho_w - \phi_f(C,C_{crit},\alpha)\cdot(1-\phi(C_f(C,C_{crit},\alpha)))\cdot\rho_w\end{array}\right]} \qquad \text{Eq. [109]}$$

$$X_{if}(C,C_{crit},\alpha,\beta) := \frac{(\phi(C) - \phi_f(C,C_{crit},\alpha)\cdot\phi(C_f(C,C_{crit},\alpha))\cdot\beta)}{(\phi(C) - \phi_f(C,C_{crit},\alpha)\cdot\phi(C_f(C,C_{crit},\alpha)))}\cdot X_{Fines} \qquad \text{Eq. [110]}$$

Repeat for the pulp and water mass balance Equations [52] and [61]

$$F_1(C, C_{crit}, \alpha) := \phi_f(C, C_{crit}, \alpha) \cdot \phi(C_f(C, C_{crit}, \alpha)) \leq \phi(C) \quad \text{Eq. [111]}$$

$$F_2(C, C_{crit}, \alpha) := -\phi_f(C, C_{crit}, \alpha) \cdot \left(-1 + \phi(C_f(C, C_{crit}, \alpha))\right) \leq 1 - \phi(C) \quad \text{Eq. [112]}$$

$$PulpCheck(C, C_{crit}, \alpha) := F_1(C, C_{crit}, \alpha) \cdot F_2(C, C_{crit}, \alpha) \quad \text{Eq. [113]}$$

Repeat for the pulp fines mass balance equations [72], [83] and [91].

$$F_3(C, C_{crit}, \alpha, \beta) := \phi(C) - \phi_f(C, C_{crit}, \alpha) \cdot \phi(C_f(C, C_{crit}, \alpha)) \cdot \beta \leq \phi(C) \quad \text{Eq. [114]}$$

$$F_4(C, C_{crit}, \alpha, \beta) := -X_{Fines} \cdot \left(-\phi(C) + \phi_f(C, C_{crit}, \alpha) \cdot \phi(C_f(C, C_{crit}, \alpha)) \cdot \beta\right) \leq \phi(C) - \phi_f(C, C_{crit}, \alpha) \cdot \phi(C_f(C, C_{crit}, \alpha)) \quad \text{Eq. [115]}$$

$$F_5(C, C_{crit}, \alpha, \beta) := \phi_f(C, C_{crit}, \alpha) \cdot \phi(C_f(C, C_{crit}, \alpha)) \cdot \beta \cdot X_{Fines} \leq \phi(C) \quad \text{Eq. [116]}$$

$$FinesCheck(C, C_{crit}, \alpha, \beta) := F_3(C, C_{crit}, \alpha, \beta) \cdot F_4(C, C_{crit}, \alpha, \beta) \cdot F_5(C, C_{crit}, \alpha, \beta) \quad \text{Eq. [117]}$$

LIST OF SYMBOLS

C = Overall consistency, defined as the mass fraction of pulp in the pulp suspension.

C_{crit} = Adjustable parameter, corresponding to the consistency at which pulp flocs first form.

C_f = Floc consistency.

C_{fmax} = Maximum floc consistency. This corresponds to the hypothetical case where all the pulp exists in flocs, and the interfloc region contains only water.

C_{if} = Interfloc consistency.

$C_m(\phi)$ = Consistency, defined as a function of the pulp volume fractioin (ϕ).

M_{fines} = Total mass of pulp fines (g).

$M_{finesFlocs}$ = Mass of pulp fines within the flocs (g).

$M_{finesif}$ = Mass of pulp fines in the interfloc region (g).

M_{pulp} = Total mass of pulp in the pulp suspension (g).

$M_{pulpFlocs}$ = Mass of pulp within the flocs (g).

M_{pulpif} = Mass of pulp in the interfloc region (g).

$M_{pulpEnt}$ = Mass of pulp entrained into the foam (g).

M_{Total} = Total mass (g).

M_w = Total mass of water (g).

M_{wFlocs} = Mass of water within the flocs (g).

M_{wif} = Mass of water in the interfloc region (g).

V_{Flocs} = Volume of the flocs (ml).

V_{Pulp} = Total volume of the pulp in the pulp suspension (ml).

$V_{pulpFlocs}$ = Volume of pulp within the flocs (ml).

V_{Total} = Total volume (ml).

V_w = Total volume of water (ml).

V_{wFlocs} = Volume of water within the flocs (ml).

X_{Fines} = Overall fines fraction of the pulp suspension, which is defined as the mass fraction of fines in the pulp.

$X_{FinesFloc}$ = Fines fraction within the flocs.

X_{if} = Fines fraction in the interfloc region.

Greek Symbols:

α: = Adjustable parameter, relating the floc volume fraction (ϕ_f) to $\phi_{Exp}(C)$.

β: = Adjustable parameter, relating the overall fines fraction to the fines fraction in the flocs (where $X_{FinesFloc} = \beta X_{Fines}$).

$\phi = \phi(C)$ = Volume fraction of pulp in the pulp suspension.

$\phi(C_f)$ = Volume fraction of pulp in the flocs.

$\phi(C_{fmax})$ = Volume fraction of pulp at the maximum floc consistency.

$\phi(C_{if})$ = Volume fraction of pulp in the interfloc region.

$\phi_{Exp}(C)$ = Experimental settled pulp volume fraction, defined as a function of C. $\phi_{Exp}(C)$ is defined as (V_{Set}/V_{Total}).

ϕ_f = Floc volume fraction.

ρ_{pulp} = Density of the cellulosic material (pulp) (= 1.5 g/cm^3).

ρ_w = Density of pure water (= 1 g/cm^3).

APPENDIX E

Correlating the Experimental Data from Chapter 5 to the Flocculation Model Derived in Chapter 6

APPENDIX E-1
Fitting the Model to the TMP-GWD Pulp (Small Bubble) Data

Equations and Parameters:

$\rho_{pulp} \equiv 1.5 \cdot \frac{gm}{cm^3}$ $\rho_w \equiv 1 \cdot \frac{gm}{cm^3}$ — Density of oven-dry pulp fibres and fines, and density of water. (ρ_{pulp} and ρ_w assumed to be constant).

$X_{Fines} = 0.3886$ — Average Fines Fraction of the TMP-GWD Pulp

$$\phi(C) = \frac{C \cdot \rho_w}{(-C \cdot \rho_{pulp} + C \cdot \rho_w + \rho_{pulp})}$$ — Volume consistency of the pulp suspension.

$$C_m(\phi) = \frac{-\phi \cdot \rho_{pulp}}{(-\phi \cdot \rho_{pulp} + \phi \cdot \rho_w - \rho_w)}$$ — Mass consistency of the pulp suspension.

$\phi_{Exp}(C) = (1 - e^{-138.9636 \cdot C})$ — Correlation for Settled Pulp Volume Fraction for TMP-GWD Pulp (From Appendix D-6).

Equations for InterFloc Properties (from Appendix D-7)

$\phi_f(C, C_{crit}, \alpha) = \alpha \cdot \phi_{Exp}(C - C_{crit}) \cdot (C > C_{crit})$ — Floc Volume Fraction

$C_{fmax}(C, C_{crit}, \alpha) = C_m\left(\frac{\phi(C)}{\phi_f(C, C_{crit}, \alpha)}\right)$ — Maximum Floc Consistency

$C_f(C, C_{crit}, \alpha) = C + \phi_f(C, C_{crit}, \alpha) \cdot \left(C_m\left(\frac{\phi(C)}{\phi_f(C, C_{crit}, \alpha)}\right) - C\right)$ — Floc Consistency

$$C_{if}(C, C_{crit}, \alpha) = \frac{\left(\phi(C) \cdot \rho_{pulp} - \phi_f(C, C_{crit}, \alpha) \cdot \phi(C_f(C, C_{crit}, \alpha)) \cdot \rho_{pulp}\right)}{\left[\begin{array}{l}\phi(C) \cdot \rho_{pulp} - \phi_f(C, C_{crit}, \alpha) \cdot \phi(C_f(C, C_{crit}, \alpha)) \cdot \rho_{pulp} \cdots \\ +(1 - \phi(C)) \cdot \rho_w - \phi_f(C, C_{crit}, \alpha) \cdot (1 - \phi(C_f(C, C_{crit}, \alpha))) \cdot \rho_w\end{array}\right]}$$ — Interfloc Consistency

$$X_{if}(C, C_{crit}, \alpha, \beta) = \frac{\left(\phi(C) - \phi_f(C, C_{crit}, \alpha) \cdot \phi(C_f(C, C_{crit}, \alpha)) \cdot \beta\right)}{\left(\phi(C) - \phi_f(C, C_{crit}, \alpha) \cdot \phi(C_f(C, C_{crit}, \alpha))\right)} \cdot X_{Fines}$$ — Interfloc Fines Fraction

The following data are taken from Appendix C:

C_{MSFeed} Feed consistency from the flotation experiments.

C_{MSFoam} Foam consistency from the flotation experiments.

C_{DDJMS} Feed consistency from DDJ foam fractionation experiments.

X_{MSFoam} Fines fraction of foam from the DDJ foam fractionation experiments.

$C_{MechInit}$ Consistency from the pulp settling experiments.

$C_{MechSet}$ Settled consistency from the pulp settling experiments.

$\phi_{MechSet}$ Settled volume fraction from the pulp settling experiments.

Number of Data for TMP-GWD (Small Bubbles) $i := \text{length}(C_{MSFeed})$ $i = 44$ $i = 0..43$

To find α and C_{crit}, define the sum squared of errors as:

$$SSE(\alpha, C_{crit}) := \sum_{i=0}^{43} \left(C_{MSFoam_i} - C_{if}(C_{MSFeed_i}, C_{crit}, \alpha)\right)^2$$

where the function "C_{if}" is defined in Appendix D-7.

Use MathCad's "minerr" solver function to find the minimum of the sum squared of errors.

Guess: $\alpha := .95$ $C_{crit} := 0.001$ $TOL = 1 \cdot 10^{-5}$

Given

$SSE(\alpha, C_{crit}) = 0$

$1 = 1$

$ANS := \text{minerr}(\alpha, C_{crit})$

$$ANS = \begin{pmatrix} 0.863 \\ 2.0753 \cdot 10^{-4} \end{pmatrix}$$

$\alpha := ANS_0$

$C_{crit} := ANS_1$

The resulting values of α and C_{crit} are as follows:

$\alpha = 0.863$ $C_{crit} = 2.0753 \cdot 10^{-4}$

Plot the results:

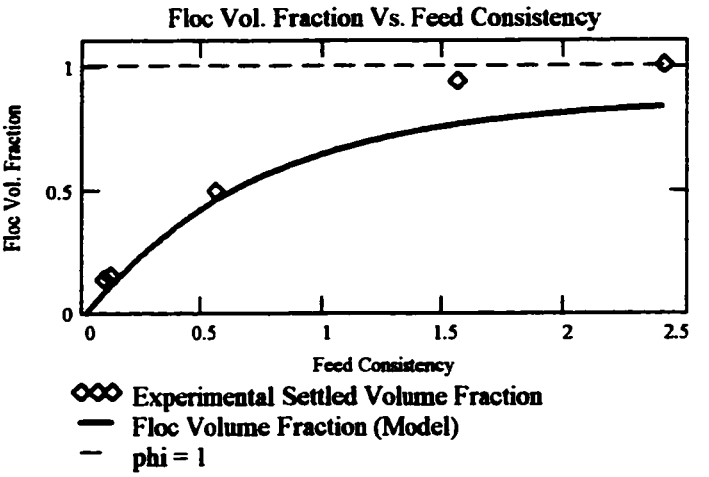

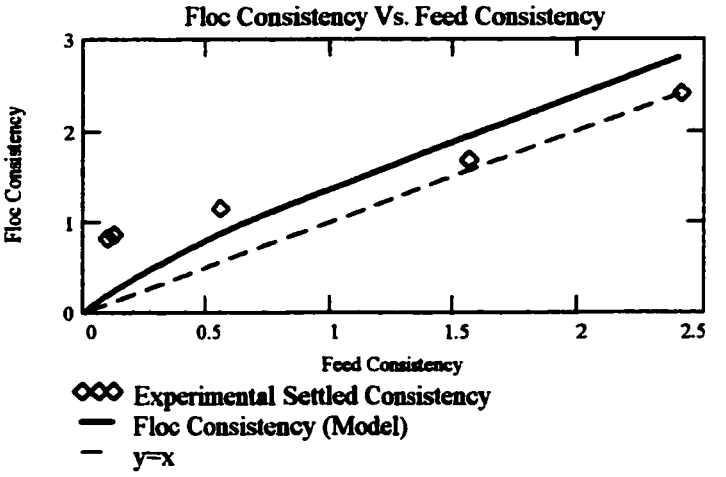

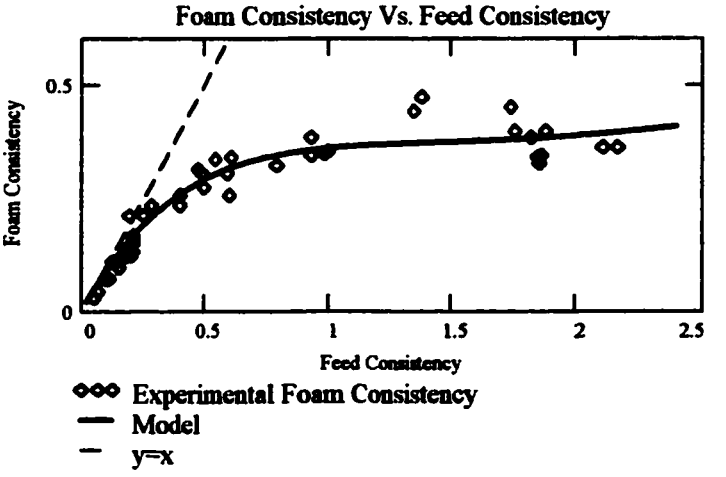

Next, use the values of α and C_{crit}, to solve for β for the InterFloc Fines Fraction.

$j := \text{length}(C_{DDJMS})$ $\quad j = 5$ $\quad j := 0..4$

Define the sum squared of errors as:

$$SSE(\beta) := \sum_{j=0}^{4} \left(X_{MSFoam_j} - X_{if}\left(C_{DDJMS_j}, C_{crit}, \alpha, \beta\right)\right)^2$$

where the function "X_{if}" is defined in Appendix D-7.

Use MathCad's "minerr" solver function to find the minimum of SSE(β).

Guess: $\beta := .95$

Given

$SSE(\beta) \equiv 0$

$1 \equiv 1$

$\beta := \text{minerr}(\beta)$

$\beta = 0.957$

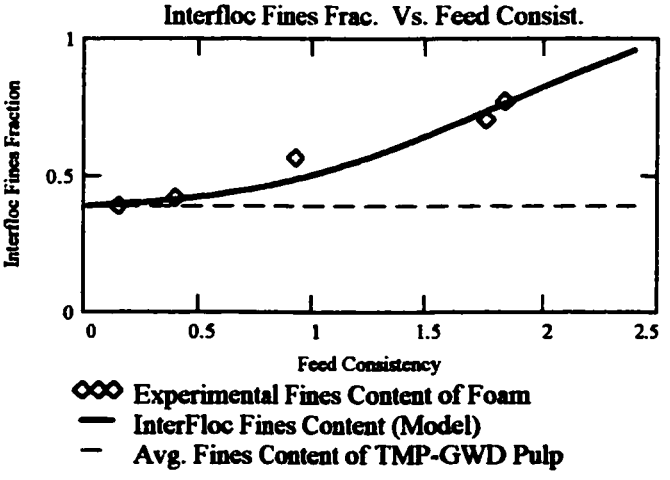

Plot the mass balance functions "PulpCheck" and "FinesCheck" from Appendix D-7 to verify the validity of the estimates of α, β and C_{crit} for the consistency range of the data.

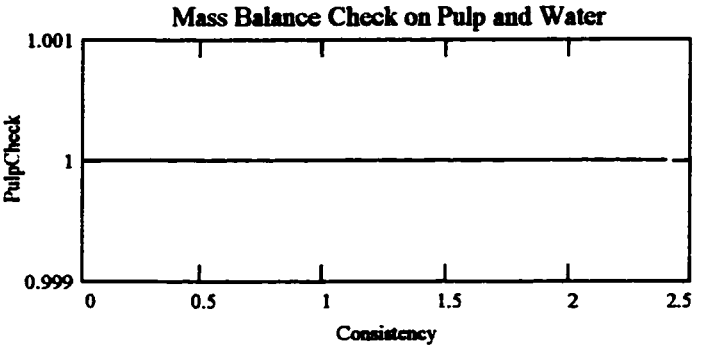

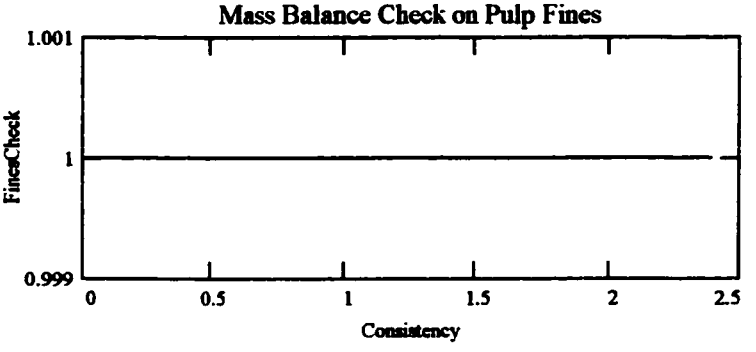

Since "PulpCheck" and "FinesCheck" = 1, the mass balances are valid.

APPENDIX E-2
Fitting the Model to the BKP (Small Bubble) Data

Equations and Parameters:

$\rho_{pulp} \equiv 1.5 \cdot \frac{gm}{cm^3}$ $\rho_w \equiv 1 \cdot \frac{gm}{cm^3}$ — Density of oven-dry pulp fibres and fines, and density of water. (ρ_{pulp} and ρ_w assumed to be constant).

$X_{Fines} = 0.1069$ — Average Fines Fraction of the BKP

$$\phi(C) = \frac{C \cdot \rho_w}{\left(-C \cdot \rho_{pulp} + C \cdot \rho_w + \rho_{pulp}\right)}$$ — Volume consistency of the pulp suspension.

$$C_m(\phi) = \frac{-\phi \cdot \rho_{pulp}}{\left(-\phi \cdot \rho_{pulp} + \phi \cdot \rho_w - \rho_w\right)}$$ — Mass consistency of the pulp suspension.

$\phi_{Exp}(C) = \left(1 - e^{-486.4652 \cdot C}\right)$ — Correlation for Settled Pulp Volume Fraction for BKP (Appendix D-6).

Equations for InterFloc Properties (from Appendix D-7)

$$\phi_f(C, C_{crit}, \alpha) = \alpha \cdot \phi_{Exp}(C - C_{crit}) \cdot (C > C_{crit})$$ — Floc Volume Fraction

$$C_{fmax}(C, C_{crit}, \alpha) = C_m\left(\frac{\phi(C)}{\phi_f(C, C_{crit}, \alpha)}\right)$$ — Maximum Floc Consistency

$$C_f(C, C_{crit}, \alpha) = C + \phi_f(C, C_{crit}, \alpha) \cdot \left(C_m\left(\frac{\phi(C)}{\phi_f(C, C_{crit}, \alpha)}\right) - C\right)$$ — Floc Consistency

$$C_{if}(C, C_{crit}, \alpha) = \frac{\left(\phi(C) \cdot \rho_{pulp} - \phi_f(C, C_{crit}, \alpha) \cdot \phi\left(C_f(C, C_{crit}, \alpha)\right) \cdot \rho_{pulp}\right)}{\left[\begin{array}{l}\phi(C) \cdot \rho_{pulp} - \phi_f(C, C_{crit}, \alpha) \cdot \phi\left(C_f(C, C_{crit}, \alpha)\right) \cdot \rho_{pulp} \cdots \\ +(1 - \phi(C)) \cdot \rho_w - \phi_f(C, C_{crit}, \alpha) \cdot \left(1 - \phi\left(C_f(C, C_{crit}, \alpha)\right)\right) \cdot \rho_w\end{array}\right]}$$ — Interfloc Consistency

$$X_{if}(C, C_{crit}, \alpha, \beta) = \frac{\left(\phi(C) - \phi_f(C, C_{crit}, \alpha) \cdot \phi\left(C_f(C, C_{crit}, \alpha)\right) \cdot \beta\right)}{\left(\phi(C) - \phi_f(C, C_{crit}, \alpha) \cdot \phi\left(C_f(C, C_{crit}, \alpha)\right)\right)} \cdot X_{Fines}$$ — Interfloc Fines Fraction

The following data are taken from Appendix C:

C_{BSFeed} Feed consistency from the flotation experiments.

C_{BSFoam} Foam consistency from the flotation experiments.

C_{DDJBS} Feed consistency from DDJ foam fractionation experiments.

X_{BSFoam} Fines fraction of foam from DDJ foam fractionation.

$C_{BKPInit}$ Consistency from pulp settling experiments.

C_{BKPSet} Settled consistency from pulp settling experiments.

ϕ_{BKPSet} Settled volume fraction from pulp settling experiments.

Number of Data for BKP (Small Bubbles): $i := \text{length}(C_{BSFeed})$ $i = 37$ $i = 0..36$

To find α and C_{crit}, define the sum squared of errors as:

$$SSE(\alpha, C_{crit}) := \sum_{i=0}^{36} \left(C_{BSFoam_i} - C_{if}(C_{BSFeed_i}, C_{crit}, \alpha)\right)^2$$

where the function "Cif" is defined in Appendix D-7.

Use MathCad's "minerr" solver function to find the minimum of the sum squared of errors.

Guess: $\alpha := .95$ $C_{crit} := 0.001$ $TOL := 1 \cdot 10^{-5}$

Given

$SSE(\alpha, C_{crit}) = 0$

$1 = 1$

$ANS := \text{minerr}(\alpha, C_{crit})$

$$ANS = \begin{pmatrix} 0.9695 \\ 0.0015 \end{pmatrix}$$

$\alpha := ANS_0$

$C_{crit} := ANS_1$

The resulting values of α and C_{crit} are as follows:

$\alpha = 0.9695$ $C_{crit} = 0.00155$

Plot the results:

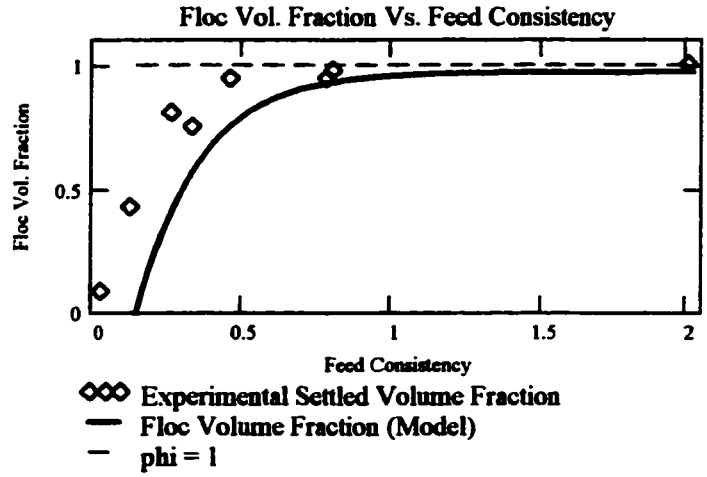

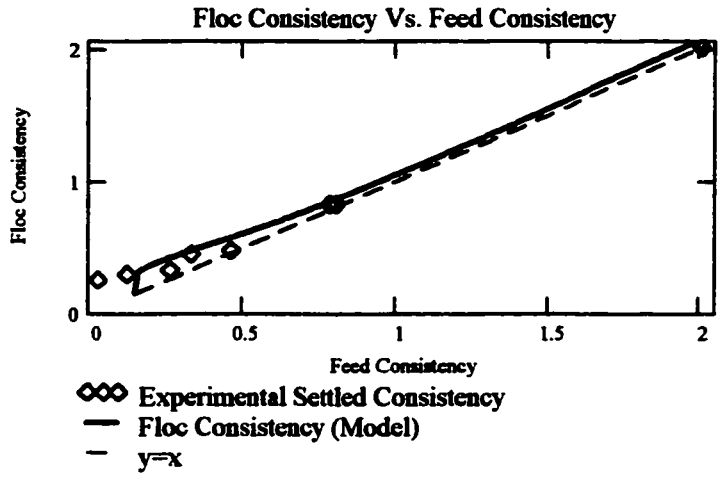

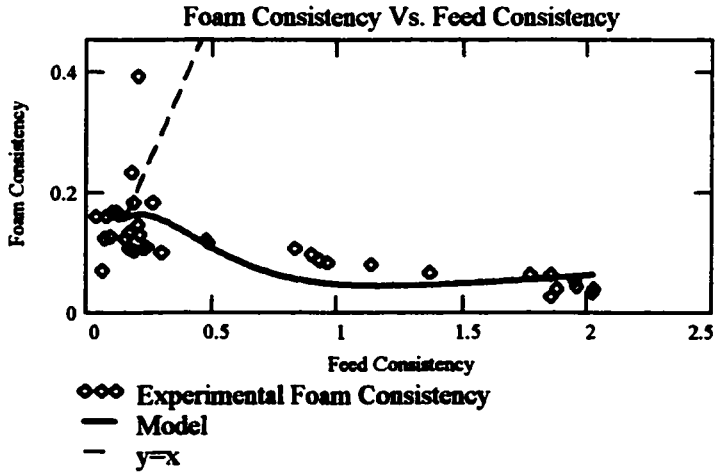

Next, use the values of α and C_{crit}, to solve for β for the InterFloc Fines Fraction.

$j := \text{length}(C_{DDJBS})$ $\quad j = 4$ $\quad j := 0..3$

Define the sum squared of errors as:

$$SSE(\beta) := \sum_{j=0}^{3} \left(X_{BSFoam_j} - X_{if}\left(C_{DDJBS_j}, C_{crit}, \alpha, \beta\right)\right)^2$$

where the function "X_{if}" is defined in Appendix D-7.

Use MathCad's "minerr" solver function to find the minimum of SSE(β).

Guess: $\beta := .95$ $\quad TOL := 1 \cdot 10^{-5}$

Given

$SSE(\beta) \equiv 0$

$1 \equiv 1$

$\beta := \text{minerr}(\beta)$

$\beta = 0.9974$

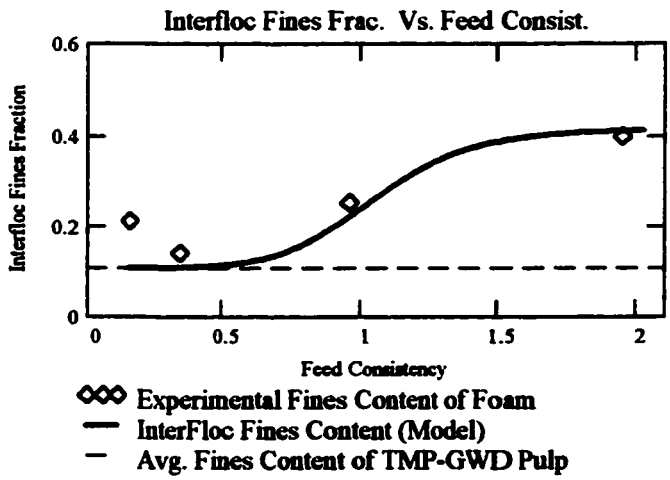

Plot the mass balance functions "PulpCheck" and "FinesCheck" from Appendix D-7 to verify the validity of the estimates of α, β and C_{crit} for the consistency range of the data.

$c = 1.001 \cdot C_{crit}, C_{crit} + 0.0001 .. 0.02025$

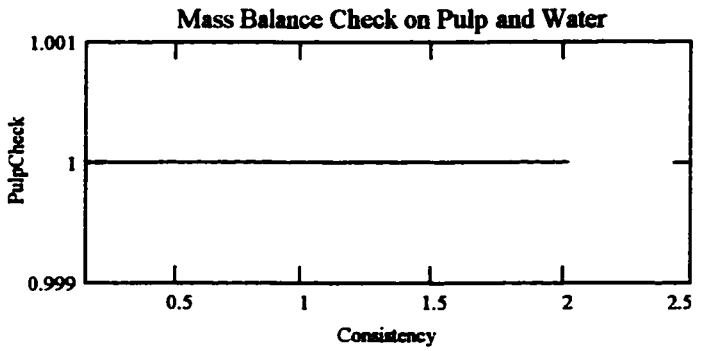

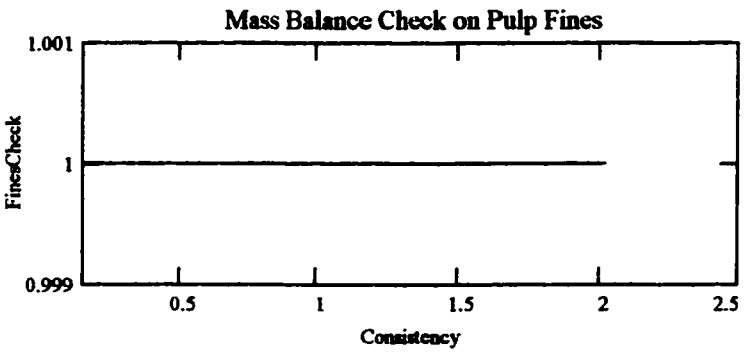

Since "PulpCheck" and "FinesCheck" = 1, the mass balances are valid.

APPENDIX E-3
Fitting the Model to the TMP-GWD Pulp (Large Bubble) Data

Equations and Parameters:

$\rho_{pulp} \equiv 1.5 \cdot \frac{gm}{cm^3}$ $\rho_w \equiv 1 \cdot \frac{gm}{cm^3}$ — Density of oven-dry pulp fibres and fines, and density of water. (ρ_{pulp} and ρ_w assumed to be constant)

$X_{Fines} = 0.3886$ — Average Fines Fraction of the TMP-GWD Pulp

$$\phi(C) = \frac{C \cdot \rho_w}{(-C \cdot \rho_{pulp} + C \cdot \rho_w + \rho_{pulp})}$$ — Volume consistency of the pulp suspension.

$$C_m(\phi) = \frac{-\phi \cdot \rho_{pulp}}{(-\phi \cdot \rho_{pulp} + \phi \cdot \rho_w - \rho_w)}$$ — Mass consistency of the pulp suspension.

$$\phi_{Exp}(C) = \left(1 - e^{-138.9636 \cdot C}\right)$$ — Correlation for Settled Pulp Volume Fraction for TMP-GWD Pulp (Appendix D-6).

Equations for InterFloc Properties (from Appendix D-7)

$$\phi_f(C, C_{crit}, \alpha) = \alpha \cdot \phi_{Exp}(C - C_{crit}) \cdot (C > C_{crit})$$ — Floc Volume Fraction

$$C_{fmax}(C, C_{crit}, \alpha) := C_m\left(\frac{\phi(C)}{\phi_f(C, C_{crit}, \alpha)}\right)$$ — Maximum Floc Consistency

$$C_f(C, C_{crit}, \alpha) := C + \phi_f(C, C_{crit}, \alpha) \cdot \left(C_m\left(\frac{\phi(C)}{\phi_f(C, C_{crit}, \alpha)}\right) - C\right)$$ — Floc Consistency

$$C_{if}(C, C_{crit}, \alpha) := \frac{\left(\phi(C) \cdot \rho_{pulp} - \phi_f(C, C_{crit}, \alpha) \cdot \phi(C_f(C, C_{crit}, \alpha)) \cdot \rho_{pulp}\right)}{\left[\begin{array}{l}\phi(C) \cdot \rho_{pulp} - \phi_f(C, C_{crit}, \alpha) \cdot \phi(C_f(C, C_{crit}, \alpha)) \cdot \rho_{pulp} \ldots \\ +(1 - \phi(C)) \cdot \rho_w - \phi_f(C, C_{crit}, \alpha) \cdot (1 - \phi(C_f(C, C_{crit}, \alpha))) \cdot \rho_w\end{array}\right]}$$ — Interfloc Consistency

$$X_{if}(C, C_{crit}, \alpha, \beta) := \frac{\left(\phi(C) - \phi_f(C, C_{crit}, \alpha) \cdot \phi(C_f(C, C_{crit}, \alpha)) \cdot \beta\right)}{\left(\phi(C) - \phi_f(C, C_{crit}, \alpha) \cdot \phi(C_f(C, C_{crit}, \alpha))\right)} \cdot X_{Fines}$$ — Interfloc Fines Fraction

The following data were taken from Appendix C:

C_{MLFeed} Feed consistency from the flotation experiments.

C_{MLFoam} Foam consistency from the flotation experiments.

C_{DDJML} Feed consistency from the DDJ foam fractionation experiments.

X_{MLFoam} Fines fraction of foam from the DDJ foam fractionation experiments.

$C_{MechInit}$ Consistency from pulp settling experiments.

$C_{MechSet}$ Settled consistency from the pulp settling experiments.

$\phi_{MechSet}$ Settled volume fraction from the pulp settling experiments.

Number of Data for TMP-GWD (Large Bubbles): $i := \text{length}(C_{MLFeed})$ $i = 21$ $i = 0..20$

To find α and C_{crit}, define the sum squared of errors as:

$$SSE(\alpha, C_{crit}) := \sum_{i=0}^{20} \left(C_{MLFoam_i} - C_{if}\left(C_{MLFeed_i}, C_{crit}, \alpha\right)\right)^2$$

$\max(C_{MLFeed}) = 0.01887$

where the function "C_{if}" is defined in Appendix D-7.

Use MathCad's "minerr" solver function to find the minimum of the sum squared of errors

Guess: $\alpha := .95$ $C_{crit} := 0.001$ $TOL := 1 \cdot 10^{-5}$

Given

$SSE(\alpha, C_{crit}) = 0$

$1 = 1$

$ANS := \text{minerr}(\alpha, C_{crit})$

$$ANS = \begin{pmatrix} 0.892 \\ 0.012 \end{pmatrix}$$

$\alpha := ANS_0$

$C_{crit} := ANS_1$

The resulting values of α and C_{crit} are as follows:

$\alpha = 0.8921$ $C_{crit} = 0.01157$

Plot the results:

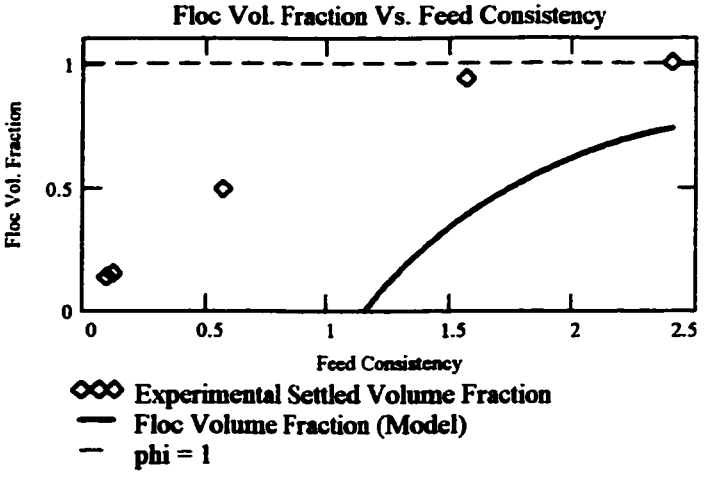

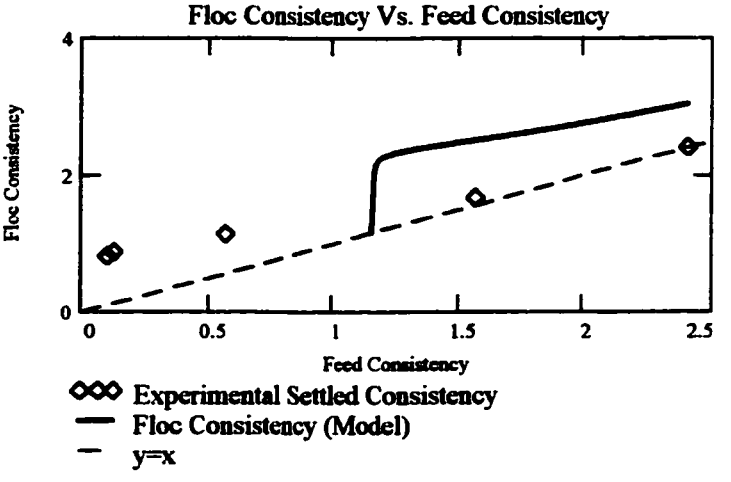

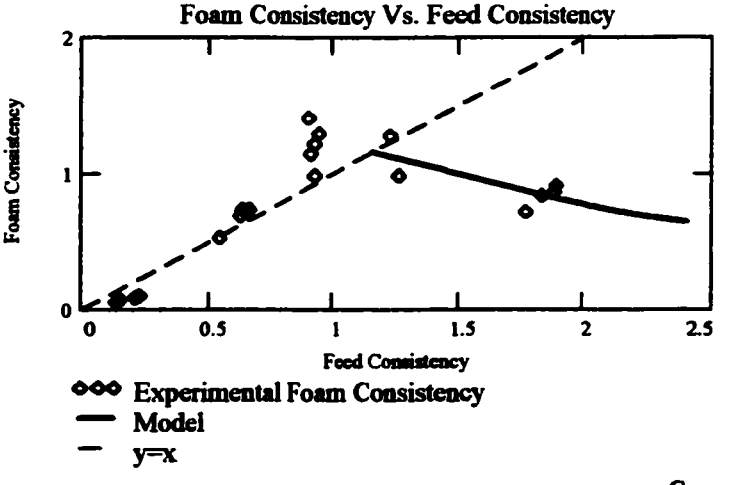

$C_{crit} = 0.012$

Next, use the values of α and C_{crit}, to solve for β for the InterFloc Fines Fraction.

$j := \text{length}(C_{DDJML})$ $\quad j = 5$ $\quad j := 0..4$

Define the sum squared of errors as:

$$SSE(\beta) := \sum_{j=3}^{4} \left(X_{MLFoam_j} - X_{if}\left(C_{DDJML_j}, C_{crit}, \alpha, \beta\right)\right)^2$$

where the function "X_{if}" is defined in Appendix D-7. Use only consistencies greater than C

Use MathCad's "minerr" solver function to find the minimum of SSE(α,Ccrit).

Guess: $\beta := .95$ $\quad TOL := 1 \cdot 10^{-5}$

Given

$SSE(\beta) \equiv 0$

$l \equiv 1$

$\beta := \text{minerr}(\beta)$

$\beta = 0.9129$

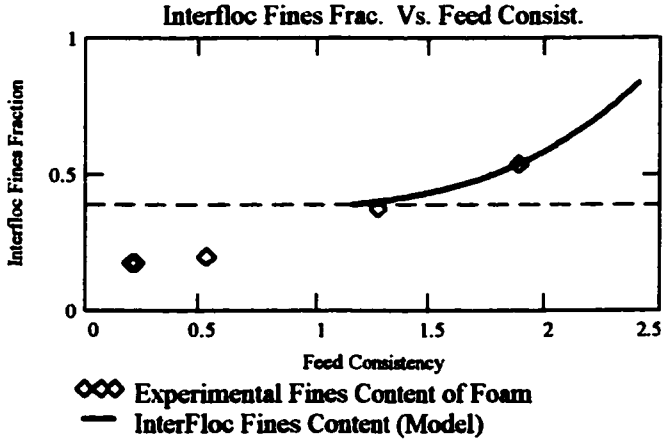

Plot the mass balance functions "PulpCheck" and "FinesCheck" from Appendix D-7 to verify the validity of the estimates of α, β and C_{crit} for the consistency range of the data.

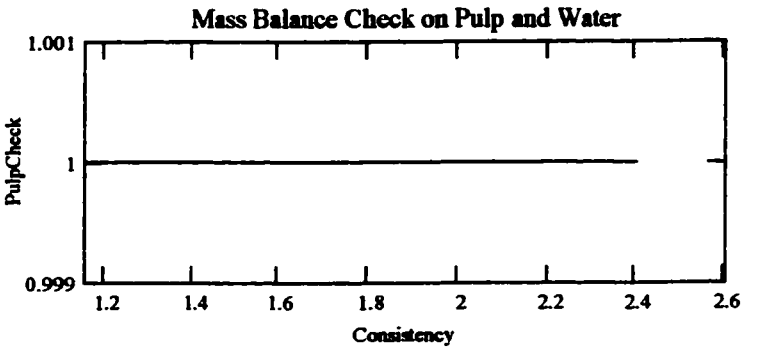

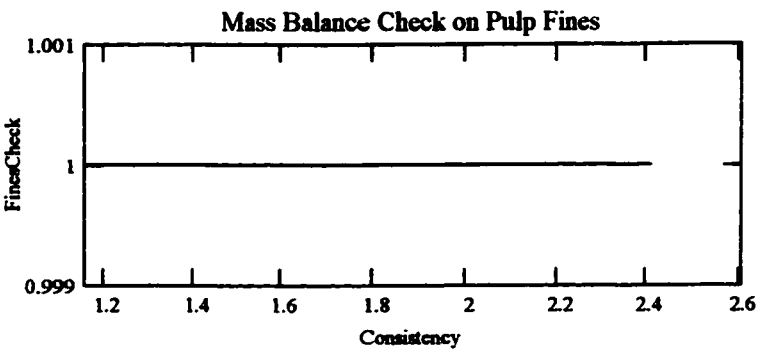

Since "PulpCheck" and "FinesCheck" = 1, the mass balances are valid.

APPENDIX E-4
Fitting the Model to the BKP (Large Bubble) Data

Equations and Parameters:

$\rho_{pulp} \equiv 1.5 \cdot \frac{gm}{cm^3}$ $\rho_w \equiv 1 \cdot \frac{gm}{cm^3}$ — Density of oven-dry pulp fibres and fines, and density of water. (ρ_{pulp} and ρ_w assumed to be constant)

$X_{Fines} := 0.1069$ — Average Fines Fraction of the BKP

$$\phi(C) := \frac{C \cdot \rho_w}{(-C \cdot \rho_{pulp} + C \cdot \rho_w + \rho_{pulp})}$$ — Volume consistency of the pulp suspension.

$$C_m(\phi) := \frac{-\phi \cdot \rho_{pulp}}{(-\phi \cdot \rho_{pulp} + \phi \cdot \rho_w - \rho_w)}$$ — Mass consistency of the pulp suspension.

$$\phi_{Exp}(C) := \left(1 - e^{-486.4652 \cdot C}\right)$$ — Correlation for Settled Pulp Volume Fraction for TMP-GWD Pulp (Appendix D-6).

Equations for InterFloc Properties (from Appendix D-7)

$$\phi_f(C, C_{crit}, \alpha) := \alpha \cdot \phi_{Exp}(C - C_{crit}) \cdot (C > C_{crit})$$ — Floc Volume Fraction

$$C_{fmax}(C, C_{crit}, \alpha) := C_m\left(\frac{\phi(C)}{\phi_f(C, C_{crit}, \alpha)}\right)$$ — Maximum Floc Consistency

$$C_f(C, C_{crit}, \alpha) := C + \phi_f(C, C_{crit}, \alpha) \cdot \left(C_m\left(\frac{\phi(C)}{\phi_f(C, C_{crit}, \alpha)}\right) - C\right)$$ — Floc Consistency

$$C_{if}(C, C_{crit}, \alpha) := \frac{(\phi(C) \cdot \rho_{pulp} - \phi_f(C, C_{crit}, \alpha) \cdot \phi(C_f(C, C_{crit}, \alpha)) \cdot \rho_{pulp})}{\left[\begin{array}{l}\phi(C) \cdot \rho_{pulp} - \phi_f(C, C_{crit}, \alpha) \cdot \phi(C_f(C, C_{crit}, \alpha)) \cdot \rho_{pulp} \cdots \\ + (1 - \phi(C)) \cdot \rho_w - \phi_f(C, C_{crit}, \alpha) \cdot (1 - \phi(C_f(C, C_{crit}, \alpha))) \cdot \rho_w\end{array}\right]}$$ — Interfloc Consistency

$$X_{if}(C, C_{crit}, \alpha, \beta) := \frac{(\phi(C) - \phi_f(C, C_{crit}, \alpha) \cdot \phi(C_f(C, C_{crit}, \alpha)) \cdot \beta)}{(\phi(C) - \phi_f(C, C_{crit}, \alpha) \cdot \phi(C_f(C, C_{crit}, \alpha)))} \cdot X_{Fines}$$ — Interfloc Fines Fraction

The following data were taken from Appendix C:

C_{BLFeed} Feed consistency from the flotation experiments.

C_{BLFoam} Foam consistency from the flotation experiments.

C_{DDJBL} Feed consistency from DDJ foam fractionation experiments.

X_{BLFoam} Fines fraction of the foam from DDJ foam fractionation experiments.

$C_{BKPInit}$ Consistency from the pulp settling experiments.

C_{BKPSet} Settled consistency from the pulp settling experiments.

ϕ_{BKPSet} Settled volume fraction from pulp settling experiments.

Number of Data for the BKP (Large Bubbles): $i := \text{length}(C_{BLFeed})$ $i = 14$ $i := 0..13$

To find α and C_{crit}, define the sum squared of errors as:

$$SSE(\alpha, C_{crit}) := \sum_{i=0}^{13} \left(C_{BLFoam_i} - C_{if}(C_{BLFeed_i}, C_{crit}, \alpha)\right)^2$$

where the function "Cif" is defined in Appendix D-7.

Use MathCad's "minerr" solver function to find the minimum of the sum squared of errors.

Guess: $\alpha := .95$ $C_{crit} := 0.001$ $TOL := 1 \cdot 10^{-5}$

Given

$SSE(\alpha, C_{crit}) \equiv 0$

$1 \equiv 1$

$ANS := \text{minerr}(\alpha, C_{crit})$

$$ANS = \begin{pmatrix} 0.888 \\ 0.01 \end{pmatrix}$$

$\alpha := ANS_0$

$C_{crit} := ANS_1$

The resulting values of α and C_{crit} are as follows:

$\alpha = 0.888$ $C_{crit} = 0.01024$

Plot the results:

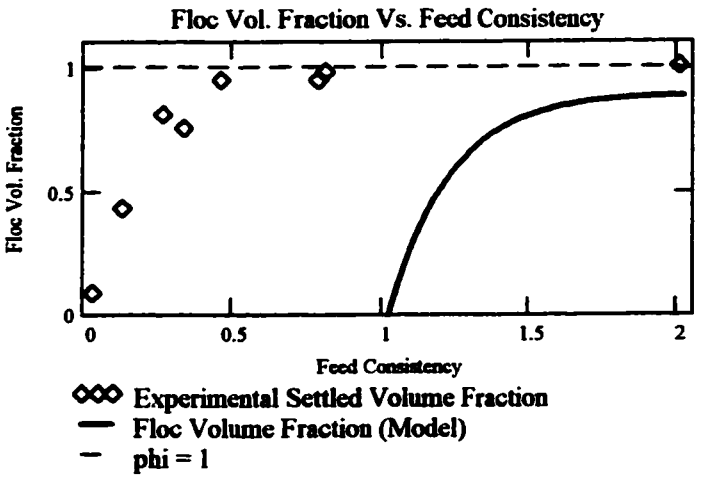

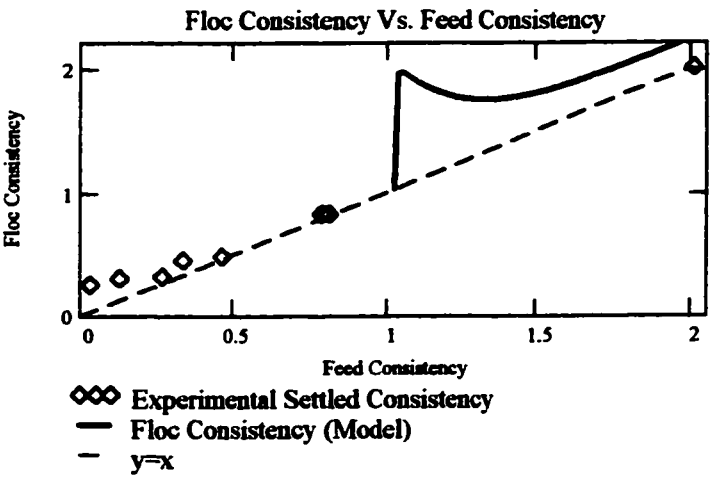

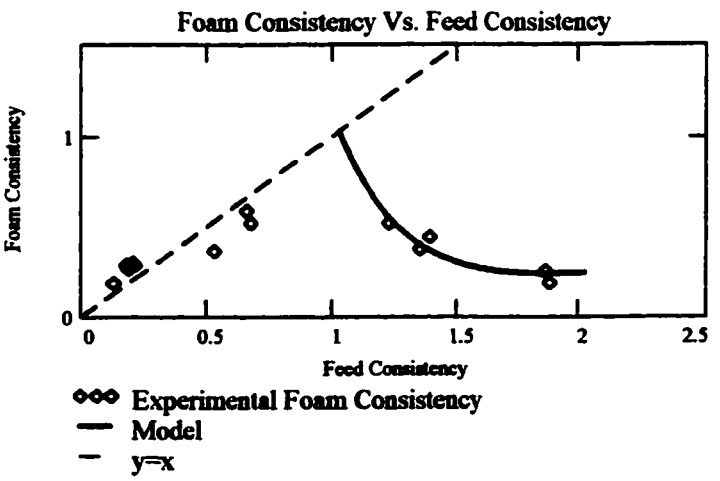

Next, use the values of α and C_{crit}, to solve for β for the InterFloc Fines Fraction.

$j := \text{length}(C_{DDJBL})$ $\quad j = 4$ $\quad j := 0..3$

Define the sum squared of errors as:

$$SSE(\beta) := \sum_{j=2}^{3} \left(X_{BLFoam_j} - X_{if}\left(C_{DDJBL_j}, C_{crit}, \alpha, \beta\right)\right)^2$$

where the function "X_{if}" is defined in Appendix D-3.

Use MathCad's "minerr" solver function to find the minimum of SSE(α,Ccrit).

Guess: $\beta := .95$ $\quad TOL = 1 \cdot 10^{-5}$

Given

$SSE(\beta) = 0$

$1 = 1$

$\beta := \text{minerr}(\beta)$

$\beta = 0.9891$

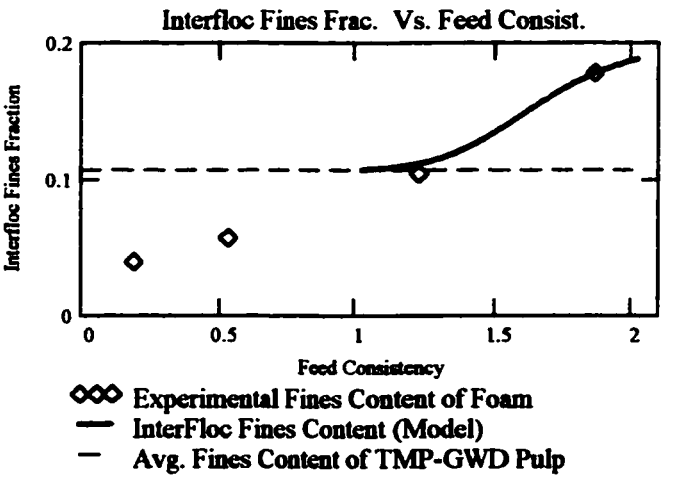

Plot the mass balance functions "PulpCheck" and "FinesCheck" from Appendix D-7 to verify the validity of the estimates of α, β and C_{crit} for the consistency range of the data.

$c = 1.001 \cdot C_{crit}, C_{crit} + 0.0001 .. 0.02025$

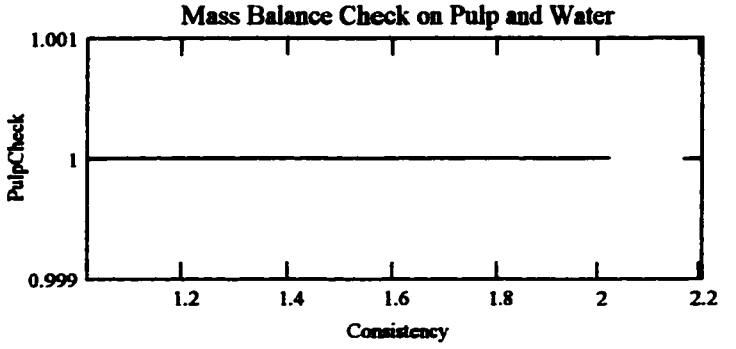

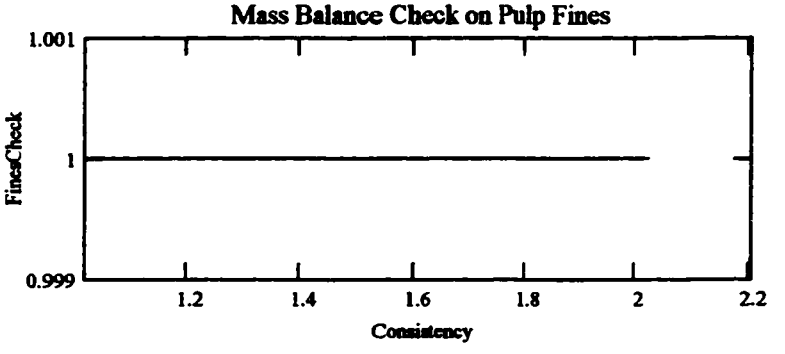

Since "PulpCheck" and "FinesCheck" = 1, the mass balances are valid.

APPENDIX E-5
Fitting the Model to the TMP-GWD Pulp (Small Bubble) Data
(Assuming a pulp density of 1.2 g/cm^3)

Equations and Parameters:

$\rho_{pulp} \equiv 1.2 \cdot \frac{gm}{cm^3}$ $\quad \rho_w \equiv 1 \cdot \frac{gm}{cm^3}$ — Density of oven-dry pulp fibres and fines, and density of water. (ρ_{pulp} and ρ_w assumed to be constant)

$X_{Fines} := 0.3886$ — Average Fines Fraction of the TMP-GWD Pulp

$$\phi(C) := \frac{C \cdot \rho_w}{(-C \cdot \rho_{pulp} + C \cdot \rho_w + \rho_{pulp})}$$ — Volume consistency of the pulp suspension.

$$C_m(\phi) := \frac{-\phi \cdot \rho_{pulp}}{(-\phi \cdot \rho_{pulp} + \phi \cdot \rho_w - \rho_w)}$$ — Mass consistency of the pulp suspension.

$$\phi_{Exp}(C) := \left(1 - e^{-138.9636 \cdot C}\right)$$ — Correlation for Settled Pulp Volume Fraction for TMP-GWD Pulp (From Appendix D-6).

Equations for InterFloc Properties (from Appendix D-7)

$$\phi_f(C, C_{crit}, \alpha) := \alpha \cdot \phi_{Exp}(C - C_{crit}) \cdot (C > C_{crit})$$ — Floc Volume Fraction

$$C_{fmax}(C, C_{crit}, \alpha) := C_m\left(\frac{\phi(C)}{\phi_f(C, C_{crit}, \alpha)}\right)$$ — Maximum Floc Consistency

$$C_f(C, C_{crit}, \alpha) := C + \phi_f(C, C_{crit}, \alpha) \cdot \left(C_m\left(\frac{\phi(C)}{\phi_f(C, C_{crit}, \alpha)}\right) - C\right)$$ — Floc Consistency

$$C_{if}(C, C_{crit}, \alpha) := \frac{\left(\phi(C) \cdot \rho_{pulp} - \phi_f(C, C_{crit}, \alpha) \cdot \phi(C_f(C, C_{crit}, \alpha)) \cdot \rho_{pulp}\right)}{\left[\begin{array}{l}\phi(C) \cdot \rho_{pulp} - \phi_f(C, C_{crit}, \alpha) \cdot \phi(C_f(C, C_{crit}, \alpha)) \cdot \rho_{pulp} \ldots \\ +(1 - \phi(C)) \cdot \rho_w - \phi_f(C, C_{crit}, \alpha) \cdot (1 - \phi(C_f(C, C_{crit}, \alpha))) \cdot \rho_w\end{array}\right]}$$ — Interfloc Consistency

$$X_{if}(C, C_{crit}, \alpha, \beta) := \frac{\left(\phi(C) - \phi_f(C, C_{crit}, \alpha) \cdot \phi(C_f(C, C_{crit}, \alpha)) \cdot \beta\right)}{\left(\phi(C) - \phi_f(C, C_{crit}, \alpha) \cdot \phi(C_f(C, C_{crit}, \alpha))\right)} \cdot X_{Fines}$$ — Interfloc Fines Fraction

The following data are taken from Appendix C:

C_{MSFeed} Feed consistency from the flotation experiments.

C_{MSFoam} Foam consistency from the flotation experiments.

C_{DDJMS} Feed consistency from DDJ foam fractionation experiments.

X_{MSFoam} Fines fraction of foam from the DDJ foam fractionation experiments.

$C_{MechInit}$ Consistency from the pulp settling experiments.

$C_{MechSet}$ Settled consistency from the pulp settling experiments.

$\phi_{MechSet}$ Settled volume fraction from the pulp settling experiments.

Number of Data for TMP-GWD (Small Bubbles) $i := \text{length}(C_{MSFeed})$ $i = 44$ $i = 0..43$

To find α and C_{crit}, define the sum squared of errors as:

$$SSE(\alpha, C_{crit}) := \sum_{i=0}^{43} \left(C_{MSFoam_i} - C_{if}(C_{MSFeed_i}, C_{crit}, \alpha)\right)^2$$

where the function "C_{if}" is defined in Appendix D-7.

Use MathCad's "minerr" solver function to find the minimum of the sum squared of errors.

Guess: $\alpha := .95$ $C_{crit} := 0.001$ $TOL = 1 \cdot 10^{-5}$

Given

$SSE(\alpha, C_{crit}) = 0$

$1 = 1$

$ANS := \text{minerr}(\alpha, C_{crit})$

$$ANS = \begin{pmatrix} 0.8623 \\ 2.0935 \cdot 10^{-4} \end{pmatrix}$$

$\alpha := ANS_0$

$C_{crit} := ANS_1$

The resulting values of α and C_{crit} are as follows:

$\alpha = 0.8623$ $C_{crit} = 2.0935 \cdot 10^{-4}$

Next, use the values of α and C_{crit}, to solve for β for the InterFloc Fines Fraction.

$j := \text{length}(C_{DDJMS})$ $\quad j = 5$ $\quad j := 0..4$

Define the sum squared of errors as:

$$SSE(\beta) := \sum_{j=0}^{4} \left(X_{MSFoam_j} - X_{if}\left(C_{DDJMS_j}, C_{crit}, \alpha, \beta\right)\right)^2$$

where the function "X_{if}" is defined in Appendix D-7.

Use MathCad's "minerr" solver function to find the minimum of SSE(β).

Guess: $\beta := .95$

Given

$SSE(\beta) = 0$

$1 = 1$

$\beta := \text{minerr}(\beta)$

$\beta = 0.9567$

Plot the mass balance functions "PulpCheck" and "FinesCheck" from Appendix D-7 to verify the validity of the estimates of α, β and C_{crit} for the consistency range of the data.

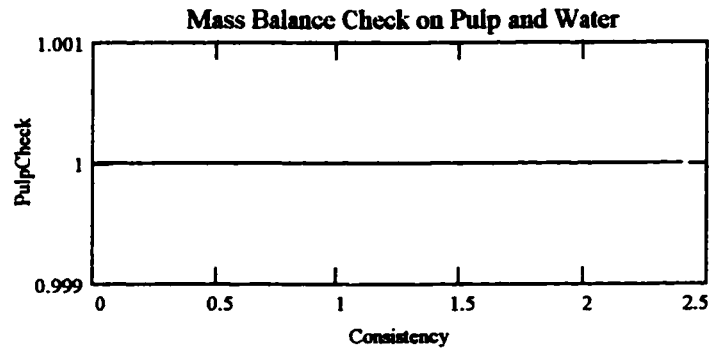

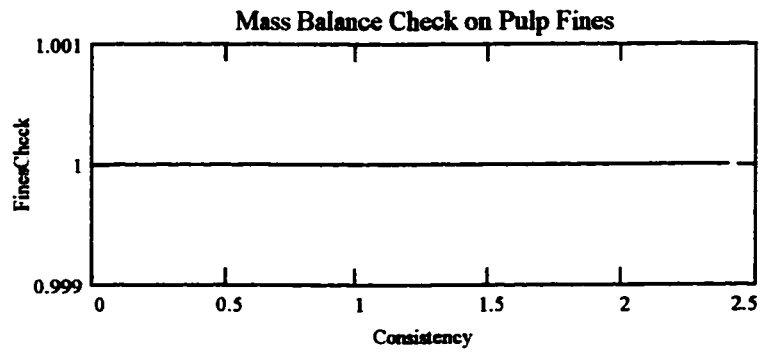

Since "PulpCheck" and "FinesCheck" = 1, the mass balances are valid.

APPENDIX E-6
Fitting the Model to the BKP (Small Bubble) Data
(Assuming a pulp density of 1.2 g/cm^3).

Equations and Parameters:

$\rho_{pulp} \equiv 1.2 \cdot \frac{gm}{cm^3}$ $\rho_w \equiv 1 \cdot \frac{gm}{cm^3}$ — Density of oven-dry pulp fibres and fines, and density of water. (ρ_{pulp} and ρ_w assumed to be constant)

$X_{Fines} = 0.1069$ — Average Fines Fraction of the BKP

$$\phi(C) = \frac{C \cdot \rho_w}{(-C \cdot \rho_{pulp} + C \cdot \rho_w + \rho_{pulp})}$$ — Volume consistency of the pulp suspension.

$$C_m(\phi) = \frac{-\phi \cdot \rho_{pulp}}{(-\phi \cdot \rho_{pulp} + \phi \cdot \rho_w - \rho_w)}$$ — Mass consistency of the pulp suspension.

$\phi_{Exp}(C) = (1 - e^{-486.4652 \cdot C})$ — Correlation for Settled Pulp Volume Fraction for BKP (Appendix D-6).

Equations for InterFloc Properties (from Appendix D-7)

$\phi_f(C, C_{crit}, \alpha) = \alpha \cdot \phi_{Exp}(C - C_{crit}) \cdot (C > C_{crit})$ — Floc Volume Fraction

$C_{fmax}(C, C_{crit}, \alpha) = C_m\left(\frac{\phi(C)}{\phi_f(C, C_{crit}, \alpha)}\right)$ — Maximum Floc Consistency

$C_f(C, C_{crit}, \alpha) = C + \phi_f(C, C_{crit}, \alpha) \cdot \left(C_m\left(\frac{\phi(C)}{\phi_f(C, C_{crit}, \alpha)}\right) - C\right)$ — Floc Consistency

$$C_{if}(C, C_{crit}, \alpha) = \frac{\left(\phi(C) \cdot \rho_{pulp} - \phi_f(C, C_{crit}, \alpha) \cdot \phi(C_f(C, C_{crit}, \alpha)) \cdot \rho_{pulp}\right)}{\left[\begin{array}{l}\phi(C) \cdot \rho_{pulp} - \phi_f(C, C_{crit}, \alpha) \cdot \phi(C_f(C, C_{crit}, \alpha)) \cdot \rho_{pulp} \cdots \\ +(1 - \phi(C)) \cdot \rho_w - \phi_f(C, C_{crit}, \alpha) \cdot (1 - \phi(C_f(C, C_{crit}, \alpha))) \cdot \rho_w\end{array}\right]}$$ — Interfloc Consistency

$$X_{if}(C, C_{crit}, \alpha, \beta) = \frac{\left(\phi(C) - \phi_f(C, C_{crit}, \alpha) \cdot \phi(C_f(C, C_{crit}, \alpha)) \cdot \beta\right)}{\left(\phi(C) - \phi_f(C, C_{crit}, \alpha) \cdot \phi(C_f(C, C_{crit}, \alpha))\right)} \cdot X_{Fines}$$ — Interfloc Fines Fraction

The following data are taken from Appendix C:

C_{BSFeed} Feed consistency from the flotation experiments.

C_{BSFoam} Foam consistency from the flotation experiments.

C_{DDJBS} Feed consistency from DDJ foam fractionation experiments.

X_{BSFoam} Fines fraction of foam from DDJ foam fractionation.

$C_{BKPInit}$ Consistency from pulp settling experiments.

C_{BKPSet} Settled consistency from pulp settling experiments.

ϕ_{BKPSet} Settled volume fraction from pulp settling experiments.

Number of Data for BKP (Small Bubbles): $i := \text{length}(C_{BSFeed})$ $i = 37$ $i = 0..36$

To find α and C_{crit}, define the sum squared of errors as:

$$SSE(\alpha, C_{crit}) := \sum_{i=0}^{36} \left(C_{BSFoam_i} - C_{if}(C_{BSFeed_i}, C_{crit}, \alpha)\right)^2$$

where the function "Cif" is defined in Appendix D-7.

Use MathCad's "minerr" solver function to find the minimum of the sum squared of errors.

Guess: $\alpha := .95$ $C_{crit} := 0.001$ $TOL := 1 \cdot 10^{-5}$

Given

$SSE(\alpha, C_{crit}) = 0$

$1 = 1$

$ANS := \text{minerr}(\alpha, C_{crit})$

$$ANS = \begin{pmatrix} 0.9694 \\ 0.0015 \end{pmatrix}$$

$\alpha := ANS_0$

$C_{crit} := ANS_1$

$\rho_{pulp} := 1.2 \cdot 10^3 \cdot kg \cdot m^{-3}$

The resulting values of α and C_{crit} are as follows:

$\alpha = 0.9694$ $C_{crit} = 0.00155$

Next, use the values of α and C_{crit}, to solve for β for the InterFloc Fines Fraction.

$j := \text{length}(C_{DDJBS}) \qquad j = 4 \qquad j := 0..3$

Define the sum squared of errors as:

$$SSE(\beta) := \sum_{j=0}^{3} \left(X_{BSFoam_j} - X_{if}\left(C_{DDJBS_j}, C_{crit}, \alpha, \beta\right)\right)^2$$

where the function "X_{if}" is defined in Appendix D-7.

Use MathCad's "minerr" solver function to find the minimum of SSE(β).

Guess: $\beta := .95 \qquad TOL = 1 \cdot 10^{-5}$

Given

$SSE(\beta) = 0$

$1 = 1$

$\beta := \text{minerr}(\beta)$

$\beta = 0.9973$

Plot the mass balance functions "PulpCheck" and "FinesCheck" from Appendix D-7 to verifty the validity of the estimates of α, β and C_{crit} for the consistency range of the data

$c = 1.001 \cdot C_{crit}, C_{crit} + 0.0001 .. 0.02025$

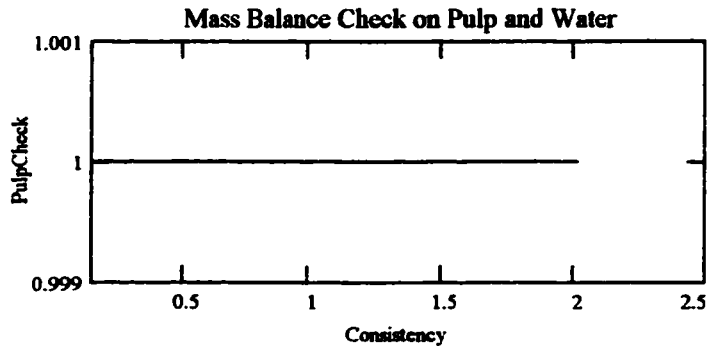

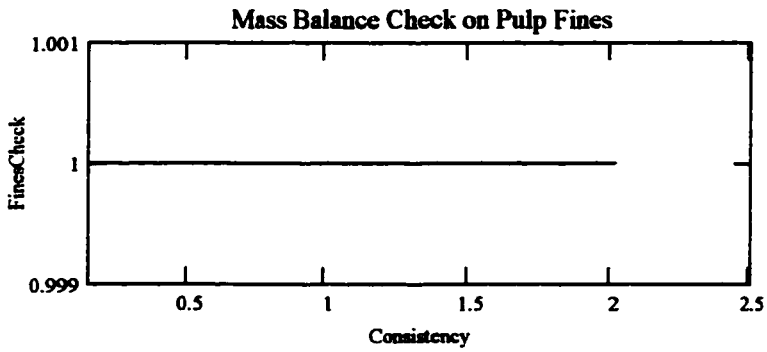

Since "PulpCheck" and "FinesCheck" = 1, the mass balances are valid.

IMAGE EVALUATION
TEST TARGET (QA-3)

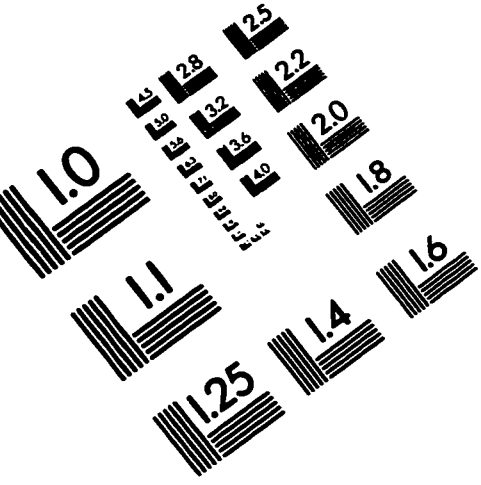

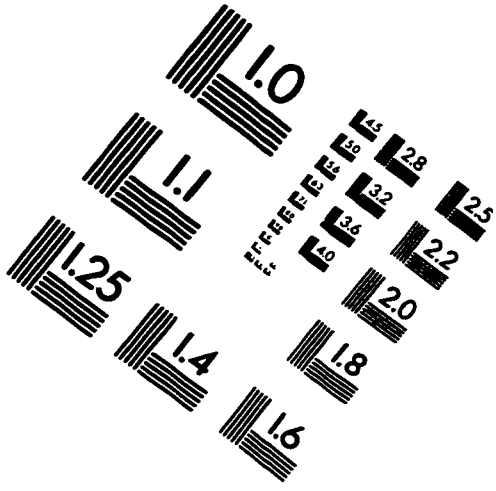

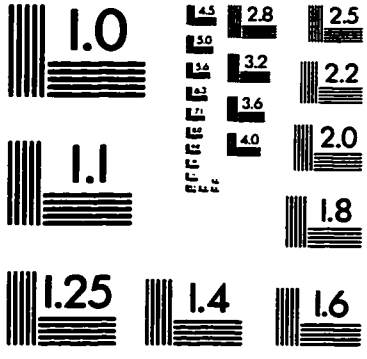

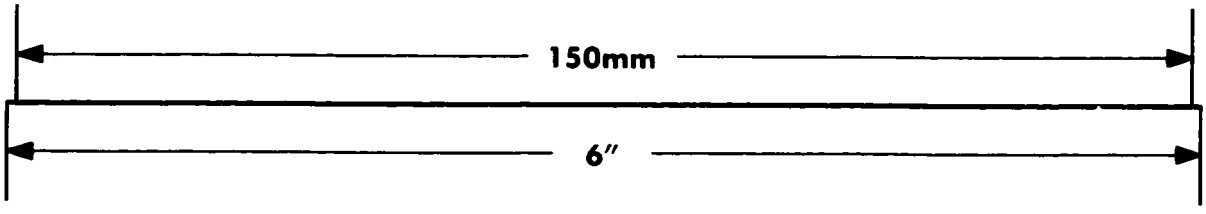

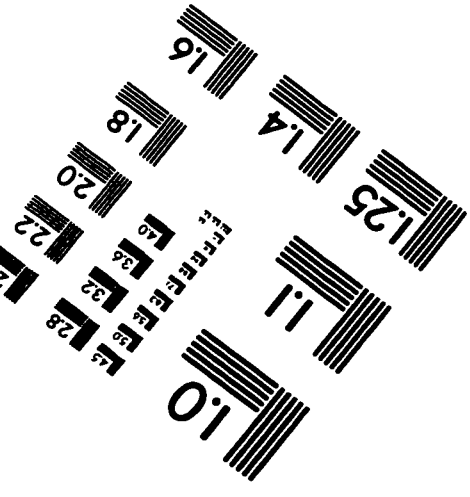

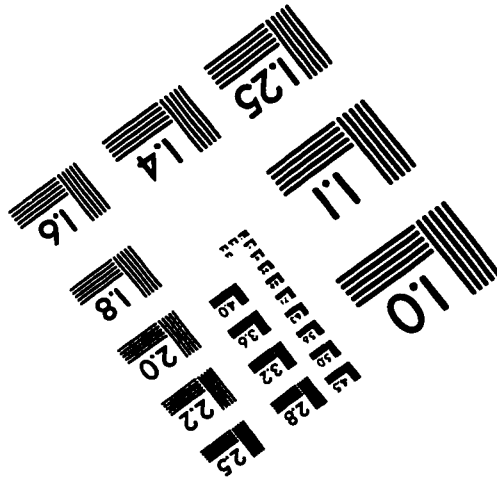

APPLIED IMAGE, Inc
1653 East Main Street
Rochester, NY 14609 USA
Phone: 716/482-0300
Fax: 716/288-5989